WILDFIRE EFFECTS ON RANGELAND ECOSYSTEMS AND LIVESTOCK GRAZING IN IDAHO

EXECUTIVE SUMMARY

SIGNIFICANT FINDINGS AND ACHIEVEMENTS

- Field sampling of rangeland vegetation for use in remote sensing studies needs to be scaled relative to the imagery used for classification.
- Field studies using multi-spectral imagery obtain better classification accuracies when vegetation is sampled categorically (chapters 1, 2, and 8).
- Trained field observers can reliably and consistently estimate the same percent cover as that calculated using high-spatial resolution (2.5mm/pixel) digital imagery (chapter 3).
- No difference was found in mean percent cover of shrubs, grasses, and bare ground in areas subjected to numerous years of fire, grazing, or fire and grazing treatments. *Note: treatments were not applied as part of this study, but rather referenced from management documents dating as far back as 1939* (chapter 9).
- The most accurate and reliable fuel load models utilize only three fuel load categories (<2 tons/acre, 2-4 tons/acre, and >4 tons/acre) for rangeland ecosystems of Idaho (chapter 8)
- Even when compared with recent fires (<3 years old), livestock grazing was found to be the most effective method to reduce fine fuel load in sagebrush-steppe rangelands (chapter 9).
- Fuel loads tend to recover to pre-fire levels within 10-12 years.
- Mountainous areas experience far higher rates of cloud-to-ground lightning strikes than rangelands of the Snake River Plain (chapter 6).
- Remote sensing imagery is a promising tool for predicting areas of potential landslide and soil erosion hazards as a result of wildfire activity (chapter 11).
- The two most applicable GIS data for landslide prediction are 1) high resolution multi-spectral imagery (e.g., IKONOS and/or Quickbird) and 2) 10mpp DEM's (e.g. USGS)(chapter 11).
- Landsat imagery, 30mpp USGS DEM's, and DEM's created from RADARSAT fine-beam imagery are too coarse for landslide and soil erosion modeling (chapter 11).
- Remote sensing imagery can reliably differentiate between burned and unburned patches of vegetation of the same species (chapter 14).
- Many Holocene millenial-scale climatic fluctuations recognized in other areas of the Northern Hemisphere are clearly visible in the regional pattern observed in this study (chapter 12).
- Within southeastern Idaho (and adjacent environs) the quantity of pine pollen in the recent past is at its highest level since human occupation 12,000 radiocarbon years ago, while the quantity of sagebrush and grass pollen is either at --or is approaching-- an all-time low (chapter 12).
- Successful M.S. thesis completion in the Department of Geology for Ms. Diane Wheeler.

In the summer of 2001, researchers at Idaho State University began an enthusiastic study to examine the effect of wildfire on Idaho's rangelands. Since that time, great strides have been made toward a better understanding of rangeland dynamics and wildfire impact. Further, new techniques and geotechnical best practices have been developed which can be implemented throughout this and other regions.

We developed an accurate and reliable fuel load model (73% overall accuracy, Kappa = 0.39) using geographic information systems (GIS), global positioning systems (GPS), and remote sensing. The fuel load model --along with other GIS datasets-- was used to develop a comprehensive wildfire risk model. These models provide land managers with a suite of tools, including predictive models of wildfire risk and identification of possible fuel load reduction areas. Local, regional, and federal land managers have benefited by using these models to proactively manage wildfire risk for communities in southeastern Idaho. This approach to wildfire management promotes rangeland sustainability and strengthens the economy of the state.

Various post-fire effects were also assessed using Geo-spatial maps and models. Landslide potential was examined using remote sensing and digital terrain modeling. Our study demonstrates that remote sensing is an effective tool to predict areas with increased landslide and erosion hazard. The tools developed by ISU researchers are particularly effective in areas with limited access. Land managers can implement remote sensing (e.g., IKONOS imagery) and digital terrain modeling (e.g., USGS 10mpp digital elevation models) techniques to rapidly and reliably predict landslide hazard following wildfire. These tools allow land managers to respond quickly and with appropriate landslide and erosion mitigation efforts.

We characterized historic vegetation patterns to better understand rangeland dynamics and better interpret historic wildfire records. Researchers found that sagebrush and grasses were more common in the past (approximately 12,000 years bp) than they are today. This finding is very interesting, especially when interpreted relative to the current wildfire focus of this study. With higher proportions of sagebrush and grasses present, we expect fuel loads would have been higher and with a greater fine fuel component. This scenario may have yielded more intense and severe wildfires. However, this speculation cannot be substantiated at this time. Indeed, with the presence of megaherbivores, it is just as likely that wildfire were rare and when they occurred, small and restricted to areas unsuited to grazing by megaherbivores.

Much progress has been made in this study and a better understanding of wildfire and its effects has been gained. At the same time, new questions have arisen that will surely yield new research directions for the scientists at Idaho State University.

FIELD COLLECTION OF FUEL LOAD, VEGETATION CHARACTERISTICS, AND FORAGE MEASUREMENTS ON RANGELANDS OF THE UPPER SNAKE RIVER PLAIN, ID FOR WILDFIRE FUEL AND RISK ASSESSMENT MODELS. A FIELD SAMPLING REPORT

Glenn Russell and Keith Weber
GIS Training and Research Center
Idaho State University
Pocatello, Ida. 83209-8130
(http://giscenter.isu.edu, e-mail: giscenter@isu.edu)

ABSTRACT

Fuel load, forage availability, and vegetation characteristics were sampled for 129 randomly generated points across the sagebrush- steppe semi- desert in southeast Idaho. We collected percent cover, fuel load, forage availability, visual obstruction, habitat type, and big sagebrush (Artemisia tridentata spp.) age estimates. Samples were stratified by fire and grazing treatments. Our study showed that bare ground, short grasses, and > 61 cm (~2 ft) big sagebrush were the dominant cover types. Visual obstruction readings, forage samples, and fuel load assessments revealed that forage availability and fuel loads were low. Calculations of big sagebrush age revealed that the age of live sagebrush plants in our study area range from 7 to 92 years.

Keywords: Grazing, Sagebrush-Steppe

INTRODUCTION

There has been a need to estimate rangeland wildfire danger since the 1940's (Burgan, 2000). Monitoring and inventory of rangeland wildfire factors, such as vegetation characteristics, litter, and percent bare-ground, are important fire hazard assessments to determine wildfire fuel load (Andersen, 1982). Modeling fuel load has become a valuable approach for the prediction of fire behavior and assessing the potential intensity and severity of wildfires (Andersen, 1982).

To effectively model wildfire potential with remotely sensed imagery, field samples of fuel load and vegetation condition needs to be collected. Ideally, correlates are then established between field data and the digital numbers recorded by the imagery. Researchers will then perform ground-truth sampling to validate the fuel load models and to assess the accuracy of the models.

Using data collected during the summer 2001 field season we will develop models to predict fuel load for our study area. Field data collected included fuel load estimations, forage material measurements, and vegetation characteristics.

Study Area

This study was conducted on land managed by the USDI BLM in the Upper Snake River Plain, Southeast Idaho (fig. 1). Sampling sites were found on Burley and Idaho Falls BLM Districts between $43^{0}36'00"$ and $42^{0}48'00"$ north Latitude and $-113^{0}35'00"$ and $-112^{0}37'59"$ west Longitude. This area is considered sagebrush-steppe semi-desert bordered by large, relatively recent lava formations to the south and west and irrigated agricultural lands to the east. This area has a history of livestock grazing and wildfire occurrence.

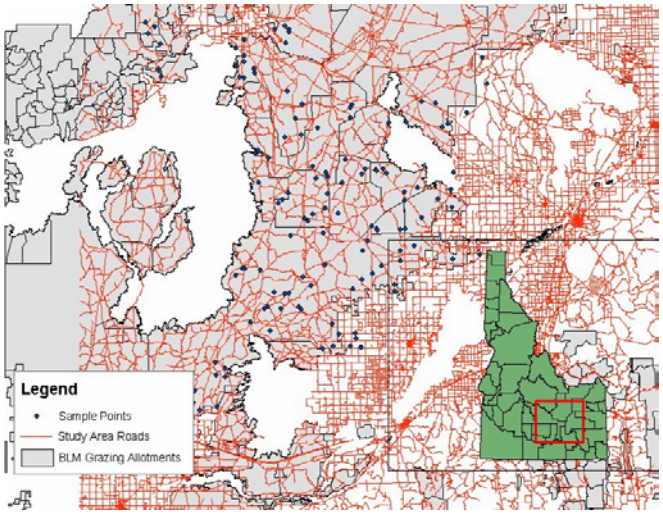

Figure 1. Map of the study area with sample points and road network.

METHODS

Experimental Design

Using ArcGIS 8.1, 129 points were randomly generated across the study area. Each point had to meet the following criteria: $\geq$ 70 meters from a road (to avoid edge effects) and $\leq$ 1000 meters from a road (to aid researchers in navigating to sample points on foot).

Sample points also had to fit our experimental design sampling strata regarding fire and livestock grazing treatments. Sample points were distributed over areas with no fire, one fire, or multiple fires, (between 1939 – 2001), and areas of livestock grazing and no livestock grazing.

Fuel Load Estimation

Fuel load estimates were made following BLM GIS Mapping Standards (BLM, 2001). Visual observations of an approximately 900 m^2 area centered over the sample point were used to make ocular estimates of:

- Assessment of the primary fuel structure of the area. (e.g. barren/rock, > 61 cm brush, short grasses)
- Assessment of the secondary fuel structure of the area. (e.g. barren/rock, > 61 cm brush, short grasses)
- Percent estimate of the fuel loading for wildfire fuels > 7.62 cm in basal diameter.
- Percent estimate of the fuel loading for wildfire fuels < 7.62 cm in basal diameter.
- Assessment of the presence of live fuels within the area.
- Estimate of the average height of all fuels.
- Estimate of the average depth of the duff component. (Duff, for this purpose, is defined as the decaying organic layer above the mineral soil.)
- Estimate of the average depth of the litter component of the stand. (Litter, for this purpose, is defined as needle cast, shed leaves and other shed vegetation matter above the duff layer.)
- Estimate of percent bare ground. (Bare ground is defined as exposed soil and rock and not covered with any vegetation, dead fuels, duff or litter.)
- Estimate of percent shrub cover.
- Estimate of the average shrub height of the big sagebrush plants in the area.
- Assessment of the current overall health of the shrub component (Decadence). (Only sagebrush shrub species were taken into consideration.)
- Estimate of percent grass cover.
- Estimate of percent forb cover.
- Estimate of percent cheatgrass cover.
- Estimate of average grass/ forb height. This includes the herbaceous and graminoid components of the area.
- Estimate of percent vegetation that would be removed due to an "average" fire. (We assume low fuel moisture, 80 degree day, 20% relative humidity, and 10 mph winds.)
- Estimate of rate of spread of an "average" fire. (We assume low fuel moisture, 80 degree day, 20% relative humidity, and 10 mph winds.)
- Assessment of the relative degree of grazing (domestic and wildlife).
- Assessment of previous fire evidence such as charcoal marks or fire scars.

Estimates were made based on field training for species identification and fuel load estimation instructed by Brandon Brown (BLM), Bryce Griffith (BLM), and Steve Pokovich (Consultant, Shoshone, ID). Glenn Burkhart (BLM) coordinated training.

Trimble Geo-Explorer II GPS receivers were used to acquire the sampling point location and record the above attributes data in a data dictionary. Approximately 50 positions per sample point were collected every 5 to 10 seconds to improve the accuracy of each location.

Forage Measurement

Data were collected to estimate available forage using a 0.44 m^2 circular hoop. The hoop was blindly tossed into each of four quadrants (NW, NE, SE, SW) centered over the sample point. All forage material within the hoop were clipped and weighed (+/- 1 g). All forb species and all grass species (except cheatgrass (*Bromus tectorum)*) were considered forage. The measurements were then used to estimate forage amount (lbs/acre) and animal units (AU/acre).

In addition to forage clipping, visual obstruction was collected to explore an alternative forage estimation method. Visual obstruction was measured using a graduated Robel pole marked with alternating 2.54 cm width bands of silver and black. The bottom of the pole had a 25 cm spike, which allowed it to stand free once the spike was pushed into the ground (Robel et al, 2000). The pole was located 10 paces (approximately 10 m) from the sample point in a 45^o bearing. Visual obstruction readings were taken from each of four cardinal directions (N, E, S, W) at a distance of 4 m with the reader's eye at an approximate height of 1 m (Robel et al, 2000). The top band totally obstructed by forage was recorded for each reading.

Other Vegetation Characteristics

GAP Analysis

Using a list of vegetation types defined by the Idaho GAP 2 dataset (2000), the observed primary vegetation type that best described the sample point was recorded.

Big Sagebrush (*Artemisia tridentata* spp.) Age Estimation

Maximum stem diameter (+/- 1 mm) of big sagebrush plants within the first 250 mm of stem height was measured. Four samples were taken at each sample point, one at each quadrant (NW, NE, SE, SW) of the sample area. The big sagebrush plant nearest the plot center within each quadrant was measured. The age of each big sagebrush plant was estimated using a modified linear regression model (6.1003+0.5769[diameter]) developed by Perryman and Olson, 2000.

Photo Points

Digital photos were taken using an Olympus D-360L in each of 4 cardinal directions (N, E, S, W) from the sample point.

RESULTS

Fuel Load Estimations

Primary and Secondary Fuel Models

Short grasses, barren/rock, and > 61 cm brush were the dominant primary fuel models found in the study area (98 %). Secondary fuel model was typically barren/rock or short grasses (77 %).

< 7.62 cm Diameter Fuels and ≥ 7.62 cm Diameter Fuels
Estimation of fuel load (kg/hectare) with basal diameter < 7.62 cm were low. More than 95 % of the sample points were estimated to have < 3 tons/acre. Fuel loads with basal diameter > 7.62 cm were low as well. Eighty percent of sample points were estimated as having < 3 tons/acre.

Average Duff and Litter Depths
Seventy-eight percent of sample points had a duff layer 2.54 – 3.81cm with no points having a mean duff depth > 7.62 cm. Litter depths were never measured > 7.62 cm with a majority (89 %) of the mean litter depths measured at < 2.54 cm.

Percent Bare Ground, Forb, Grass, and Shrub Cover
The percent bare ground was estimated as > 25 % at 71% (*n* = 92) of sample points. Forb Cover was rarely (*n* = 7) > 25 % cover. Seventy-six percent of the sample points were estimated to have < 5 % forb cover. A majority of sample points (*n* = 105) had a percent grass cover > 26 %. There were no sample points without grass species. In particular, cheatgrass, a non-native invasive species, was the dominant plant at many sample sites (*n* = 20). Percent cover of cheatgrass ranged from 0 - > 50%. Percent shrub cover was the most variable vegetation type.

Mean Shrub, Grass, and Forb Height
Mean shrub height was rarely (*n* = 5) > 91 cm (~3 ft). The majority (*n* = 69) was 30 – 91 cm. Sixty-six percent of sample points had a mean forb and grass height < 7 in.

Fire and Grazing Evidence
Fire was evident in 65 % of sample points and 69 % of sample points showed evidence of grazing. Thirty-six percent and 31% of sample sites had signs of light grazing and heavy grazing respectively.

Big Sagebrush Age Estimation
The mean age of big sagebrush plants was 38.8 yrs (*n* = 348). The minimum age was 7.9 yrs. and maximum age was 92.6 yrs.

Forage Measurements
Using AUM Analyzer software (Sheley, 1999), forage amount and available Animal Units (AU) were calculated for all sample points. Mean forage was 87.8 kg/hectare and mean AU was 0.097 AU/acre. The mean visual obstruction reading was 3.81 cm.

DISCUSSION
Collection of field data began July 4, 2001 and concluded August 8, 2001. Initially, our study had only 114 randomly generated sample points but after further review, these points were not meeting our experimental design criteria. Therefore, an additional 15

points were randomly generated and sampled allowing us to better meet our criteria (table 1).

Table 1. Stratification of sample points collected during the summer of 2001.

	Fires			
Treatment	**0**	**1**	**>1**	**Total**
Grazing	17	14	20	51
No grazing	33	28	17	78
Total	50	42	37	129

Fuel Loads Estimations and GAP Analysis

The large ranges recorded as interval data for percent cover (e.g. 1 – 25 %, 26 - 50%, >51%) may not accurately describe the vegetative community at the sample point. For instance, percent cover could only be recorded at very high (>51%). At some sample points, cheatgrass was clearly > 75%. An area of 75% cheatgrass would appear to be a highly infested while a moderately infested are could be 51 % cover. However, to accurately assess percent cover, a finer graduated, more diagnostic approach will be needed rather than ocular estimates.

GAP vegetation type observations may be too specific to accurately represent these areas. For instance, a sample point may be recorded as big sagebrush when 40 percent cover is big sagebrush but the remaining 60 percent are bare ground with bunchgrasses. Two methods that could improve agreement are; 1) record secondary habitat types or 2) increase the number of habitats to include mixed habitat (e.g. big sagebrush with short grasses).

Estimates of fuel load of plants with basal diameters < 7.62 cm and $\geq$ 7.62 cm seemed low (< 3 tons/acre). Fuel loads were not recorded > 3 kg/hectare even in areas with larger, older big sagebrush plants. Further analysis may reveal that this is significantly correlated to percent bare ground and the grass types (rhizomonous or bunchgrass) present at the sample points. However, BLM fuel load guidelines are also used for forested areas which would have higher values for $\geq$ 7.62 cm basal diameter fuels. This suggests that a more graduated characterization of fuel loads specific to Sagebrush Steppe communities may better describe the fuel loads in our study area. High values for < 7.62 cm fuels would be expected in areas of rhizomonous tall grasses and forbs. This suggests that fuel load models should be re-evaluated and sub-divided into additional models for particular vegetation types such as sagebrush-steppe.

Forage Measurements

Southeast Idaho experienced severe drought during the spring and summer of 2001 and our low forage measurement seems to support this. The visual obstruction reading (mean = 3.81 cm) suggests that forage is extremely limited across the study area. This may also indicate our method of measurement is not conducive for bunchgrass communities where bare ground cover is typically high (>40%). Benkobi et al (2000) found visual obstruction method conducive for Nebraska sandhills which consisted of mostly rhizomonous species of grasses thus allowing for readings > ours. Many sample

points had readings = 0 for this measurement because the nearest bunchgrasses would be inches to feet away and not obstructing the view of the pole in one of the cardinal directions from the reader. With rhizomonous species, there is an increased likelihood that grasses would be obstructing the view of pole in all directions. We believe the percent bare ground at each sample point may be a factor in this measurement. Vegetation in our study area included bunchgrasses with high percent bare ground (>40%), which may not be applicable for these methods.

A low visual obstruction average seems to coincide with low forage availability (0.097 AU/acre). Since both methods have low values, this correlates intuitively with a drought year where precipitation has limited forage growth.

Big Sagebrush Age

Big sagebrush age calculations reveal that the mean age of big sagebrush is 38 years with a minimum of 7.9 years and maximum of 92 years. We believe the minimum value (min = 7.9 yrs) may be overestimated and questions the validity of our modified linear regression model. A young big sagebrush plant could have a diameter of 1 mm and, based on our calculation, it would be nearly 6 years old. Our model may have a bias towards older big sagebrush and may not be an accurate calculation of age for young big sagebrush plants.

The dial-caliper had a maximum caliper width of 150 mm. When big sagebrush plants had diameter > 150 mm, the value was recorded as "150+" (n = 18). Further, 150 mm diameter plants are estimated to be 92 years of age. This suggests these plants have not experienced an intense fire in over 92 years.

ACKNOWLEDGEMENTS

This study was made possible by a grant from the National Aeronautics and Space Administration Goddard Space Flight Center. ISU would also like to acknowledge the Idaho Delegation for their assistance in obtaining this grant.

REFERENCES

Andersen, H.E., 1982. Aids to Determining Fuel Models for Estimating Fire Behavior, USDA, FS, General Technical Report INT-122.

Benkobi, L., Uresk, D.W., Schenbeck, G., and King, R.M. 2000. Protocol for monitoring standing crop in grasslands using visual obstruction, J. Range Mange. 53:627-633.

Bureau of Land Management (BLM), Upper Snake River District, 2001. Field Survey Project for Fuels Management Planning GIS Mapping Standards.

Burgan, R.E., Klaver, R.W., and Klaver, J.M. 2000. Fuel Models and Fire Potential from Satellite and Surface Observations, USDA, FS, Rocky Mountain Research Station, Missoula, MT.

Burgan, R.E. and Shasby, M.B. 1984. Mapping Broad-Area Fire Potential From Digital Fuel, Terrain, and Weather Data, Journal of Forestry 8:228-231.

Chuvieco, E. and Congalton, R.G., 1989. Application of Remote Sensing and Geographic Information Systems to Forest Fire Hazard Mapping, Remote Sens. Environ, 29:147-159.

Miller, R.F., Svejcar, T.J., and West, N.E. Implications of Livestock Grazing in the Intermountain Sagebrush Region: Plant Composition, Ecological Implications of Livestock Herbivory in the West.

Perryman, B.L. and Olson, R.A. 2000. Age-stem diameter relationships of big sagebrush and their management implications. J. Range Manage. 53:342-346.

Robel, R.J., Briggs, J.N., Dayton, A.D., and Hulbert, L.C. 2000. Relationships between visual obstruction measurements and weight of grassland vegetation. J. Range Manage. 23:295-297.

Sheley, Roger, 1999. AUM Analyzer Software, Montana State University.

FIELD COLLECTION OF FUEL LOAD AND VEGETATION CHARACTERISTICS WILDFIRE RISK ASSESSMENT MODELING: 2002 FIELD SAMPLING REPORT

Keith T. Weber and J. Ben McMahan
GIS Training and Research Center
Idaho State University
Pocatello, ID 83209-8130
(http://giscenter.isu.edu, e-mail: giscenter@isu.edu)

ABSTRACT

Fuel load and vegetation characteristics were collected at 370 sample points across sagebrush-steppe regions in southeast Idaho. We collected visual estimations of fuel load (tons/acre), percent cover of major ground cover types (shrub, grass, litter/duff, bare ground, and cheatgrass), and basal stem measurements of big sagebrush (Artemisia tridentata spp.). These data were collected to validate fuel load and wildfire risk models created following the 2001 field season and to refine and rebuild these models in order to improve upon their accuracies. These data will also be used in other projects conducted at the GIS Training and Research Center including fuzzy classification of sagebrush-steppe vegetation, modeling of invasive weed distribution and density, and other wildfire research conducted as part of the NASA-funded Wildfire Effects on Rangeland Ecosystems and Livestock Grazing project.

Keywords: Grazing, Snake River Plain, Sagebrush-Steppe

INTRODUCTION

Field measurements and observations collected during the summer of 2001 were used to create a series of models (e.g. fuel load, comprehensive wildfire risk, etc.) for the NASA-funded *Wildfire Effects on Rangeland Ecosystems and Livestock Grazing* project. During the 2002 summer field season, additional data was collected to determine the accuracy of these models. These data were also used to refine and rebuild the fuel load and wildfire risk models, and to create new components for a comprehensive wildfire risk assessment (cf. chapter 8).

Study Area

This study was conducted on land managed by the United States Department of the Interior Bureau of Land Management (USDI BLM) in the Upper Snake River Plain, Southeast Idaho. Sampling sites were located in Burley and Idaho Falls BLM Districts, and had a spatial extent of approximately 110 x 115 km (min x: 520000, max x: 630000, min y: 170000 max y: 285000, Idaho Transverse Mercator, GCS: NAD27, Datum: NAD27, Clarke's 1866). This area is a sagebrush-steppe semi-desert bordered by large, relatively recent lava formations to the south and west and irrigated agricultural lands to the north, south, and east, and has a history of livestock grazing and wildfire occurrence.

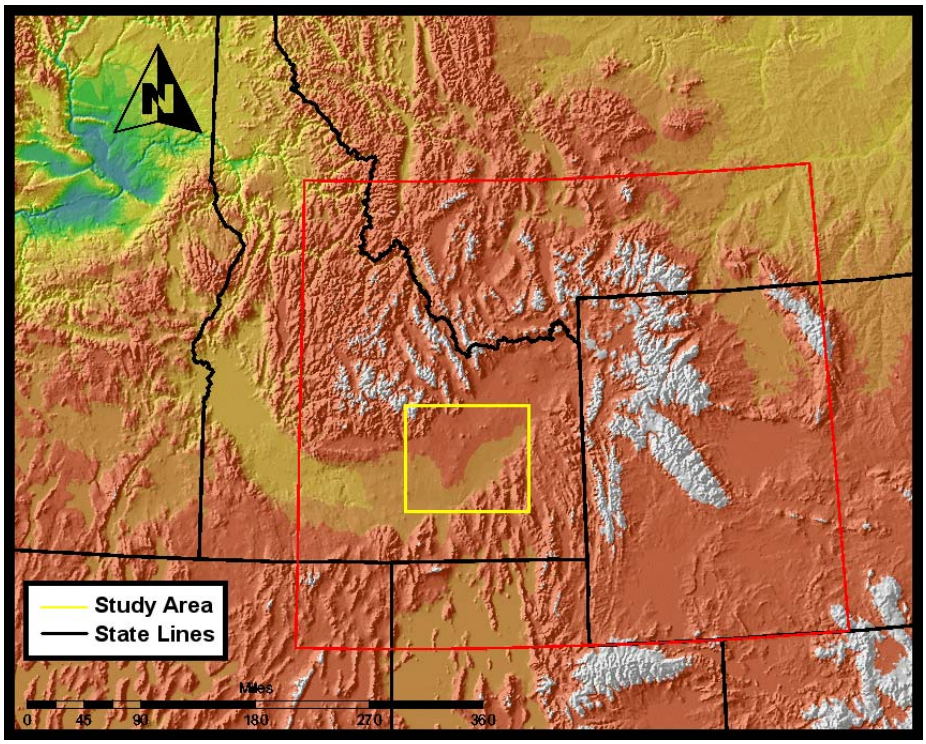

Figure 1. Study Area for NASA Wildfire Livestock (NWL) interactions project shown in yellow (light gray), Area Of Concern (AOC) for the ISU GIS Training & Research center shown in red (dark gray).

METHODS

Traditional methods of quantifying vegetation cover are time intensive and may not reliably represent the patterns necessary for use in landscape scale remote sensing analyses. We collected data at our sample points (n = 370) that better represents how large-scale remote sensing platforms image the landscape (e.g. Landsat ETM7+, 30m pixels, ~150km x 150km extent). We gathered ocular estimates of fuel load, vegetation type and percent cover, and dominant shrub species/height within an area representing approximately four Landsat pixels (~3600m^2 (60x60m)).

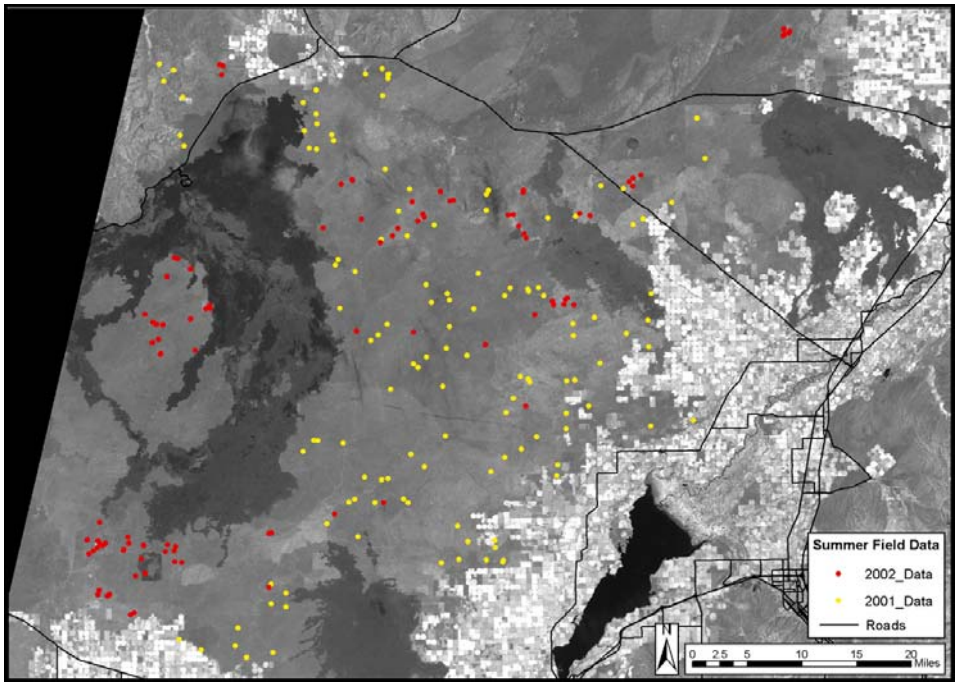

Figure 2. Sample points for summer 2001 field season (n = 128) (yellow/light gray) and 2002 summer field season (n = 370) (red/dark gray).

Fuel Load Estimation

Fuel load was estimated based on the same five categories of fuel load found in this area during the 2001 field season (cf. chapter 1). These categories were 0.74 tons/acre, 1.0 tons/acre, 2.0 tons/acre, 4.0 tons/acre, and 6.0 tons/acre. We stratified our sample point collection so that each fuel load category in the fuel load model would have at least 25 points for validation. Note: following USDA-USFS fuel load identification guidelines (Anderson 1982), only three fuel load/fire behavior categories are applicable to this area (0.74 tons/acre, 4.0 tons/acre, and 6.0 tons/acre). In order to increase the number of fuel load types available for modeling, technicians created two intermediate categories (1.0 tons/acre and 2.0 tons/acre) to better account for the continuum of fuel load levels between 0.74 tons/acre and 4.0 tons/acre.

Vegetation Estimation

We estimated ground cover immediately adjacent to each sample point for five general cover types (shrub, grass, cheatgrass (a dominant invasive weed found in the study area and included within the grass cover estimation as well), litter and duff, and bare ground). Percent cover for each of these vegetation types were estimated using categorical breaks of 0%, 1-5%, 6-15%, 16-

25%, 26-35%, 36-50%, 51-75%, 76-95%, and 96-100%. For each sample, the dominant shrub species (e.g., sagebrush, rabbitbrush, other, or none) and mean shrub height category (0-50cm, 51-100cm, 101-150cm, >150cm, or none) was also recorded.

Big Sagebrush (*Artemisia tridentata* spp.) Age Estimation

Maximum basal stem diameter (+/- 1 mm) of big sagebrush plants was measured (within the first 25 cm of stem height). Four samples were taken at each sample point, one within each quadrant (northwest, southeast, southwest, and northwest) centered over the sample point. The big sagebrush plant nearest the plot center in each quadrant was measured. If no big sagebrush plant was within 30 meters of the sample point, a null measurement was recorded. The age of each big sagebrush plant was estimated using a modified linear regression model (6.1003 + 0.5769 * [diameter]) (Perryman and Olson, 2000).

Photo Points

Digital photos were taken using an Olympus D-360L in each of 4 cardinal directions (north, east, south, and west) from the sample point.

RESULTS AND DISCUSSION

Sample points were collected in order to validate our existing fuel load model (created following the 2001 summer field season) and produce an improved model. Points were stratified by treatment (fire and grazing, Table 1). As a result, sample points were spatially clustered (Figure 3). Inferences drawn from observed differences in vegetation should take into consideration the distribution of sampling used for this study.

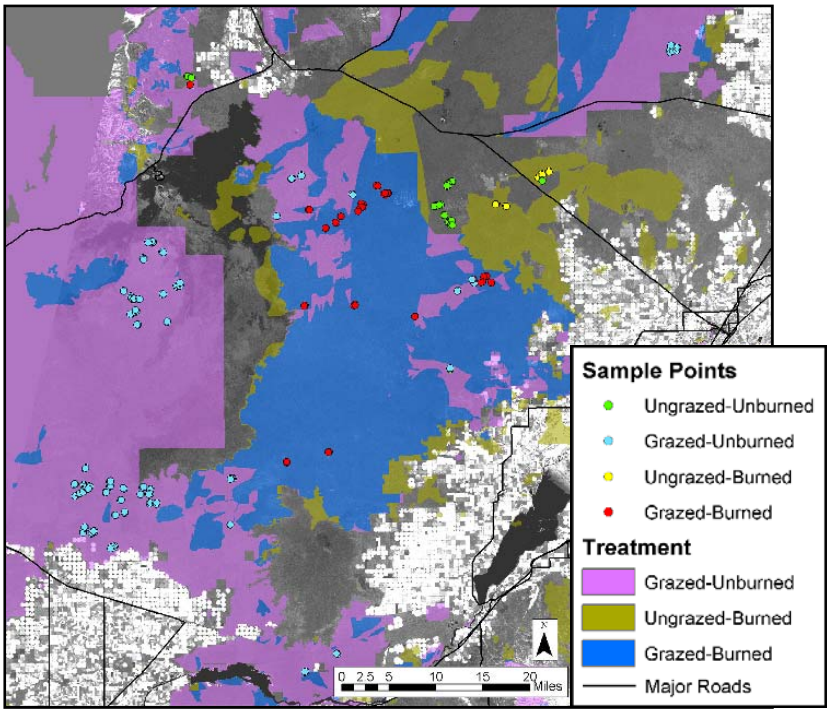

Figure 3. Sample points symbolized by treatment. Spatial extent of the treatment types is also displayed.

Table 1. Stratification of treatments.

	Fires			
Treatment	**0**	**1**	**>1**	**Total**
Grazing	211	6	3	220
No grazing	74	55	21	150
Total	285	61	24	370

The mean fuel load was 2.3 tons/acre (std. dev. = 1.31, *n* = 370) and the median fuel load class was 2.0 tons/acre (skewness = 0.31). The vegetation found at these sites is perhaps best characterized using mode since categorical data was recorded (Table 2). Shrub and grass cover was most commonly estimated in the 16-25% category, with big sagebrush (*Artemesia tridentata*) being the most common shrub species. Cheatgrass (*Bromus tectorum*) was found at most sample locations with a mean, median, and mode cover class in the 1-5% category. Litter cover was typically 16-25% and bare ground comprised 26-35% of all sample locations.

Field samples recorded in 2001 yielded similar results for several of the sampled parameters. Bareground was typically estimated in the 26-50% category (note: modified categories were implemented in 2002 so direct comparisons are not possible) while litter was estimated at <25%. In contrast however, is the fact that grass cover was most commonly estimated at 26-50% in 2001 compared to 16-25% in 2002. This is primarily due to the presence and abundance of cheatgrass in 2001, which in many cases comprised all grassy cover at sample locations.

Big Sagebrush Age Estimation

The mean age of big sagebrush plants sampled in the region was 25.4 Years (std. dev = 10.9, minimum 10.7, maximum 75.9, *n* = 187). Further analysis of the sagebrush age study can be found in chapter 5.

CONCLUSIONS

The 2002 field season was successful in many ways. First, data were gathered to support a reliable validation of preliminary fuel load models developed using 2001 field data. Second, many (*n* = 370) vegetation samples were recorded that add either directly or indirectly to our knowledge base regarding the ecological dynamics acting on rangelands in the Intermountain West.

ACKNOWLEDGEMENTS

This study was made possible by a grant from the National Aeronautics and Space Administration Goddard Space Flight Center. ISU would also like to acknowledge the Idaho Delegation for their assistance in obtaining this grant.

LITERATURE CITED

Perryman, B.L., and Olson, R.A. 2000. Age-Stem Diameter Relationships of Big Sagebrush and Their Management Implications. Journal of Range Management, v53 pp342-346, May 2000.

THE "POLE CAM": CORROBORATING FIELD ESTIMATIONS WITH HIGH SPATIAL RESOLUTION IMAGERY

Ben McMahan, Dan Narsavage, and Keith T. Weber
GIS Training and Research Center
Idaho State University
Pocatello, ID 83209-8130
(http://giscenter.isu.edu, e-mail: giscenter@isu.edu)

ABSTRACT

Traditional methods of quantifying vegetation cover are time intensive and may not represent patterns necessary for use in landscape scale remote sensing analyses. We used visual assessments to determine percent cover at the scale of four LANDSAT pixels (~60m^2). To compare visual assessments with ground cover characteristics, we took RGB images using a digital camera mounted on a four-meter pole. We used maximum likelihood classification to assign pixels to one of five classes (shrub, grass, litter/duff, bare ground, and shadow). We calculated proportions of each class and compared them to our ocular assessments to determine the difference between observed and actual percent cover.

Keywords: remote sensing, field estimates, correlation

INTRODUCTION

Point-quarter, Daubenmire frame, and line transect are common methods to characterize vegetation cover and structure but are also time consuming and tend to collect data at scales that are impractical for remote sensing image analysis (e.g., Landsat ETM 7+ with 30mpp resolution and approximately 150km x 150km scene extent). Ocular estimates of vegetation cover (e.g., using shrub, grass, litter, and bare ground categories) has proven to be a successful method to characterize vegetation for use in remote sensing studies (cf. chapters 1 and 2). However, no studies known to the authors have evaluated the agreement between estimates made by field observers and cover classifications derived with image processing techniques. The primary reason for this is surely the lack of high-spatial resolution imagery necessary to support such a study. The recent (c. 1999) commercial availability of high spatial resolution multi-spectral imagery changed this, and made it possible --albeit theoretically-- to classify sites using <2.5mpp imagery.

METHODS

During the summer of 2002, we collected field vegetation samples (n = 370) using ocular estimates of vegetation type and percent cover within a 30 meter radius of each sample point. This area approximated four Landsat pixels (60 x 60m). To test the agreement between ocular and remote sensing estimates, we developed a method using small plots (~2m x 3m) that were digitally imaged using a 3.3 mega-pixel camera. The digital camera was mounted to a four-meter pole and used to acquire three aerial RGB images at each of 19 plots (a subset of the original 370 sample sites) using the highest resolution setting on the camera (1600 x 1200 pixels). The camera's lens was always parallel to the ground. This was ensured by the use of a bubble level and "kickstand" attachment for the pole. Imagery was downloaded (n = 57) and opened with ENVI software .We digitized training polygons for five vegetation classes on each image (shrub, grass, litter, bare ground, and shadow), and generated a maximum likelihood supervised classification of each image. We then calculated the percent cover of each class as a proportion of the area not classified as shadow. These proportions were then compared with ocular estimations of percent cover.

RESULTS

Based on maximum likelihood supervised classification of the pole-cam photos, shrub cover was underestimated in the field an average of 3% per plot, grass cover was overestimated in the field an average of 8% per plot, litter was overestimated in the field an average of 23% per plot, and bare ground was underestimated in the field an average of 10% per plot (Figures 1 and 2).

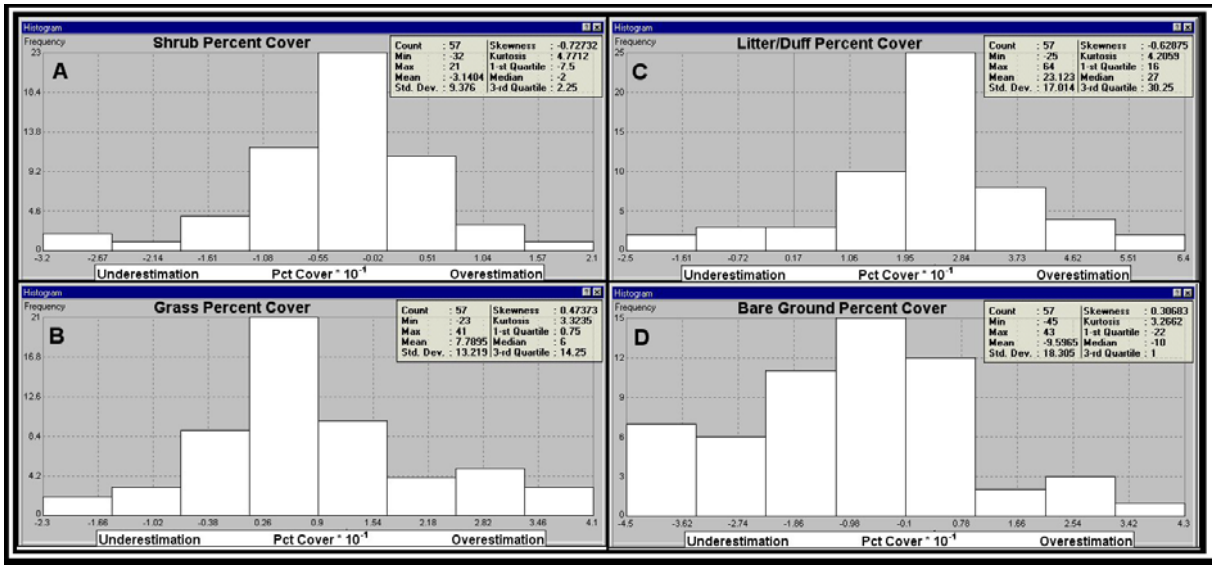

Figure 1. Distribution of agreement between ocular estimations and classifications of vegetation cover.

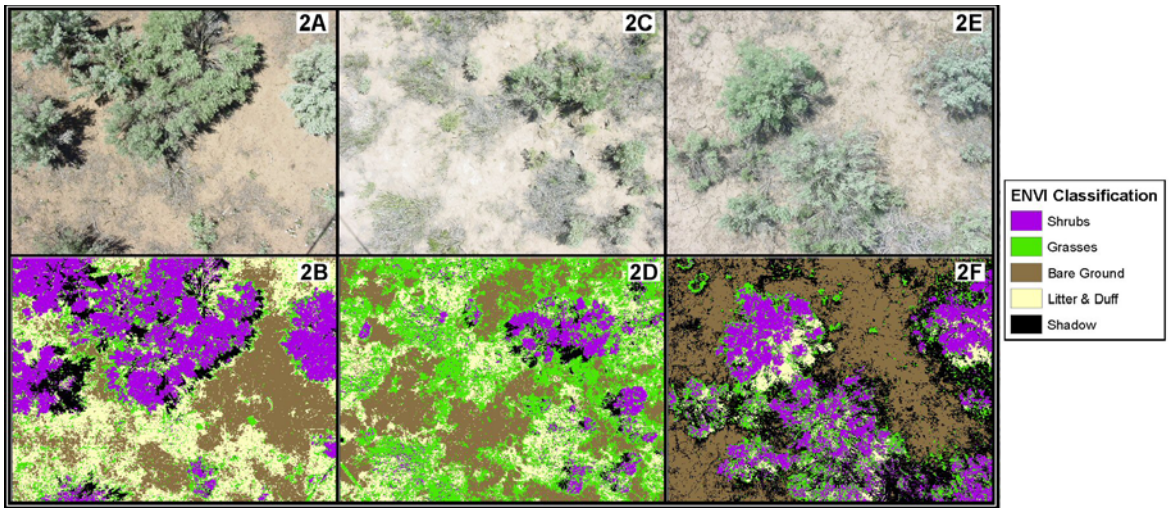

Figure 2. Original "pole-cam" photos (A, C, and E) and ENVI classifications (B,D, and F) .

DISCUSSION

We were satisfied with the agreement between ocular estimates and remote sensing classifications. The relatively small difference between ocular estimates and ENVI's classification gives us confidence in the precision of our field estimates. The differences between the ocular estimations and ENVI classifications of shrub, grass, and bare ground cover were all <10%. Further, the ocular estimations implemented in our remote sensing studies are always recorded in ordinal classes where classes have a range of 15%. This suggests that under most circumstances, field estimates will agree well with remote sensed imagery.

There were four systematic errors that had an effect on accuracy, all of which help explain the errors between ENVI's classification and ocular estimations. 1) The 'core' areas of grass clumps were occasionally mis-classified as shrubs by ENVI. This helps account for some of the overestimation of shrubs (cf. Figure 2b, 2d, and 2f). 2) The edge of shrubs were often mis-classified as grass resulting in a moderate underestimation to the shrubs category and an overestimation of the grass category (cf. Figure 2b and 2f). 3) Dry shrub branches were often mis-classified as litter resulting in moderate overestimation of litter and minor underestimation of shrubs (cf. Figure 2f). 4) Desiccation cracks in the soil were occasionally mis-classified as grass resulting in a minor overestimation of grass (cf. Figure 2f).

These four errors amplify differences between estimations and classifications and are the result of imagery having similar RGB values within different classes (e.g., the bright green of young green rabbitbrush looks quite similar to grass, and woody branches of sagebrush look similar to litter within the visible portions of the electromagnetic spectrum recorded by the digital camera). This error could be resolved with the use of a multispectral sensor that incorporates one or more bands in the near-infrared portion of the electromagnetic spectrum.

AKNOWLEDGEMENTS

This study was made possible by a grant from the National Aeronautics and Space Administration Goddard Space Flight Center. ISU would also like to acknowledge the Idaho Delegation for their assistance in obtaining this grant.

LITERATURE CITED

ENVI, 2003. Environment for Visualizing Images. RSI Inc., Boulder, Colo. 80301.

COMPARISON OF TWO STANDING CROP ESTIMATORS IN SAGEBRUSH-STEPPE COMMUNITIES

Keith T. Weber and Glenn P. Russell
GIS Training and Research Center
Idaho State University
Pocatello, ID 83209-8130
(http://giscenter.isu.edu, e-mail: giscenter@isu.edu)

ABSTRACT
The use of direct sampling (using Daubenmire frame or hoop sampling) to estimate standing crop is widely used and effective, but time consuming. Visual obstruction is a non-destructive and less intensive alternative. Benkobi et al. found visual obstruction a reliable technique in Nebraska grasslands. We applied the same techniques in sagebrush-steppe communities and found visual obstruction routinely underestimated forage availability and was only weakly correlated with hoop sampling measurements ($R^2 = 0.14$).

Keywords: Grazing, Daubenmire frame, Direct harvest, Visual Obstruction, Robel.

INTRODUCTION

Accurately assessing standing crop on rangeland is important for livestock and wildlife management (Webb 1942, Benkobi et al. 2000, Thoma et al. 2002). Reliably calculating forage biomass and available AU's allows land managers to correctly prescribe stocking rates and promote healthy and sustainable rangelands. Using the direct-harvest (or hoop sampling) method (Daubenmire 1959, Milner and Hughes 1968, Pieper 1978, Pieper1988) is both destructive and time-intensive. However this technique has been demonstrated to be an accurate estimator of standing crop (Cochran 1977, Pieper 1988, Benkobi et al, 2000, Holechek et al 2001). For this reason, we assumed standing crop estimates derived from direct harvest accurately reflected existing range productivity. We then applied a non-destructive visual obstruction method (Benkobi et al. 2000) to estimate standing crop. Statistical comparisons were made to test correlation of visual obstruction results with accepted standing crop estimates. While Benkobi et al. (2000) demonstrated that visual obstruction correlated well with direct harvest and the weight-estimation (or double-sampling) methods (Pechanec and Pickford 1937) in Nebraska grasslands ($R^2 = 0.88$), this method has not been validated in sagebrush-steppe communities. The sagebrush-steppe community typically has a high bare ground component along with substantial shrub cover making visual obstruction more difficult to apply successfully.

The objective of this study was to determine the utility of the visual obstruction estimator as an alternative to direct harvest in sagebrush-steppe communities of the Upper Snake River Plain, Idaho. If proven reliable, the visual obstruction method would offer a more productive means to estimate standing crop.

METHODS

This study was conducted on land managed by the USDI BLM, Upper Snake River District in southeast Idaho. Sample points were located between $43^0$36'00" and $42^0$48'00" N latitude and –$113^0$35'00" and -$112^0$37'59" W longitude. This area is considered sagebrush-steppe semiarid-desert and is bordered by large, relatively recent lava formations (2000 years BP) to the south and west and irrigated agricultural lands to the east. This area has a history of livestock grazing and wildfire occurrence (Figure. 1).

One-hundred and twenty-eight sample points were randomly generated across the study area. Each point was located $\geq$70 m from a road to avoid edge effects. Sample points were stratified by grazing treatment (grazed versus ungrazed), fire history, and control. Fire history was determined using an historic wildfire (1939-2001) geographic information systems data set with samples categorized into no-fire, one-fire, or multiple-fire treatment classes (Table 1).

Two methods were used to estimate standing crop at each sample point. Firtst, direct harvest in which a 0.44 m^2 hoop was blindly tossed into each of four quadrants (NW, NE, SE, SW) centered over the sample point. All current year' above ground growth of grass and forbs (Shoop and McIlvain 1963) within the hoop was clipped and weighed (+/- 1 g). Standing crop (kg ha^{-1}) was calculated with "AUM Analyzer" software (Sheley 1999) by entering the four hoop sample weights and applying a dry-weight correction factor based on current phenology. Second, visual obstruction was measured using a modified Robel pole marked with alternating 2.54 cm bands of silver and black. Affixed to the bottom of

the pole was a 25 cm spike that allowed it to stand free once the spike was pushed into the ground. The pole was located 10 paces (approximately 10m) from the sample point. One reading was made from each of four cardinal directions (N, S, E, and W). The observer stood 4m from the pole with his eye approximately 1m above the ground. The top band totally obstructed by forage was recorded. If sagebrush or other non-forage shrub was obstructing view of the pole, the observer simply stepped aside. These techniques are consistent with those reported by Benkobi et al. 2000.

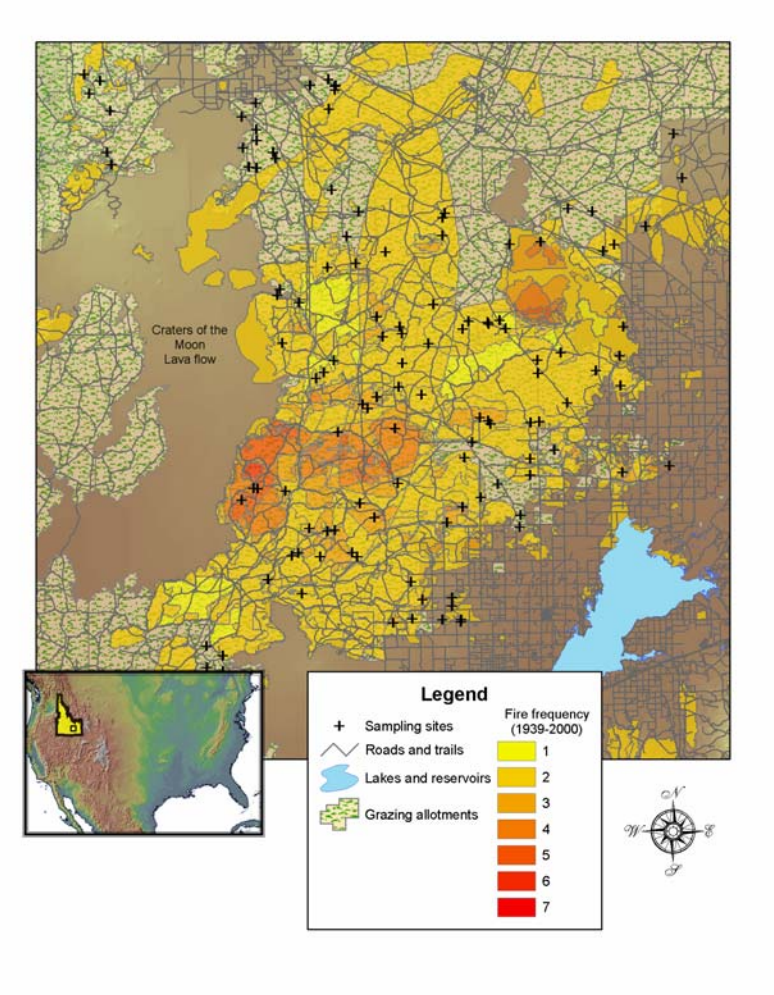

Figure 1. Study area with field sampling sites indicated.

Table 1. Stratification of treatments at sampling sites.

Sample Points	Fire Frequency				
Grazing	0	1	> 1	Total	Percent
Grazed	17	14	20	51	40
Ungrazed	33	28	17	78	60
TOTALS	50	42	37	129	100
Percent	39	33	29		100

Linear regression was used to determine the predictability of standing crop (as measured by direct harvest) using the mean of four visual obstruction readings per site.

RESULTS AND DISCUSSION

The mean, minimum, and maximum weight of clipped vegetation was 14, 0, and 95 g respectively. Mean standing crop was 87.8 kg ha^{-1}. The mean, minimum, and maximum visual obstruction reading was 3.81, 0.0, and 31.75 cm, respectively. There was no statistically significant relationship between measured standing crop and visual obstruction readings ($R^2 = 0.14$).

Many of the sample points had readings of 0 because the nearest plant did not obstruct our view of the pole. The visual obstruction method is best applied in grassland areas with 1) relatively high standing crop (≥300 kg ha^{-1}) and 2) grass species like those found in the Nebraska sandhills (e.g., Little bluestem (*Schizachyrium scoparium spp.*, prairie sand reed (*Calamovilfa longifolia spp.*), and needle-and-thread (*Stipa comata spp.*)) and northeast Kansas (Robel et al 1970). Further, we believe areas with a high bare-ground component are poor candidates for the visual obstruction method.

Other estimation techniques exist (Shoop and McIlvain 1963, Pearson and Miller 1972, Holmes 1974, Pieper 1988, Holechek et al. 2001) that may improve the efficiency of standing crop estimation. However, until other techniques are validated in sagebrush-steppe ecosystems, accurate standing crop estimates can only be achieved using standard hoop sampling techniques.

ACKNOWLEDGEMENTS

This study was made possible by a grant from the National Aeronautics and Space Administration Goddard Space Flight Center. ISU would also like to acknowledge the Idaho Delegation for their assistance in obtaining this grant.

LITERATURE CITED

Benkobi, L., D. W. Uresk, G. Schenbeck, and R. M. King. 2000. Protocol for monitoring standing crop in grasslands using visual obstruction. J. Range Manage. 53:627-633.

Cochran, W.G. 1977. Sampling techniques, 3rd ed. John Wiley Sons, Inc. New York, N.Y. 428 pp.

Daubenmire, R. 1959. A canopy-coverage method of vegetational analysis. Northwest Sci. 33(1)43-64.

Holechek J., R. D. Pieper, and C. H. Herbel. 2001. Range management: principles and practices, 4th ed. Prentice-Hall, Upper Saddle River, N.J. 587pp.

Holmes, C. W. 1974. The Massey grass meter. Dairy farming annual. pp.26-30.

Miller, R.F., T.J. Svejcar, and N.E. West. 1994. Implications of Livestock Grazing in the Intermountain Sagebrush Region: Plant Composition, Ecological Implications of Livestock Herbivory in the West. Society for Range Management. 297pp.

Milner, C. and R.E. Hughes. 1968. Methods for the measurement of primary production of grasslands. Blackwell Scientific Publications, Oxford, Great Britain.

Pearson, R.L. and L.D. Miller. 1972. Remote spectral measurements as a method for determining plant cover. US/IBP Grassland Biome Tech. Rep. no. 167, Colorado State Univ., Fort Collins, Colo.

Pechanec, J.F. and G.D. Pickford. 1937. A weight estimate method for determination of range or pasture production. J. Amer. Soc. Agron. 29:894-904.

Pieper, R.D. 1978. Measurement techniques for herbaceous and shrubby vegetation. New Mexico State Univ., Las Cruces, N.M.

Pieper, R.. D. 1988. Rangeland vegetation productivity and biomass, pp. 449-467. *In* P. T. Tueller (ed),Vegetation Science Applications for Rangeland Analysis and Management. Kluwer Academic Publishers, Norwell, Mass. 581pp.

Robel, R.J., J.N. Briggs, A.D. Dayton, and L.C. Hulbert. 1970. Relationships between visual obstruction measurements and weight of grassland vegetation. J. Range Manage. 23:295-297.

Sheley, R. 1999. AUM Analyzer Software, Montana State University, Bozeman, Mont.

Shoop, M.C. and E.H. McIlvain. 1963. The micro-unit forage inventory method. J. Range Manage. 16:172-179.

Thoma, D.P., D.W. Bailey, D.S. Long, G.A. Nielsen, M.P. Henry, M.C. Breneman, and C. Montagne. 2002. Short -term monitoring of rangeland forage conditions with AVHRR imagery. J. Range Manage. 55:383-389.

Webb, W.L. 1942. A method for wildlife management mapping in forested areas. J. Wild. Manage. 6:38-43.

SAGEBRUSH AGE ESTIMATION IN THE UPPER SNAKE RIVER PLAIN, IDAHO

Dan Narsavage and Keith T. Weber
GIS Training and Research Center
Idaho State University
Pocatello, ID 83209-8130
(http://giscenter.isu.edu, e-mail: giscenter@isu.edu)

ABSTRACT
During the summer 2002, sagebrush plants (n = 611) growing in the sagebrush-steppe region of southeastern Idaho were sampled to estimate age. Techniques used follow those described by Perryman and Olsen (2002) and include measurement of maximum stem diameter. Stem diameter measurements are then applied to a linear regression equation fit for various sub-species of Big Sagebrush (*Artemesia tridentata*). Sagebrush age estimates were analyzed for overall trend and compared by treatment (grazing and past wildfire). No treatment effects were detected, however a positive correlation was observed between average sagebrush age and percent shrub cover.

Keywords: Field sampling, GIS, range.

INTRODUCTION

One of the focuses of ISU's Geographic Information Systems (GIS) Training and Research Center is on performing spatial analysis of rangeland ecosystems. While methodological and practical constraints have prevented our determination of the age of sagebrush individuals and stands in the past, the significance of such determinations is undeniable. Now, new methods developed by Perryman and Olson (2000) and adapted by ISU's GIS Training and Research Center make it possible to determine the age of sagebrush plants and to study how factors such as grazing, historic wildfires, and total shrub cover affects or correlates with the age of sagebrush plants. The data gathered here may shed light on relationships between these variables and may aid range managers in making decisions about prescribed fire and grazing management. This report focuses on a portion of Idaho's Eastern Snake River Plain (Figure 1) and is intended to study the relationships mentioned above, as well as assess the feasibility of the methods used.

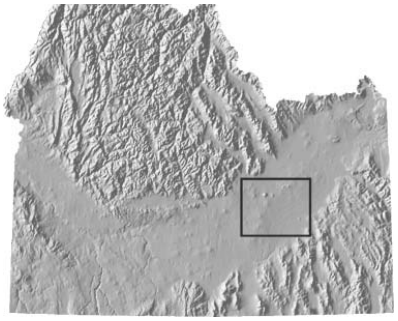

Figure 1: Hillshade image of southern Idaho showing this study's Area of Concern (AOC)

METHODS

Point data describing ground cover and sagebrush diameter (measured in mm) was estimated by GIS Center technicians during the summer of 2002 (n=370). Each point was randomly selected and represents the center of a circle with a 30-meter radius. This circle is bisected by two lines, one running east-west and the other running north-south. These lines effectively divide the circle into quadrants. The maximum diameter (in mm), within the lowest 25cm of stem, of the sagebrush plant closest to the center of the circle in each of the four quadrants (NW, NE, SE, and SW) was measured. Associated with each sample point were as many as four and as few as zero sagebrush stem diameters, depending on whether a sagebrush plant was available for sampling in each quadrant. Zeros were entered into the database to represent quadrants containing no sagebrush plants (McMahan and Sauder 2002).

To estimate sagebrush age, an equation developed by Perryman and Olson (2000) (modified for Eastern Idaho by ISU GIS Training and Research Center technicians) was employed (equation 1)

$$Age = 6.1003 + 0.5769(diameter)$$

Where; Diameter is the largest stem diameter (mm) within 25cm of the plant's base
Age is the age of the sagebrush plant in years.

Using spatial join operations in ArcMap 8.2, grazing treatment data (i.e., whether the point had been grazed by livestock or not) was incorporated into the database. Data describing the number of historic wildfires between the years of 1939 and 2001 was also added to the database using the Surface - point Z-value extractor Avenue script (spPntzval.ave) in ArcView 3.2.

With this information, I used Microsoft® Excel for basic processing. Descriptive statistics and graphs were generated illustrating the relationship between estimated sagebrush age and other factors such as treatment (grazing and/or wildfire), and total shrub cover (figures 2 and 3, respectively). Plants growing in areas where no fire or grazing had occurred were used as a control population for comparison with plants in areas known to have been grazed, burned, or both.

RESULTS

Descriptive statistics, generated in Excel, regarding treatment and percent shrub cover are presented in tables 1 and 2. These statistics are graphed in figures 2 and 3. Standard error was used to plot error bars, not standard deviation.

Table 1: Descriptive statistics regarding sage age versus grazing and fire treatment data.

Treatment	***Control***	***Grazing Only***	***Fire Only***	***Fire & Grazing***	***No Fire, Unknown Grazing***
Mean	27.86	28.24	27.78	30.76	29.44
Standard Error	0.80	1.57	1.90	3.00	0.60
Median	26.29	26.29	26.58	27.16	27.73
Mode	19.95	23.98	15.91	28.02	18.79
Standard Deviation	9.56	10.77	11.07	13.44	11.48
Range	55.96	47.88	46.73	58.27	65.77
Minimum	13.02	14.18	12.45	15.91	10.14
Maximum	68.98	62.06	59.18	74.17	75.91
Count	144	47	34	20	366

Table 2: Descriptive statistics regarding sage age versus shrub cover data.

Shrub cover	***1-5%***	***6-15%***	***16-25%***	***26-35%***	***36-50%***
Mean	25.94	27.75	29.00	31.47	36.52
Standard Error	1.27	0.91	0.57	1.61	3.46
Median	25.14	25.71	26.87	29.75	32.64
Mode	23.98	19.95	18.79	33.79	26.29
Standard Deviation	8.82	11.65	10.35	12.17	15.10
Range	39.81	62.31	62.88	62.31	58.27
Minimum	10.14	12.45	6.10	13.60	16.48
Maximum	49.94	74.75	68.98	75.91	74.75
Count	48	163	324	57	19

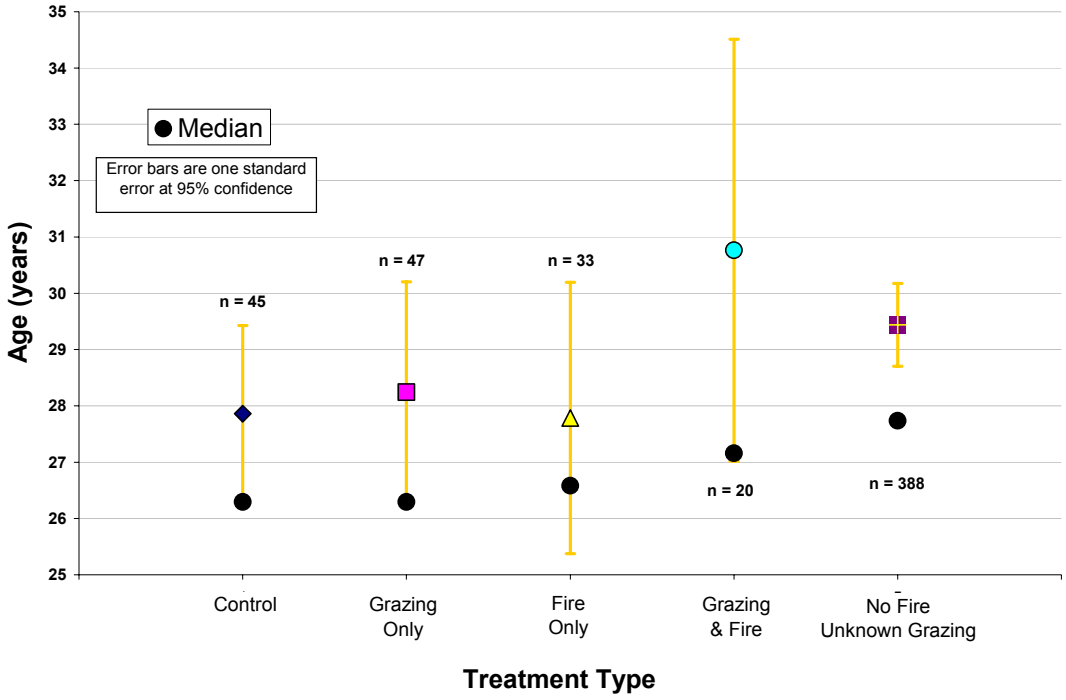

Figure 2: Average age of sagebrush plants versus grazing and fire treatments

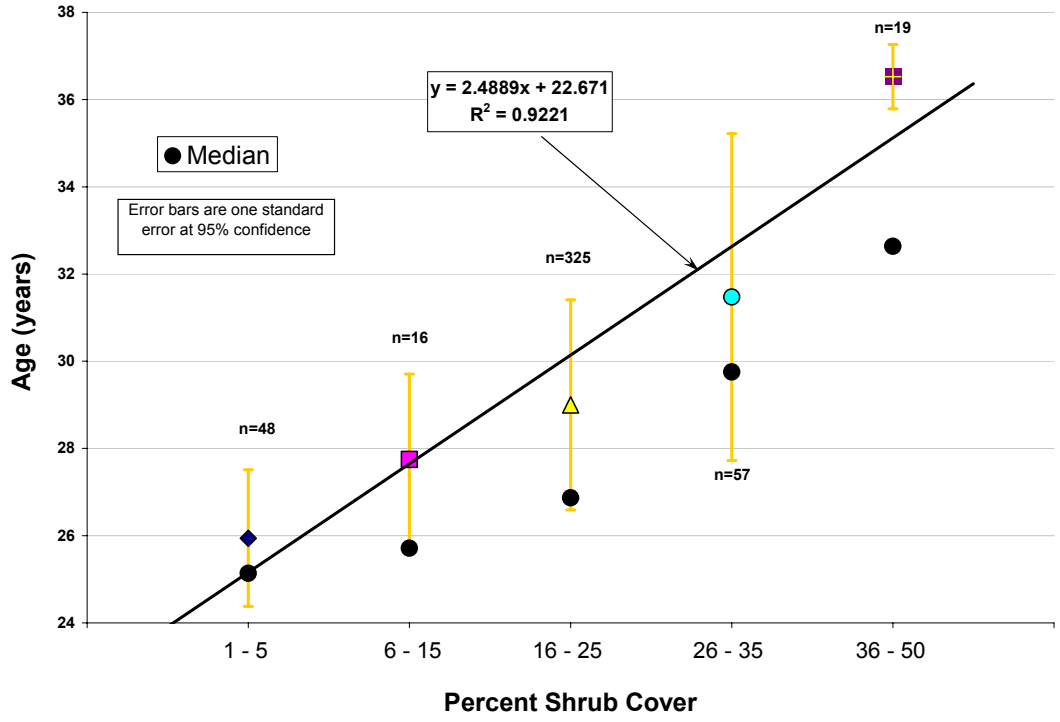

Figure 3: Average age of sagebrush versus percent shrub cover

DISCUSSION

It is clear in figures 2 and 3 that no difference exists in mean or median sagebrush age between burned versus unburned areas. Similarly, there is no difference in sagebrush age in grazed versus ungrazed areas. Figure 3 shows a gradual increase in average estimated age with increasing shrub cover. T-tests indicate this trend is not significant (95% confidence), however linear regression analysis reveals a trend line that describes the mean sagebrush ages with an R^2 value of 0.9221.

Little can be said from this exercise regarding how average age of sagebrush plants in a stand is affected by grazing and/or fire. Based upon our data, it appears that any treatment effect on the average age of sagebrush plants is insignificant compared to other factors not addressed by this study.

In many plant communities, one would expect large, dense stands to contain some old individual plants. The data in figure 3, while within statistical error bounds, illustrates trend which supports this presumption. However, Thomas Windholz (pers. comm.) indicated that, with large standard errors, the means themselves may have little significance.

ERROR ASSESSMENT

Perryman and Olson's (2000) methods for developing their technique and equation included collection of a section of sagebrush stem. Part of the stem was then cut and sanded so that annual growth rings could be counted. Diameter measurements took place after the samples were uprooted, cut, and sanded. At this point in the procedure, it is unclear how knowledge of the vertical position of the measurement on the stem, even simply whether or not the measurement was taken above the soil, could be assured. This is a source of error untouched by Perryman and Olson (2000), and we are unsure how to assess this in the report short of making the reader aware.

ACKNOWLEDGEMENTS

This study was made possible by a grant from the National Aeronautics and Space Administration Goddard Space Flight Center. ISU would also like to acknowledge the Idaho Delegation for their assistance in obtaining this grant.

LITERATURE CITED

McMahan, J.B., and J. Sauder, 2002. 2002 Rangeland wildfire field sampling geodatabase, http://giscenter.isu.edu/research/techpg/nasa_wildfire/Nwl.htm

Perryman, B. L., and R. A. Olson, 2000. Age-stem diameter relationships of big sagebrush and their management implications. J Range Management. 53: 342-346.

Windholz, T., 2002. personal communication, December 4, 2002

MODELING LIGHTNING AS AN IGNITION SOURCE OF RANGELAND WILDFIRE IN SOUTHEASTERN IDAHO

Keith T. Weber, Ben McMahan, Paul Johnson, and Glenn Russell
GIS Training and Research Center
Idaho State University
Pocatello, ID 83209-8130
(http://giscenter.isu.edu, e-mail: giscenter@isu.edu)

ABSTRACT

Cloud-to-ground lightning strike events are a common source of wildfire ignition. In Southeast Idaho, most lightning-ignited wildfires occur during the summer and early fall. During this time, large areas of hot, high pressures zones occur within the basin and range topography of the Intermountain west. Precipitation inputs are minimal as weather patterns originate from monsoonal flows from the south (Fox 2000). Thunderstorm occurrences increase with atmospheric instability, which is influenced by topography, humidity, and temperature. Effects of topography on lightning strikes have not been previously analyzed using a geographic information system. Our objective was to model lightning strike events across Southeast Idaho using lightning strike data collected from mid-June to mid-September 1998-2000 (n = 42,666). We further analyzed coincidence of precipitation during storm events to better understand wildfire ignition potential. Our results show lightning strike events are substantially more frequent in areas in close proximity to mountains and that wildfire risk in mountainous areas is approximately twice predicted for the Snake River Plain.

Keywords: Lightning, wildfires, GIS.

INTRODUCTION

Wildfires are an increasing problem in Idaho because fuel stockpiles have developed during a century of fire suppression and because the prevalence of cheat grass (*Bromus tectorum*) has made the fuels on Idaho rangelands much more flammable. A particularly destructive fire season involving a number of extremely large wildfires occurred in the Intermountain West during the year 2000. Due to accumulated fuel loads many of these fires burned more intensely and severely than witnessed before. Consequently, soils in some of the more severely burned areas were sterilized and important nutrients volatized.

Southeastern Idaho's climate is fairly xeric and brittle (Savory 1999). Rangelands in this area will require many years to recover from wildfire events like those experienced in 2000. To further compound this problem, non-native species like cheatgrass will likely invade these sites and subsequently alter the future fire regime.

Lightning is a natural wildfire ignition source. In many areas of the intermountain west, the potential for lightning to ignite a fire is enhanced during "dry" thunderstorm events (i.e., a storm event accompanied by little (<0.25cm) or no rainfall). Characteristics of individual cloud-ground lightning strikes also influence ignition potential.

We examined the spatial distribution, polarity and multiplicity of lightning strike events, coincident precipitation, fuel load and continuity of fuel to develop a wildfire-associated-lightning model. This study was based upon data describing field conditions and lightning strike events that occurred between June 15 and September 15, 1998-2002.

METHODS

Our study area (18,800km^2) was contained within a single Landsat 7 ETM+ scene (path 39 row 30) in southeastern Idaho. All lightning strikes included in this study were located between 43^{0}36'00" and 42^{0}48'00" N latitude and –113^{0}35'00" and -112^{0}37'59" W longitude. This area is considered sagebrush-steppe semiarid-desert and has a history of livestock grazing and wildfire occurrence.

We acquired cloud-to-ground lightning strike events (n=42,666) from Global Atmospherics (2000). Visual observation of the spatial distribution of lightning strikes overlaid upon a digital terrain hillshade model indicated a strong relationship between frequency of lightning strike events and proximity to mountains.

For purposes of this study, mountains were defined as having slope ≥5%, elevation ≥500m above minimum relative elevation for the region and a minimum mapping unit of 25 ha. Elevation in the Rocky Mountain (RM) region ranged from 1386-3231m while elevation in the adjacent Snake River Plain (SRP) region ranged from 1258-2300m. The relationship between frequency of lightning strike and proximity to mountains was evaluated using use-availability and regression analyses.

We acquire precipitation data from AgriMet (2002). Six weather stations were selected to represent RM and SRP regions. Individual storm events were identified by date and time. The extent of each storm event was determined by the spatial extent (minimum and maximum X, Y coordinates) of lightning strikes. The weather station

within the extent of the storm event or closest to each storm event was then examined for coincident precipitation. The precipitation recorded for the selected station was then assigned to the storm event. This process was repeated for all storm events (n=163).

Statistical analysis was performed to determine the relationship between precipitation and RM versus SRP storm events using regression analyses. Polarity of charge and multiplicity of strikes was examined in the same fashion.

Another associated wildfire risk component is fuel continuity. Horizontal fuel continuity was estimated using fuel load measurements (Anderson 1982) and vegetation cover characteristics (n=370). Maximum-likelihood supervised classification was used to produce a horizontal fuel continuity model for the region. Validation of this model was accomplished using boot-strap methods.

Results of lightning strike pattern, coincident precipitation, and continuity of fuel analyses were ranked to describe relative risk and combined into a final wildfire-associated-lightning model.

RESULTS AND DISCUSSION

During the fire season (1998-2000) 42,801 lightning strikes were recorded. Nearly 8% were positive strikes (n=3,372). Typically, 10% (DeCoursey et al 1983) to 20% (Brookhouse 1999) of all lightning strikes are positively charged. Wildfire ignition risk due to lightning is primarily a function of long continuing current. Long continuing current occurs with 80% of all positive strikes and 10% of negative strikes. The proportion of positively charged lightning strikes was equal in the RM and SRP regions.

Lightning strikes did not occur randomly within the study area. Based upon use-availability analysis (i.e., Chi-square and Bonferroni-Z) the number of lightning strikes in the RM region was twice its proportion of land area. In contrast, the number of lightning strikes in the SRP was half of its proportion of land area. In foothill regions (that area within 10km of a mountain) the frequency of lightning strikes was readily predicted using proximity to mountains ($y = -759.24\text{Ln}(x) + 1939$, $R^2 = 0.985$, where y = frequency of lightning strikes and x = proximity to mountain in km). A relative risk model was then produced for lightning strike events where mountain areas were assigned a value of 2.0, foothills were given a value of 1.0, and the SRP region was given a value of 0.5. We realize however, that actual risk could be effectively reduced if heavy precipitation occurred during storm events.

Average rainfall in the study area during the entire fire season (1-June through 15-September) was only 3.6cm (RM) and 4.6cm (SRP) for 1998-2000. Precipitation -- albeit very little-- in both the RM and SRP regions occurred concurrently nearly 70% of the time. Twenty-three percent of storm events in the RM region had coincident precipitation (≥0.25cm) while 36% of storm events in the SRP region had coincident precipitation. Due to the uniform and minimal amount of rainfall associated with storm events in both the RM and SRP regions, we conclude that coincident precipitation had no measurable effect upon our study. However, higher precipitation events would effect wildfire risk.

Results of the fuel continuity model predict clusters of highly continuous fuel in the RM region as well as portions of the SRP region. Pixels were classified with values ranging from 0.0 (low fuel continuity (e.g., isolated pockets of vegetation within lava flows)) to 5.0 (high fuel continuity (e.g., areas with high percent cover of grass and shrubs). Overall accuracy (67%) of this model was determined using boot-strapping techniques.

The lightning strike events relative risk model and fuel continuity model were multiplied together to produce a final wildfire-associated-lightning model (fig. 1). Based upon these results, wildfire risk in the RM region is approximately twice that found in the SRP rangelands.

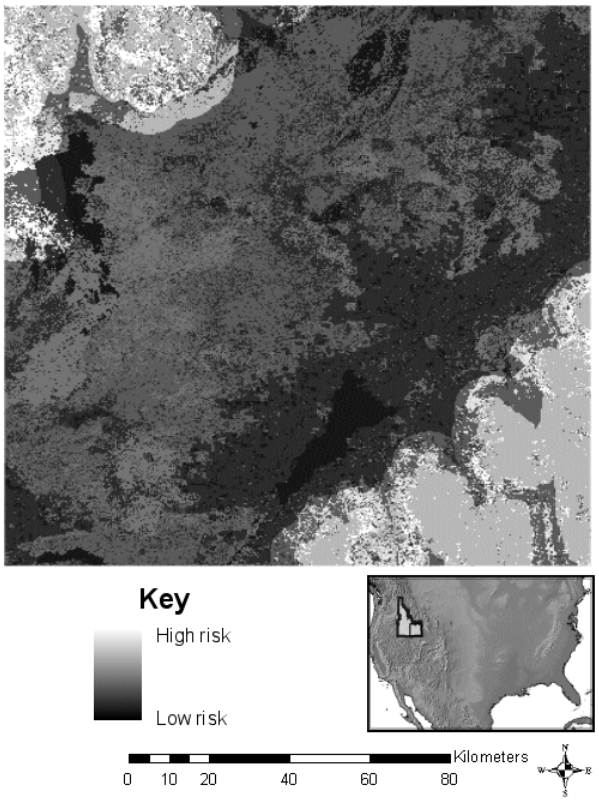

Figure 1. Final wildfire-associated-lighting risk model for the study area.

ACKNOWLEDGEMENTS
This study was made possible by a grant from the National Aeronautics and Space Administration Goddard Space Flight Center. ISU would also like to acknowledge the Idaho Delegation for their assistance in obtaining this grant.

LITERATURE CITED
Agrimet. 2002. Historical archive data access.
http://mac1.pn.usbr.gov/agrimet/webarcread.html

Andersen, H.E., 1982. Aids to Determining Fuel Models for Estimating Fire Behavior, USDA Forest Service General Technical Report INT-122.

Brookhouse, P. 1999. Lightning detection and operations systems in North America. Conference Proceedings, Australian Bushfire Conference, Albury Australia.

DeCoursey, D. G., Chameides, W.L., McQuigg, J., Frere, M.H., Nicks, A.D. 1983. Thunderstorms in Agriculture and in Forest Management, *In*: The Thunderstorm in Human Affairs. University of Oklahoma Press, Norman, Oklahoma.

Global Atmospherics 2000. Lightning strike products. http://www.lightningstorm.com/

FUZZY CLASSIFICATION OF HETEROGENEOUS VEGETATION IN A COMPLEX ARID ECOSYSTEM

Ben McMahan, Keith T. Weber, and Joel Sauder
GIS Training and Research Center
Idaho State University
Pocatello, ID 83209-8130
(http://giscenter.isu.edu, e-mail: giscenter@isu.edu)

ABSTRACT
Traditional methods of remote sensing classification may not accurately portray the complexity of ecosystems where vegetation type and structure is diverse and variable. We used fuzzy classification to better characterize the complexity and heterogeneity of sagebrush-steppe vegetation on the Upper Snake River Plain in southeast Idaho. Unlike supervised classification where pixels are classified into discrete categories, fuzzy systems classify each pixel into multiple categories based on estimated membership in each class. Field data (n = 370) collected in summer 2002 were used as training sites for supervised classification and fuzzy classification. We compared the results of supervised and fuzzy classification to determine which produced a more accurate depiction of land cover. Our results show fuzzy classification produces more accurate predictions of sagebrush and grass cover compared to supervised classification. Additionally, there is an apparent relationship between fuzzy membership and percent cover of sagebrush, which provides the user vegetation structure information as well.

Keywords: Remote sensing, sagebrush, grasslands.

INTRODUCTION

Vegetation modeling can be problematic in ecosystems where vegetation types are heterogeneous or are poorly represented by large pixels. Fuzzy classification offers an alternative to crisp logic (supervised classification) by evaluating pixels based on their membership into each category. Fuzzy membership is based on fuzzy set theory, which assumes that membership to a given category will range from complete membership (100%) to non-membership (0%), and that pixels may be classified as partial members into two or more categories (Gopal and Woodcock, 1994).

The Upper Snake River Plain (SRP) in southeastern Idaho is a sagebrush-steppe ecosystem, where sagebrush (Artemesia spp.), forb, and grass species comprise a majority of the vegetation. Bare soil, lava flows of various ages, and cryptobiotic crust are also present. The complexity of SRP vegetation types has been poorly classified by previous landscape-scale mapping attempts (e.g. GAP and NLCC classifications, 2000) with accuracies of <50% in sagebrush and grassland areas. These classifications also perform poorly in their representation of percent cover of vegetation, which is an important characteristic of the ecosystem (Connely, et al, 2000).

Fuzzy logic can be used to classify satellite imagery based by calculating membership to homogeneous sagebrush and grassland training sites. If a correlation between membership and percent cover can be established, fuzzy classification will function as a better technique for producing land cover maps which include information on vegetation structure. Fuzzy classification has also been shown to improve classification accuracy of land cover types when compared to maximum likelihood supervised classification (Bardossy and Samaniego, 2002).

METHODS

Field data (n = 370) were used to create training sites for maximum likelihood supervised classification and fuzzy classification of Landsat 7 ETM+ imagery of the SRP (acquired August 07, 2002). Seven base images and indices (PVI, NDVI, SAVI, tasseled cap greenness, tasseled cap moistness, Landsat 7 band 5, and PCA composite 2) were created with this imagery and each was used as a training image in the models. These were chosen because they best characterized the spectral variability within the training sites. We created two models for each classification system (supervised and fuzzy): one that used two homogenous classes of training sites (sagebrush and grass), and one that used three classes of training sites (sagebrush, grassland and mixed). Sagebrush sites had >15% cover of sage and <15% cover of grass. Grass sites had <15% sage cover and >15% grass cover. Mixes sites had >15% cover of both sage and grass. Spectral signatures were extracted using these training sites from the base imagery and classify the imagery using both supervised and fuzzy classification. Supervised classification produces an image where each pixel is classified as having 100% membership in a category (e.g. sagebrush or grassland). Fuzzy classification produces a series of images where the membership of each pixel is determined based on spectral similarity to training sites and user confidence of homogeneity of training sites (z-score).

We validated the supervised classifications using traditional error matrices. Validation of fuzzy classification is problematic because fuzzy results must be converted into crisp categories (Congalton and Green, 1999). We validated fuzzy classification using two methods: 1) flexible error matrix validation described in Congalton and Green (1999), and 2) a simple presence-absence threshold validation. To test for a significant relationship between fuzzy membership and percent cover of sagebrush and grass an ANOVA (Analysis Of Variance) was used.

RESULTS

The two-class and three-class supervised classifications had an accuracy of 33.7% and 47.5%, respectively. The results of fuzzy classification using a z-score of 1.5 generated the most accurate results by minimizing type 1 and type 2 errors. The flexible error matrix validation showed the two-class fuzzy model had an accuracy of 39.5%, while the three-class model had an accuracy of 50.5%. The presence/absence threshold procedure showed the two-class fuzzy model had an accuracy of 65.6% predicting sagebrush cover and of 44.8% predicting grass cover. The three-class fuzzy model had an accuracy of 65.9% predicting sagebrush cover and 48.0% predicting grass cover. The ANOVA demonstrated a significant relationship between sagebrush membership and percent sagebrush cover ($F=8.114$, $P < 0.0001$). No significant relationship was detected between grass membership and percent grass cover.

DISCUSSION

Both classifications appear to perform at least as well as currently available vegetation maps (e.g. GAP or NLCC). The supervised classification did not have as much flexibility in classifying diversity in the region, and subsequently accuracy suffered. The improved accuracy of fuzzy classification demonstrates the utility of fuzzy logic systems for classification of heterogeneous vegetation in complex ecosystems. Additionally, since fuzzy classification is able to utilize remotely sensed data with coarse spatial resolution and still produce accurate results, it is more practical for landscape-scale analyses compared to other methods (e.g. hyperspectral or fine spatial resolution multispectral data).

A limitation of fuzzy classification using coarse-scale data is the increased heterogeneity of training classes. Higher spatial resolution multispectral data would allow for smaller, more homogeneous training sites that should yield improved results. The necessity to convert fuzzy results into crisp data for validation illustrates another limitation of fuzzy classifications. Validating relationships between membership and vegetation structure (such as those demonstrated in this study) are less susceptible to this limitation, as the process does not require prior conversion to crisp data. A final limitation of our application is the nature of training classes used in this study. Sagebrush and grass vegetation types present difficulties regarding how a sensor images these targets. Sagebrush has open spaces between branches as well as dead and dying limbs which do not reflect spectra the way “pure” sagebrush pixels would. Further, the elongated vertical growth-form of grasses means most of the plants biomass is perpendicular to the viewing angle of a satellite. Increased spatial resolution will help, but these issues are characteristic of the general problems associated with accurate representation of complex vegetation types and structures.

In conclusion, fuzzy classification provides a means by which vegetation heterogeneity and variability can be modeled if a relationship between fuzzy membership and percent cover can be reliably established. Even if such relationships cannot be established, fuzzy classification produces more accurate vegetation cover "maps" compared to other methods. Improved classification accuracy and the potential to model vegetation structure and density will prove useful to land managers. This is especially true in areas where existing classifications do not adequately portray the complexity of vegetation found in the region. Further research will attempt to establish a stronger correlation between fuzzy membership and vegetation structure using imagery with improved spatial resolution.

ACKNOWLEDGEMENTS
This study was made possible by a grant from the National Aeronautics and Space Administration Goddard Space Flight Center. ISU would also like to acknowledge the Idaho Delegation for their assistance in obtaining this grant.

LITERATURE CITED
Bardossy, A., and L. Samaniego. 2002. Fuzzy Rule-Based Classification of Remotely Sensed Imagery. IEEE Transactions on Geoscience and Remote Sensing 40 i2:p362(13).

Congalton, R. G., and K. Green. 1999. Assessing the Accuracy of Remotely Sensed Data. CRC Press, Boca Raton, FL. 137 pp.

Connelly, J.W., et al. 2000. Guidelines to Manage Sage Grouse Populations and Their Habitats. Wildlife Society Bulletin 28(4):967-985.

Gopal, S., and C. Woodcock, 1994. Theory and Methods for Accuracy Assessment of Thematic Maps Using Fuzzy Sets. Photogrammetric Engineering and Remote Sensing 60:181-188.

National GAP Analysis. 2000. GAP-Homepage. www.gap.uidaho.edu 1 Oct 2002.

National Land Cover Characterization. 2000. NLCC-Homepage. http://landcover.usgs.gov/nationallandcover.html 1Oct 2002.

WILDFIRE RISK MODEL VALIDATION

Ben McMahan and Keith T. Weber
GIS Training and Research Center
Idaho State University
Pocatello, ID 83209-8130
(http://giscenter.isu.edu, e-mail: giscenter@isu.edu)

ABSTRACT
Field samples (n = 128) collected during summer 2001 were used to create a series of fuel load and wildfire risk models. Field data collected during the summer 2002 field season (n = 370) were used to determine the accuracy of these models, as well as to refine and rebuild the existing models. Using this new data, we created an updated wildfire risk model that included components on ignition risk, risk of spread, fuel moisture, fuel load, physical characteristics, and response time. We validated these models using a number of error matrix validation procedures, with the resulting accuracies ranging from 30% - 92%. The wildfire risk components provide land managers and local agencies with an additional tool for use in their decision making process.

Keywords: Fuel load, wildfire risk, model validation, Snake River Plain, SE Idaho

INTRODUCTION

Field samples (n = 128) collected during summer 2001 were used to create a series of fuel load and wildfire risk models for a NASA-funded *Wildfire Effects on Rangeland Ecosystems and Livestock Grazing* research project. During the summer 2002 field season we collected validation samples (n = 370) to determine the accuracy of these models. We then used these data to refine and rebuild the fuel load and wildfire risk models, and to create new components for an updated comprehensive wildfire risk assessment.

METHODS AND RESULTS

During the 2001 field season, technicians noted that only three of the fuel load classes described in Anderson (1982) were present in our study area: 0.74 tons/acre (grass areas), 4.0 tons/acre (sagebrush areas), and 6.0 tons/acre (juniper-woodland areas). Two new fuel load classes (1.0 tons/acre and 2.0 tons/acre) were created to more accurately represent the continuum between grass and sagebrush areas (0.74 and 4.0 tons/acre). In the Anderson fuel load classes, 1.0 tons/acre would be included in 0.74 tons/acre class, and 2.0 tons/acre would be included in 4.0 tons/acre class.

The overall accuracy of the 2001 and 2002 fuel load models were quantified in two ways. One where each fuel load class (0.74, 1.0, 2.0, 4.0, and 6.0 tons/acre) was included in the error matrix (yielding a conservative accuracy assessment), and one where classes were combined to represent the three original Anderson fuel load classes (1982).

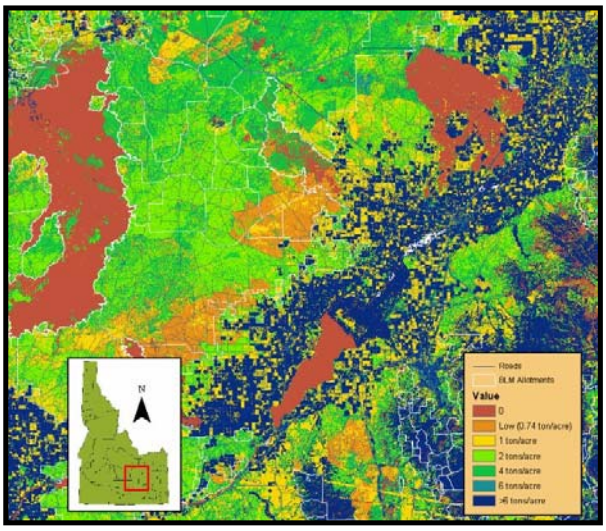

Figure 1. Initial fuel load model developed in 2001.

2001 Model Validation

Models created following the field season of 2001 included fuel load, emergency response time, lightning strike pattern, vegetation moisture, and topographic effects (slope and aspect). The fuel load model was created using maximum likelihood supervised classification, and as such was the only model where accuracy could be assessed using validation data. The overall accuracy of the 2001 fuel load model (Figure 1) was 30.27% using conservative estimates (Table 1) and 65.41% using the expanded/combined estimate method (Table 2).

Table 1 - Conservative error assessment of 2001 Fuel Load Model (5 classes)

		Field Estimation of Fuel load (tons/acre)							
	Fuel load class	0.00	0.74	1.00	2.00	4.00	6.00	Total	User's Accuracy
Modeled Fuel load (tons/acre)	0.00	0	0	0	1	1	0	2	0.00
	0.74	0	7	6	6	7	1	27	0.26
	1.00	0	25	21	26	16	0	88	0.24
	2.00	0	12	21	59	74	2	168	0.35
	4.00	0	12	23	25	25	0	85	0.29
	6.00	0	0	0	0	0	0	0	0.00
	Total	0	56	71	117	123	3	370	
	Producer's Accuracy	0.00	0.13	0.30	0.50	0.20	0.00		0.30

Note: Kappa statistic = 0.04

Table 2 - Expanded error assessment of 2001 Fuel Load Model (3 classes)

		Field Estimation of Fuel load (tons/acre)					
	Fuel load class	0.00	0.74 - 1.00	2.00 - 4.00	6.00	Total	User's Accuracy
Modeled Fuel load (tons/acre)	0.00	0	0	2	0	2	0.00
	0.74 - 1.00	0	59	55	1	115	0.51
	2.00 - 4.00	0	68	183	2	253	0.72
	6.00	0	0	0	0	0	0.00
	Total	0	127	240	3	370	
	Producer's Accuracy	0.00	0.46	0.76	0.00		0.65

Note: Kappa statistic = 0.23

Model Re-Building/refinement

Ignition Risk Model (component model no. 1)

There are two primary sources of wildfire ignition in the Intermountain west. Anthropogenic ignition sources account for approximately 55-90% of wildfires (Larimer County, Colo 2003). These fires are frequently started unintentionally by careless use/disposal of cigarettes, fireworks, and campfires. Ignition sites are characteristically close in proximity to municipalities, homes and campsites. Consequently they are also in close proximity to roads. This fact allowed us to model anthropogenic ignition sources using roads as a surrogate indicator for ignition risk.

Lightning strikes account for approximately 10-45% of wildfires. During the fire season (typically July-September) dry-thunderstorms are commonplace. Such storms are characterized as having little or no rainfall (< 0.25") and a large number of cloud-to-ground lightning strikes (e.g., a storm event on July 26, 2000 recorded 2,599 cloud-to-ground lightning strikes). The ignition risk model first modeled each source independently, and then combined them to create a single ignition source model.

Anthropogenic Ignition Sources

The 2002 anthropogenic ignition risk model was created using a maximum-likelihood classification (Wang 1990, Lillesand and Kiefer 2000) of vegetation types consistent with

increased risk of anthropogenic ignition, a distance-from-roads proximity model (to account for probability of ignition), and a vegetation moisture model to adjust for relative moisture content and the real risk of ignition.

Vegetation types consistent with increased risk of anthropogenic ignition model:

We created a maximum likelihood supervised classification using our 2002 field data as training sites for vegetation types consistent with increased risk of human-caused ignition events. For this model, we focused on presence of fine fuels (grass, litter/duff) as a primary component of ignition risk, and shrub presence as a secondary component of risk. The five classes consisted of:

Low-risk (shrub, grass, and litter/duff cover < 15%) (weight = 1)

Moderate-risk (shrub cover > 15% and *either* grass cover or litter/duff cover > 15%) (weight = 2)

High-risk (shrub cover < 15% and *both* grass cover and litter/duff cover > 15%) (weight = 3)

Severe-risk (all categories > 15%) (weight = 4)

Distance-from-roads model:

We buffered a vector transportation coverage (including roads, railroads, etc.) by 30, 60, and 90 meters and weighted each buffer region (3, 2, and 1 respectively, with 0 being the value for all areas >90 meters from a transportation vector) to account for increased risk related to proximity to roads. This coverage was converted to a grid for use in creating the final anthropogenic ignition risk model.

Vegetation moisture model:

We used a tasseled cap transformation (Kauth and Thomas 1976) to create a relative vegetation moisture grid and reclassed the grid to values between -1 and 1 in order to account for the impact the relative vegetation moisture would have on the risk of ignition.

Final 2002 Anthropogenic Ignition Risk Model:

The three models were added together in image calculator using their respective weightings (1-4 for vegetation, 0-3 for proximity to roads, and -1 to 1 for vegetation moisture) to create an image with values between 0 and 8. This image was reclassed to fit between 0 and 5 to create the final anthropogenic risk model.

Lightning Ignition-Risk Model

The 2002 lightning ignition risk model was created using a maximum-likelihood classification (Wang 1990, Lillesand and Kiefer 2000) of vegetation types consistent with increased risk of ignition, a lightning strike potential model (cf. chapter 6), and a vegetation moisture model to adjust for relative moisture content and the real risk of ignition.

Vegetation types consistent with increased risk of anthropogenic ignition model:

We created a maximum-likelihood supervised classification (Wang 1990, Lillesand and Kiefer 2000) using our 2002 field data as training sites for vegetation types consistent with increased risk of lightning caused ignition events. For this model, we focused on the presence of woody vegetation (e.g., shrubs and trees) as the primary risk and the presence of fine fuels as the secondary risk. Our risk categories were:

Low-risk (shrub, grass, and litter/duff cover < 15%) (risk rating = 1)
Moderate-risk (shrub cover < 15% and *both* grass cover and litter/duff cover > 15%) (risk rating = 2)
High-risk (shrub cover > 15% and *either* grass cover or litter/duff cover > 15%) (risk rating = 3)
Severe-risk (all categories > 15%) (risk rating = 4)

Lightning Potential Model:

The lightning potential model was created using data acquired from global atmospherics. The model building process and results are discussed in detail in chapter 6. Risk of lightning strike was classified as 1 (>10km from mountains), 2 (6-10km from mountains), and 3 (<6km from mountains).

Vegetation moisture model:

We used a tasseled-cap transformation (Kauth and Thomas 1976) to create a relative vegetation moisture model and reclassified the model into values ranging between -1 and 1. This was done to account for the effect vegetation moisture would have on ignition risk.

Final 2002 Lightning Ignition Risk Model:

The three models described above were summed together with ArcMap raster calculator (values were 1-4 for vegetation type, 1-3 for lightning strike potential, and -1 to 1 for vegetation moisture). This yielded a model where values ranged from 1 to 8, with 8 being the highest ignition risk level. This model was reclassified so that the values ranged between 0 and 5 to create the final ignition risk model.

Final Ignition-Risk Model (model component no.1)

The Anthropogenic Ignition Risk model and Lightning Ignition Risk model were summed together to create the Final Ignition Risk model (Figure 2) where risk values range between 0 and 10. This formed component 1 of the comprehensive wildfire risk model and was given an overall weighting of 22.5%.

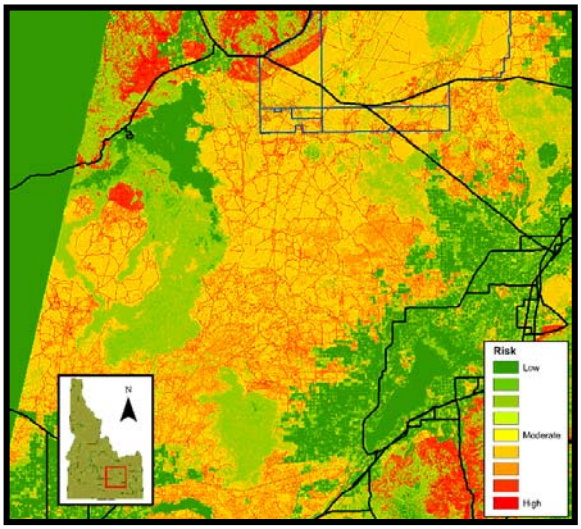

Figure 2. Component 1- Ignition risk model

Fuel Continuity Model (model component no. 2)

The 2002 fuel continuity model (Figure 3) was created using a maximum likelihood classification of vegetation types consistent with risk of escalated rate of spread following an ignition event. This model attempts to delineate area where *both* fine fuels (grass and cheatgrass) and shrubs (sagebrush, rabbitbrush, etc.) are present. Risk categories were assigned as follows:

No risk (sage <5%, grass/cheatgrass <15%) weight = 0
Low risk (sage <5% and grass/cheatgrass 16-50%) weight = 1
Moderate risk (sage 6-25% and grass/cheatgrass 16-50%) weight = 2
High risk (sage 26-50% and grass/cheatgrass <15%) weight = 3
Severe risk (sage 26-50% and grass/cheatgrass 16-50%) weight = 4

The output of the classification was reclassified into values ranging from 0 - 10 for consistency. The fuel continuity model is component 2 of the comprehensive wildfire risk model (weight 22.5%).

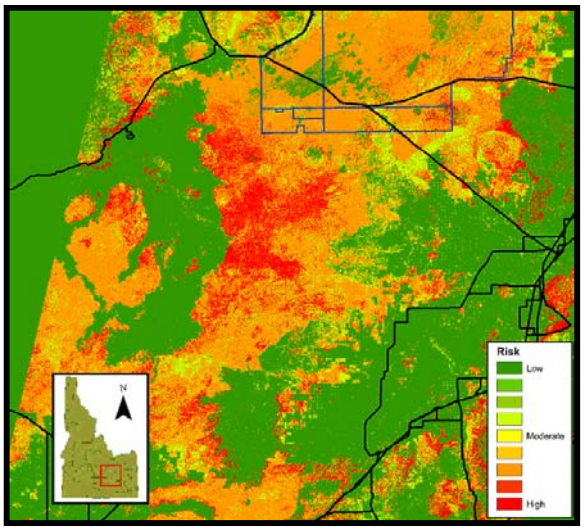

Figure 3. Component 2- Fuel continuity model.

Fuel Moisture Model (model component no. 3)

The 2002 fuel moisture model (Figure 4) was created using the vegetation moisture component of a tasseled cap transformation (Kauth and Thomas 1976) of Landsat ETM7+ imagery combined with the 2002 fuel load model (component 4). We combined the fuel load model (component 4, values 0-10) and the vegetation moisture model (values -1 to 1) by multiplying the two images using ArcMap raster calculator, and reclassifying output to values ranging from 0 - 10. The lowest values are areas that have both low fuel load levels and relatively moist vegetation. Moderate values represent either dry/moderate fuel load levels or wet/heavy fuel load levels. High values represent high fuel load levels that are also dry. This model was weighted 22.5% in the final comprehensive wildfire risk model).

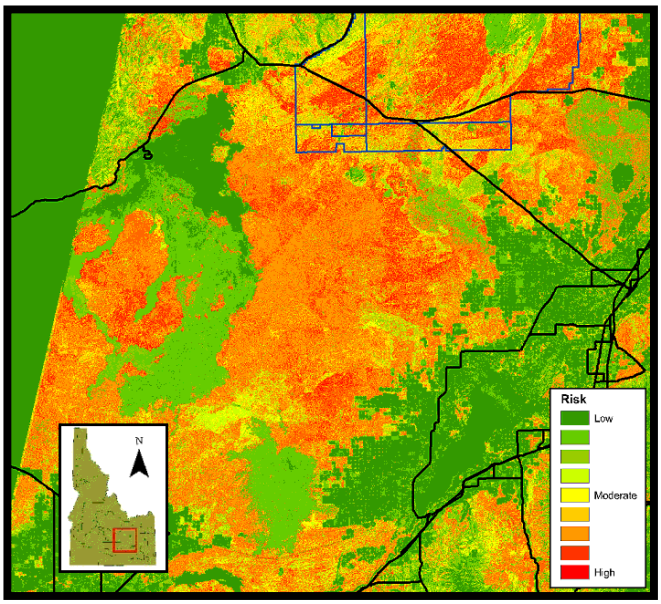

Figure 4. Component 3- Fuel moisture model.

Fuel Load Model (component model no. 4)

The 2002 fuel load model (Figure 5) was created using maximum likelihood classification. We used 2002 field data (n = 370) to create training sites for each of the five fuel load classes (0.74, 1.0, 2.0, 4.0, and 6.0 tons/acre). We applied a 30 m buffer to these points and converted the resulting polygons into a grid for use as a training site image in Idrisi. To account for the effect of bare soil on spectral signatures, each fuel load class (with the exception of 6.0 tons/acre) was divided into two sub-classes based on an arbitrary threshold of bare soil present at each sample point, resulting in nine fuel load classes. Following the creation of the maximum likelihood supervised classification model, each sub-class was then reclassified into its original fuel load category for validation and further model development (e.g., fuel moisture and comprehensive wildfire risk models). The fuel load classes were reclassified to values between 0 - 10 (0 - no fuel, 2 - 0.74 tons/acre, 4 - 1.0 tons/acre, 6 - 2.0 tons/acre, 8 - 4.0 tons/acre, and 10 - 6.0 tons/acre). This model formed component 4 of the comprehensive wildfire risk model (weight 22.5%).

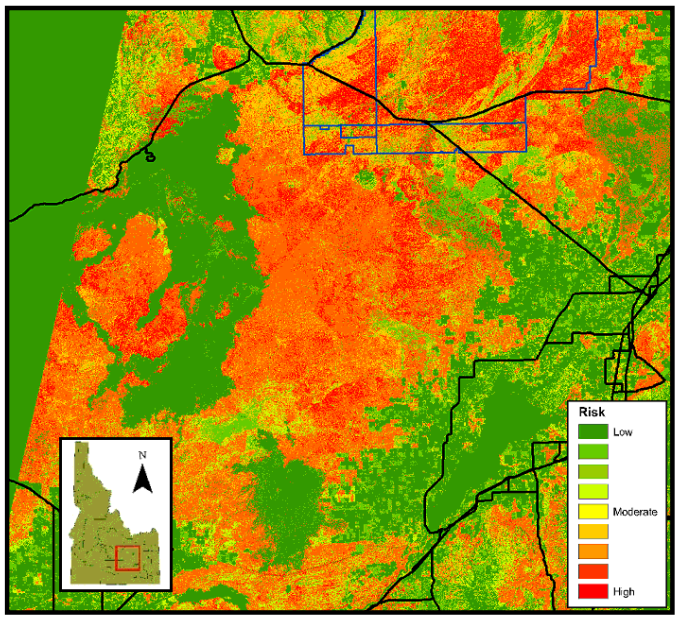

Figure 5. Component 4- Fuel load model developed in 2002.

Suppression Difficulty/Terrain associate risk model (component model no. 5)
Slope and aspect models were created using a digital elevation model for the entire AOC (80 mpp) to represent areas of increased risk due to increased fire spread rate on steep slopes, increased severity (e.g., southwestern facing slopes), and increased suppression difficulty (steep slopes where firefighting machinery would have difficulty accessing the fire). The Snake River plain is relatively flat, so slope and aspect has less impact on fire risk in this area compared to other, more mountainous areas within the AOC. The slope and aspect models were reclassified to values between 0 - 5 and summed together to form component 5 (values range from 0 to 10) of the comprehensive wildfire risk model (weight 10%) (Figure 6).

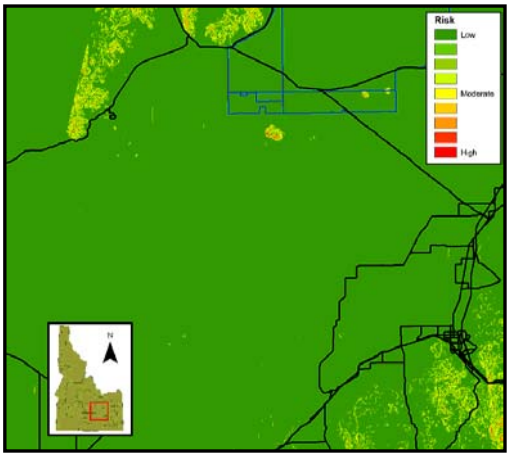

Figure 6. Component 5- Terrain associated risks.

Comprehensive Wildfire Risk Model

The five component models described above were weighted (component 1: Fuel load = 22.5%, component 2: Ignition risk = 22.5%, component 3: Fuel continuity 22.5%, component 4: Fuel moisture 22.5%, and component 5: Terrain associated risk (slope/aspect influences) 10%) and combined using ArcMap image calculator to create the 2002 comprehensive wildfire risk model (Figure 7). This model shows areas of increased risk for significant wildfire events given the potential for ignition and spread of the fire.

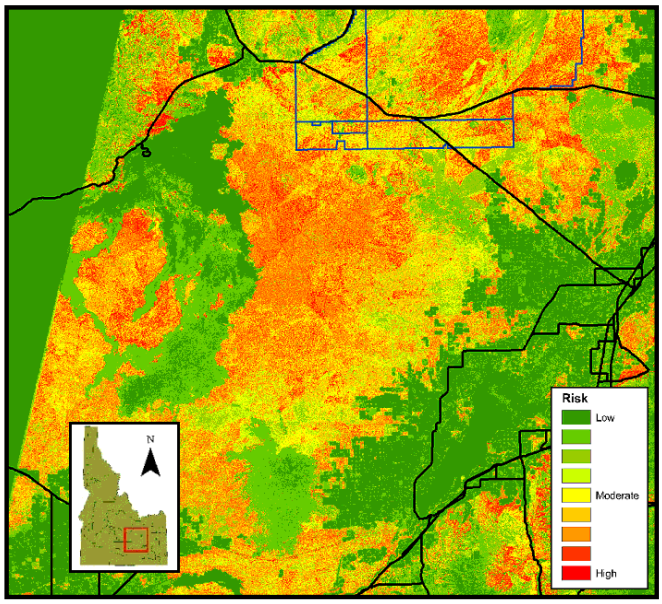

Figure 7. Comprehensive wildfire risk model

Comprehensive Wildfire Risk Model (with response time)

To account for suppression efforts by various agencies to control wildfires following ignition and detection, a response time model was developed to delineate areas that may be at increased risk due to their isolation, as well as areas that may experience decreased risk due to quick response. We created a response time model using ESRI's Network Analyst software. This model was combined with the existing comprehensive wildfire risk model (figure 7) to create a comprehensive wildfire risk model (w/response time) (Figure 8). The weightings used for each component of this risk model were 90% comprehensive wildfire risk model, and 10% response time model.

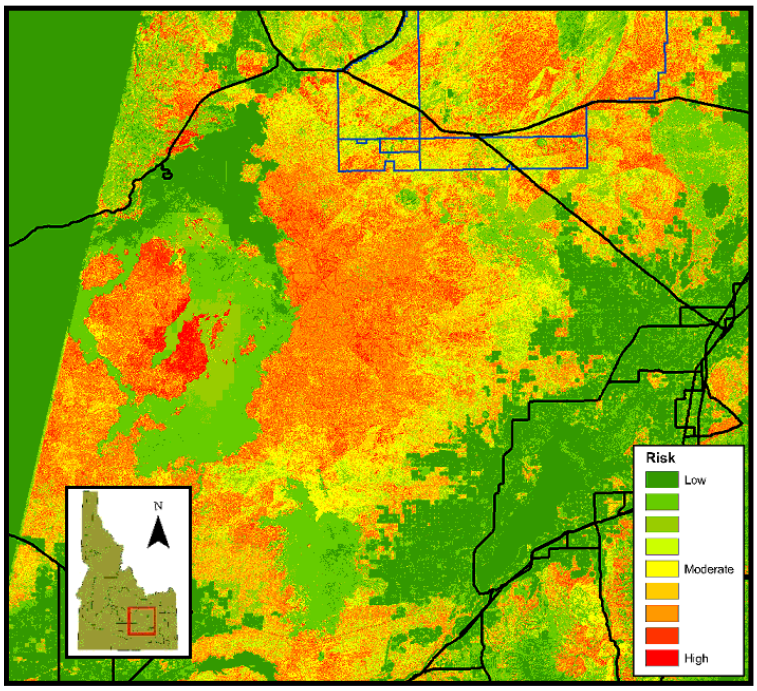

Figure 8. Comprehensive wildfire risk model including response time.

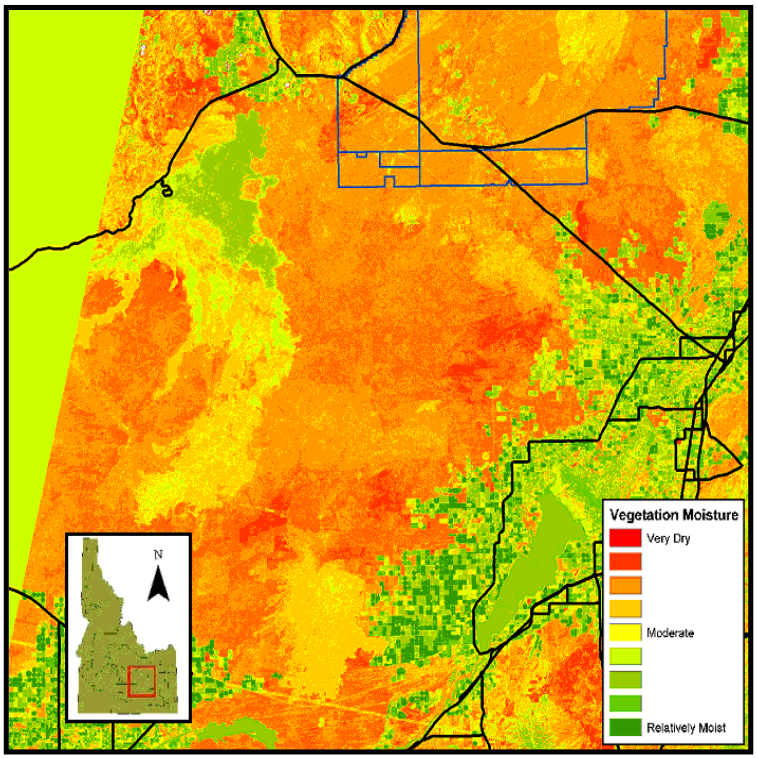

Figure 9. Vegetation moisture model (relative moisture estimates derived from Tasseled-cap transformation.

DISCUSSION

Assessment of Error and Bias

Each component of the comprehensive wildfire risk model was validated independently using three methodologies. The first was a standard error matrix (i.e., contingency table) where each predicted (modeled) class was compared against the measured (field) class at all sample point locations. The second method was a modified error matrix where similar classes were combined and accuracy determined using these super-classes. The third validation procedure used fuzzy set theory (Congalton and Green 1999) whereby a threshold of acceptable error was first established. This validation procedure allowed us to better address the difficulties associated with using multispectral imagery to delineate vegetation types having similar spectral signatures. In our case, the fuzzy set threshold was +/-1 class (i.e., this validation procedure determined whether the predicted (modeled) class was within one class of the field-observed class). We did not employ all three methods for each component. The results of these tests are reported in the text as *standard/expanded, clumped, and fuzzy-set-theory* accuracies, respectively. Note: Error matrices were calculated using the entire sample point data set (n = 370) to develop and validate the model unless stated otherwise. We explored the use of a validation subset (n = 185) and development subset (n = 185) and found no difference in resulting accuracy (chapter 10). This may be a result of our large sample size and the relatively small effect that each individual sample point had on the multi-dimensional data cloud for each spectral signature. Alternatively, it may be attributable to the relative homogeneity of our training sites. Since the results of the validation did not differ, we opted for the simpler process of including all points in both model development and accuracy assessment.

Ignition Risk Model

This model was developed as described above. Note however, that some sub-components of the ignition risk model do not involve image processing/classification but rather GIS spatial analysis based upon empirical proximity to roads or mountains, etc. This makes validation quite challenging since risk of ignition does not have a field-based dataset to compare with modeled values. Further, measuring ignition risk in the field is extremely difficult --if not impossible. As a result, the accuracy assessment of this model was in essence an assessment of the vegetation type sub-component of the ignition risk model. Further, vegetation type was collected at 267 points. Thus, validation was performed with 267 samples instead of 370.

The standard/expanded accuracy assessment used four classes of ignition risk (overall accuracy was 52% (Table 3)). In the second (clumped) assessment, the two middle classes (moderate and high risk and ignition) were combined, resulting in an increase in overall accuracy (73% (Table 4)). Using the fuzzy-set-theory method, the ignition risk model yielded an overall accuracy of 85% (cf. highlighted cells, Table 3).

Table 3 - Standard/expanded accuracy assessment of vegetation types used in the ignition risk model (Kappa = 0.253).

		Risk of Ignition					
		Low	moderate	high	severe	Total	User's Accuracy
Modeled risk of ignition	Low	6	6	4	3	19	0.32
	moderate	4	90	24	6	124	0.73
	High	2	32	30	9	73	0.41
	severe	0	25	12	14	51	0.27
	Total	12	153	70	32	267	
	Producer's Accuracy	0.50	0.59	0.43	0.44		0.52

Table 4 - Clumped accuracy assessment of vegetation types used in the ignition risk model. Note: the mod-high category consists of moderate and high categories (cf. table 3) (Kappa = 0.256).

		Risk of Ignition				
		Low	mod-high	severe	Total	User's Accuracy
Modeled risk of ignition	low	6	10	3	19	0.32
	mod-high	6	176	15	197	0.89
	severe	0	37	14	51	0.27
	Total	12	223	32	267	
	Producer's Accuracy	0.50	0.79	0.44		0.73

Fuel Continuity Model

The overall accuracy of the fuel continuity model was determined using standard/expanded methodology (overall accuracy = 67.84% (Table 5)) and fuzzy-set-theory methodology (overall accuracy = 92.97% (cf. highlighted cells, Table 5)).

Table 5: Accuracy assessment of the fuel continuity model (Kappa = 0.21).

		Field estimated fuel continuity						
	class	none	low	moderate	high	severe	Total	User's Accuracy
Modeled fuel continuity	none	3	4	2	0	0	9	0.33
	low	0	17	8	1	0	26	0.65
	moderate	7	57	227	24	11	326	0.70
	high	0	0	0	0	0	0	0.00
	severe	0	1	4	0	4	9	0.44
	Total	10	79	241	25	15	370	
	Producer's Accuracy	0.30	0.22	0.94	0.00	0.27		0.68

Fuel Moisture Model

The fuel moisture model was a combination of the fuel load model (component 4, Figure 5) and the vegetation moisture model (Figure 9). To validate the accuracy of the vegetation moisture model we first reclassified the Idaho GAP vegetation dataset into three categories (i.e., wet, moderately moist, and dry, table 6). We also reclassified our vegetation moisture model (with index values ranging from -1.0 to 1.0) into three similar categories (-1.0 - -0.2, -0.2 - 0.2, 0.2 - 1.0). Accuracy was estimated as the percent agreement between these two layers as determined using standard cross-tabulation techniques (Rosenfield and Fitzpatric-Lins 1986, Carstensen 1987). Overall agreement was only 17% (Table 7), however there was very high agreement between the vegetation moisture model's wet and dry classes and the equivalent GAP-derived wet and dry classes (98% and 92% respectively). Some of the disagreement observed is attributable to the coarse nature of the GAP vegetation dataset (2.5 ha MMU) and to vegetation changes (e.g. fires, urban development and agricultural conversion) that have occurred since the last release of GAP data (2002).

Table 6- Reclassification applied to Idaho GAP dataset (2002) to determine agreement with vegetation moisture models.

Moisture category	GAP Vegetation Type
Wet	wet meadows, riparian, wetland, open water
Moderately-wet	deciduous forest, coniferous forest
Dry	high desert vegetation types (grass, shrubs, juniper), lava, barren

Table 7- Cross-tabulation agreement between GAP-derived vegetation moisture categories and our vegetation moisture model.

		GAP-derived moisture category				
	class	Wet	moderately-wet	Dry	Total	User's agreement
Vegetation Moisture model	wet	625,212	31	10,753	635,996	0.98
	mod-wet	4,755,339	526,003	11,798,562	17,079,904	0.03
	dry	192,254	6,554	2,402,117	2,600,925	0.92
	Total	5,572,805	532,588	14,211,432	20,316,825	
	Producer's agreement	0.11	0.99	0.17		0.17

Fuel Load Model

The overall accuracy of the fuel load model was determined using the three methodologies introduced earlier (standard/expanded, clumped, and fuzzy set). For the standard/expanded accuracy assessment, each fuel load class (0.74, 1.0, 2.0, 4.0, and 6.0 tons/acre) was used in the calculation yielding an overall accuracy of 47%. (Table 8). The clumped accuracy assessment, combined the fuel load classes as originally developed by Anderson (1982) (overall accuracy = 73%, table 9). Our revised model represents an improvement in classification accuracy of 13% (cf. Table 2). Estimated accuracy using fuzzy-set-theory methodology (Congalton and Green 1999) was 83% (cf. highlighted cells, Table 8).

Table 8- Standard/expanded accuracy assessment of fuel load modeling (Kappa = 0.27)

		Field Estimation of Fuel load (tons/acre)							
	Fuel load class	0.00	0.74	1.00	2.00	4.00	6.00	Total	User's Accuracy
Modeled Fuel load (tons/acre)	0.00	0	0	0	0	0	0	0	0.00
	0.74	0	24	13	8	3	0	48	0.50
	1.00	0	7	22	17	9	0	55	0.40
	2.00	0	13	18	44	27	0	102	0.43
	4.00	0	12	18	46	80	0	156	0.51
	6.00	0	0	0	1	1	3	5	0.60
	Total	0	56	71	116	120	3	366	
	Producer's Accuracy	0.00	0.43	0.31	0.38	0.67	1.00		0.47

Table 9 - Fuel load model accuracy assessment using USFS categories (Kappa = 0.39)

		Field Estimation of Fuel load (tons/acre)					
	Fuel load class	0.00	0.74 - 1.00	2.00 - 4.00	6.00	Total	User's Accuracy
Modeled Fuel load (tons/acre)	0.00	0	0	0	0	0	0.00
	0.74 - 1.00	0	66	37	0	103	0.64
	2.00 - 4.00	0	61	197	0	258	0.76
	6.00	0	0	2	3	5	0.60
	Total	0	127	236	3	366	
	Producer's Accuracy	0.00	0.52	0.83	1.00		0.73

Suppression Difficulty/Physical Risks Model

The suppression difficulty/physical risks model was created using a digital elevation model (DEM) of our study area (80mpp). Vertical positional error for this model was assumed to be the same as the error reported for standard USGS DEM's (+/- 15 meters for 90% of all well-defined points (USGS 1990)).

Wildfire Risk Model and Wildfire Risk Model (with response time)

The final wildfire risk models are weighted composites of the previously described components. It is not possible to determine the accuracy of the final wildfire risk models apart from independently assessing the accuracy of its components.

Each component of the comprehensive wildfire risk model can be used independently to explore specific types of risk (e.g., suppression difficulty, risk of ignition, risk of spread following ignition, etc.). The ignition model (component 1) is useful for identifying vegetation types consistent with increased risk. The ignition model can also be used to account for temporal variations in ignition risk (seasonality as related to phenology and vegetation moisture content, use patterns (recreational, professional, and holidays (e.g. increased recreational use on holiday weekends and firework use on and around July 4)). While the ignition risk model provides a description of areas composed of vegetation types consistent with increased risk of wildfire

ignition, other factors can alter the risk (especially those that vary temporally) and must be understood and evaluated to determine the real risk at a specific time or place.

The fuel continuity model (component 2) focuses on vegetation structure characteristics to identify regions having elevated risk of wildfire spread following ignition. This model is also sensitive to the effects of temporal fluctuations resulting from phenology and weather, but less sensitive to patterns of human use. The fuel continuity model is useful to identify regions of highly continuous fuel. These areas may be candidates for fuel load reduction prescriptions (using fire, planned grazing, mechanical treatments or a combination of treatments depending on the primary fuel type.

The fuel moisture model (component 3) identifies relative risk of wildfire spread based on a combination of the amount of relative moisture (vegetation moisture) and fuel load. This model allows land managers to identify regions that not only have a large amount of fuel, but dry fuel as well. This model is susceptible to fluctuations in weather and phenology. Phenological status of plants alters the relative moisture content of vegetation as the growing season progresses. Precipitation also alters vegetation moisture but it does so over localized areas. While this model provides an overview of fuel moisture content, land managers will need to adjust the model based on seasonality and recent weather events that may have affected the model.

The fuel load model (component 4) predicts tonnage of fuel present at any given location within the study area. This model allows managers to identify regions of high fuel load that may be a consideration for fuel load reduction prescription.

The slope/aspect/suppression difficulty model (component 5) provides an overview of the topography within the study area. Severe topographic characteristics hinder fire suppression efforts and increase the rate of fire spread.

The power of these models lies in their combined use as it pertains to the particular needs of land managers. This is especially relevant when considering areas that may be candidates for fuel load reduction prescriptions. Recent studies at ISU's GIS TReC have shown that both fire and grazing can effectively reduce fuel load, with grazing more selectively removing herbaceous material, and fire removing varying levels of fuel, depending on the intensity of the fire (Weber et. al in-review, 2003). In addition, land managers can now identify regions to be protected (e.g., cultural resource and significant natural resources (habitat of threatened or endangered species)) in case wildfires threaten those regions.

CONCLUSIONS

These models provide land managers with a number of tools and applications, including predictive models of wildfire risk, identification of regions that may be candidates for fuel load reduction, identification of regions with high wildfire risk containing important cultural and natural resources, and identification of regions that where homes and structures are at risk. Local, regional, and federal agencies will benefit by using these models to 1) coordinate land management efforts to reduce fire suppression expenditures by implementing alternative means by which wildfire risk may be reduced, and 2) prevent catastrophic wildfire events that result in loss of human life, destruction of property, and damage to cultural and natural resources.

ACKNOWLEDGEMENTS
This study was made possible by a grant from the National Aeronautics and Space Administration Goddard Space Flight Center. ISU would also like to acknowledge the Idaho Delegation for their assistance in obtaining this grant.

LITERATURE CITED

Andersen, H.E., 1982. Aids to Determining Fuel Models for Estimating Fire Behavior, USDA Forest Service General Technical Report INT-122.

Carstensen, L.W., 1987. "A Measure of Similarity for Cellular Maps," The American Cartographer, 14, 4, 345-358.

Kauth, R. J., and Thomas, G. S., 1976. The Tasseled Cap - A Graphic Description of the Spectral Temporal Development of Agricultural Crops As Seen By Landsat. *Proceedings of the Symposium on Machine Processing of Remotely Sensed Data*, Purdue University, West Lafayette, Indiana, 41-51.

Larimer County Commission, 2003. Is Wildfire Really a Problem in Larimer County? (Website visited on 8-Sep-2003, http://www.co.larimer.co.us/wildfire/wildfire_really_problem.htm

Lillesand, T. M. and R. W. Kiefer. 2000. Remote Sensing and Image Interpretation. 4th ed. John Wiley & Sons.

Rosenfield, G.H., and K. Fitzpatric-Lins, 1986. "A Coefficient of Agreement as a Measure of Thematic Classification Accuracy," Photogrammetric Engineering and Remote Sensing, 52, 2, 223-227.

U.S. Geological Survey. 1990. Digital Elevation Models- Data Users Guide 5. Reston, Va.

Wang, F., 1990. Fuzzy Supervised Classification of Remote Sensing Images, *IEEE Transactions on Geoscience and Remote Sensing*, 28(2): 194-201.

EFFECT OF LIVESTOCK GRAZING AND FIRE HISTORY ON FUEL LOAD IN SAGEBRUSH-STEPPE RANGELANDS

Keith T. Weber, Ben McMahan, and Glenn Russell
GIS Training and Research Center
Idaho State University
Pocatello, ID 83209-8130
(http://giscenter.isu.edu, e-mail: giscenter@isu.edu)

ABSTRACT
Measuring, modeling, and managing wildfire risk is an important and challenging task for land managers. We examined the effect of livestock grazing and previous wildfire events on fuel load in southeastern Idaho as part of a wildfire risk-livestock interaction study. Fuel load was estimated using ordinal fuel load classes at 128 sample sites stratified by current livestock grazing and documented wildfire occurrence (1939-2000). Fifty-nine percent of previous wildfire sites (n = 46) had a docuemented fire within the past 2 years. Livestock grazing was the most effective means to reduce fuel load (P < 0.0005) compared to recent wildfire (P < 0.05) and livestock grazing with previous wildfire (P < 0.05). Livestock grazing provides a viable management tool for fuel load reduction prescriptions that avoids the negative effect of extreme fire intensity where fuel load is high.

Keywords: Idaho, wildfire.

INTRODUCTION

There has been a critical need to predict and manage rangeland wildfire danger since the 1940's (Burgan and Shasby 1984, Burgan et al. 2000). Various studies have been conducted to measure fuel load and model fire behavior (Deeming et al. 1977, Anderson 1982, Andrews and Bradshaw 1997), while other studies have been conducted to determine the effect of various vegetation treatments on fuel load (Madany and West 1983, Tsiouvaras et al.1989, Blackmore and Vitousek 2000). In this study, we examined the effect of livestock grazing and previous wildfire on fuel load levels in sagebrush-steppe rangelands of southeastern Idaho.

Litter, percent bare-ground, vegetation composition, structure, and senescence are important components in the estimation of fuel load (Anderson 1982). Fuel load models have become a valuable tool for predicting fire behavior (Anderson, 1982) and managing wildfire risk. Understanding the factors that influence fuel load is also of value. This is especially true when management alternatives could be implemented to reduce fuel load and wildfire risk.

Study Area

This study was conducted on land managed by the USDI BLM, Upper Snake River District in southeastern Idaho. Sample points were located between $43^0$36'00"N and $42^0$48'00"N latitude and $-113^0$35'00"W and $-112^0$37'59"W longitude. This area is sagebrush-steppe semi-desert, with a history of livestock grazing and wildfire. Historically, sheep were the primary grazer. Currently, both sheep and cattle graze this area with cattle being the primary grazer. Deferred and seasonal grazing systems are used in the study area on allotments which range in area from 1,153 to 128,728 ha.

MATERIALS AND METHODS

Fuel load was estimated during the summer 2001 at 128 sample points randomly located across the study area (fig. 1). Fuel load estimation followed USDI BLM procedures (Anderson 1982). Each point was located $\geq$ 70 m from roads and other mapped features (e.g., fence lines) to avoid edge effects. Sample points were stratified by grazing treatment (grazed versus ungrazed) and fire history. Fire history was determined using an historic wildfire (1939-2000) GIS data set with samples categorized into no-fire, one-fire, or multiple-fire treatment classes (Table 1). Grazing treatment was determined using grazing allotment data provided by the USDI BLM. Each allotment was attributed as either being grazed (1) or not grazed (0).

Table 1.: Stratification of sampling points by treatment.

Treatment	Wildfire occurence (1939-2000)			
	0	1	>1	Total
Grazed	16	13	20	49
Ungrazed	34	28	17	79
Total	50	41	37	128

Field observations were made within an area approximately 900 m^2 in size (the area occupied by 1, 30x30 m Landsat pixel) centered over each sample point. Fuel load estimates were made following "Field Survey Project for Fuels Management Planning GIS Mapping Standards" (BLM 2001) and Anderson (1982). Visual estimates made at each sample point included: (1) fuel load, (2) presence/absence of live fuels, and (3) percent bare ground. Fuel load was determined by comparing field observations with Fire Behavior Fuel Model descriptions provided in Anderson (1982) which enumerated thirteen fuel model groups having fuel loads ranging from 0.74 (grass group model 1) to 58.1 tons/acre (logging slash group model 13). The fuel load class that best fit field observations was used as the fuel load estimate.

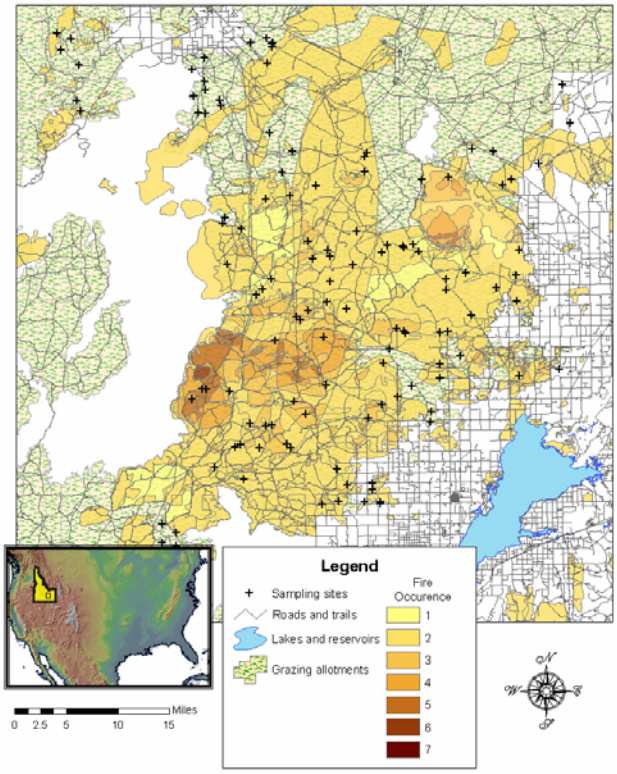

Figure 1. Sample locations, public land grazing allotments, and fire occurrence (1939-2000) for the study area.

Each sample point was classified into four categories representing the treatment type(s) found at that site; 1) grazed with previous wildfire, 2) grazed without previous wildfire, 3) no grazing with previous wildfire, and 4) no grazing or previous wildfire (i.e., control). A "previous wildfire" is one having occurred within the past 60 years, although most (59%) areas have had a fire in the past two years. Using these four categories, the effect of grazing and wildfire treatment on fuel load was tested using factorial ANOVA. We recognize the ordinal nature of our data violates the assumptions of both homogeneity of variance and normality. However, ANOVA is robust to these violations (Zar 1998) and should be fairly robust to a violation in homoscedasticity since each treatment contained approximately equal sample size. To further address these violations, we applied non-parametric Kruskal-Wallis and Mann-Whitney U with Bonferroni correction. While

these non-parametric tests may have provided greater confidence and reliability in our results, they did not allow us to assess the interaction among treatments. For this reason, we examined the results from both factorial ANOVA and non-parametric tests.

RESULTS

Of 13 possible fire behavior fuel models we encountered three (types 1, 2, and 6) in the field (Anderson 1982). Fire behavior fuel models one and two belonged to the grass group, while model six belonged to the shrub group. The models used in this study correspond with National Fire Danger Rating System models of "annual" and "perennial" grasses, and "sagebrush/grass" and "inter. brush" shrub models (Deeming and Brown 1975, Deeming et al. 1977). Five ordinal fuel load classes were described during field sampling in the summer of 2001 (Table 2).

Table 2. Ordinal fuel load categories and associated fire behavior models

	Fuel Model Descriptions (Anderson 1982)		
	Grass group		Shrub group
Fuel load class	Model 1	Model 2	Model 6
1 (0.74 kg ha^{-1})	X		
2 (1.00 kg ha^{-1})	X	X	
3 (2.00 kg ha^{-1})	X	X	
4 (4.00 kg ha^{-1})		X	
5 (6.00 kg ha^{-1})			X

Grasses were the dominant fuel load component (>50% grass cover in all grazed areas and 26-50% grass cover in burned areas that had not been grazed) in all treatment types except the control, where shrubs were the dominant fuel load component (31-60% shrub cover)(Table 3). Grazed areas consistently had a higher percent grass cover (>51%, n = 49) compared to ungrazed areas (26-50%, n = 79).

Table 3. Median vegetation cover class by treatment type.

Treatment	Grass (%)	Shrub (%)	Forb (%)	n
Grazing and fire	>51%	1-5%	1-5%	33
Grazing without fire	>51%	1-5%	1-5%	16
Fire without grazing	26-50%	1-5%	1-5%	45
Control	26-50%	31-60%	1-5%	34

Seventy-eight sample points were in areas of previous wildfire. The mean number of years since a fire was 16.3 (fig. 2) with most sites (n = 46) having a fire in the previous 2 years. The remaining sample sites (n = 50) had no record or indication of a wildfire since 1939. Mean fuel load was 1.34 kg ha^{-1} (n = 44) in all areas with a wildfire in the past 2 years, 1.59 kg ha^{-1} (n = 19) in non-grazed areas with a wildfire in the past 2 years, and 1.25 kg ha^{-1} (n = 27) in grazed areas with a wildfire in the past 2 years.

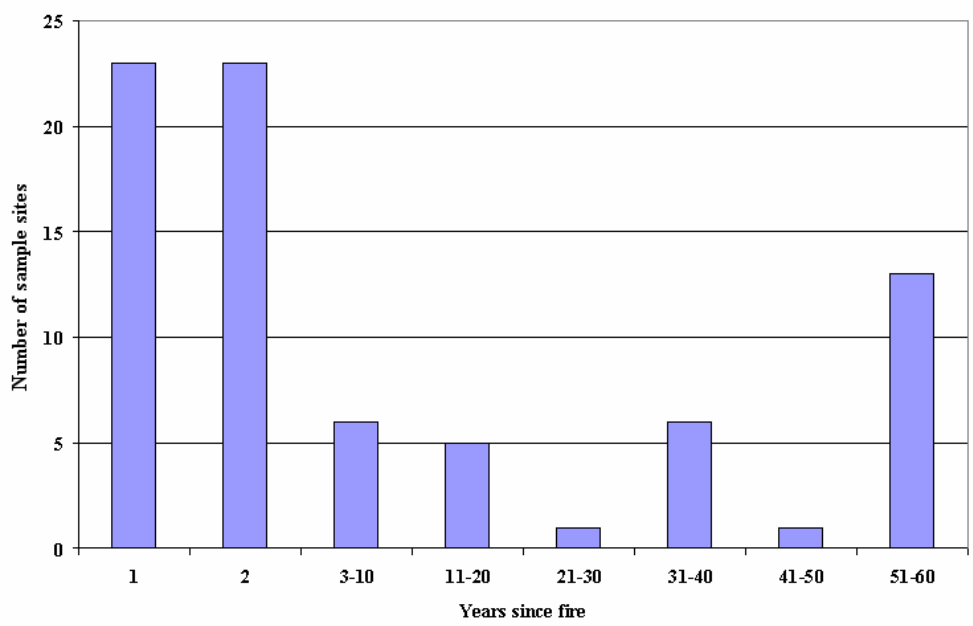

Figure 2. The number of years since a fire occurrence at sampling sites (1939-2000). Mean years since fire = 16.3. Fifty sample sites had not burned during this period (>60 yrs.).

Fuel load was decreased significantly by previous wildfire and/or grazing treatment (Fig. 3). The most significant treatment effect however, was grazing ($P < 0.0005$, Table 4). The effect of grazing and previous wildfire on fuel load was significant ($P<0.05$) as was the effect of fire alone ($P<0.01$) and the effect of grazing alone ($P<0.01$). Non-parametric Kruskal-Wallis analysis revealed a significant difference in fuel load among the four treatments and control categories ($P<0.00005$). A post-hoc non-parametric Mann-Whitney U test with Bonferroni correction was used to evaluate the effect of each treatment on fuel load. Once again, a significant effect was observed for both grazing ($P<0.01$) and fire ($P<0.01$) treatments. However, when tested against the effect of fire with grazing, fire alone did not produce significant results ($P=0.84$).

Table 4. Effect of treatment on fuel load[1].

Treatment	Type III Sum of Squares	df	Mean Square	F	P
Fire	13.77	1	13.77	7.62	0.00665
Grazing	33.10	1	33.10	18.32	0.00004
Grazing and Fire	8.48	1	8.48	4.69	0.03223
Error	224.03	124	1.81		
Total	287.15	127			

[1] Dependent Variable: Fuel load estimate.

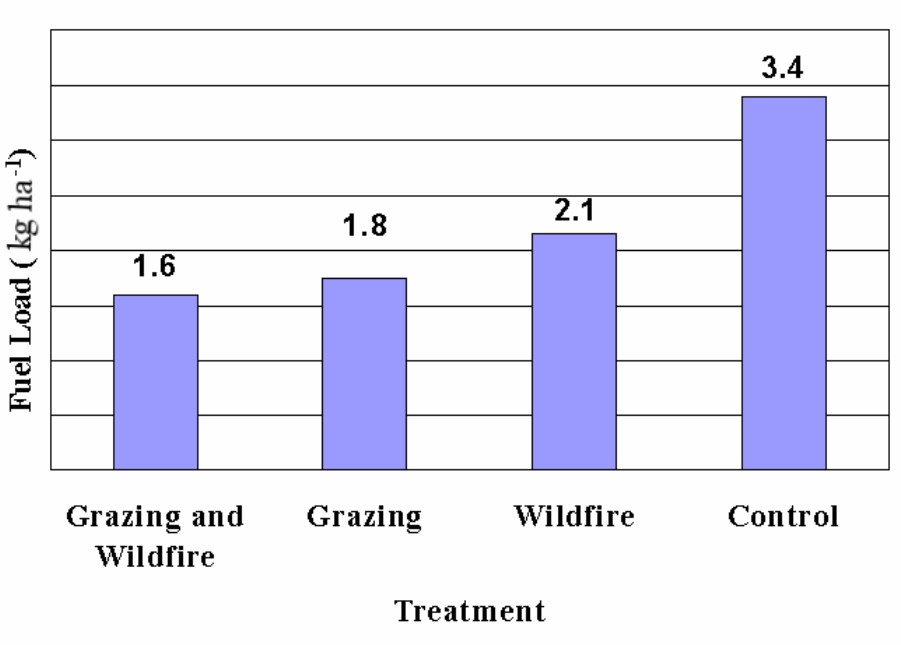

Figure 3. Mean fuel load (kg ha-1) by treatment type. Fuel load estimations are from field observations.

DISCUSSION

Historic fire suppression efforts have interrupted the natural fire cycle allowing fuel loads to reach unprecedented levels. Recent catastrophic wildfires, such as those seen in Idaho, Montana, Colorado, and Arizona, have the potential to produce extremely intense and severe burns. While these fires reduce fuel load, they may also sterilize soils (Wells et al. 1979). These extensive fires may result in loss of biodiversity and the destruction of critical habitat for native plants and animals, which often leads to invasion by cheatgrass (B*romus tectorum)* and other invasive species.

This study examined the effect of and interaction between two fuel load reduction treatments (livestock grazing and wildifire). We found livestock grazing to be as effective in reducing the primary fuel load component of the sagebrush-steppe ecosystem (herbaceous material) when compared to wildfire. Additionally, grazing reduces fuel load in a more selective fashion (Archer 1999) avoiding the potential sterilizing effect that an extremely intense fire may have on soil.

Studies in other regions have reported results that corroborate well with our findings. Within montane forests of Zion National Park, Madany and West (1983) considered livestock grazing the primary factor in the reduction of herbaceous cover. Tsiouvaras et al. (1989) reported that grazing by goats effectively reduced 1- and 10-hour fuel load in coastal forest areas of California. Similarly, Blackmore and Vitousek (2000) found grazing in dry forest ecosystems of Hawaii to be an effective means to reduce continuity of fuels, fire intensity, and fire risk.

CONCLUSIONS

In conclusion, livestock grazing can be viewed as a viable land management tool for fuel load reduction prescriptions when proper consideration has been given to other ecological effects not discussed here.

ACKNOWLEDGEMENTS

This study was made possible by a grant from the National Aeronautics and Space Administration Goddard Space Flight Center. ISU would also like to acknowledge the Idaho Delegation for their assistance in obtaining this grant.

LITERATURE CITED

Anderson, H.E., 1982. Aids to Determining Fuel Models for Estimating Fire Behavior, USDA Forest Service General Technical Report INT-122.

Andrews P. L. and L. S. Bradshaw. 1997. FIRES: Fire Information Retrieval and Evaluation System- A Program for Fire Danger Rating Analysis. USDA Forest Service, General Technical Report INT-GTR-367. August 1997, Ogden, Utah 84401.

Archer, S. 1999. Woody Plant Encroachment into Southwestern Grasslands and Savannas: Rates, Patterns, and Proximate Causes. pp 13-68 *in* Ecological Implications of Livestock Herbivory in the West (2nd Edition), Vavra M., W. A. Laycock, and R. D. Pieper (Eds.), Society for Range Management, Denver, Colo.

Bureau of Land Management (BLM), Upper Snake River District, 2001. Draft-Field Survey Project for Fuels Management Planning GIS Mapping Standards (May 9, 2001). 51pp.

Blackmore, M. an d P. M. Vitousek. 2000. Cattle Grazing, Forest Loss, and Fuel Loading in a Dry Forest Ecosystem at Pu'u Wa'aWa'a Ranch, Hawai'i. Biotropica 32(4a):625-632.

Burgan, R.E., Klaver, R.W., and Klaver, J.M. 2000. Fuel Models and Fire Potential from Satellite and Surface Observations, USDA, FS, Rocky Mountain Research Station, Missoula, MT.

Burgan, R.E. and Shasby, M.B. 1984. Mapping Broad-Area Fire Potential From Digital Fuel, Terrain, and Weather Data, J. For. 8:228-231.

Deeming, J. E. and J. K. Brown. 1975. Fuel Models in the National Fire-Danger Rating System. J. For. 73:347-350.

Deeming, J. E., R. E. Burgan, and J. D. Cohen. 1977. The National Fire-Danger Rating System-1978. USDA Forest Service, General Technical Report INT-39. October 1977. Ogden, Utah 84401.

Madany, M. H. and N. E. West. 1983. Livestock Grazing-Fire Regime Interactions within Montane Forests of Zion National Park, Utah. Ecology 64(4):661-667.

Tsiouvaras, C. N., N. A. Havlik, and J. W. Bartolome. 1989. Effects of Goats on Understory Vegetation and Fire Hazard Reduction in a Coastal Forest in California. Forest Science. 35(4):1125-1131.

Wells, C. G., R. E. Campbell, L. F. DeBano, C. E. Lewis, R. L. Fredriksen, E. C. Franklin, R. C. Froelich, and P. H. Dunn. 1979. National Fire Effects Workshop (1978:Denver, Colo.). USDA Forest Service General Technical Report WO-7. 34pp.

Zar, J. H. 1998. Biostatistical Analysis (4th Edition). Prentice-Hall, 929 pp.

VALIDATION ALTERNATIVES FOR CLASSIFIED IMAGERY

Ben McMahan and Keith T. Weber
GIS Training and Research Center
Idaho State University
Pocatello, ID 83209-8130
(http://giscenter.isu.edu, e-mail: giscenter@isu.edu)

INTRODUCTION

The only reliable means to determine the accuracy of models developed from remotely sensed imagery or geographic information system (GIS) analyses is to perform a validation test. This is typically accomplished by assembling a standard contingency table (or confusion matrix). The matrix is developed by selecting numerous sample points representing each category of the model and determining if the observed field value at that location agrees with the value predicted by the GIS model (e.g., classified imagery). Errors are then reported as omission, commission, and overall error. The Kappa statistic (Titus et al. 1984) gives yet another calculation for classification accuracy, expressed as how much better (or worse) the classification is relative to chance alone.

Validation is typically performed using sample points collected independent of training site data. While this process may seem statistically rigorous, it can be unproductive if researchers have limited field availability or a short field season. In such cases, models will be built in year 1 and not validated until year 2. Changes that can occur in one year can be fairly substantial and it is felt that errors in validation may result because of this temporal delay. To address this, we collected all field data necessary for both model production and validation during the summer of 2002. We then experimented with various bootstrapping (*n* random subsets of the data are

created and tested for consistency of performance) validation iterations to determine the optimum number of field samples needed for classification relative to the number of validation samples.

Within the literature on validation procedures, a number of different methods can be employed to assess the accuracy of the models. One of the most common methods is subset validation (mentioned above), which involves the use of training and test subsets of the data, where the model is built with the training subset and subsequently validated with the test subset. Other more comprehensive validation procedures such as cross-validation (also known as leave-one-out validation) or bootstrapping also exist (Weiss and Kulikowski 1991, Efron and Tibshirani 1993.

METHODS

We iteratively classified fuel load models (with five fuel load categories) using various randomly selected subsets of field data (n = 370) and maximum likelihood classifier. Training site sample sizes were 22, 44, 66, 88, 133, 185, and 370. Validation was performed using all un-used sample points save for the last iteration where all points were used for both model development and validation.

RESULTS

The resulting accuracy of models created with a training subset (n = 185) and validated with a test subset (n = 185) were nearly identical to the results from models developed and validated using the entire dataset (n = 370) (Table 1). During each classification iteration the variance for each spectral signature was calculated for each band of imagery used (i.e., Landsat ETM+ bands 3, 4, and 5) (Figure 1).

Table 1. Comparison of accuracy assessment using 50% of field samples for model developement and 100% for model development and validation.

	All Point Technique	Subset Validation
Overall accuaracy	47.27%	48.28%

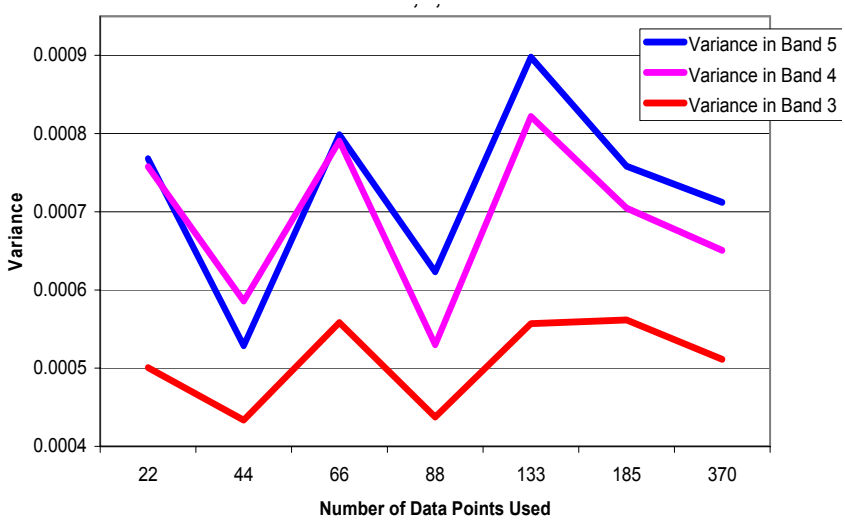

Figure 1. Variance of spectral signatures using different subsets of training sites.

DISCUSSION

The fact that accuracy is nearly identical when using 185 sample points compared to all 370 sample points indicates it is legitimate to perform validation using the same training sites employed to build the model. However, a word of caution is merited. If the total number of points collected is relatively small, then the influence of each individual sample point on the output model (regardless of classification technique selected) will increase. At some point, the classified value at each sample point will perfectly reflect the original value of the sample point. In such cases, accuracy will be 100% and the alert user should suspect a problem. A less obvious example exists as one approaches the scenario described. In this case we expect accuracies to artificially soar. Therefore we consider it prudent to first test the reliability of your sample dataset by performing a 50/50 development/validation classification and compare the resulting accuracy with a development/validation classification where all sample points are used. To employ this technique then, users must ensure they have a collected a large number of field observations that truly captures the variability between and among each category being classified.

ACKNOWLEDGEMENTS

This study was made possible by a grant from the National Aeronautics and Space Administration Goddard Space Flight Center. ISU would also like to acknowledge the Idaho Delegation for their assistance in obtaining this grant.

LITERATURE CITED

Efron, B. and Tibshirani, R.J. (1993), An Introduction to the Bootstrap, London: Chapman & Hall.

Titus, K., Mosher, J.A., Williams, B.K. (1984) Chance-corrected classification for use in discriminant analysis: ecological applications. *American Midland Naturalist*, 111, 1-7.

Weiss, S.M. and Kulikowski, C.A. (1991), Computer Systems That Learn, Morgan Kaufmann.

THE USE OF REMOTE SENSING IMAGERY FOR EVALUATION OF POST-WILDFIRE SUSCEPTIBILITY TO LANDSLIDE AND EROSION HAZARDS IN THE SALMON-CHALLIS NATIONAL FOREST, LEMHI COUNTY, IDAHO

Diane K. Sprague-Wheeler
Department of Geosciences
Idaho State University
Pocatello, ID 83209-8130

ABSTRACT

Remote sensing and field-based research is used to investigate landslide and soil erosion hazards resulting from wildfire activity in central Idaho. This study focuses on four areas in the Salmon-Challis National Forest (SCNF). Field-based research is performed on three sites (one kilometer (km^2) each) to test the remote sensing imagery and to use as ground-truth for the larger, fourth site (570 km^2). Two relative hazard maps, one for landslides and one for erosion, are developed for each of these areas. The classification system for the maps includes slope, aspect, burn severity, understory vegetation cover (for erosion only), hydrology, bedrock geology, and soil characteristics. Each parameter is assigned a relative hazard ranking of ordinal numbers. Results indicate that digital elevation models are useful in providing comprehensive slope and aspect analysis. High-resolution multispectral data can be used successfully to map areas of high burn severity and unburned areas, although mapping areas of low to moderate burn severities proved more difficult. The imagery can also be used to assess vegetation cover; however, it cannot distinguish between understory and overstory vegetation cover. The kappa statistic is used to assess the accuracy of the remote sensing data. Results indicate that the remote sensing data corresponds well to field mapping when using a bootstrap accuracy check. However, in the pixel-by-pixel comparison, kappa values are considered low. The greatest difference between the relative hazard maps using field data and remote sensing is that the imagery classifies each 4-meter pixel, whereas field mapping tends to classify larger areas based upon similar features. This study has produced a well-documented methodology of landslide and soil erosion hazard assessment and a qualification of the relative importance of land cover parameters in the SCNF.

Keywords: GIS, satellite

INTRODUCTION

PROBLEM STATEMENT

The 2000 wildfires of central Idaho burned thousands of square kilometers of forest and grazing land and are estimated to have cost millions of dollars in firefighting and damage to infrastructure, natural resources, and the environment (USFS, 2001a). It may be impossible to assess the full extent of damage to natural resources and the pristine environments of areas such as the Salmon-Challis National Forest (SCNF) (Figure 1). One detrimental effect of large wildfires is the widespread impact of increased landslides and soil erosion by water resulting from the removal of vegetation (Bailey, 1971; McKean et al., 1991; Dragovich et al., 1993a,b). Sediment transport in burned areas affects watersheds and water quality for aquatic wildlife. Degradation of wildlife habitat is accelerated by sediment loading of streams from landslides. Sediment and other materials transported after fires may be deposited in stream channels, which may change stream morphology, especially channel form, and particle size and distributions. In addition, wildfires affect new vegetation growth and this affects habitat, sediment stability, and future wildfire regimes.

Currently, field study is the primary tool for investigating the potential for landslides and erosion after wildfires (Benavides-Solorio and MacDonald, 2001; Cannon, 2001; Cannon et al., 2001a,b; Meyer et al., 2001). This can be especially difficult and time-consuming in remote areas with limited access and large, diverse landscapes. For example, the SCNF, located in central Idaho, contains over 10,000 square kilometers (km²) of land. This area is extensive and heavily forested; thus field investigations to identify and map landslide and soil erosion hazards are limited. This study evaluates the

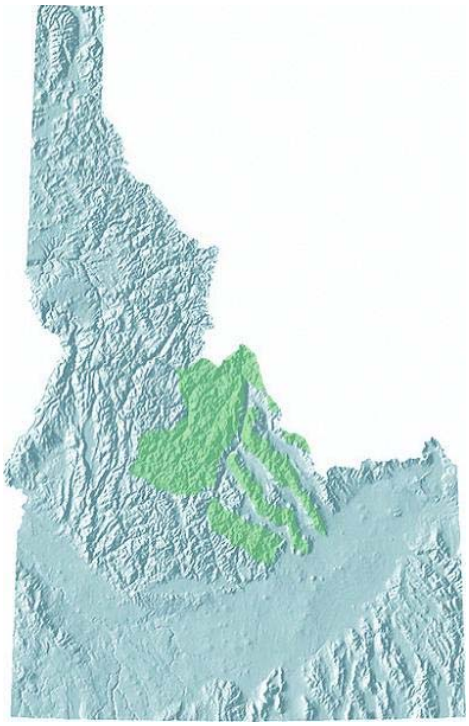

Figure 1. Topographic map of Idaho. Areas highlighted in green indicate the approximate location of the Salmon-Challis National Forest.

usefulness of remote sensing imagery in assessing relative landslide and erosion hazards and develops a relative hazard ranking system for landslide and erosion hazards in the SCNF. This methodology was first developed and validated on three one-km² sites, and then applied to a 570 km² area of the SCNF to assess large-scale applicability. The hypothesis of this study is that field studies and remote sensing methods can be used to identify land cover parameters that influence susceptibility to post-fire erosion and landslides.

BACKGROUND

Wildfire History

Decades of fire suppression have led to an unnatural buildup of fuels within forests, contributing to the development of intense wildfires (USFS, 2001b). Complete fire suppression has disrupted normal ecological cycles and changed the structure and make-up of forests. Years of fire suppression have created fuel ladders, and consequently forests experience more of the high-severity, stand-replacing fires. In addition, a general warming cycle over the past century is thought to have increased the frequency of wildfires (Meyer et al., 1992). As noted by the United States Forest Service (USFS) (2001b), decades of aggressive fire suppression have drastically changed the look and fire behavior of forests and rangelands. Compared to forests a century ago, forests today are denser and have smaller, less fire-resistant trees. The composition of forests has changed from more fire-resistant species such as ponderosa pine, aspen, and cottonwood, to non-fire resistant species such as grand fir, Douglas fir, and lodgepole pine (Gough and Lamb, 2000; Idaho Forest Products Commission, 2003; Keep Idaho Green, 2003). As a result, studies show that wildfires today tend to burn hotter and faster than those of the past (USFS, 2001b).

Scientists have understood for some time that fire is an essential part of the forest ecosystem. Not only are forests adapted to wildfires, they are in large part dependent upon them. For example, lodgepole pine produces two types of cones. As noted by Carey and Carey (1989), one type opens upon reaching maturity and falls to the ground, where, unless it lands in a nurturing (i.e., soil and nutrient rich) environment, it is quickly eaten by rodents and birds. The other type of cone only opens at temperatures of 49º Celsius (C), an unlikely temperature to be reached in forests without fire. Fires leave behind a rich ash bed in which the seeds from these cones can quickly germinate and become established. Plants normally rely on the slow decomposition of organic material for their nutrients, and ash from fire contains a dense concentration of these nutrients. Ash provides a natural fertilizer for plants and does not require additional breakdown to be accessible to the root systems of the plants. Higher levels of sunlight resulting from the destruction of forest canopy also stimulate plant growth. Carey and Carey (1989) report that when old-growth timber is removed, total plant species increase thirty-fold within 3-20 years. Streams benefit from fire to some extent by the addition of ash that increases in-stream vegetation, and by increased available sunlight that increases water temperature and stimulates aquatic productivity.

There are numerous wildfires every year in the U.S. Between the 40-year period of 1960-2000, there was an average of 135,826 wildfires and 16,415 km² burned each year (NIFC, 2001) (Table 1). The largest number of fires occurred in 1981, while the most area burned in 2000. Wildfires are started in a variety of ways, including lightning

Table 1. Total wildfires and area burned in the U.S. between the 40-year period of 1960-2000 (NIFC, 2001).

Year	Number of Fires	Area Burned (km^2)	Year	Number of Fires	Area Burned (km^2)
2000	122,827	34,084	1979	163,196	12,087
1999	93,702	22,913	1978	218,842	15,827
1998	81,043	9,428	1977	173,998	12,758
1997	89,517	14,863	1976	241,699	20,679
1996	115,025	27,120	1975	134,872	7,249
1995	130,019	9,371	1974	145,868	11,651
1994	114,049	19,117	1973	117,957	7,751
1993	97,031	9,350	1972	124,554	10,688
1992	103,830	9,946	1971	108,398	17,314
1991	116,953	9,056	1970	121,736	13,268
1990	122,763	22,067	1969	113,351	27,070
1989	121,714	13,200	1968	125,371	17,126
1988	154,573	29,942	1967	125,025	18,853
1987	143,877	16,805	1966	122,500	18,512
1986	139,980	13,388	1965	113,684	10,733
1985	133,840	17,947	1964	116,358	16,986
1984	118,636	9,171	1963	164,183	28,817
1983	161,649	20,560	1962	115,345	16,507
1982	174,755	9,640	1961	98,517	12,287
1981	249,370	19,482	1960	103,387	18,123
1980	234,892	21,290			

strikes and human activities, such as campfires, smoking, incendiary, equipment, railroads, juveniles, and miscellaneous (NIFC, 2001). During 1988 to 1997, lightning strikes were responsible for burning the most area while miscellaneous human activities caused the greatest number of fires (Table 2).

Lightning strikes were a major contributing factor to the extensive wildfires that occurred in the western U.S. during summer 2000. These wildfires were a result of two primary factors: drought-like conditions accompanied by dry storms that produced thousands of lightning strikes and windy conditions, and an unnatural buildup of brush and trees created by the effects of aggressively suppressing all wildfires for more than a century (USFS, 2001b). Two of the largest of these fires, the Clear Creek Fire and the Salmon-Challis Forest Wilderness Fire, occurred within the SCNF. Collectively these two fires are known as the Salmon-Challis National Forest Fire; they burned approximately 1,619 km^2 of forest and grazing land. This fire, one of the top five largest fires in the U.S. during 2000, is estimated to have cost millions of dollars in firefighting and damage to infrastructure, natural resources, and the environment (NIFC, 2001).

Table 2. Number of wildfires and area burned in the U.S. by cause between the 10-year period of 1988-1997 (NIFC, 2001)

Year	Cause	Number of Fires	Area Burned (km²)
1988	Human	138,238	14,403
	Lightning	16,335	15,539
1989	Human	107,318	8,419
	Lightning	14,396	4,791
1990	Human	105,784	7,023
	Lightning	16,979	15,052
1991	Human	104,777	7,091
	Lightning	12,164	1,961
1992	Human	89,701	5,699
	Lightning	14,245	4,244
1993	Human	87,725	4,720
	Lightning	9,305	4,626
1994	Human	94,265	7,751
	Lightning	19,801	11,379
1995	Human	120,045	5,886
	Lightning	9,974	3,489
1996	Human	99,606	13,618
	Lightning	15,560	13,504
1997	Human	79,484	3,985
	Lightning	10,033	10,836
10-Year Average	**Human**	**102,694**	**7,859**
	Lightning	**13,879**	**8,542**

Mass Wasting/Erosion Terminology

There are numerous types of surficial processes defined in the literature, so it is prudent to define the terminology used in this study. This study considers the propensity for rapid mass wasting, rather than distinguishing the specific mechanisms and types of mass wasting. Mass wasting is a general term that can include landslides, slumps, debris flows, mud flows, earth flows, rock falls, soil creep, etc.

This study focuses on landslides and flows, because these are the two processes most likely to affect water quality within watersheds. Landslides are defined as the rotational or planar movement of a discrete mass that takes place along a well-defined failure surface. A flow has continuous, internal deformation without the development of a failure surface. Many types of flows are recognized in the literature, and flows observed in motion are generally classified by the type and rate of movement, whereas flows not observed in motion are classified by the morphology and sediment type of flow deposits (Easterbrook, 1999). Herein, this study will use the term landslide to include all landslides and flows.

Flowing water removes soil from slopes through a variety of erosional processes, including sheet wash, rilling, and gullying. As noted by Selby (1993), sheet wash is the process by which soil is detached due to raindrop impact and entrained by water runoff. Flow velocities typically range

from 0.015 to 0.30 meters (m) per second. Rills are small channels, a few centimeters (cm) to tens-of-centimeters in cross-section, that are usually discontinuous and not connected to a stream channel system. Rills may deepen and widen to form gullies. Gullies are typically over 0.3 m wide and 0.6 m deep. Herein, this study will use the term erosion to include the processes of sheet wash, rilling, and gullying.

The Relationship Between Wildfires and Landslides/Erosion

Undisturbed lodgepole and ponderosa pine forests typically have high infiltration rates, lack overland flow, and experience low erosion rates (Benavides-Solorio and MacDonald, 2001). Reduction of infiltration rates can lead to overland flow (e.g. sheet wash) and increased rill erosion. Wildfires can make forests more susceptible to sediment transport processes in a number of ways. For example, fires may create water repellent soils, they may remove the protective layer of litter/duff covering the forest floor, and they may remove vegetation that stabilizes slopes and reduces surface runoff.

Numerous studies have observed a wettable surface layer that overlies a water-repellent layer following fires in watersheds. Water repellent soils are those which will hold a drop of water for at least a few seconds before penetration (Doerr et al., 2000). Strong water repellency can be created when vaporized organic compounds move downward due to the temperature gradient and condense in lower soil layers. Doerr et al. (2000) observed little change in water repellency of soils at temperatures less than 175º C. At temperatures between 175-200º C water repellency was intensified. Hydrophobic substances are fixed to soil particles around 250º C, but destroyed above 270-300º C. These findings indicate that cooler fires will cause water repellency at the surface, and hotter fires will produce water repellency at greater depth. Soil temperatures would be highest at the ground surface during a fire and decrease with depth. Repellency is increased with longer sustained heating times. The longevity of water repellency is hard to predict because it is very site specific and depends on soil temperature, soil type, organic compounds, and climatic conditions. Several studies indicate that water repellency can cause reduction in soil infiltration capacity, enhanced overland flow and accelerated erosion, development of preferential flow, rainsplash detachment, soil loss by both water and wind, and generation of debris flows (Doerr et al., 2000; Benavides-Solorio and MacDonald, 2001; Huffman et al., 2001; Meyer et al., 2001).

Wildfires may burn away the protective litter layer on the forest floor and thus increase the rate of precipitation delivery to the soil and the occurrence of rainsplash detachment (Martin and Moody, 2001). This results in higher rates of surface runoff and erosion. Most studies indicate that the greatest increase in runoff and erosion occur within the first few years after the wildfire, but this is dependent upon climatic conditions.

Fires may also destroy vegetation that removes moisture from the soil via evapotranspiration, which may eventually lead to increased overland flow. In addition, vegetation increases slope stability and thus the removal of small types of vegetation, such as bushes and grass, has immediate consequences for erosion. Similar to the removal of litter, this results in higher rates of surface runoff and rainsplash detachment, and increases the rate at which precipitation is delivered to the soil (Cooke and Doornkamp, 1990). Large tree roots are effective in making slopes less susceptible to deep-seated landslides (Selby, 1993). Tree roots near the surface can

be completely incinerated by high-severity fires. In some cases, the roots can be burned but it will take 5-6 years for them to completely decay, at which time they are rendered useless for slope stability (Meyer et al., 2001). It has been suggested by various studies that shallow landslides are more probable in burned and/or logged areas after the tree roots decay, an effect that occurs 4-10 years after tree mortality (Gray and Megahan, 1981; Clayton and Megahan, 1986; Meyer et al., 2001).

Setting

The study area is the Yellowjacket Mountains in the SCNF, Lemhi County, Idaho (Figure 2). Much of the study area is very steep, with narrow canyons and slopes up to 40º (Figure 3). The elevation generally ranges from 2,000-3,000 m (all elevations are above sea level).

Four specific study sites were selected for this study (Figures 2, 3). Sites #1 and #2 are located within the Panther Creek watershed. Panther Creek, a tributary to the Middle Fork of the Salmon River, drains a 1,378 km² area within the Middle Salmon-Panther subbasin. Site #3 is located within the Camas Creek watershed, which is part of the Lower Middle Fork of the Salmon River subbasin. Camas Creek is also a tributary to the Middle Fork of the Salmon River. These particular sites were selected due to their varying slopes and aspects, burn severity, amount of understory vegetation cover, hydrology, bedrock geology, and soil characteristics in order to provide a diverse range of conditions for this study. Site #4 is a 570 km² area of the SCNF that was selected to encompass the three smaller study sites.

As noted by B. Rieffenberger (oral comm., 2002), these subbasins have a wide range of climates due to varying elevations, and local topography and aspects. Climate can range from a near desert environment in lower elevations to near alpine environment in upper elevations. Maximum summer temperatures can exceed 38° C in the lower elevations, and winter temperatures can be well below -18° C at all elevations. Snowfall contributes most of the annual precipitation, although rain is common in late spring and early summer. High-intensity, short-duration thunderstorms occur primarily in July and August. These storms tend to move in an easterly direction along the Salmon River Canyon. In the study areas, located south of the Salmon River Canyon, thunderstorms generally approach from the west or from the north. The average precipitation ranges from 38 cm per year along the lower elevations to 102 cm per year at the higher elevations.

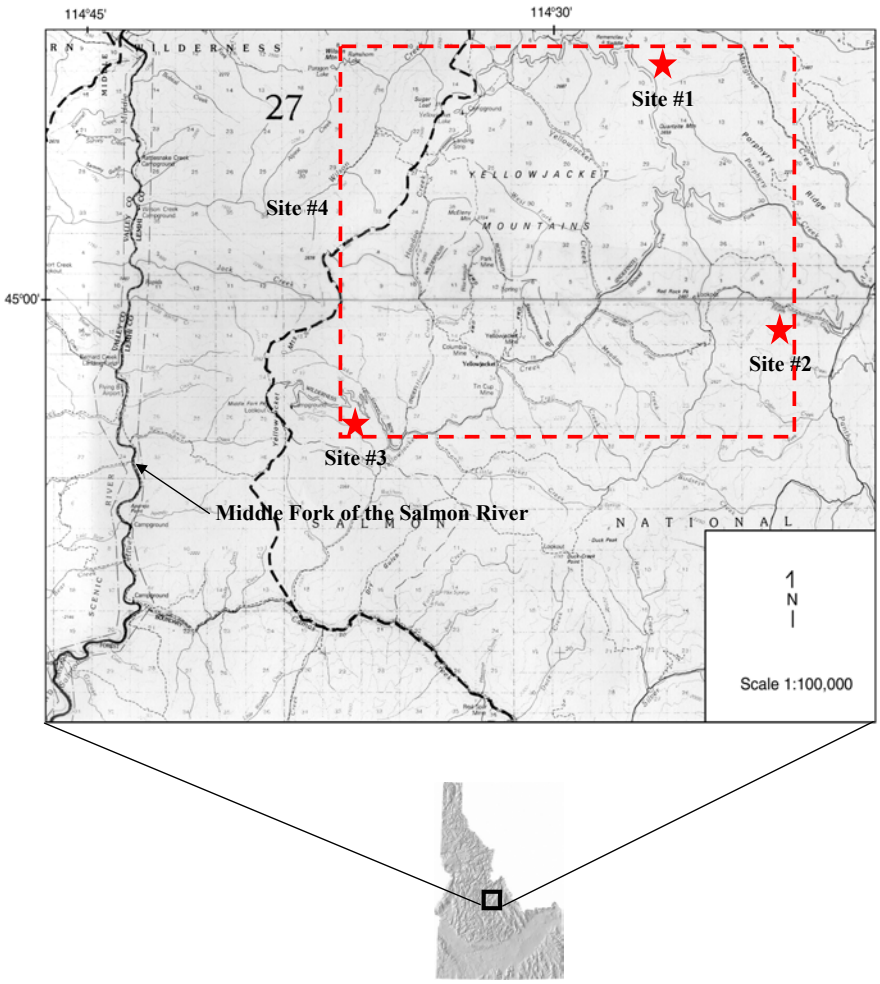

Figure 2. Map showing the approximate locations of the four selected study areas within the Yellowjacket Mountains in the Salmon-Challis National Forest, Lemhi County, Idaho (modified from Idaho Transportation Department, 1996). Sites #1-3 are indicated in red.

Figure 3. Relief map of Site #4 and the approximate locations of Sites #1-3 (indicated by red stars). Streams are shown by blue lines. (Derived from IKONOS imagery, 4-m resolution.).

Landforms within the watersheds of the Middle Fork of the Salmon River are highly variable. The lower elevations tend to consist of oversteepened canyons and rock outcrops. The middle elevations are characterized by mountainous slopes ranging from 10° up to 40°. Upper elevations are dominated by broad and gently-sloping ridge tops and mountain slopes.

The watersheds of the Middle Fork of the Salmon River are dominantly subalpine and Douglas fir forests, and include ponderosa pine, lodgepole pine, and Douglas fir (Rieffenberger, 2000). Lodgepole pines are common especially in old burn areas. The forest undergrowth consists primarily of bunchgrass, pinegrass, and beargrass.

PREVIOUS WORK

Geologic Mapping

Ross (1934) first mapped the geology of the Yellowjacket Mountains. It has been geologically mapped and interpreted most recently by Ekren (1988), Evans and Connor (1993), Winston et al. (1999), and Tysdal (2000). A compilation of these maps has been constructed for this study (Figure 4). There are seven main bedrock types significant to the study areas. They include (1) the "Type" Yellowjacket Formation; (2) the Hoodoo Quartzite; (3) the informal argillaceous member of the "Cobalt" Yellowjacket Formation of the Middle Proterozoic Belt Supergroup (Winston et al., 1999); (4) Ordovician or Middle Proterozoic granites; (5) granitic rocks of the Idaho Batholith; (6) Tertiary granites of the Casto and Crags Plutons, and (7) the Challis Volcanic Group. Each of these seven main bedrock types possesses distinct soil-forming and sediment yield characteristics.

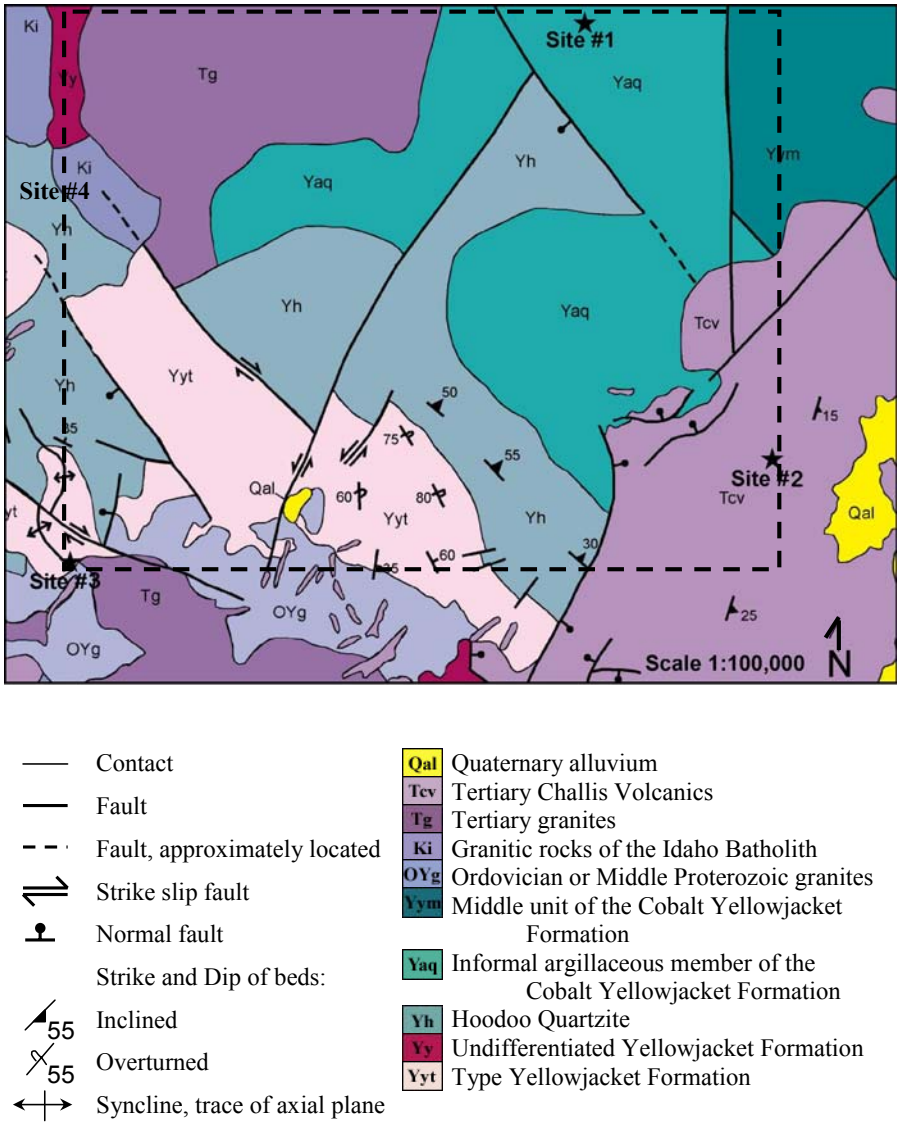

Figure 4. Simplified geologic map of the study areas compiled from Ross (1934), Ekren (1988), Evans and Connor (1993), and Winston et al. (1999). Sites #1-3 are indicated by black stars and Site #4 is bound by the thick black dotted line.

Type Yellowjacket Formation

Since its first usage by Ross (1934), the name Yellowjacket Formation has been generously applied to any slightly metamorphosed, nonfossiliferous, medium to dark gray, micaceous quartzite and siltite of Middle Proterozoic age in central Idaho. The name Yellowjacket Formation as used in this inclusive sense is stratigraphically located both above and below the Hoodoo Quartzite. Winston et al. (1999) determined that the Type Yellowjacket is in conformable contact below the Hoodoo, and thus they subdivided the unit formerly lumped together as "Yellowjacket" into the Type Yellowjacket, which lies below the Hoodoo, and the Cobalt Yellowjacket, which lies above the Hoodoo.

The Type Yellowjacket Formation is correlative to the informal lower member of the Yellowjacket as described by Evans (1999). It is primarily composed of gray to greenish-gray siltite and argillaceous siltite with minor carbonate and fine-grained quartzite layers. It is primarily slope-forming and weathers to sand and silt; thus movement may occur as debris flow or as soil creep in those areas with relatively thick soil development.

Hoodoo Quartzite
The Hoodoo Quartzite is generally massive, although intricately jointed in some places (Ross, 1934; Ekren, 1988). Bedding is indistinct; however, beds 0.3-1.0 m thick can be found that are distinctly crossbedded (Ekren, 1988). This unit is indurated and fairly resistant to weathering. Little or no movement is expected to occur in this unit, as this rock weathers into angular fragments of quartzite.

Argillaceous Quartzite of the Cobalt Yellowjacket Formation
The Cobalt Yellowjacket Formation is correlative to the informal middle and upper members of the Yellowjacket as described by Evans (1999). Winston et al. (1999) further subdivides the middle member, the lower section that stratigraphically overlies the Hoodoo Formation, as the informal argillaceous quartzite member of the Cobalt Yellowjacket Formation. This lower section is composed of light gray siltite and fine-grained quartzite alternating with black argillite. Sand and silt consistently penetrate downward into cracks developed within the argillite layers. Large (30 cm-scale) trough and planar cross-beds and hummocky cross stratification are common. Also present are ripple cross-laminations and local rip-up clasts (Tysdal, 2000). This member is primarily slope-forming and weathers to sand and silt. Movement may occur as debris flow or as soil creep in those areas with relatively thick soil development.

Ordovician or Middle Proterozoic Granites
The Ordovician or Middle Proterozoic granites are intrusive rocks that consist of diorite, quartz diorite, gabbro, granite, syenite, and quartz syenite (Ross, 1934; Ekren, 1988). These rocks are primarily ledge-forming and weather to form grus.

Granitic Rocks of the Idaho Batholith
The Mesozoic granitic rocks of the Idaho batholith include undifferentiated granitic rocks, migmatite, quartz diorite, and quartz monzonite (Ross, 1934). These rocks are primarily ledge-forming and weather to form grus.

Tertiary Granite
The Tertiary granites include the Eocene granitic rocks of the Casto Pluton and the Crags Pluton (Ross, 1934; Ekren, 1988). The Casto Pluton consists of pink granite and light-gray quartz monzonite. The granites of the Crags Pluton include quartz monzonite and granodiorite. These granites are ledge-forming and weather to form grus.

Challis Volcanic Group
The Eocene Challis Volcanic Group unconformably overlies all Proterozoic units. As noted by Fisher and Johnson (1995), the Challis Volcanics range from magnesium-rich basalt to alkali rhyolite. The predominant rock is intermediate in composition (dacite and rhyodacite). The Challis Volcanics include voluminous ash-flow tuffs, lavas, and hypabyssal intrusives

interbedded with fluvial and lacustrine sedimentary rocks. Hydrothermally altered rocks, which are typically highly silicified, bleached, and stained with iron oxides, are common. The Challis Volcanics are intruded by the pink granites of the Casto Pluton. The Challis Volcanics are ledge-forming and weather to medium- to fine-grained sand. Movement may occur as debris flow or as soil creep in those areas with relatively thick soil.

Remote Sensing Studies

Several studies have investigated the applicability of remote sensing methods to assess landslide hazards. Moeremans and Dautrebande (2000) used synthetic aperture radar (SAR) imagery to evaluate spatial and temporal soil moisture variation, which is crucial information for hydrologists wanting to predict flood events. Kimura and Yamaguchi (2000) demonstrated that SAR data can be used to investigate kilometer-scale landslides by using interferograms to detect and evaluate displacement patterns and landslide behavior. McKean et al. (1991) used Landsat Thematic Mapper (TM) imagery to explore the effect of vegetation type on debris flow occurrence. They found root strength and evapotranspiration to be important variables in the occurrence of shallow landslides. McKean et al. (1991) found that remote sensing can be used to measure soil depth indirectly by the type of vegetation present. Pickup and Marks (2000) used airborne gamma radiometrics and digital elevation models (DEMs) to investigate patterns of erosion and deposition by analyzing K, Th, and U content. Gamma ray signatures of these elements are determined by lithology but change with weathering, erosion, and deposition. Nachtergaele and Poesen (1999) assessed ephemeral gully erosion rates by utilizing temporally sequential high-altitude stereo aerial photographs. Singhroy et al. (2000) and Singhroy and Mattar (2000) evaluated the usefulness of interferometric SAR (InSAR) and high-resolution (8 m) RADARSAT imagery in identifying meter-scale landslide features, thereby assisting in hazard mapping. They found InSAR data to be the most useful for detailed geomorphic characterization and identification of landslide features in high relief terrains, and RADARSAT data useful for identifying more regional landslide features in mountainous areas.

Landslide Studies

Many studies have investigated landslide hazards. A review of several studies particularly relevant to this study is provided in this section.

Meyer et al. (2001) conducted sediment transport studies in the South Fork Payette River basin in west-central Idaho. They found evidence to indicate that sediment yields in this region are not constant over time, and that climatic variations and related fire regime changes may exert a strong influence on the probability of major erosional events. This study compared sediment yields in the study area to longer term estimates of sediment yields by alluvial fan stratigraphy and work by other investigators. This study also investigated the distinction between saturation-failure events and runoff-generated events after fires and their differing causal factors. Meyer et al. (2001) found that after stand-replacing fires in the Idaho batholith region, storms of sufficient intensity and duration can initiate sediment transport in the form of large debris flows to flood events. Sediment-charged flows are initiated by different mechanisms and at different times over the post-fire period. Intense precipitation occurring within the first few post-fire years produces runoff from bare, burned slopes, which creates progressive sediment bulking on slopes and in channels. Runoff-related events are suppressed by vegetation regrowth, the litter layer, and the lessening of water-repellent soil conditions within the first 5 years or so following fire. Several

years after fire when tree root strength has been lost, saturation and failure of colluvium occurs during prolonged and heavy winter-spring rainfall and often with snowmelt. Slopes remain susceptible to saturation-induced slope failures until deep roots have been reestablished, regardless of vegetation regrowth.

Cannon (2001) and Cannon et al. (2001a,b) have extensively studied debris flow initiation after fires in drainage basins located in Colorado, New Mexico, and southern California. Their studies indicate that debris flows are not the dominant erosive response from burned basins; rather, most of the burned basins evaluated produced sediment-laden streamflow or no discernible response. They classed debris flows into two groups, Type 1 and Type 2. Type 1 debris flows consist of poorly sorted, matrix supported, and up to boulder-sized materials. Most of these types of flows are initiated through a process of progressive sediment bulking of surface runoff. These flows are produced from basins in which 5-100% of the basin experienced moderate to high burn severity. Most of these flows occur without the presence of a water-repellent soil layer. Type 2 debris flows consist primarily of poorly-sorted sand and gravel-sized material in an abundant matrix that is rich in charcoal and ash. Type 2 debris flows transport finer material and thus are less destructive than Type 1 debris flows. Type 2 debris flows appear to be initiated exclusively through runoff dominated processes, and tend to occur in areas with a discontinuous water-repellent layer. They may be produced from basins that experience anywhere from 8-100% burn.

Gritzner et al. (2000) utilized 30-m DEM's to test Geographic Information System (GIS) modeling, chi-square analysis, Bayesian probability modeling, and cumulative frequency curves to predict landslide locations in the Middle Fork Payette River basin in Idaho. Evidence suggests that slope and elevation are significantly related to landslide occurrence in the study area. They attribute the perplexing relationship between elevation and landslides to the location of logging roads at certain elevations. The locations of these logging roads were not adequately mapped so they could not be included in the input data. Their study found that GIS offers a useful method of documenting many key variables driving landslide risk and developing maps of landslide hazard, and that usefulness of this methodology is limited by the coarse resolution of the 30-m DEM's.

Benavides-Solorio and MacDonald (2001) used field study and rainfall simulation on small plots of land in the Colorado Front Range to evaluate those factors contributing to landslide hazards in Colorado. Site variables such as burn severity, percent vegetative cover, soil water repellency, soil moisture, time elapsed since burning, and slope angles were evaluated in relation to how they corresponded to runoff and sediment yields. Final analysis indicated that burn severity did not significantly affect runoff rates, but had a significant impact on the sediment yield. Sediment yield of high-severity fire plots produced 4.5-4.8 times as much sediment as moderate severity plots, and 10-26 times as much sediment as low severity and unburned plots. A similar study by Johansen et al. (2001) indicates that the runoff from burned plots was about 45% of the total precipitation applied, and only 23% from the unburned plots. However, burned plots generated 25 times more sediment than unburned plots.

METHODS

FIELD STUDY

The three specific study areas (Sites #1-3) within the Yellowjacket Mountains were identified during June of 2001 (Figures 2, 3). Site #4 was evaluated with remote sensing data only and is discussed in Chapter 3. Sites #1-3 are approximately one km² each and were selected due to the varying slopes, aspects, burn severity, amount of understory vegetation cover, hydrology, bedrock geology, and soil characteristics exhibited. These parameters were mapped in the field during June, July, and August of 2001 and 2002.

In order to assess the relative landslide and erosion hazards of the study areas, two relative hazard classification systems were developed for this study. One relative hazard classification system is specifically for landslides, and considers parameters including: slope, aspect, burn severity, hydrology, bedrock geology, and soil characteristics (Table 3). The other relative hazard classification system is specifically for erosion, and considers the same parameters with the addition of understory vegetation cover (Table 4). In order to develop a relative hazard map, every parameter within each system was assigned a relative hazard ranking of ordinal numbers 0-10, with 10 being more likely to influence the occurrence of landslides or erosion and zero most likely to have no effect. This range was specifically selected so that parameters could be given different weighting in the classification system. For example, parameters hypothesized to have more influence on the occurrence of landslides and erosion were assigned values closer to 10, whereas parameters hypothesized to have less influence on the occurrence of landslides and erosion were assigned values closer to zero. The rankings of each parameter were compared to other parameter ranking values within the classification system in order to verify that the numbers were accurately weighted. For example, it is hypothesized for this study that an area of high burn severity (ranked with a value of 10) has the same propensity for landslides and erosion as an area with surface water present (also ranked with a value of 10). The following sections describe the assignment of ordinal numbers to the aforementioned parameters.

Table 3. Relative hazard ranking values for landslides within study areas (SF = Safety Factor).

Slope	Aspect	Hydrology
>55° (SF < 0.5) = 10 35-55° (0.5 ≤ SF < 1.0) = 9 20-34° (1.0 ≤ SF ≤ 2.0) = 2 0-19° (SF > 2.0) = 1	North = 1 East & West = 2 South = 3	Surface water present = 10 Surface water not present = 0
		Geology
		Sandstones/siltstones = 1 Granites = 2 Challis Volcanics = 4
	Burn Severity	**Soil Characteristics**
	High = 10 Moderate = 9 Low = 8 Unburned = 0	Sand = 4 Silt = 5 Clay = 3

Table 4. Relative hazard ranking values for erosion within study areas.

Slope	Aspect	Hydrology
50-90° = 10 45-49° = 9 40-44° = 8 35-39° = 7 30-34° = 6 25-29° = 5 20-24° = 4 15-19° = 3 10-14° = 2 5-9° = 1 0-4° = 0	North = 3 East & West = 2 South = 1	Surface water present = 10 Surface water not present = 0
	Burn Severity	**Geology**
	High = 10 Moderate = 9 Low = 8 Unburned = 0	Sandstones/siltstones = 1 Granites = 2 Challis Volcanics = 4
	Understory Vegetation Cover	**Soil Characteristics**
	0-25% = 5 26-50% = 4 51-75% = 3 >75% = 2	Sand = 4 Silt = 5 Clay = 3

Slope

Slope is perhaps one of the most significant factors influencing landslides and erosion (Dunne and Leopold, 1978; Ritter et al., 1995; Wilson et al., 2001). Slope was measured quantitatively in the field using a hand-held clinometer. Slope rankings are calculated differently for landslides and erosion, because the factors that influence these processes are different. For landslides, slope stability represents a balance between driving forces (shear stress) and resisting forces (shear strength). This ratio is known as the Factor of Safety equation (Ritter et al., 1995):

$$\text{Factor of Safety} = \frac{c + (\gamma h \cos^2\theta - ')\tan\phi}{(\gamma h \sin\theta \cos\theta)}$$

where c = cohesion, kilonewtons/square meters (kN/m²)
γ = weight, kilonewtons/cubic meters (kN/m³)
h = height of the water table above the slide plane, m
' = pore pressure, kN/m²
ϕ = friction angle, degrees
θ = slope angle, degrees

Shear stress and shear strength were not measured quantitatively in the field; therefore, slope rankings for the landslide hazard classification system were determined by calculating the Factor of Safety for slopes in the study areas between 0-90º (Figure 5, Table 5). Soils in the field areas are generally dry, and saturation values are assumed to be zero for this study. Soils are predominantly cohesionless and cohesion is expected to play a smaller role than the friction angle, thus cohesion values are assumed to be zero for this study. A friction angle of 35º was assumed to be representative of the soil types (mostly sandy) in the field areas.

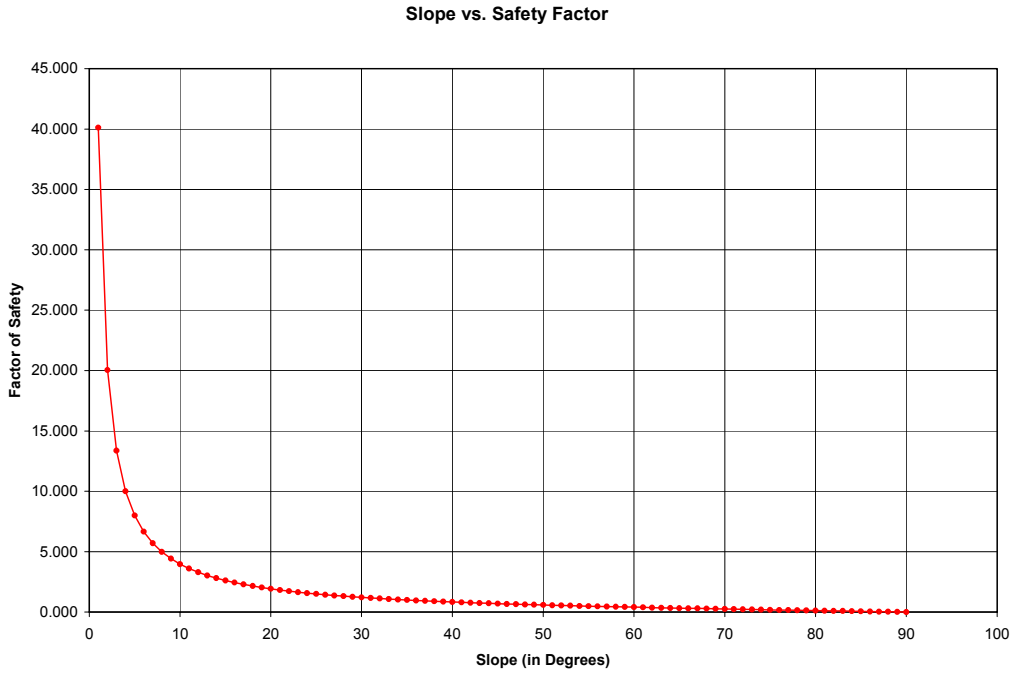

Figure 5. The relationship between slopes and Safety Factors (SF) in dry, cohesionless soils with a friction angle of 35º. Slopes with a SF greater than 1 indicate stable slopes, and values below 1 indicate a slope is prone to failure.

Slopes with a Safety Factor greater than 1 indicate stable slopes, and values below 1 indicate slope failure. Therefore, slopes with a Safety Factor greater than 2 (0-19º) are assumed to be most stable and ranked with a value of 1. Slopes with a Safety Factor of 1-2 (20-34º) are assumed to be stable and assigned a value of 2. Slopes with a Safety Factor of 0.5-1.0 (35-55º) have attained the critical value of 35º and are much more prone to failure than slopes of 34º or less; therefore, these slopes are ranked with a value of 9. Slopes with a Safety Factor less than 0.5 (greater than 55º) are assumed to be most prone to failure and assigned a value of 10.

Slope rankings for the erosion hazard classification system were determined by calculating the sine of the slope angle between 0-90º. In general, steeper slopes will be more prone to erosion due to several factors. The most important factor is the increasing shear stress with increasing slope steepness. In addition, water runoff will have a higher velocity on steeper slopes and thus be able to move more sediment and sediments with larger particle size. Rainsplash detachment on steeper slopes will move sediments greater distances down slope. For this study, it is hypothesized that erosion will increase with increasing slope (and hence, increasing shear stress). Therefore, slopes between 0-4º are ranked with a value of zero, slopes between 5-9º are ranked with a value of 1, and slopes between 10-14º are ranked with a value of 2. Slopes between 15-19º are ranked with a value of 3, slopes between 20-24º are ranked with a value of 4, and slopes between 25-29º are ranked with a value of 5. Slopes between 30-34º are ranked with a value of 6, slopes between 35-39º are ranked with a value of 7, slopes between 40-44º are ranked with a value of 8, and slopes between 45-49º are ranked with a value of 9. Slopes of 50º and greater are ranked with a value of 10, because such steep slopes will be highly prone to erosion where there is soil present.

Table 5. The relationship between slopes and Safety Factors (SF) in dry, cohesionless soils with a friction angle of 35º.

Slope, degrees	Safety Factor	Slope, degrees	Safety Factor	Slope, degrees	Safety Factor
1	40.115	31	1.165	61	0.388
2	20.051	32	1.121	62	0.372
3	13.361	33	1.078	63	0.357
4	10.013	34	1.038	64	0.342
5	8.003	35	1.000	65	0.327
6	6.662	36	0.964	66	0.312
7	5.703	37	0.929	67	0.297
8	4.982	38	0.896	68	0.283
9	4.421	39	0.865	69	0.269
10	3.971	40	0.834	70	0.255
11	3.602	41	0.805	71	0.241
12	3.294	42	0.778	72	0.228
13	3.033	43	0.751	73	0.214
14	2.808	44	0.725	74	0.201
15	2.613	45	0.700	75	0.188
16	2.442	46	0.676	76	0.175
17	2.290	47	0.653	77	0.162
18	2.155	48	0.630	78	0.149
19	2.034	49	0.609	79	0.136
20	1.924	50	0.588	80	0.123
21	1.824	51	0.567	81	0.111
22	1.733	52	0.547	82	0.098
23	1.650	53	0.528	83	0.086
24	1.573	54	0.509	84	0.074
25	1.502	55	0.490	85	0.061
26	1.436	56	0.472	86	0.049
27	1.374	57	0.455	87	0.037
28	1.317	58	0.438	88	0.024
29	1.263	59	0.421	89	0.012
30	1.213	60	0.404	90	0.000

Aspect

Slope aspect has been found to influence hillslope processes such as landslides and erosion in several studies (Crozier et al., 1980; Churchill, 1982; Dragovich et al., 1993a). Many studies have found that the greatest percentage of landslides occurs on equator-facing slopes, and only a small percentage occurs on pole-facing slopes. Selby (1993) notes that more insolated slopes in humid environments undergo more wetting/drying cycles with greater soil cracking. This leads to more macropore development, higher infiltration, and higher pore-water pressures. Increased soil cracking may also increase the water holding capacity, so that soils on sunny slopes may exceed or hold their liquid limit volume of water (Selby, 1993). However, Churchill (1982) found that erosion is more pronounced on pole-facing slopes in humid environments because the dry conditions on equator-facing slopes reduce weathering and fluvial erosion.

Slope aspect was evaluated in the field by using a Brunton compass. Since several studies have demonstrated that most landslides occur on equator-facing slopes, in the relative hazard classification system for landslides, southern slopes were assigned a value of 3, eastern and western slopes a value of 2, and northern slopes a value of 1. Due to Churchill's (1982) findings that erosion is more pronounced on pole-facing slopes, in the relative hazard classification system for erosion, southern slopes were assigned a value of 1, eastern and western slopes a value of 2, and northern slopes a value of 3. The parameter of aspect is hypothesized to have less influence on slope stability than the parameter of slope, hence the lower ranking values.

Burn Severity

Many studies have shown dramatic increases in the amount of landslides and erosion following forest fires (Benavides-Solorio and MacDonald, 2001; Cannon, 2001; Cannon et al., 2001a,b; Meyer et al, 1992; Meyer et al., 2001). This study considers burn severity to be a major factor influencing landslides and erosion, similar to the influence of slope. As defined by Key and Benson (2002), burn severity is the degree of environmental change caused by fire. Thus, field estimation of burn severity requires consistent judgment on the part of the observers.

For this study, two researchers evaluated burn severity in the study areas and compared findings to obtain as much consistency as possible. Burn severity was assessed by using the Landscape Assessment methodology (Key and Benson, 2002), which provides burn severity factor ratings as follows: % green is the percentage of crown foliage (living or dead) unaltered by fire relative to estimated pre-fire crown volume; % black is the black (non-living) crown foliage that actually caught fire, stems and leaves included, relative to estimated pre-fire crown volume; and % brown is the percentage of tree canopy affected by scorch or girdling, without direct flame contact, relative to estimated pre-fire crown volume plot-wide. In this study, areas with greater than 50% black are considered to be high severity and ranked with a value of 10. Areas with less than 50% black but greater than 50% brown are considered moderate severity and ranked with a value of 9. Areas with greater than 50% green and less than 50% brown or black are considered as low severity and assigned a value of 8. Unburned areas are not immune from landslides or erosion due to other factors (e.g., slope, surface hydrology), but the parameter of burn severity is intended to isolate burn effects. Therefore, unburned areas were assigned a value of zero.

Understory Vegetation Cover

Vegetation helps to stabilize slopes by various mechanisms and to varying degrees. Vegetation removes moisture from the soil via evapotranspiration, and roots enhance soil cohesion (Dragovich et al., 1993b). Leafy vegetation decreases the rate at which precipitation is delivered to the soil, so the absence of this type of vegetation may lead to erosion by surface runoff and rainsplash detachment. The presence of vegetation to intercept precipitation is particularly significant after storm events. Understory vegetation cover, such as brush and grass, is effective in reducing surface erosion such as rilling, gullying, and sheet wash, but is not significant in reducing large-scale mass movements such as landslides. Therefore, the ranking of understory vegetation cover is only relevant to erosion.

Understory vegetation cover was visually estimated in the field. For erosion considerations, slopes exhibiting understory vegetation cover from 0-25% are assumed to be less stable for the reasons previously stated, and were assigned a value of 5. Slopes with increasing cover are

assumed to be increasingly stable, and thus slopes with 26-50% cover were assigned a value of 4, slopes with 51-75% cover were assigned a value of 3, and slopes with greater than 75% cover were assigned a value of 2. The parameter of understory vegetation cover is hypothesized to have a slightly greater influence than the parameter of aspect, and much less influence than the parameters of slope and burn severity.

Hydrology

Areas with surface water present are significantly more likely to experience landslides and erosion than dry areas. This is because water is a primary contributor to erosion, and perched groundwater causes increased pore water pressure in soils which contributes to the increased likelihood of landslides (Dunne and Leopold, 1978). It is difficult to assess the influence of streams without an understanding of the hillslope hydrology, and it is not clear if streams within the study areas are fed by groundwater systems or originate from snow melt at higher elevations. Therefore, areas with surface water such as springs and streams were ranked with a value of 10. Areas lacking evidence of surface water are not immune from landslides or erosion due to other factors (e.g., slope, burn severity), but the parameter of hydrology is intended to isolate hydrological effects. Therefore, areas lacking evidence of surface water were ranked with a value of zero. The parameter of hydrology is hypothesized to have as much influence on slope stability as the parameters of slope and burn severity, and a much greater influence than the parameters of aspect and understory vegetation cover.

Bedrock Geology

The geology of Sites #1-3 was mapped in the field at a scale of 1:24,000; however, assigning a relative hazard classification system to the bedrock geology was fairly difficult because the relationships between rock lithology and landslides and erosion within the study areas have not been previously studied. In addition to the lithology, landslides may also be influenced by structural features, such as bedding planes and jointing, within the unit. Soil can slide down-slope along bedding planes in areas where dip-slopes are parallel to bedding (Dragovich et al., 1993a). Bedrock units that contain no bedding planes or significant jointing may be stronger than units that display these structural features. Lithology is assumed to have less influence on landslides and erosion than several other parameters considered in this study, so the parameter of bedrock geology was given less weight in the overall ranking.

As previously stated, there are seven main bedrock types within the study sites, and each bedrock type possesses distinct soil-forming and sediment yield characteristics. The Type Yellowjacket Formation and the Cobalt Yellowjacket Formation are primarily slope-forming and weather to sand and silt; thus movement may occur as debris flow or as soil creep in those areas with relatively thick soil development. These units within the study areas are ranked with a relative value of 1 because they are highly cohesive and have little soil development. Slopes are more prone to landslides in cases where the bedding plane orientation is the same as the slope direction; thus these areas would be assigned a value of 2. This circumstance was not evidenced in Sites #1-3, and the geologic map of Site #4 is at too gross of a scale (1:100,000) relative to the slope dataset (10 m) for determination of this circumstance. The Hoodoo Quartzite is highly indurated and fairly resistant to weathering. Little or no movement is expected to occur in this unit, as this rock weathers into angular fragments of quartzite. Areas with these lithologies are also ranked with a relative value of 1. The Ordovician or Middle Proterozoic granites, Mesozoic granitic rocks of the Idaho batholith, and Tertiary granites are primarily ledge-forming and

weather to form grus. This type of lithology is not as cohesive as the Type Yellowjacket and Cobalt Yellowjacket formations so these units are ranked with a value of 2. The Challis Volcanics are ledge-forming and weather to medium- to fine-grained sand. Movement may occur as debris flow or as soil creep in those areas with relatively thick soil development. A small meter-scale landslide was observed in the Challis Volcanics in Site #2 during year 2001 field studies, and this lithology is considerably more friable than the other relevant lithologies. Therefore, areas with this lithology are ranked with a value of 4. The parameter of bedrock geology is hypothesized to have a similar influence on slope stability as that of aspect, a slightly lesser influence than the parameter of understory vegetation cover, and much less influence than the parameters of slope, burn severity, and hydrology.

Soil Characteristics

Soil characteristics can influence landslides and erosion in two primary ways. First, different soil types have different infiltration capacities. Coarse-textured soils such as sands have larger pores that allow them to drain more easily than the fine pore structures in clays (Dunne and Leopold, 1978). As noted by Dragovich et al. (1993b), cohesive fine-grained soils are generally more likely to undergo deep-seated failures, and non-cohesive coarse-grained soils tend to fail by shallow processes.

The second important consideration is how easily soil can be transported, which affects erosion processes. Silt, which is smaller in size than sand, can be easily picked up by water and transported. Clay is more cohesive in nature, and thus is not as easily entrained. Taking all of these variables into consideration, silt was assigned a value of 5, sand a value of 4, and clay a value of 3. The parameter of soil characteristics is hypothesized to have a similar influence on slope stability as that of understory vegetation cover, a slightly greater influence than the parameters of aspect and bedrock geology, and much less influence than the parameters of slope, burn severity, and hydrology.

Soils were evaluated in the field by digging soil pits to bedrock depth, and then classifying the soil texture and color according to the Unified Soil Classification System (USCS)(McCarthy, 2002). Soil moisture and organic content were visually evaluated and, in general, soils were found to be dry with little organic content.

REMOTE SENSING STUDY

Potential sites for this study were first identified by using Landsat-7 Enhanced Thematic Mapper (ETM+) imagery and aerial photographs taken one month after the fires of summer 2000. The potential sites were compared to archived Landsat-5 TM data to contrast the amount of vegetation present prior to these fires.

Two IKONOS 11-bit images were used to evaluate the four sites chosen for this study. IKONOS is a commercial (owned by Space Imaging, Inc.) high-resolution Earth imaging satellite that provides 4-m multispectral spatial resolution. The two images were acquired September 9, 2001, at 18:40 and 18:41 Greenwich Mean Time (GMT) with a sun elevation of 48° and an azimuth angle of 159°. The multispectral data includes the following wavelengths of the electromagnetic spectrum: blue = 444.7-516.0 nanometers (nm); green = 506.4-595.0 nm; red = 631.9-697.7 nm; and near-infrared (NIR) = 757.3-852.7 nm. ENVI 3.5 (RSI, 2002) was used to mosaic and

evaluate the IKONOS imagery. The digital number (DN) values were converted to radiance values prior to all classifications by:

(DN_i) / (Radiometric Calibration Coefficient)
where i = 1 to z; z = number of pixels in image

Note: Radiance values were calculating based on conversion values provided by Space Imaging (Table 6).

Table 6. Calibration coefficients for IKONOS imagery (Space Imaging, 2002) (mW = megawatts, sr = steradian).

Radiometric Calibration Coefficient	Blue	Green	Red	NIR
$DN/(mW/cm^2 \times sr)$	728	727	949	843

Supervised and unsupervised classifications and transformations were then performed using all bands to determine which site parameters (burn severity, amount of understory vegetation cover, hydrology, bedrock geology, and soil characteristics) could be analyzed with the imagery. Burn severity and vegetation cover can be assessed with supervised classifications and transformations using ENVI 3.5 (RSI, 2002). It was not necessary to use IKONOS imagery to assess slope and aspect, as these features can be readily evaluated using 10-m DEM's. The hydrology within Sites #1-3 was in the form of small springs and streams less than 2 m, and so could not be detected by IKONOS data. Bedrock geology could not be assessed using IKONOS data because there are relatively few rock outcrops within the study areas, and most are obscured by vegetative cover. To assess the geology of Sites #1-4 remotely, a geologic map was compiled from pre-existing data mapped at a scale of 1:100,000 and digitized for this study. Soil type and soil characteristics are difficult to evaluate without adequate ground exposure and hyperspectral imagery. The following sections describe the assessments of burn severity and vegetative cover using IKONOS imagery.

Burn Severity Assessment

Burn severity can be mapped based on the reflectivity of soils and vegetation in the four multispectral bands. Burn severity was assessed by performing supervised and unsupervised classifications, and these classifications were then used to evaluate relative susceptibility to landslides and erosion. In contrast to supervised classifications, unsupervised classifications require minimal input from the analyst. The two unsupervised algorithms experimented with in this study were the IsoData and K-Means classifications. In these classifications, the software performs numerical operations that search for natural groupings of the spectral properties of pixels. The computer selects the class means and covariance matrices to be used in the classification. Neither of these algorithms produced results similar to the field mapping results.

Supervised classifications for burn severity were performed by selecting regions of interest or training classes that correlate with a specific burn severity (Figure 6). For example, there were four classes of burn severity mapped in the field (high, moderate, low, and unburned). An additional training class was developed for areas of high reflectance (outcrops, roads, and bare

ground) as these features would be incorrectly classified using burn severity classifications only. Thus a total of five training classes in each study site were utilized.

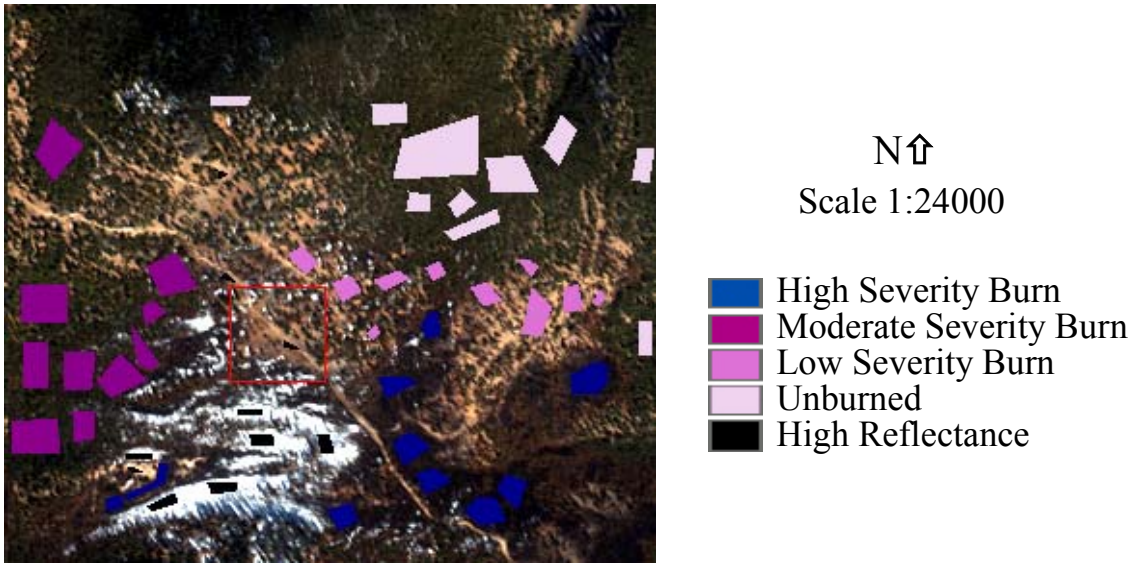

Figure 6. Training sites of Site #2. Red box indicates small meter-scale landslide observed during summer 2001 field study.

The accuracy of training site selection may be assessed using a bootstrap method. This is done by simply selecting extra training sites (bootstrap sites) that will not be used in the classification. These bootstrap training classes may then be compared to the classification results to evaluate the overall accuracy.

As noted by Jensen (1996), the general rule is that if training data are being extracted from *n* bands, then at least 10*n* pixels of training data are necessary for each class. Four IKONOS bands (blue, green, red, and NIR) were used to extract the training data in this study. Jensen's (1996) recommendation was modified for this study to reflect the small areal extent of Sites #1-3. For the three smaller study sites (Sites #1, #2, and #3), twelve areas of each training class (five training classes) were selected for a total of sixty training sites for burn severity in each study site. Training sites ranged in size between 1 and 1,000 pixels. Ten of the twelve sites were used for classification, and the remaining two were used for a bootstrap method accuracy check. For the larger study site (Site #4), fifty-five areas of each type of training site were selected for a total of two hundred and seventy-five training sites for burn severity. Fifty of the fifty-five sites were used for classification, and the remaining five were used for a bootstrap method accuracy check.

The four classes of burn severity were ranked with the same values as those used in field mapping. High burn severity was ranked with a value of 10, moderate severity was ranked with a value of 9, low burn severity was ranked with a value of 8, and unburned areas were ranked with a value of zero. The training class developed for areas of high reflectance (outcrops, roads, and bare ground) was assigned a value of zero so that these features would not influence the burn severity classifications.

The parallelepiped, spectral angle mapper (SAM), maximum likelihood, and minimum distance algorithms were evaluated to ascertain which classification algorithm yielded results matching closest to field mapping results. The parallelepiped algorithm uses a range of minimum and maximum DN values to classify each pixel in parallelograms fitted over the scatterplot data. This method is computationally simple, but there can be difficulty if training categories overlap. If a pixel value lies above the lower threshold and below the higher threshold for all *n* bands being classified, it is assigned to that class. If the pixel value falls in multiple classes, the pixel is assigned to the last class matched. This algorithm did not provide results similar to field mapping results, possibly due to training category overlap.

The SAM algorithm compares the angle between the endmember spectrum (considered as an *n*-dimensional vector, where *n* is the number of bands) and each pixel vector in *n*-dimensional space. Smaller angles represent closer matches to the reference spectrum. This algorithm uses the spectral pattern of the data rather than the statistical distribution pattern (Sohn and Rebello, 2002). SAM did not predict moderate burn severity appropriately, and all burn severities were overpredicted.

The maximum likelihood algorithm assumes that the statistics for each training class are normally distributed and assigns each pixel to the class that has the highest probability. This is a complex, statistically-based algorithm that requires large computations. No probability threshold was set for this classification. This algorithm yielded slightly better results than the parallelepiped algorithm. It is likely that this algorithm did not provide results similar to field mapping because, in this case, the statistics for each training class are not normally distributed.

The minimum distance algorithm uses the mean vectors of each endmember to calculate the Euclidean distance from each unknown pixel to the mean vector for each class. Pixels are classified to the nearest class. This is a mathematically simple technique but may sometimes be insensitive to different degrees of variance in the data. The maximum standard deviation from the mean and the maximum distance error thresholds were both set to zero. This algorithm provided results in best agreement with the field mapping data. Therefore, this algorithm was used for subsequent analysis. The accuracy of all burn severity classifications was assessed by comparing the bootstrap training sites to the minimum distance classifications (discussed in Section 4.2). Accuracy was also assessed using a pixel-by-pixel statistical comparison of field and remote sensing data, which is discussed in Section 2.4.

Vegetation Cover Assessment

There are several methods of assessing vegetation cover with remote sensing data, including the Composite Burn Index (CBI), the Normalized Burn Ratio (NBR), the Normalized Difference Vegetation Index (NDVI), and the Soil-Adjusted Vegetation Index (SAVI). The CBI is designed to correlate burn severity effects on vegetation as measured in the field to those observed with Landsat TM data (Key and Benson, 1999a). The NBR is a temporal index formulated from Landsat TM bands 4 and 7 and compares temporal indices to discriminate burn characteristics (Key and Benson, 1999b). The NDVI is the difference of the NIR band and the red band divided by the sum of the NIR band and the red band, or (NIR-Red)/(NIR+Red). The SAVI proposed by Huete (1988) is similar to the NDVI with added terms to adjust for different brightnesses of background soil. SAVI is the NDVI multiplied by (1 + L), where L varies between 0-1

depending on the amount of visible soil (note that when L = 0, SAVI = NDVI). When the amount of visible soil in unknown, L = 0.5 is often used. For this study, it is expected that L will vary greatly due to the disparity of burn severities and thus SAVI was not used.

This study utilizes the NDVI to specifically assess vegetation cover displayed by IKONOS data. The NDVI is a widely-used transformation because it is a good indicator of biomass. NDVI values fall between -1 and +1. Higher NDVI values indicate more green vegetation and appear bright. For example, green vegetation generally has NDVI values greater than zero, soils have values close to zero, and water has values less than zero.

In order to determine what NDVI values should represent the ranking values used for understory vegetation cover, NDVI values were compared to field mapping results. These comparisons indicate that study areas with 0-25% understory vegetation cover typically have NDVI values from -1 to -0.5, and thus were assigned a value of 5. Since these areas do not contain water, the low values may be due to the heterogeneous soil cover and ash. Study areas with 26-50% cover have NDVI values between -0.5 and zero, and were assigned a value of 4. Areas with 51-75% cover have NDVI values between zero and 0.5 and were assigned a value of 3. Areas with greater than 75% cover have NDVI values from 0.5 to 1.0 and were assigned a value of 2. NDVI values were imported into ArcMap 8.2 (ESRI, 2002) and reclassified according to these findings. Accuracy was assessed using a pixel-by-pixel statistical comparison of field and remote sensing data, which is discussed in Section 2.4.

GEOGRAPHIC INFORMATION SYSTEM (GIS) STUDY

ArcView 3.3 (ESRI, 2002) was used to create GIS coverages for this study. Coverages were created for each study site and the respective parameters measured in the field, including slope, aspect, burn severity, amount of understory vegetation cover, hydrology, bedrock geology, and soil characteristics. Slope and aspect coverages were developed by using USGS 10-m DEMs rather than by measurements made in the field in order to provide a more comprehensive assessment.

ArcMap 8.2 (ESRI, 2002) was used to convert the GIS coverages from field measurements into raster images. To produce a relative hazard map for landslides, the coverages for slope, aspect, burn severity, hydrology, bedrock geology, and soil characteristics were summed using raster arithmetic. The raster images for slope and aspect were produced with 10-m USGS DEMs, and therefore the arithmetic product has a resolution of 10-m. To produce a relative hazard map for erosion, the sum of these coverages was added to the coverages for understory vegetation cover.

The NDVI transformations and minimum distance classifications were imported into ArcMap 8.2 (ESRI, 2002) and converted to raster images. Unfortunately, there are no soil or fine-resolution hydrology GIS coverages or maps available for the study sites. The 1:100,000-scale geological map that was compiled and digitized specifically for this study was imported to represent the bedrock geology of each site. To produce a relative hazard map for landslides using information not directly obtained from field measurements, raster arithmetic was used to sum the 10-m USGS DEMs for slope and aspect, 4-m minimum distance classifications for burn severity, and the 1:100,000-scale compiled map for bedrock geology. The arithmetic product has a resolution of 10-m (note that the resolution of the geologic map is significantly coarser). To

produce a relative hazard map for erosion, the sum of these coverages was added to the 4-m NDVI raster image for understory vegetation cover.

STATISTICAL COMPARISON OF FIELD AND REMOTE SENSING DATA

The ranking of the parameters derived from field mapping versus remote sensing data were compared by calculating the kappa coefficient, K. K is a measure of association used to describe and test the degree of agreement in classifications (Koch, 1983; Kraemer, 1983). Classification results are grouped into a contingency table to summarize the proportions of correct and incorrect classifications. For example, a simple summary table, known as a 2x2 confusion matrix or error matrix, is as follows:

	Actually Present	Actually Absent
Predicted Present	a	b
Predicted Absent	c	d

where a, b, c, and d represent frequencies of occurrence of possible outcomes from N total outcomes (Welhan, 2003). Actual agreement is indicated by the major diagonal and chance agreement is indicated by the row and column totals (Congalton and Green, 1999). For a 2 x2 confusion matrix, K is defined as:

$$K = \frac{[(a+d) - \{((a+c)(a+b)) + ((b+d)(c+d))\}] / N}{N - [\{((a+c)(a+b)) + ((b+d)(c+d))\}] / N]}$$

Burn severity, vegetation cover, and geology were compared; slope and aspect were not, as these parameters were assessed using the same data source (USGS 10-m DEMs). It is important to note that the final hazard maps were not compared because different parameters could possibly result in the same sum, and thus results would be misleading. For example, an area with high severity burns and no surface water would result in a hazard ranking of 10. This same hazard ranking could also be obtained by an unburned area with surface water.

The field mapping results (and ranking of the specific parameters) are considered the baseline or "accepted" data for the purposes of this study. The remote sensing data was compared to this baseline information. The ranking maps for each of the three parameters for both the landslide and erosion studies at each site were reclassified into values that, when the remote sensing values were subtracted from the field mapping values, would yield unique values (field mapping reclassification values are 25, 50, 75, and 100, and remote sensing reclassification values are 1, 5, 11, and 19) (Table 7). The actual numbers of pixels corresponding to the values in the shaded portion of the table were used to calculate K. The range of K is typically 0-1, with zero corresponding to chance agreement and 1 corresponding to perfect agreement.

Table 7. An example of the 4x4 confusion matrix used to assess the accuracy of the remote sensing burn severity data to field mapping results. The values in the shaded areas will be replaced by the number of pixels corresponding to those values.

		Remote Sensing Reclassification Values			
		1	**5**	**11**	**19**
Field Mapping Reclassification Values	**25**	24	20	14	6
	50	49	45	39	31
	75	74	70	64	56
	100	99	95	89	81

RESULTS

FIELD STUDY AND GIS

Each of the three study sites is approximately one km² and varies in elevation between approximately 1,700-2,600 m. Each site exhibits varying slopes, aspects, burn severity, amount of understory vegetation cover, hydrology, bedrock geology, and soil characteristics. These parameters were mapped in the field during June, July, and August of 2001. Field studies during June, July, and August of 2002 investigated active mass wasting processes and evaluated landslide and erosion hazard susceptibility predictions. The following sections detail the field-based data.

Site #1: Quartzite Mountain

Site #1 is located north of Quartzite Mountain (Figure 2) and covers an area of 0.90 km². Elevation ranges between 2,347-2,621 m. The predominant types of vegetation are Douglas fir and pinegrass.

Parameters

Slope and Aspect

Slopes range between 0-36° (Figure 7) and the predominate aspect is northern (Figure 8).

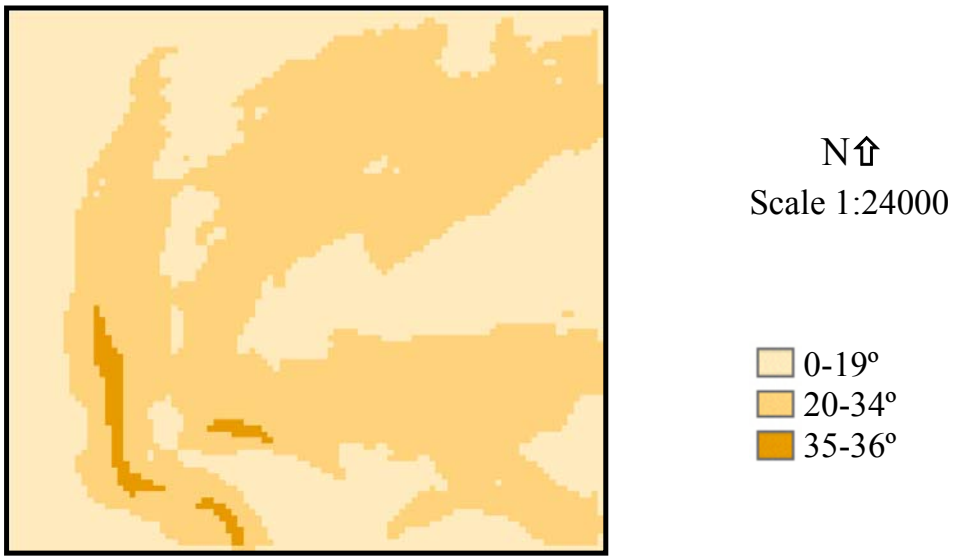

Figure 7. Slopes of Site #1. (Derived from USGS Blackbird Mountain DEM, 10-m resolution.)

Figure 8. Aspects of Site #1. (Derived from USGS Blackbird Mountain DEM, 10-m resolution.)

Burn Severity

The burn intensities of Site #1 include all degrees of severity (Figure 9). High severity burns, ranked with a value of 10 for this study, cover 80% of the total site area. Moderate severity burns were ranked with a value of 9 and cover 8% of the site. Low severity burns were ranked with a value of 8 and cover 9% of the site. A small area of the site, 3%, is unburned and was ranked with a value of zero.

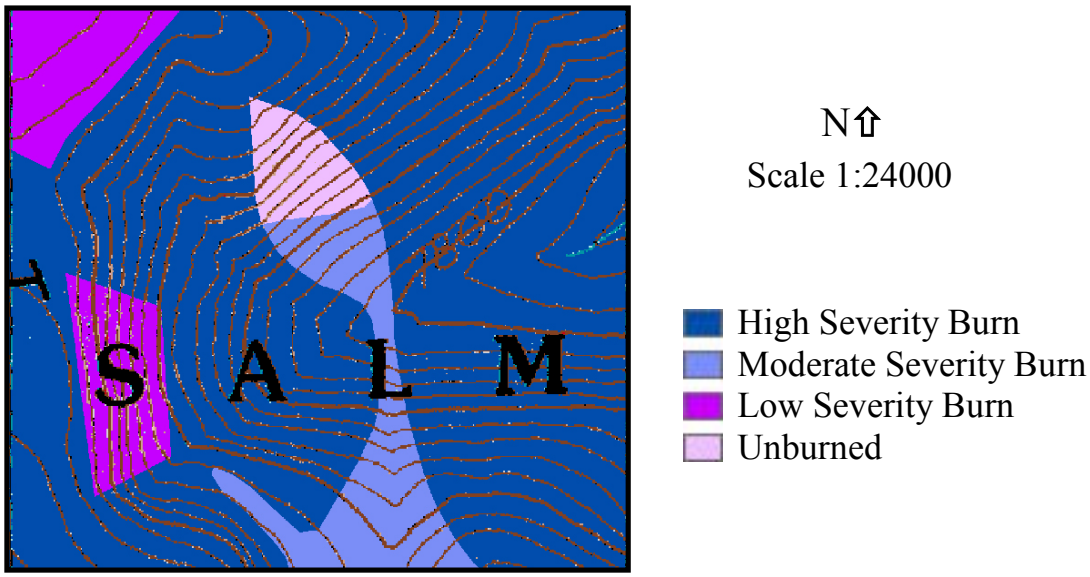

Figure 9. Burn severities of Site #1. (Base map from USGS Blackbird Mountain 7.5 Minute Quadrangle.)

Understory Vegetation Cover

Most of this site, 81% of the total area, has 0-25% understory vegetation cover (Figure 10). These areas were ranked with a value of 5. The remaining 19% of the area has greater than 75% cover, and was ranked with a value of 2.

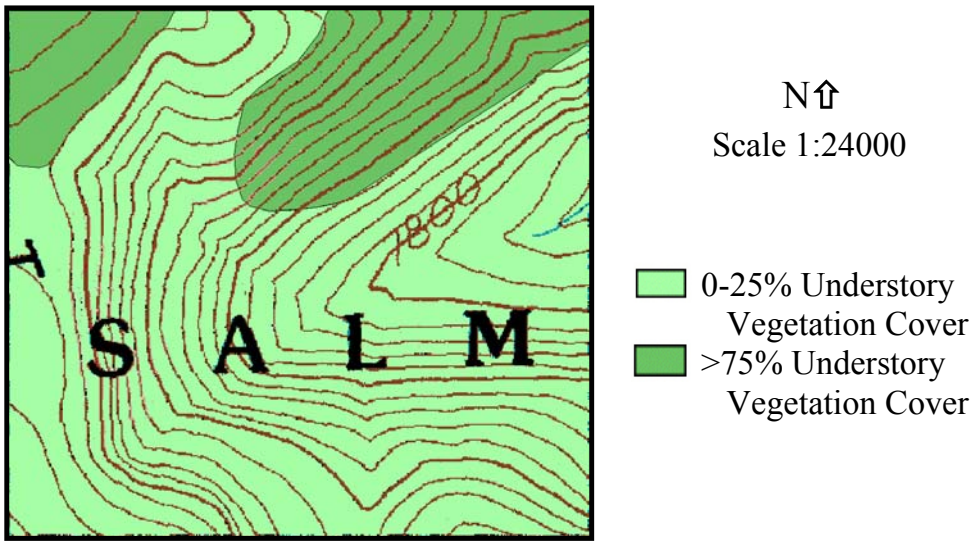

Figure 10. Understory vegetation cover of Site #1. (Base map from USGS Blackbird Mountain 7.5 Minute Quadrangle.)

Hydrology

A large percentage of this site, 96%, contains no surface water (Figure 11). These areas were ranked with a value of zero. Only 4% of the site has surface water, which is in the form of small springs that originate in the south and west portions of the site and feed into a small creek at the east side of the site. These areas were ranked with a value of 10.

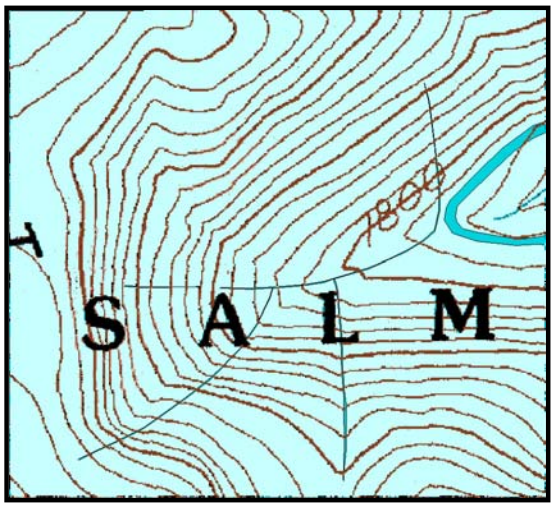

Figure 11. Hydrology of Site #1. (Base map from USGS Blackbird Mountain 7.5 Minute Quadrangle.)

Geology

The bedrock in most of the study area consists of west-dipping thin-bedded microlaminated fine-grained sandstone (Figure 12). These rocks are mapped as "type" or "lower" Yellowjacket Formation by Ekren (1988) and Tysdal (2000). Winston et al. (1999) mapped these units as the argillaceous quartzite unit of Ekren (1988) which lies stratigraphically above the Hoodoo Quartzite. In the southeast portion of the study area, the bedrock consists of west-dipping thin-bedded siltite and fine-grained sandstone with characteristic convoluted cracks in silt filled with fine sand. These rocks are identical to outcrops of the Wallace Formation along the Salmon River and are mapped as Apple Creek Formation by Tysdal (2000). A south-dipping normal fault mapped by Tysdal (2000) runs along the prominent gully in the southeast part of the study area and separates the two stratigraphic units. As this site is primarily composed of cohesive sandstones and siltstones, it was ranked with a value of 1.

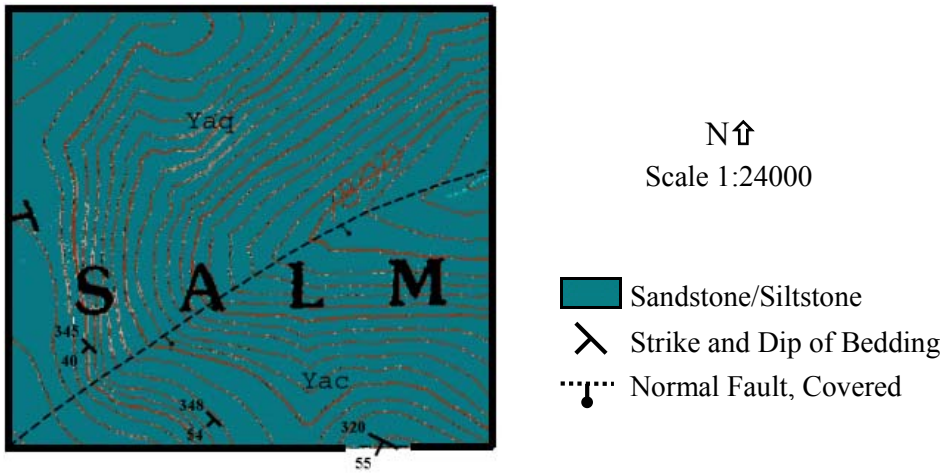

Figure 12. Geology of Site #1. A south-dipping normal fault runs along the prominent gully and separates fine-grained sandstone (Yaq) from siltite and fine-grained sandstone (Yac). (Base map from USGS Blackbird Mountain 7.5 Minute Quadrangle.)

Soil Characteristics
All of the soil evaluated in this site is sandy silt, which was assigned a value of 5 (Figure 13).

Landslide and Erosion Hazard Ranking
The relative hazard map for landslides incorporates the parameters of slope, aspect, burn severity, hydrology, bedrock geology, and soil characteristics. The relative values for landslide hazard range between 9-31, with 9 being relatively less likely to experience landslides and 31 being more likely (Figure 14). Small areas with high values occur in the southern and northeastern portion of the site. The northern portion of this site has a large area with moderately high values.

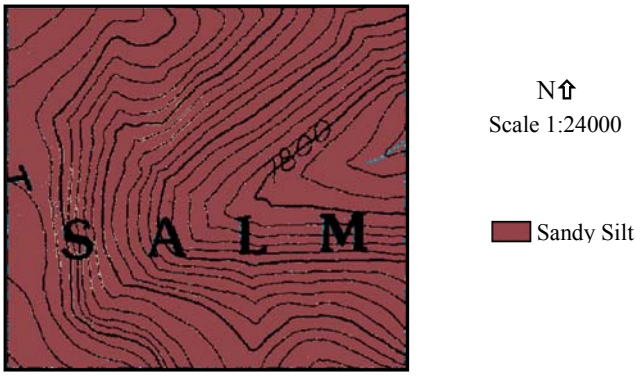

Figure 13. Soil type of Site #1. (Base map from USGS Blackbird Mountain 7.5 Minute Quadrangle.)

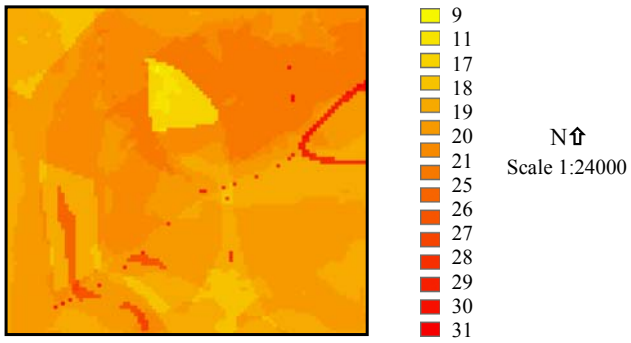

Figure 14. Relative landslide hazard for Site #1. Areas relatively more likely to experience landslides have higher values. (Derived from USGS Blackbird Mountain DEM, 10-m resolution.)

The relative hazard map for erosion incorporates the parameters of slope, aspect, burn severity, understory vegetation cover, hydrology, bedrock geology, and soil characteristics. The relative values for erosion hazard range between 12-40, with 12 being relatively less likely to experience erosion and 40 being more likely (Figure 15). Small areas with high values occur in the southwestern and northeastern portion of the site. The southeastern portion of this site has a large area with moderately high values.

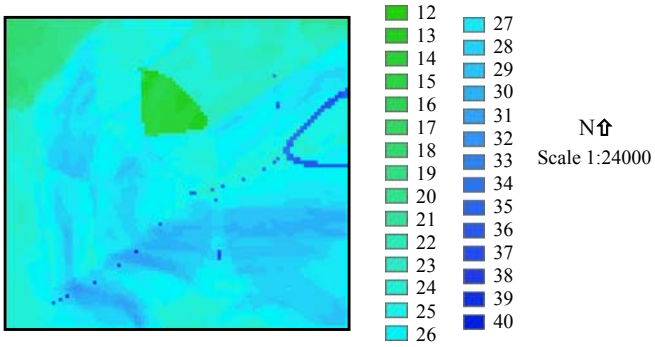

Figure 15. Relative erosion hazard for Site #1. Areas relatively more likely to experience erosion have higher values. (Derived from USGS Blackbird Mountain DEM, 10-m resolution.)

Site #2: Fourth of July Creek

Site #2 is located south of Fourth of July Creek (Figure 2) and covers an area of 1.2 km². Elevation ranges between 2,134-2,438 m. The predominant types of vegetation are Douglas Fir and pinegrass.

Parameters

Slope and Aspect

Slopes range from 1-39° (Figure 16) and aspects are predominantly eastern and western (Figure 17).

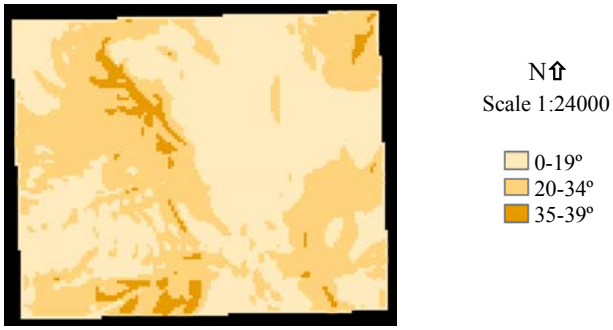

Figure 16. Slopes of Site #2. (Derived from USGS Duck Creek Point DEM, 10-m resolution.)

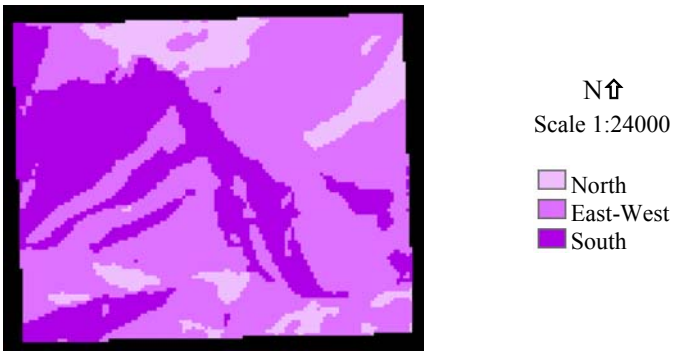

Figure 17. Aspects of Site #2. (Derived from USGS Duck Creek Point DEM, 10-m resolution.)

Burn Severity

The burn intensities of Site #2 include all degrees of severity (Figure 18). High severity burns, ranked with a value of 10 for this study, cover 25% of the total site area. Moderate severity burns were ranked with a value of 9 and cover 32% of the site. Low severity burns were ranked with a value of 8 and cover 14% of the site. Unburned areas cover 29% of the site area and were ranked with a value of zero.

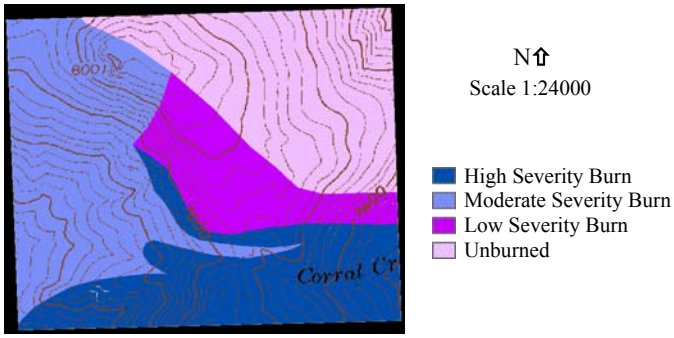

Figure 18. Burn severities of Site #2. (Base map from USGS Duck Creek Point 7.5 Minute Quadrangle.)

Understory Vegetation Cover

A small area comprising 5% of the total site area has 0-25% understory vegetation cover and was ranked with a value of 5. Another 27% of the site area has 26-50% cover and was assigned a value of 4. The remaining 68% of the total area has greater than 75% cover and was ranked with a value of 2 (Figure 19).

Hydrology

This particular site contains no surface water, and was thus ranked with a value of zero (Figure 20).

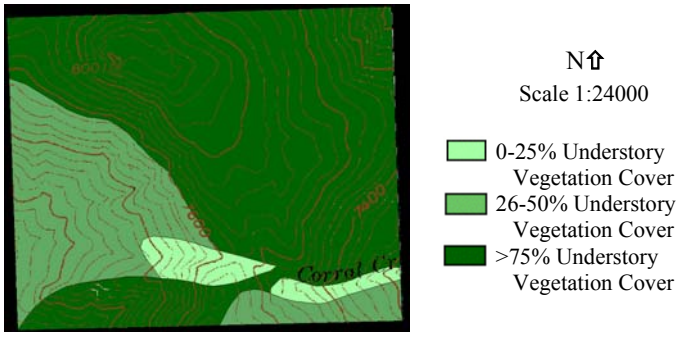

Figure 19. Understory vegetation cover of Site #2. (Base map from USGS Duck Creek Point 7.5 Minute Quadrangle.)

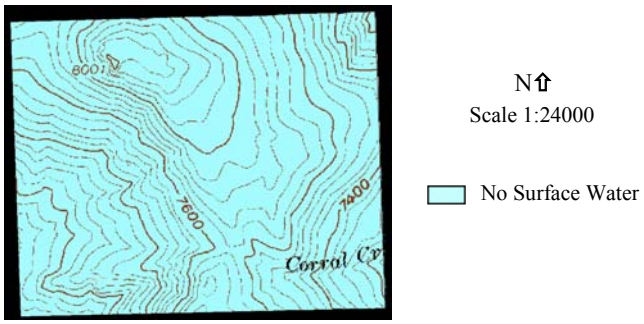

Figure 20. Hydrology of Site #2. (Base map from USGS Duck Creek Point 7.5 Minute Quadrangle.)

Geology

The geology of this area consists of the Challis Volcanic Group within the Panther Creek graben, including epiclastic bedded lapilli tuffs, welded tuffs, and minor rhyolite lavas (Figure 21). As noted by Fisher et al. (1995), the study area is underlain by east-dipping strata assigned to units consisting of flow-layered rhyolite. This site was ranked with a value of 4, as this lithology is considerably more friable than any other lithologies investigated in this study.

Soil Characteristics

Clayey silt and sandy silt cover 25% of the site (Figure 22). Although both soils are predominantly silt, the clay component makes the clayey silt slightly more cohesive and thus less easily entrained. The sand component of the sandy silt makes the soil grain size slightly larger overall and also less easily entrained; however, the sand component may increase the infiltration capacity of the soil slightly. Taking all of these variables into consideration, the clayey silt and the sandy silt were both ranked with a value of 5. Silty sand covers the remaining 75% of the site and was assigned a value of 4.

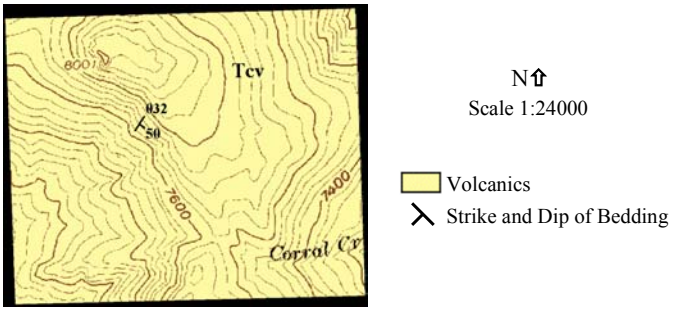

Figure 21. Geology of Site #2. This site consists of the Challis Volcanic Group (Tcv), including epiclastic bedded lapilli tuffs, welded tuffs, and minor rhyolite lavas. (Base map from USGS Duck Creek Point 7.5 Minute Quadrangle.)

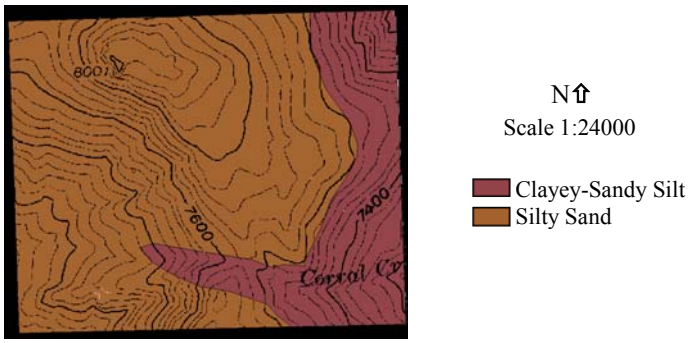

Figure 22. . Soil type of Site #2. (Base map from USGS Duck Creek Point 7.5 Minute Quadrangle).

Landslide and Erosion Hazard Ranking

The relative hazard map for landslides incorporates the parameters of slope, aspect, burn severity, hydrology, bedrock geology, and soil characteristics. Relative values for landslide hazard range between 10-31, with 10 being relatively less likely to experience landslides and 31 being more likely (Figure 23). The highest values occur in the southern and northwest portions of the site.

The relative hazard map for erosion incorporates the parameters of slope, aspect, burn severity, understory vegetation cover, hydrology, bedrock geology, and soil characteristics. The relative values for erosion hazard range between 11-34, with 11 being relatively less likely to experience erosion and 34 being more likely (Figure 24). The highest values occur in the southern and northwestern portions of the site.

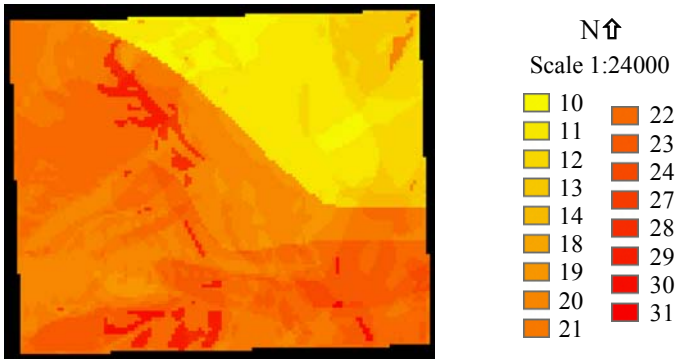

Figure 23. Relative landslide hazard for Site #2. Areas relatively more likely to experience landslides have higher values. (Derived from USGS Duck Creek Point DEM, 10-m resolution).

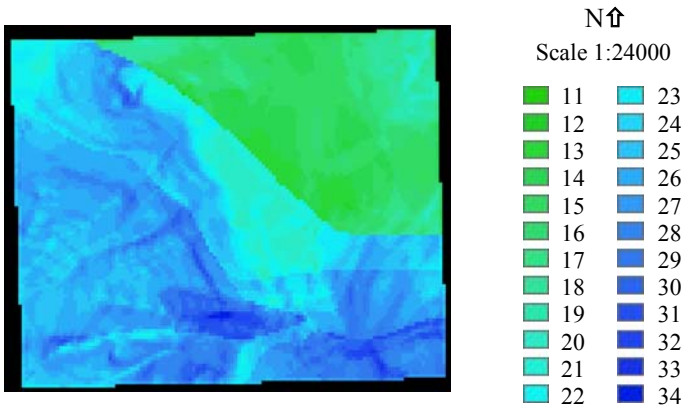

Figure 24. Relative erosion hazard for Site #2. Areas relatively more likely to experience erosion have higher values. (Derived from USGS Duck Creek Point DEM, 10-m resolution).

Site #3: Lake Creek

Site #3 is located west of Lake Creek (Figure 2) and covers an area of 0.95 km². Elevation ranges between 1,707-2,195 m. The predominant types of vegetation are Douglas fir, ponderosa pine, pinegrass, and bunch grass.

Parameters

Slope and Aspect

Slopes range from 0-56° (Figure 25) and the predominant aspect is eastern (Figure 26).

Figure 25. Slopes of Site #3. (Derived from USGS Yellowjacket DEM, 10-m resolution).

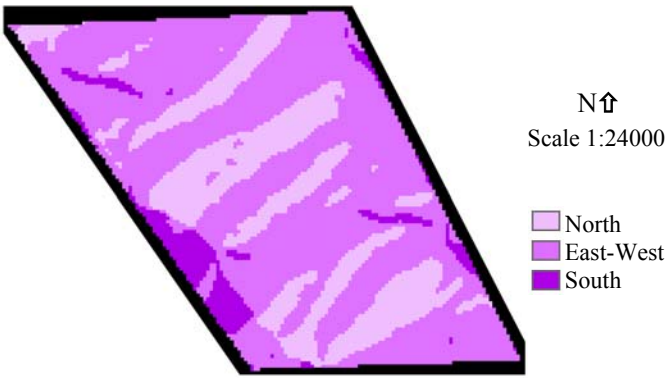

Figure 26. Aspects of Site #3. (Derived from USGS Yellowjacket DEM, 10-m resolution).

Burn Severity
High severity burns cover 50% of Site #3 and were ranked with a value of 10 (Figure 27). Moderate severity burns were ranked with a value of 9 and cover 19% of the site. Low severity burns were ranked with a value of 8 and cover 4% of the site. Unburned areas cover 27% of the site area and were ranked with a value of zero.

Understory Vegetation Cover
Approximately 14% of the site area has 26-50% cover and was assigned a value of 4 (Figure 28). Another 20% of the site area has 51-75% cover and was assigned a value of 3. The remaining 66% of the site has greater than 75% cover, and was ranked with a value of 2.

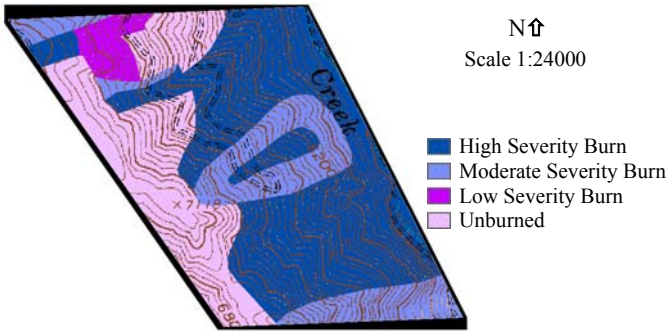

Figure 27. Burn severities of Site #3. (Base map from USGS Yellowjacket 7.5 Minute Quadrangle).

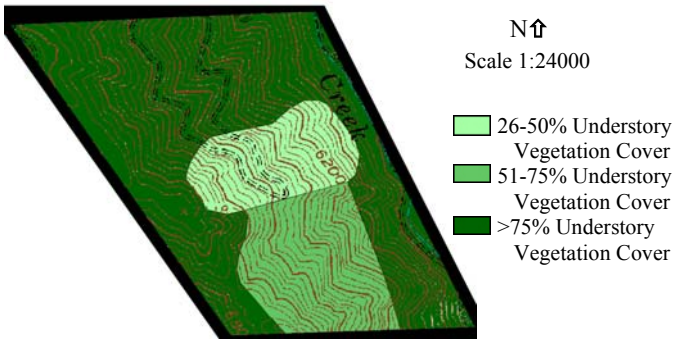

Figure 28. Understory vegetation cover of Site #3. (Base map from USGS Yellowjacket 7.5 Minute Quadrangle).

Hydrology
A large percentage of this site, 98%, contains no surface water (Figure 29). These areas were ranked with a value of zero. Only 2% of the site has surface water, which is in the form of a stream (Lake Creek) along the eastern perimeter of the site, and was ranked with a value of 10.

Figure 29. Hydrology of Site #3. (Base map from USGS Yellowjacket 7.5 Minute Quadrangle).

Geology

The bedrock of this site is primarily coarse-grained granodiorite (mapped by Ekren (1988) as Ordovician in age) and was ranked with a value of 2 (Figure 30). A ridge at the western portion of the site is intruded by northeast-trending dikes mapped as quartz porphyry intrusions of the Challis Volcanics and thus ranked with a value of 4.

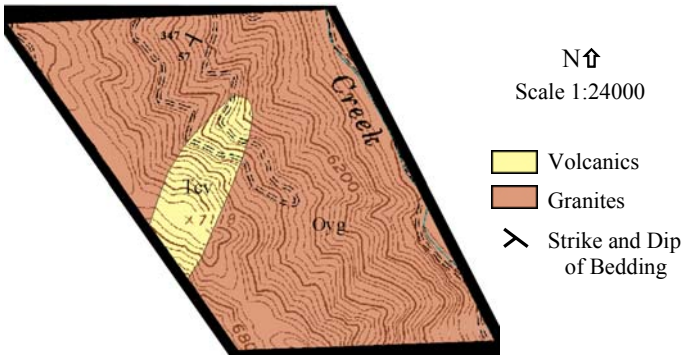

Figure 30. Geology of Site #3. The bedrock of this site is primarily coarse-grained granodiorite (Oyg). A ridge at the western portion of the site is intruded by northeast-trending dikes of quartz porphyry intrusions (Tcv). (Base map from USGS Yellowjacket 7.5 minute quadrangle).

Soil Characteristics

Approximately 83% of the soil evaluated in this site is silty sand, which was assigned a value of 4 (Figure 31). The remaining 17% of the soil is clayey-sandy silt and was assigned a value of 5.

Landslide and Erosion Hazard Ranking

The relative hazard map for landslides incorporates the parameters of slope, aspect, burn severity, hydrology, bedrock geology, and soil characteristics. Relative values for landslide hazard range between 8-30, with 8 being relatively less likely to experience landslides and 30 being more likely (Figure 32). The highest values occur in the central and eastern portions of the site.

Figure 31. Soil type of Site #3. (Base map from USGS Yellowjacket 7.5 Minute Quadrangle).

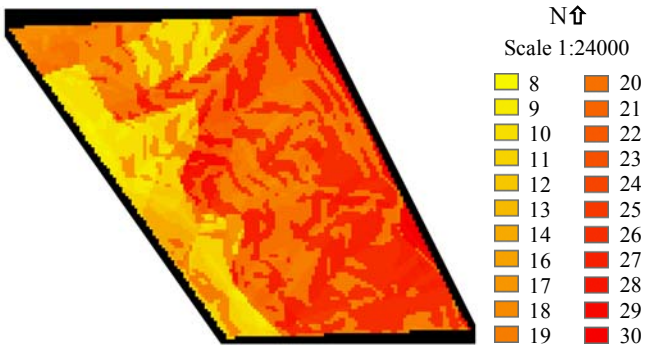

Figure 32. Relative landslide hazard for Site #3. Areas relatively more likely to experience landslides have higher values. (Derived from USGS Yellowjacket DEM, 10-m resolution).

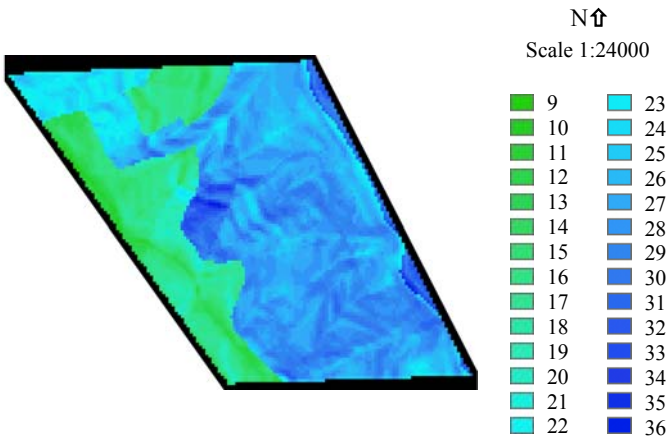

Figure 33. Relative erosion hazard for Site #3. Areas relatively more likely to experience erosion have higher values. (Derived from USGS Yellowjacket DEM, 10-m resolution).

The relative hazard map for erosion incorporates the parameters of slope, aspect, burn severity, understory vegetation cover, hydrology, bedrock geology, and soil characteristics. The relative values for erosion hazard range between 9-36, with 9 being relatively less likely to experience erosion and 36 being more likely (Figure 33). The highest values occur in the central and eastern portions of the site.

REMOTE SENSING STUDY AND GIS

Burn severity and amount of vegetation cover were analyzed for Sites #1-4 using IKONOS imagery. Burn severity was assessed using a minimum distance algorithm and vegetation cover was assessed using an NDVI transformation. As previously stated, there are no soil or fine-resolution hydrology GIS coverages or maps available for the study sites; therefore, soil characteristics and hydrology were not evaluated by remote sensing or GIS methods. Pre-existing geological maps were digitized to provide bedrock geology coverage for this aspect of the study. USGS 10-m DEM's provided slope and aspect coverages. Therefore, the parameters evaluated with remote sensing data include slope, aspect, burn severity, vegetation cover (for erosion only), and geology.

The accuracy of remote sensing image interpretations for Sites #1-3 was evaluated by comparing them to field mapping results. The accuracy of remote sensing image interpretations for Site #4 could only be evaluated by comparing interpretations at Sites #1-3 (within Site #4) to results obtained from field mapping results.

Site #1: Quartzite Mountain

Parameters

Burn Severity

The burn intensities of Site #1 include all degrees of severity (Figure 34). High severity burns, ranked with a value of 10 for this study, cover 65% of the total site area. Moderate severity burns were ranked with a value of 9 and cover 18% of the site. Low severity burns were ranked with a value of 8 and cover 6% of the site. A small area of the site, 4%, is unburned and was ranked with a value of zero. About 7% of the site are areas of rock outcrops/roads and high reflectance and were ranked with a value of zero.

Vegetation Cover

The NDVI values for this site range from -0.220 to 0.657. Approximately 30% of this site has 26-50% vegetation cover (Figure 35). These areas were ranked with a value of 4. Most of the site, 69% of the total area, has 51-75% cover, and was ranked with a value of 3. The remaining 1% of the area has greater than 75% cover and was ranked with a value of 2.

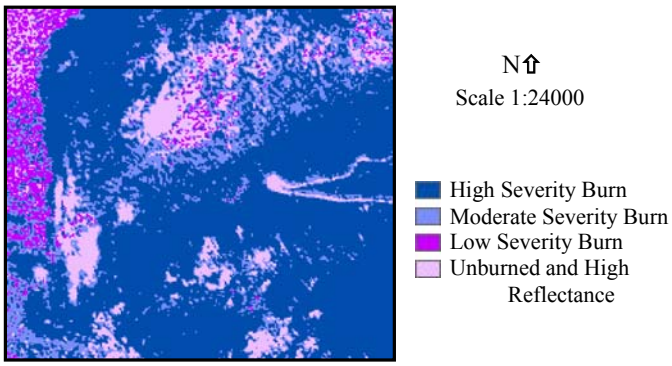

Figure 34. Burn severity of Site #1 assessed with a minimum distance algorithm. Areas of high reflectance include rock outcrops and roads. (Derived from IKONOS imagery, 4-m resolution).

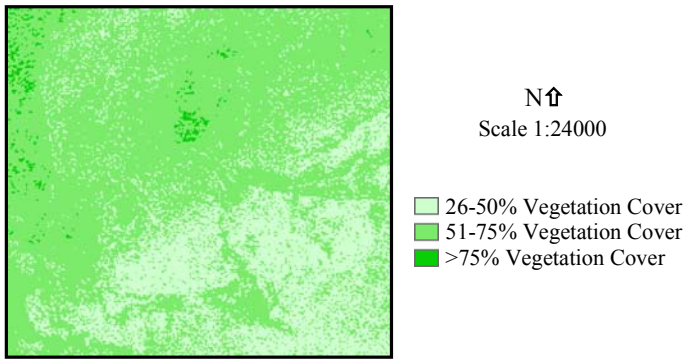

Figure 35. Vegetation cover of Site #1 assessed with an NDVI transformation. (Derived from IKONOS imagery, 4-m resolution).

Geology

The digitized map agrees with field mapping in that this site is primarily composed of sandstones and siltstones (Figure 12). This site was thus ranked with a value of 1.

Landslide and Erosion Hazard Ranking

The relative hazard map for landslides incorporates the parameters of slope, aspect, burn severity, and bedrock geology. The relative values for landslide hazard range between 3-22, with 3 being relatively less likely to experience landslides and 22 being more likely (Figure 36). The highest values occur in the southwest and northern portions of the site.

The relative hazard map for erosion incorporates the parameters of slope, aspect, burn severity, vegetation cover, and bedrock geology. The relative values for erosion hazard range between 4-26, with 4 being relatively less likely to experience erosion and 26 being more likely (Figure 37). The highest values occur in the southern and southwest portions of the site.

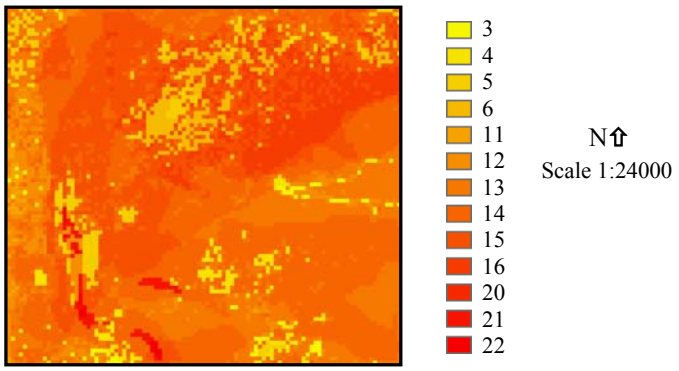

Figure 36. Relative landslide hazard for Site #1. Areas relatively more likely to experience landslides have higher values. (Derived from USGS Blackbird Mountain DEM, 10-m resolution, and IKONOS imagery, 4-m resolution).

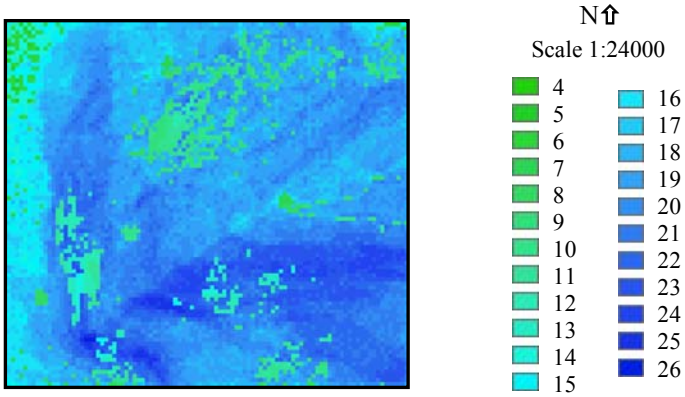

Figure 37. Relative erosion hazard for Site #1. Areas relatively more likely to experience erosion have higher values. (Derived from USGS Blackbird Mountain DEM, 10-m resolution, and IKONOS imagery, 4-m resolution).

Site #2: Fourth of July Creek

Parameters

Burn Severity

The burn severities of Site #2 include all degrees (Figure 38). High severity burns, ranked with a value of 10 for this study, cover 23% of the total site area. Moderate severity burns were ranked with a value of 9 and cover 27% of the site. Low severity burns were ranked with a value of 8 and cover 27% of the site. A small area of the site, 19%, is unburned and ranked with a value of zero. About 4% of the site are areas of rock outcrops/roads and high reflectance and were ranked with a value of zero.

Vegetation Cover

The NDVI values for this site range from -0.207 to 0.692. Approximately 3% of the site area has 26-50% vegetation cover and was ranked with a value of 4 (Figure 39). Most of this site, 79% of the total area, has 51-75% vegetation cover. These areas were ranked with a value of 3. The remaining 18% of the area has greater than 75% cover and was ranked with a value of 2.

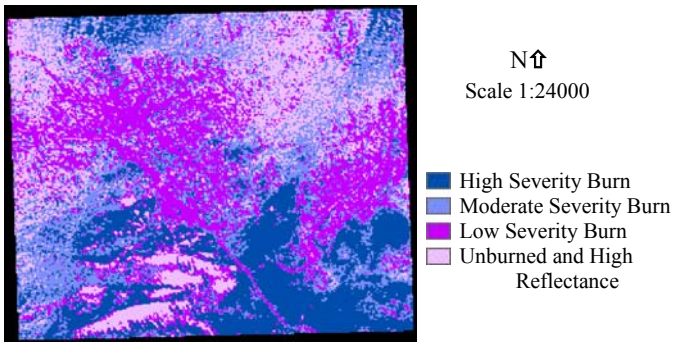

Figure 38. Burn severity of Site #2 assessed with a minimum distance algorithm. Areas of high reflectance include rock outcrops and roads. (Derived from IKONOS imagery, 4-m resolution).

Geology

The digitized map agrees with field mapping in that this site primarily consists of the Challis Volcanic Group and was thus ranked with a value of 3 (Figure 21).

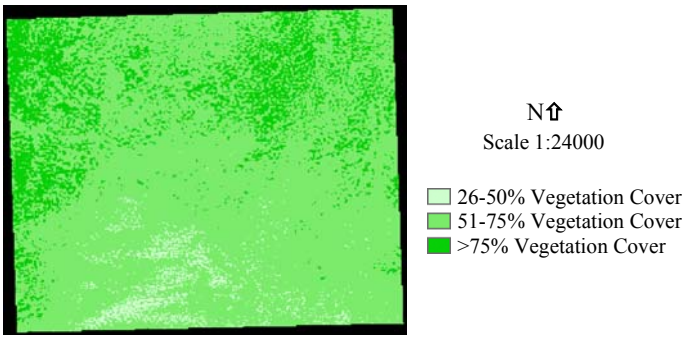

Figure 39. Vegetation cover of Site #2 assessed with an NDVI transformation. (Derived from IKONOS imagery, 4-m resolution).

Landslide and Erosion Hazard Ranking

The relative hazard map for landslides incorporates the parameters of slope, aspect, burn severity, and bedrock geology. The relative values for landslide hazard range between 6-26, with 6 being relatively less likely to experience landslides and 26 being more likely (Figure 40). The highest values occur in the southwest, northeast, and northwest portions of the site.

The relative hazard map for erosion incorporates the parameters of slope, aspect, burn severity, vegetation cover, and bedrock geology. The relative values for erosion hazard range between 7-28, with 7 being relatively less likely to experience erosion and 28 being more likely (Figure 41). The highest values occur in the southwest, northeast, and northwest portions of the site.

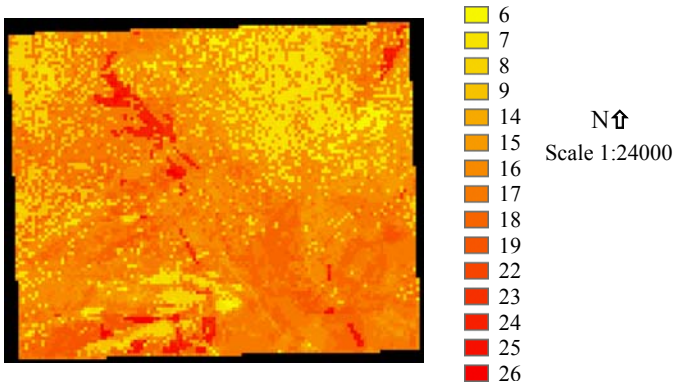

Figure 40. Relative landslide hazard for Site #2. Areas relatively more likely to experience landslides have higher values. (Derived from USGS Blackbird Mountain DEM, 10-m resolution, and IKONOS imagery, 4-m resolution).

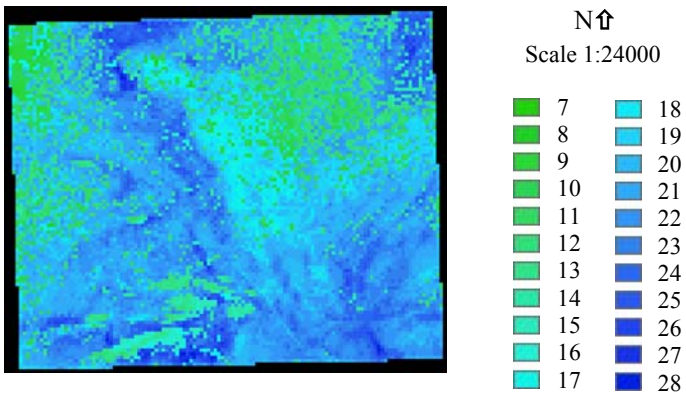

Figure 41. Relative erosion hazard for Site #2. Areas relatively more likely to experience erosion have higher values. (Derived from USGS Blackbird Mountain DEM, 10-m resolution, and IKONOS imagery, 4-m resolution).

Site #3: Lake Creek

Parameters

Burn Severity

The burn intensities of Site #3 include all degrees of severity (Figure 42). High severity burns, ranked with a value of 10 for this study, cover 32% of the total site area. Moderate severity burns were ranked with a value of 9 and cover 17% of the site. Low severity burns were ranked with a value of 8 and cover 27% of the site. A small area of the site, 19%, is unburned and thus ranked with a value of zero. About 5% of the site are areas of rock outcrops/roads and high reflectance and were ranked with a value of zero.

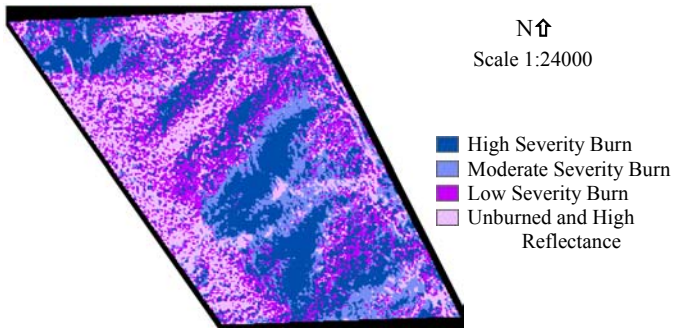

Figure 42. Burn severity of Site #3 assessed with a minimum distance algorithm. Areas of high reflectance include rock outcrops and roads. (Derived from IKONOS imagery, 4-m resolution).

Vegetation Cover

The NDVI values for this site range from -0.309 to 0.710. Most of this site, 85% of the total area, has 51-75% vegetation cover (Figure 43). These areas were ranked with a value of 3. Approximately 3% of the site area has 26-50% vegetation cover and was ranked with a value of 4. The remaining 12% of the area has greater than 75% cover and was ranked with a value of 2.

Geology

The bedrock of this site is primarily coarse-grained granodiorite (mapped by Ekren as Ordovician in age) which was ranked with a value of 2 (Figure 44). The digitized map shows a large area covered by northeast-trending quartz porphyry intrusions (ranked with a value of 4), larger than the area indicated by field mapping. The digitized map also shows an area of granite in the northwest corner not indicated by field mapping; however, this granite was ranked with the same value (2) as the granodiorite and thus not distinguished on the map.

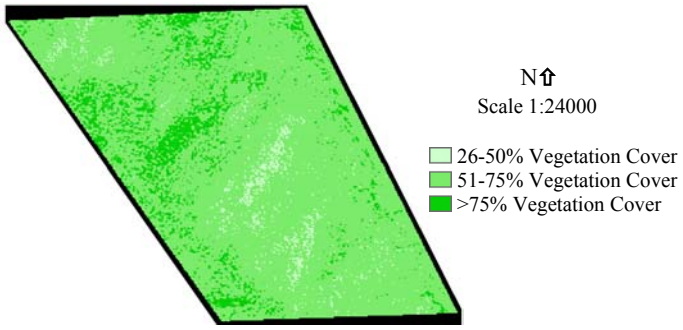

Figure 43. Vegetation cover of Site #3 assessed with an NDVI transformation. (Derived from IKONOS imagery, 4-m resolution).

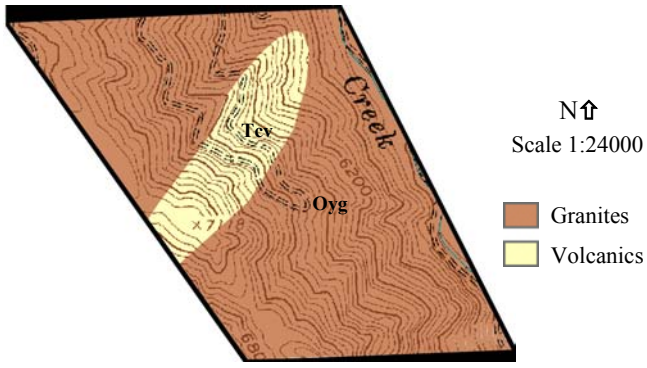

Figure 44. Geology of Site #3. The bedrock of this site is primarily coarse-grained granodiorite (Oyg). A ridge at the western portion of the site is intruded by northeast-trending dikes of quartz porphyry intrusions (Tcv). No attitudes available on source map.

Landslide and Erosion Hazard Ranking

The relative hazard map for landslides incorporates the parameters of slope, aspect, burn severity, and bedrock geology. The relative values for landslide hazard range between 3-25, with 3 being relatively less likely to experience landslides and 25 being more likely (Figure 45). The highest values occur in the eastern two-thirds of the site.

The relative hazard map for erosion incorporates the parameters of slope, aspect, burn severity, vegetation cover, and bedrock geology. The relative values for erosion hazard range between 5-29, with 5 being relatively less likely to experience erosion and 29 being more likely (Figure 46). The highest values occur in the eastern two-thirds of the site.

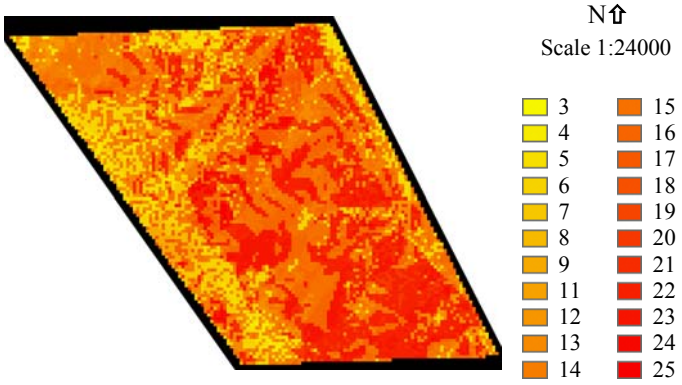

Figure 45. Relative landslide hazard for Site #3. Areas relatively more likely to experience landslides have higher values. (Derived from USGS Blackbird Mountain DEM, 10-m resolution, and IKONOS imagery, 4-m resolution).

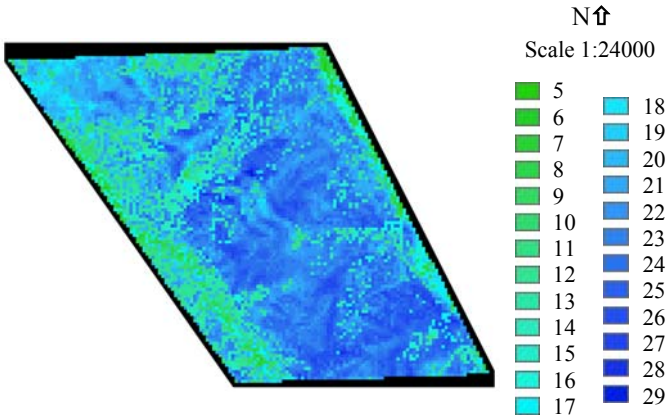

Figure 46. Relative erosion hazard for Site #3. Areas relatively more likely to experience erosion have higher values. (Derived from USGS Blackbird Mountain DEM, 10-m resolution, and IKONOS imagery, 4-m resolution).

Site #4: Salmon-Challis National Forest

Parameters

The parameters evaluated for Site #4 include slope, aspect, burn severity, vegetation cover (for erosion only), and geology. These are the same parameters used to evaluate Sites #1-3 with remote sensing data.

Slope and Aspect

Slopes range between 0-75° (Figure 47) and the predominate aspects are eastern and western (Figure 48).

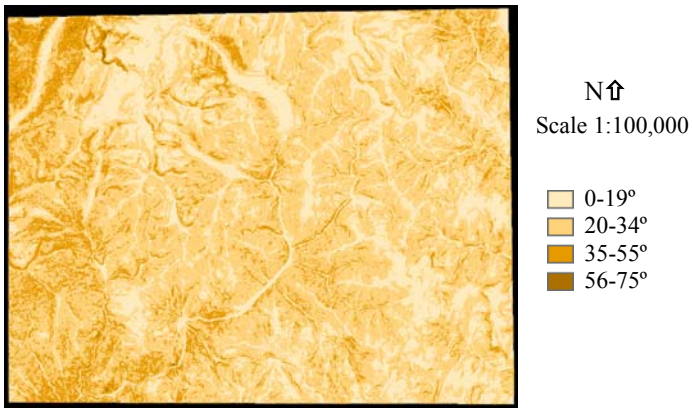

Figure 47. Slopes of Site #4. (Derived from the following USGS DEMs, 10-m resolution: Hoodoo Meadows, Blackbird Mountain, Blackbird Creek, Opal Lake, Duck Creek Point, and Yellowjacket).

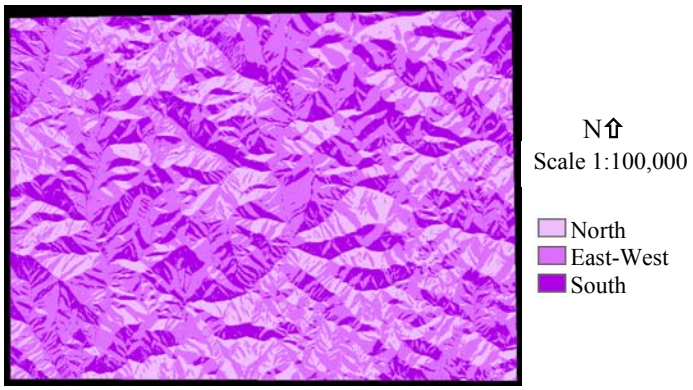

Figure 48. Aspects of Site #4. (Derived from the following USGS DEMs, 10-m resolution: Hoodoo Meadows, Blackbird Mountain, Blackbird Creek, Opal Lake, Duck Creek Point, and Yellowjacket).

Burn Severity

The burn intensities of Site #4 include all degrees of severity (Figure 49). High severity burns, ranked with a value of 10 for this study, cover 11% of the total site area. Moderate severity burns were ranked with a value of 9 and cover 12% of the site. Low severity burns were ranked with a value of 8 and cover 45% of the site. The remaining 25% of the total site area is unburned and ranked with a value of zero. About 7% of the site are areas of rock outcrops/roads and high reflectance and were ranked with a value of zero.

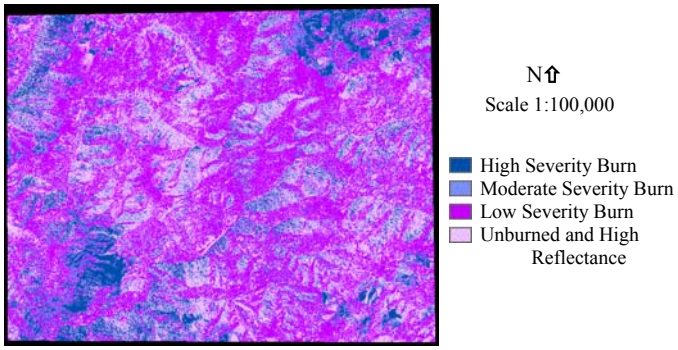

Figure 49. Burn severities of Site #4 assessed with a minimum distance algorithm. Areas of high reflectance include rock outcrops and roads. (Derived from IKONOS imagery, 4-m resolution).

Vegetation Cover

The NDVI values for this site range from -1.0 to 0.767. Most of this site, 78% of the total area, has 51-75% vegetation cover (Figure 50). These areas were ranked with a value of 3. Approximately 21% of the area has greater than 75% cover and was ranked with a value of 2. Only 1% of the site area has 26-50% vegetation cover and was ranked with a value of 4, and less than 1% of the area has 0-25% cover and was ranked with a value of 5.

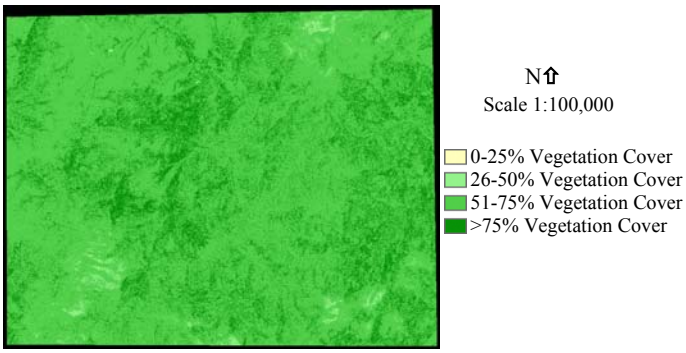

Figure 50. Vegetation cover of Site #4 assessed with an NDVI transformation. (Derived from IKONOS imagery, 4-m resolution).

Geology

There are seven types of bedrock in this site (Figure 51). Units assigned a ranking value of 1 include the Type Yellowjacket Formation, the Hoodoo Quartzite, and the informal argillaceous member of the Cobalt Yellowjacket Formation. Units assigned a ranking value of 2 include the Ordovician or Middle Proterozoic granites, the granitic rocks of the Idaho Batholith, and the Tertiary granites of the Casto and Crags Plutons. The Challis Volcanic Group and minor areas of Quaternary alluvium were ranked with a value of 4.

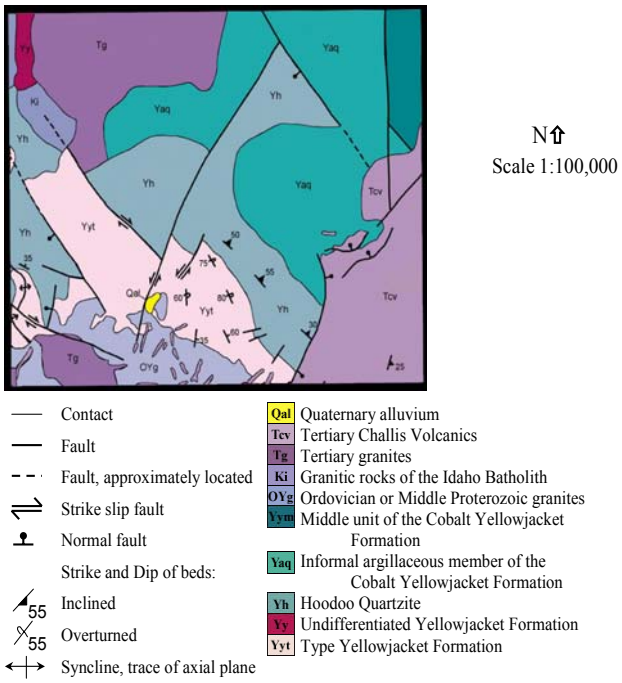

Figure 51. Geology of Site #4. The bedrock of this site consists of seven main bedrock types and Quaternary alluvium. (Source map from compiled from Ross (1934), Ekren (1988), Evans and Connor (1993), and Winston et al. (1999)).

Landslide and Erosion Hazard Ranking

The relative hazard map for landslides incorporates the parameters of slope, aspect, burn severity, and bedrock geology. The relative values for landslide hazard range between 3-27,

with 3 being relatively less likely to experience landslides and 27 being more likely (Figure 52). The highest values occur in the northwestern and southwestern portions of the site.

The relative hazard map for erosion incorporates the parameters of slope, aspect, burn severity, vegetation cover, and bedrock geology. The relative values for erosion hazard range between 4-31, with 4 being relatively less likely to experience erosion and 31 being more likely (Figure 53). The highest values also occur in the northwestern and southwestern portions of the site.

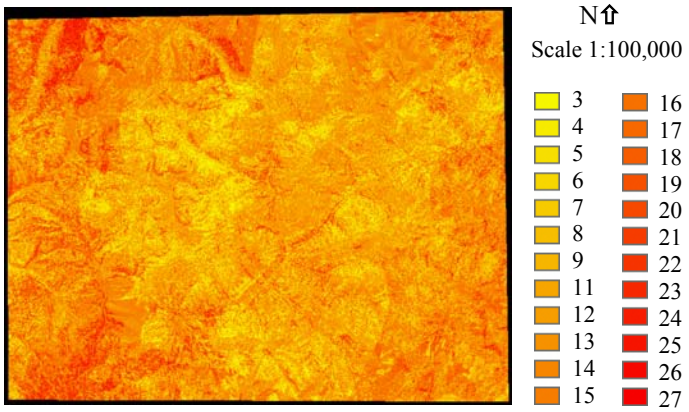

Figure 52. Relative landslide hazard for Site #4. Areas relatively more likely to experience landslides have higher values. (Derived from USGS Blackbird Mountain DEM, 10-m resolution, and IKONOS imagery, 4-m resolution).

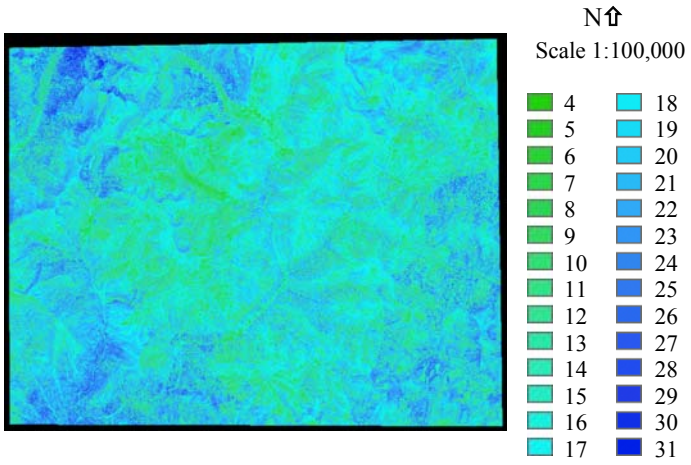

Figure 53. Relative erosion hazard for Site #4. Areas relatively more likely to experience erosion have higher values. (Derived from USGS Blackbird Mountain DEM, 10-m resolution, and IKONOS imagery, 4-m resolution).

DISCUSSION

FIELD STUDY

The relative hazard maps using field data incorporated the parameters of slope, aspect, burn severity, hydrology, geology, and soil characteristics for landslides; and slope, aspect, burn severity, understory vegetation cover, hydrology, geology, and soil characteristics for erosion.

Field mapping was performed at scales appropriate to the parameters being mapped. For example, burn severity was mapped at a scale of tens-of-meters, whereas hydrology was mapped at meter-scale resolution. The relative hazard maps of all three sites generated with field data correspond well to observations made in the field regarding areas relatively more likely to experience landslides and erosion. Areas of highest relative risk to landslides and erosion are assumed to be those within 40-50% of the maximum ranking values. Therefore, areas of highest relative risk to landslides have values of 25 and greater and areas of highest relative risk to erosion have values of 30 and greater.

Site #1: Quartzite Mountain
The areas of highest relative risk to landslides are those areas with slopes greater than 34º, surface water, and low to high burn severities. These areas are located in the northeast and southwest portions of the site. The areas of highest relative risk to erosion are those areas with north-facing slopes greater than 29º, moderate to high burn severities, 0-25% understory vegetation cover, and surface water. These areas are located in the southern and eastern portions of the site. These results agree with field observations because steep slopes, surface water, and low to high burn severities are all represented by high values in the ranking system. The geology and soil characteristics are consistent throughout the site, so they do not influence spatial changes in the hazard maps. During field study in July 2002, centimeter-scale rilling over an area approximately 5 m² was observed in the southwest corner of the site in the same area predicted by the hazard maps to be susceptible to both landslides and erosion.

Site #2: Fourth of July Creek
The areas of highest relative risk to landslides are those areas with slopes greater than 34º and low to high burn severities. These areas are located in the southern and northwest portions of the site. The areas of highest relative risk to erosion are those areas with north-facing slopes greater than 20º, moderate to high burn severities, and 0-25% understory vegetation cover. These areas are also located in the southern and northwest portions of the site. The presence of clayey-sandy silt (ranked with a value of 5) along the eastern portion of the site does not significantly influence the overall risk assessment. The geology is consistent throughout the site and there is no surface water, so these parameters do not influence spatial changes in the hazard maps.

Site #3: Lake Creek
The areas of highest relative risk to landslides are those areas with slopes greater than 34º, surface water, and low to high burn severities. These areas are located throughout the western and southern portions of the site. The areas of highest relative risk to erosion are those areas with north-facing slopes greater than 34º, low to high burn severities, and surface water. These areas are also located throughout the western and southern portions of the site. Geology and soil characteristics vary only slightly throughout the site, and do not influence spatial changes in the hazard maps. Surprisingly, understory vegetation cover does not appear to significantly influence the erosion hazard map. This may be because slope, burn severity, and surface water are more heavily weighted in the ranking system and thus override the effects of understory vegetation cover.

Summary
For Sites #1-3, the areas of highest relative risk to landslides are those areas with slopes greater than 34º, surface water (except Site #2, which has no surface water), and low to high burn severities. This is to be expected, as these three parameters are given the highest weighting in the overall ranking system.

The areas in Sites #1-3 of highest relative risk to erosion are the steepest, north-facing slopes. Sites #1 and #2 are influenced by moderate to high burn severities and low understory vegetation cover (0-25%). Site #3 exhibits more burn severity heterogeneity and so is influenced by a larger range of burn severities (low to high), and does not appear to be affected by understory vegetation cover. Sites #1 and #3 are affected by surface water, but again, Site #2 has no surface water.

REMOTE SENSING
The relative hazard maps using remote sensing data incorporated the parameters of slope, aspect, burn severity, and geology for landslides; and slope, aspect, burn severity, vegetation cover, and geology for erosion. In general, the relative hazard maps for each site generated with remote sensing data correspond well to areas predicted from field mapping. The greatest difference is that the remote sensing imagery classifies each 4-m pixel, whereas field mapping tends to group areas together at scales of tens-of-meters. Areas of highest relative risk to landslides and erosion are assumed to be those within 30-35% of the maximum ranking values. Therefore, areas of highest relative risk to landslides have values of 20 and greater and areas of highest relative risk to erosion have values of 22 and greater.

Most of the surface water within Sites #1 and #3 is in the form of small springs and streams less than 2 m, which cannot be detected by remote sensing data. This omission significantly affected the comparisons between field mapping and remote sensing data because areas with surface water present were assigned a high value (10) in the ranking system. Areas with surface water are significantly more likely to experience landslides and erosion than in areas without surface water. In order to detect the water bodies found in the study sites, remote sensing imagery with at least 1-m resolution would be required. A higher-resolution platform than IKONOS, such as Digital Globe's Quickbird (2.4 m multispectral resolution and 0.6 m panchromatic resolution), may provide such resolution; however, the cost of this data may be prohibitive for large areas such as the SCNF. Another consideration is that surface water fluctuates seasonally, and thus the season at which remote sensing imagery is acquired becomes more important. In addition, springs are often obscured by vegetation.

Soil is an important parameter because soils can influence landslides and erosion due to their infiltration capacities and the ease by which they may be transported. Unfortunately, it is difficult to evaluate soil type directly with IKONOS or similar multispectral remote sensing platforms. Although hyperspectral remote sensing platforms can be used to evaluate soil mineralogy, these platforms cannot be used to directly analyze grain size. In addition, heavily vegetated areas such as the study areas prevent direct observation of the ground.

It is important to note that the NDVI transformation used to assess vegetation cover cannot distinguish between understory and overstory vegetation cover. Remote sensing classifications

for burn severity and vegetation cover may overlap, causing the results to be overpredictive. Conversely, if the overstory is unburned and the understory is burned, results may be underpredictive. Another potential problem with using NDVI values is that this transformation does not model areas of exposed soil well. This is because soil may contain organic materials and chemical constituents that will influence the reflectivity from the red band.

Statistical Evaluation of Minimum Distance Classifications

The accuracy of the minimum distance classifications was assessed using the bootstrap method. A confusion matrix was generated to show the accuracy of each classification by comparing the classification results with ground-truth information (i.e. bootstrap training sites). The overall accuracy (total number of pixels classified correctly divided by the total number of pixels), kappa coefficient, confusion matrix, errors of commission (percentage of extra pixels in class), errors of omission (percentage of pixels left out of class), producer accuracy (probability that a pixel in the classification image is put into class *X* given the ground-truth class is *X)*, and user accuracy (probability that the ground-truth class is *X* given a pixel is put into class *X* in the classification image) was assessed for Sites #1-4 (Tables 8-11). For Site #1, the overall accuracy is 82.27% and K = 0.69. For Site #2, the overall accuracy is 62.40% and K = 0.50. For Site #3, the overall accuracy is 72.82% and K = 0.52. For Site #4, the overall accuracy is 71.04% and K = 0.59. Although these values are relatively high for remote sensing classifications, the errors of commission and omission are high in some cases. For example, in Site #1, low and high severity burns were often incorrectly classified as moderate severity burns, resulting in a high error of commission (81.61%). In Site #2, unburned and moderate severity burns were incorrectly classified as low severity burns, resulting in a commission error of 50.73%. Low severity burns were classified as unburned and moderate severity

Table 8. The overall accuracy, kappa coefficient, confusion matrix, errors of commission and omission, and producer and user accuracy assessed for the minimum distance classification of Site #1.

Minimum Distance Classification	Ground-Truth Pixels					
	High Reflectance	Unburned	Low Severity	Moderate Severity	High Severity	Total
Unclassified	0	0	0	0	0	0
High Reflectance	327	0	0	0	0	327
Unburned	0	106	157	14	0	277
Low Severity	0	22	502	21	0	545
Moderate Severity	34	3	206	98	192	533
High Severity	14	0	78	37	2578	2707
Total	375	131	943	170	2770	4389
Commission (%)	0.00	61.73	7.89	81.61	4.77	
Omission (%)	12.80	19.08	46.77	42.35	6.93	
Producer Accuracy (%)	87.20	80.92	53.23	57.65	93.07	
User Accuracy (%)	100.00	38.27	92.11	18.39	95.23	
Overall Accuracy 82.27%						
Kappa Coefficient = 0.69						

Table 9. The overall accuracy, kappa coefficient, confusion matrix, errors of commission and omission, and producer and user accuracy assessed for the minimum distance classification of Site #2.

Minimum Distance Classification	Ground-Truth Pixels					
	High Reflectance	Unburned	Low Severity	Moderate Severity	High Severity	Total
Unclassified	0	0	0	0	0	0
High Reflectance	332	0	8	0	0	340
Unburned	0	1598	155	879	0	2632
Low Severity	105	183	539	262	5	1094
Moderate Severity	2	873	276	1434	10	2595
High Severity	2	38	37	419	1497	1993
Total	441	2692	1015	2994	1512	8654
Commission (%)	2.35	39.29	50.73	44.74	24.89	
Omission (%)	24.72	40.64	46.90	52.10	0.99	
Producer Accuracy (%)	75.28	59.36	53.10	47.90	99.01	
User Accuracy (%)	97.65	60.71	49.27	55.26	75.11	
Overall Accuracy 62.40%						
Kappa Coefficient = 0.50						

burns, which resulted in an omission error of 52.10%. In Site #3, unburned and high severity burns were incorrectly classified as low severity burns, resulting in a commission error of 69.47%. Low severity burns were classified as unburned and high severity burns, which resulted in an omission error of 56.95%. Low and high severity burns were incorrectly classified as moderate severity burns, resulting in an error of commission of 56.81%. In Site #4, unburned and moderate severity burns were incorrectly classified as low severity burns, resulting in a commission error of 96.70%. Low severity burns were classified as unburned and high reflectance, which resulted in an omission error of 60.18%. Low and high severity burns were incorrectly classified as moderate severity burns, resulting in a commission error of 87.66%. Moderate severity burns were classified as unburned and high severity burns, which resulted in an omission error of 51.89%. This information indicates that areas of low and moderate burn severities particularly are not predicted well by the minimum distance classification for burn severity.

Taking into consideration the difficulties discussed above, the overall accuracies for Sites #1-4 are good (none less than 62.40%), and kappa values are all greater than 0.50. Site #1 yielded the highest overall accuracy and kappa values (82.27% and 0.69, respectively). This is probably because this site exhibits 80% high severity burns, which

Table 10. The overall accuracy, kappa coefficient, confusion matrix, errors of commission and omission, and producer and user accuracy assessed for the minimum distance classification of Site #3.

Minimum Distance Classification	Ground-Truth Pixels					
	High Reflectance	Unburned	Low Severity	Moderate Severity	High Severity	Total
Unclassified	0	0	0	0	0	0
High Reflectance	231	1	4	2	5	243
Unburned	0	795	118	24	26	963
Low Severity	0	239	229	68	214	750
Moderate Severity	21	1	41	450	529	1042
High Severity	0	23	140	174	2661	2998
Total	252	1059	532	718	3435	5996
Commission (%)	4.94	17.45	69.47	56.81	11.24	
Omission (%)	8.33	24.93	56.95	37.33	22.53	
Producer Accuracy (%)	91.67	75.07	43.05	62.67	77.47	
User Accuracy (%)	95.06	82.55	30.53	43.19	88.76	
Overall Accuracy 72.82%						
Kappa Coefficient = 0.52						

Table 11. The overall accuracy, kappa coefficient, confusion matrix, errors of commission and omission, and producer and user accuracy assessed for the minimum distance classification of Site #4.

Minimum Distance Classification	Ground-Truth Pixels					
	High Reflectance	Unburned	Low Severity	Moderate Severity	High Severity	Total
Unclassified	0	0	0	0	0	0
High Reflectance	7289	0	12	3	0	7304
Unburned	0	15957	145	2	0	16104
Low Severity	1110	5286	227	211	43	6877
Moderate Severity	9	2576	166	459	511	3721
High Severity	0	2854	20	279	8520	11673
Total	8408	26673	570	954	9074	45679
Commission (%)	0.21	0.91	96.70	87.66	27.01	
Omission (%)	13.31	40.18	60.18	51.89	6.11	
Producer Accuracy (%)	86.69	59.82	39.82	48.11	93.89	
User Accuracy (%)	99.79	99.09	3.30	12.34	72.99	
Overall Accuracy 71.04%						
Kappa Coefficient = 0.59						

are predicted well by the minimum distance classification. In general, it appears that the minimum distance classifications for burn severity correspond very well to the ground-truth or

validation areas mapped in the field. Sites #2, #3, and #4 had slightly lower overall accuracies (62.40%, 72.82%, and 71.04%, respectively) and kappa values (0.50, 0.52, and 0.59, respectively). These sites exhibit more burn heterogeneity, including more low and moderate severity burns, which were not predicted as well by the minimum distance classifications.

Site #1: Quartzite Mountain
With the remote sensing analysis, the areas of highest relative risk to landslides (values of 20 and greater) are those areas with slopes greater than 34º and moderate to high burn severities. These areas are located in the southwest portion of the site. The areas of highest relative risk to erosion (values of 22 and greater) are those areas with north-facing slopes greater than 19º, moderate to high burn severities, and 26-50% vegetative cover. These areas are located in the southern portion of the site. The geology is consistent throughout the site and thus does not influence spatial changes in the hazard maps. The minimum distance algorithm appears to correlate fairly well with burn severities observed in the field, although the western edge and northeastern portion of the site are classified as lower-severity burns than were observed in the field. The NDVI values appear to be more correlated to burn severity than to understory vegetation cover as mapped in the field. This site is dominated by high severity burns with little vegetation cover, so the large areas of bare soil present may affect the NDVI values as discussed above. In situations such as this, it may be advantageous to use SAVI rather than NDVI values. The rilling observed in the southwest corner of the site during field study in July 2002 is within the same area predicted by both the field-based and remotely-sensed hazard maps to be susceptible to both landslides and erosion.

Site #2: Fourth of July Creek
The areas of highest relative risk to landslides are those areas with slopes greater than 34º and low to high burn severities. These areas are located in the northeast and northwest portions and southern edge of the site. The areas of highest relative risk to erosion are those areas with north-facing slopes greater than 24º and low to high burn severities. These areas are located in the northeast and northwest portions and southern edge of the site. The geology is consistent throughout the site and thus does not influence spatial changes in the hazard maps. Vegetation cover does not appear to significantly influence the erosion hazard map results, which is likely due to the more heavily weighted parameters (slope, burn severity, and surface water) overriding the effects of vegetation cover. The minimum distance algorithm appears to correlate fairly well with high burn severity and unburned areas observed in the field except at the western edge of the site, where burn severity was underpredicted possibly due to areas of rock outcrop. Areas of low to moderate burn severity are also generally correlative with what was observed in the field. The NDVI values for this site appear to be better correlated to understory vegetation cover than to burn severity as mapped in the field. This is likely due to the fact that burn severity (and thus soil exposure) is more heterogeneous in this site.

Site #3: Lake Creek
The areas of highest relative risk to landslides are those areas with slopes greater than 34º and low to high burn severities. These areas occur throughout the site, except in the northwest corner where values are much lower. The areas of highest relative risk to erosion are those areas with north-facing slopes greater than 29º, low to high burn severities, and 26-75% vegetation cover. These areas also occur throughout the site, except in the northwest corner where values are much

lower. The geology varies but does not significantly influence overall hazard rankings. The minimum distance algorithm appears to correlate fairly well with burn severities observed in the field, although burn severity was underpredicted in the northeastern and southeastern portions of the site. The NDVI values for this site appear to be better correlated to understory vegetation cover than to burn severity as mapped in the field. Again, this may be due to the fact that burn severity (and thus soil exposure) is more heterogeneous in this site.

Site #4: Salmon-Challis National Forest
The highest relative values for both landslide and erosion hazards occur in the northwestern and southwestern portions of the site. These areas appear to be most influenced by slopes greater than 34° and moderate to high burn severities. This is expected, as these parameters are weighted most heavily in the ranking system. The parameters of aspect, geology, and vegetation vary throughout the site but do not significantly influence the overall hazard rankings because they were given less weight in the ranking system.

The burn intensities of Site #4 include all degrees of severity. For this particular site, training classes for the minimum distance algorithm were selected visually from the remote sensing data. Training classes were selected within Sites #1-3 for purposes of ground-truthing, and others were selected without the aid of field observations. It is important to collect training sites from areas distributed throughout the site so that influences of shadow and other variables in the imagery may be taken into account. Although training classes were selected from all slope aspects, it appears that many unburned areas in shadow were incorrectly classified as high severity burned areas. This may be corrected using several different methods including histogram stretching; topographic corrections based on sun elevation, sun azimuth angle, slope, and aspect; and masking shadowed areas by masking slopes with a particular slope angle and aspect .

Summary
For Sites #1-4, the areas of highest relative risk to landslides are those areas with slopes greater than 34º. Sites #2-4 exhibit more burn severity heterogeneity than Site #1 and thus they are influenced by a larger range of burn severities (low to high), whereas Site #1 is most affected by moderate to high burn severities. Steep slopes and low to moderate burn severities are given the highest weighting in the overall ranking system, so it is expected that these parameters would be most influential in the landslide hazard maps.

The areas in Sites #1-4 of highest relative risk to erosion are generally the steepest, north-facing slopes. Site #1 is influenced by moderate to high burn severities, whereas Sites #2 and #3 exhibit more burn severity heterogeneity and so are influenced by a larger range of burn severities (low to high). Site #1 is affected by moderate vegetation cover (26-50%), although the NDVI values appear to be more correlated to burn severity than to vegetation cover. This may be due to the large areas of bare soil present in this site. Site #3 is affected by a greater range of vegetation cover (26-75%). Sites #2 and #4 do not appear to be influenced by vegetation cover, which may be due to the more heavily weighted parameters (slope and burn severity) overriding the effects of vegetation cover.

STATISTICAL COMPARISON OF FIELD AND REMOTE SENSING DATA
Statistical comparisons between field mapping results and remote sensing data were obtained by calculating the kappa coefficient, K. This is a direct, pixel-by-pixel comparison, rather than a

comparison between groups of pixels as in the traditional bootstrap accuracy check. It was not necessary to compare slope and aspect between field mapping results and remote sensing data because they were assessed using the same data source (USGS 10-m DEMs). Burn severity, vegetation cover, and geology for each site were compared individually and the results discussed below. As previously stated, the range of K is 0-1, with zero corresponding to chance agreement and 1 corresponding to perfect agreement.

Site #1: Quartzite Mountain

The remote sensing data for burn severity was compared to field mapping results using a 4x4 confusion matrix (because there were four different ranking values for burn severity in this site) (Table 12). Although the remote sensing data visually appear to predict the areas of high burn severity well, the comparison yielded K = 0.15.

In order to ascertain whether the classification system for burn severity could be improved, the ranking values for burn severity were reclassified. The first reclassification grouped unburned and low severity burns together and assigned them a value of 2 (Table 13). Moderate and high burn severity were grouped together and assigned a value of 10. Recalculating kappa resulted in K = 0.39, which is a substantial improvement. A second reclassification maintained the original values for unburned and high burn severity (zero and 10, respectively) but grouped low and moderate severity burns and assigned these areas a value of 9 (Table 14). Recalculating kappa resulted in K = 0.15, which is the same as the original. A third reclassification grouped all areas into two classes, either unburned (assigned a value of zero) or burned (assigned a value of 10) (Table 15). This yielded K = 0.27, which is a notable improvement. Overall, it appears that the first reclassification yields the best results for this site (K = 0.39). This is most likely attributed to 80% of the total site area exhibiting high burn severity, which was predicted well by the remote sensing data.

Table 12. The 4x4 confusion matrix used to assess the accuracy of the remote sensing burn severity data to field mapping results at Site #1. Ranking values are noted in parentheses. Shaded areas contain actual number of pixels.

		Remote Sensing Reclassification Values			
		1 (0)	**5 (8)**	**11 (9)**	**19 (10)**
Field Mapping Reclassification Values	**25 (0)**	468	237	346	191
	50 (8)	650	1068	876	1823
	75 (9)	91	68	944	3176
	100 (10)	791	1696	8172	31,508
		K = 0.15			

Table 13. The 2x2 confusion matrix used to assess the accuracy of reclassified remote sensing burn severity data to field mapping results at Site #1. Ranking values are noted in parentheses. Shaded areas contain actual number of pixels.

		Remote Sensing Reclassification Values	
		1 (2)	**5 (10)**
Field Mapping Reclassification Values	**25 (2)**	2423	3236
	50 (10)	2646	43800
		K = 0.39	

Table 14. The 3x3 confusion matrix used to assess the accuracy of reclassified remote sensing burn severity data to field mapping results at Site #1. Ranking values are noted in parentheses. Shaded areas contain actual number of pixels.

		Remote Sensing Reclassification Values		
		1 (0)	**5 (9)**	**11 (10)**
Field Mapping Reclassification Values	**25 (0)**	468	583	191
	50 (9)	741	2956	4999
	75 (10)	791	9868	31,508
		K = 0.15		

Table 15. The 2x2 confusion matrix used to assess the accuracy of reclassified remote sensing burn severity data to field mapping results at Site #1. Ranking values are noted in parentheses. Shaded areas contain actual number of pixels.

		Remote Sensing Reclassification Values	
		1 (0)	**5 (10)**
Field Mapping Reclassification Values	**25 (0)**	468	774
	50 (10)	1532	49,331
		K = 0.27	

The remote sensing data for vegetation cover was compared to the field mapping results using a 2x2 confusion matrix. The field mapping results have rankings of 2 and 5, and the remote sensing results have rankings of 2, 3, and 4. Therefore, rankings were reclassified into values of 2 and not 2 (Table 16). This comparison yielded K = 0.16.

In order to evaluate whether the classification system for vegetation cover could be improved, the ranking values were reclassified (Table 17). A visual inspection of the remote sensing data for this site indicates that high burn severity areas have NDVI values less than -0.05 and

unburned areas have NDVI values greater than 0.2. Therefore, ranking values were reclassified so that NDVI values from -1 to 0.2 had a value of 5, and NDVI values from 0.2 to 1 had a value of 2. This resulted in K = 0.33, which is a substantial improvement and indicates difficulty in correctly predicting areas of intermediate vegetation cover.

The geology of the remote sensing data agreed perfectly with the field mapping results and because there were no discrepancies, K = 1.0.

Table 16. The 2x2 confusion matrix used to assess the accuracy of the remote sensing vegetation cover data to field mapping results at Site #1. Ranking values are noted in parentheses. Shaded areas contain actual number of pixels.

		Remote Sensing Reclassification Values	
		1 (2)	**5 (not 2)**
Field Mapping Reclassification Values	**25 (2)**	491	10,379
	50 (not 2)	158	45,246
		K = 0.16	

Table 17. The 2x2 confusion matrix used to assess the accuracy of the reclassified remote sensing vegetation cover data to field mapping results at Site #1. Ranking values are noted in parentheses. Shaded areas contain actual number of pixels.

		Remote Sensing Reclassification Values	
		1 (2)	**5 (5)**
Field Mapping Reclassification Values	**25 (2)**	4267	6603
	50 (5)	4187	41,217
		K = 0.33	

Site #2: Fourth of July Creek

The remote sensing data for burn severity was compared to the field mapping results using a 4x4 confusion matrix (because there were four different ranking values for burn severity in this site) (Table 18). This comparison yielded K = 0.22. The remote sensing data predicts areas of high burn severity very well.

The values for burn severity were reclassified the same as for Site #1. The first reclassification grouped unburned and low severity burns together and assigned them a value of 2 (Table 19). Moderate and high burn severity were grouped together and assigned a value of 10. Recalculating kappa resulted in K = 0.18, indicating this is not a better classification than the original. A second reclassification maintained the original values for unburned and high burn severity (zero and 10, respectively) but grouped low and moderate severity burns and assigned these areas a value of 9 (Table 20). Recalculating kappa resulted in K = 0.27, which is an

improvement. A third reclassification grouped all areas into two classes, either unburned (assigned a value of zero) or burned (assigned a value of 10) (Table 21). This yielded K = 0.28, which is similar to the second reclassification. Overall, it appears that the second and third reclassifications yield the best results for this site. This is probably because burn severity is highly variable within this site, and field mapping results indicate 29% of the total site area is unburned.

Table 18. The 4x4 confusion matrix used to assess the accuracy of the remote sensing burn severity data to field mapping results at Site #2. Ranking values are noted in parentheses. Shaded areas contain actual number of pixels.

		Remote Sensing Reclassification Values			
		1 (0)	**5 (8)**	**11 (9)**	**19 (10)**
Field Mapping Reclassification Values	**25 (0)**	7841	4981	6897	1254
	50 (8)	676	4468	2516	2174
	75 (9)	5085	7034	6780	3862
	100 (10)	246	3316	2963	9445
		K = 0.22			

Table 19. The 2x2 confusion matrix used to assess the accuracy of reclassified remote sensing burn severity data to field mapping results at Site #2. Ranking values are noted in parentheses. Shaded areas contain actual number of pixels.

		Remote Sensing Reclassification Values	
		1 (2)	**5 (10)**
Field Mapping Reclassification Values	**25 (2)**	17,966	12,841
	50 (10)	15,681	23,050
		K = 0.18	

Table 20. The 3x3 confusion matrix used to assess the accuracy of reclassified remote sensing burn severity data to field mapping results at Site #2. Ranking values are noted in parentheses. Shaded areas contain actual number of pixels.

		Remote Sensing Reclassification Values		
		1 (0)	**5 (9)**	**11 (10)**
Field Mapping Reclassification Values	**25 (0)**	7841	11,878	1254
	50 (9)	5761	20,798	6036
	75 (10)	246	6279	9445
		K = 0.27		

Table 21. The 2x2 confusion matrix used to assess the accuracy of reclassified remote sensing burn severity data to field mapping results at Site #2. Ranking values are noted in parentheses. Shaded areas contain actual number of pixels.

		Remote Sensing Reclassification Values	
		1 (0)	**5 (10)**
Field Mapping Reclassification Values	**25 (0)**	7841	13,132
	50 (10)	6007	42,558
		K = 0.28	

The remote sensing data for vegetation cover was compared to the field mapping results using a 3x3 confusion matrix. The field mapping results have rankings of 2, 4, and 5, and the remote sensing results have rankings of 2, 3, and 4. Therefore, rankings were reclassified into values of 2, 4, and not 2 or 4 (Table 22). This comparison yielded K = 0.01.

The ranking values for vegetation cover were then reclassified in the same manner as for Site #1 (Table 23). Visual inspection of the remote sensing data for this site indicates that high burn severity areas have NDVI values less than -0.05 and unburned areas have NDVI values greater than 0.2. Therefore, ranking values were reclassified so that NDVI values from -1 to 0.2 had a value of 5, and NDVI values from 0.2 to 1 had a value of 2. This resulted in K = 0.17, which is a substantial improvement.

The geology of the remote sensing data agreed perfectly with the field mapping results and because there were no discrepancies, K = 1.0.

Table 22. The 3x3 confusion matrix used to assess the accuracy of the remote sensing vegetation cover data to field mapping results at Site #2. Ranking values are noted in parentheses. Shaded areas contain actual number of pixels.

		Remote Sensing Reclassification Values		
		1 (2)	**5 (4)**	**11 (not 2 or 4)**
Field Mapping Reclassification Values	**25 (2)**	9540	1083	38,846
	50 (4)	3163	584	15,379
	75 (not 2 or 4)	18	688	2958
		K = 0.01		

Table 23. The 2x2 confusion matrix used to assess the accuracy of the reclassified remote sensing vegetation cover data to field mapping results at Site #2. Ranking values are noted in parentheses. Shaded areas contain actual number of pixels.

		Remote Sensing Reclassification Values	
		1 (2)	**5 (5)**
Field Mapping Reclassification Values	**25 (2)**	33,942	12,940
	50 (5)	11,856	9704
		K = 0.17	

Site #3: Lake Creek

The remote sensing data for burn severity was compared to the field mapping results using a 4x4 confusion matrix (because there were four different ranking values for burn severity in this site) (Table 24). This comparison yielded K = 0.16. The remote sensing data predicts areas of high burn severity well.

The values for burn severity were then reclassified the same as for Sites #1 and #2. The first reclassification grouped unburned and low severity burns together and assigned them a value of 2 (Table 25). Moderate and high burn severity were grouped together and assigned a value of 10. Recalculating kappa resulted in K = 0.27, which is a notable improvement. A second reclassification maintained the original values for unburned and high burn severity (2 and 10, respectively) but grouped low and moderate severity burns and assigned these areas a value of 9 (Table 26). Recalculating kappa resulted in K = 0.16, indicating this is not a better classification than the original. A third reclassification grouped all areas into two classes, either unburned (assigned a value of zero) or burned (assigned a value of 10) (Table 27). This yielded K = 0.32, which is a substantial improvement. Overall, it appears that the third reclassification yields the best results for this site. This is probably because burn severity is highly variable within this site, and field mapping results indicate 27% of the total site area is unburned.

The remote sensing data for vegetation cover was compared to the field mapping results using a 3x3 confusion matrix (both field mapping and remote sensing results have rankings of 2, 3, and 4) (Table 28). This comparison yielded K = 0.06.

Table 24. The 4x4 confusion matrix used to assess the accuracy of the remote sensing burn severity data to field mapping results at Site #3. Ranking values are noted in parentheses. Shaded areas contain actual number of pixels.

		Remote Sensing Reclassification Values			
		1 (0)	**5 (8)**	**11 (9)**	**19 (10)**
Field Mapping Reclassification Values	**25 (0)**	6048	4825	1070	2439
	50 (8)	215	504	439	1007
	75 (9)	1036	2268	3308	3713
	100 (10)	3685	7665	4855	11,035
		K = 0.16			

Table 25. The 2x2 confusion matrix used to assess the accuracy of reclassified remote sensing burn severity data to field mapping results at Site #3. Ranking values are noted in parentheses. Shaded areas contain actual number of pixels.

		Remote Sensing Reclassification Values	
		1 (2)	**5 (10)**
Field Mapping Reclassification Values	**25 (2)**	11,592	4955
	50 (10)	14,654	22,911
		K = 0.27	

Table 26. The 3x3 confusion matrix used to assess the accuracy of reclassified remote sensing burn severity data to field mapping results at Site #3. Ranking values are noted in parentheses. Shaded areas contain actual number of pixels.

		Remote Sensing Reclassification Values		
		1 (2)	**5 (9)**	**11 (10)**
Field Mapping Reclassification Values	**25 (2)**	6048	5895	2439
	50 (9)	1251	6519	4720
	75 (10)	3685	12,520	11,035
		K = 0.16		

Table 27. The 2x2 confusion matrix used to assess the accuracy of reclassified remote sensing burn severity data to field mapping results at Site #3. Ranking values are noted in parentheses. Shaded areas contain actual number of pixels.

		Remote Sensing Reclassification Values	
		1 (0)	**5 (10)**
Field Mapping Reclassification Values	**25 (0)**	6048	8334
	50 (10)	4936	34,794
		K = 0.32	

The ranking values for vegetation cover were then reclassified the same as was done for Sites #1 and #2 (Table 29). Visual inspection of the remote sensing data for this site indicates that high-severity burned areas have NDVI values less than -0.05 and unburned areas have NDVI values greater than 0.2. Ranking values were thus reclassified so that NDVI values from -1 to 0.2 had a value of 5, and NDVI values from 0.2 to 1 had a value of 2. This resulted in K = 0.14, which is a notable improvement.

Table 28. The 3x3 confusion matrix used to assess the accuracy of the remote sensing vegetation cover data to field mapping results at Site #3. Ranking values are noted in parentheses. Shaded areas contain actual number of pixels.

		Remote Sensing Reclassification Values		
		1 (2)	**5 (3)**	**11 (4)**
Field Mapping Reclassification Values	**25 (2)**	5951	30,851	482
	50 (3)	263	10,356	679
	75 (4)	309	7265	554
		K = 0.06		

Table 29. The 2x2 confusion matrix used to assess the accuracy of the reclassified remote sensing vegetation cover data to field mapping results at Site #3. Ranking values are noted in parentheses. Shaded areas contain actual number of pixels.

		Remote Sensing Reclassification Values	
		1 (2)	**5 (5)**
Field Mapping Reclassification Values	**25 (2)**	32,396	16,186
	50 (5)	3485	4643
		K = 0.14	

The remote sensing data for geology was compared to the field mapping data by using a 2x2 confusion matrix (because there were 2 different ranking values for geology in this site, 2 and 3) (Table 30). This resulted in K = 0.63.

Table 30. The 2x2 confusion matrix used to assess the accuracy of the remote sensing geology data to field mapping results at Site #3. Ranking values are noted in parentheses. Shaded areas contain actual number of pixels.

		Remote Sensing Reclassification Values	
		1 (2)	**5 (3)**
Field Mapping Reclassification Values	**25 (2)**	793,867	62,353
	50 (3)	12,117	78,532
		K = 0.63	

To summarize the findings for Sites #1-3, it appears that the first reclassification, which grouped unburned and low severity burns together and moderate and high burn severity together, yielded the highest kappa (0.39) for Site #1. This is probably because 80% of the total site area has high burn severity, which was predicted well by the remote sensing data. The third reclassification, which grouped all areas into classes of either unburned or burned, yielded the highest kappas for Sites #2 and #3 (0.28 and 0.32, respectively). This is attributed to the highly variable burn severity within these two sites. The minimum distance classifications do not predict areas of low and moderate severities as well as unburned and high severity burn areas.

In Sites #1-3, the kappa values for vegetation cover were low (0.16, 0.01, and 0.06, respectively). When the ranking values were reclassified so NDVI values from -1 to 0.2 had a value of 5 and NDVI values from 0.2 to 1 had a value of 2, the kappa values improved substantially (0.33, 0.17, and 0.14, respectively). It is not clear whether this is a true improvement, or is the result of reducing the number of classes compared (four for the original and two for the reclassification). There are two possible explanations for the low kappa values in vegetation cover. First, the NDVI transformations may not distinguish between understory and overstory vegetation cover. Second, NDVI values may be affected by high reflectivity soils.

The geology for Sites #1-3 was well predicted by the remote sensing data (i.e., the digitized compilation geology map). The geology of the remote sensing data agreed perfectly with the field mapping results in Sites #1 and #2, so K = 1.0. The remote sensing data for geology in Site #3 differed only slightly from the field mapping data, such that K = 0.63.

CLIMATE CONSIDERATIONS

Drought conditions, which have affected the study areas, have made it impossible to test the predictions made by the relative hazard maps. As noted by National Climatic Data Center

(2003), the current national-scale drought began in November 1999 and first peaked in August 2000. The drought peaked again in July 2002. Therefore, there simply has not been enough water (i.e. snow pack) available to initiate landslides or erosion since the wildfires of 2000.

CONCLUSIONS

This study demonstrates that remote sensing imagery is a promising tool in predicting areas of potential landslide and soil erosion hazards as a result of wildfire activity. For this study, remote sensing and DEM analyses can be used to evaluate slope, aspect, burn severity, and vegetation cover, which are important factors in determining landslide and erosion hazards. However, these analyses cannot be used to evaluate hydrology, geology, and soil characteristics. The methodology developed in this study is applicable for identifying and mapping landslide and erosion hazards in large, remote areas that have limited access. This is especially significant for land management, because this methodology requires fewer personnel and takes less time than traditional field mapping techniques. It is therefore a less expensive undertaking, even considering the cost of high-resolution remote sensing data. Another valuable aspect of this methodology is that it can be performed much quicker than field mapping, thus enabling land managers to respond faster and more efficiently with landslide and erosion mitigation efforts.

The types of remote sensing data most useful in this methodology are IKONOS data and USGS 10-m DEM's. IKONOS is fairly expensive, and thus the methodology developed for this study may also be performed using Landsat data for a significant cost reduction. If Landsat data are to be used, it would be most practical to use USGS 30-m DEM's because the compilation risk maps will only be as accurate as the coarsest-resolution source data available. In addition, USGS 30-m DEM's are more widely available than 10-m DEM's. An important consideration is the ability to obtain remote sensing imagery with resolutions sufficient for mapping site-specific parameters. The resolution of the remote sensing data should be appropriate for the particular hillslope processes being assessed.

It is important to note that relative hazard classification systems should be developed specifically for the regional area to be assessed. Classification systems may consider site-specific parameters, but should certainly include parameters of slope, burn severity, surface hydrology, understory vegetation cover (for erosion only), and soil characteristics. These parameters are all weighted most heavily in this study. Although understory vegetation cover and soil characteristics are generally considered to be significant factors influencing hillslope processes, field observations in Sites #1-3 do not indicate that these parameters substantially influence the likelihood of landslides and erosion. The parameters of aspect, geology, and are also important, but may not contribute significantly to the overall hazard maps and were ranked accordingly for this study. Obviously, the more parameters are used for assessment, the more comprehensive the hazard maps will be.

Either a supervised classification or NDVI transformation may be used to assess burn severity, although this study found a supervised classification to be most correlative to field mapping results. If both types of algorithms are used (as with this study), it should be noted that NDVI transformations cannot distinguish between understory and overstory vegetation cover. For example, a high NDVI value may be obtained from an area with burned understory and unburned overstory. This would be underpredictive and result in a low hazard ranking. In addition, results

for burn severity and vegetation cover assessment may overlap, causing the findings to be overpredictive. Another potential problem with using NDVI values is that this transformation is affected by high reflectivity soils. In areas with high soil visibility, it may be more effective to use the SAVI or other vegetation indices that take soil into account.

Two methods were used to assess the accuracy of the remote sensing classifications. The bootstrap method, which compares field-validated data to remote sensing classifications, yielded kappa values equal to or greater than 0.50. The second method was a direct, pixel-by-pixel comparison between field mapping and remote sensing classifications. The kappas produced with this method were equal to or less than 0.22. Visual comparisons between field mapping results and remote sensing data correlate fairly well; however, these kappa values yielded poorer results than expected.

There are several hypotheses for the differences in these kappa values. First, there may be slight differences between the georeferencing of the field and remote sensing data, which may be exaggerated by the pixel-by-pixel comparison. Second is the subjective bias at which boundaries are mapped in the field. Boundary locations and scale are subjective. This bias is not present in the 4-m resolution supervised classifications of the remote sensing data. Third, the remote sensing imagery classifies each 4-m pixel, whereas field mapping tends to group areas together at scales of tens-of-meters.

It is important to realize that kappa does not provide a measure of spatial correlation between two data sets. However, there may be an inherent difference in the spatial autocorrelation between the bootstrap and pixel-by-pixel methods. For example, the classes in the remote sensing data change more rapidly than the classes of the field mapping over a discrete spatial distance due to the remote sensing data 4-m pixel size. This spatial dependency is exaggerated in the pixel-by-pixel method (versus the bootstrap method). In other words, in the field mapping results, there is a higher likelihood that the pixel value at one geographic location will be related to the pixel next to it than in the pixel-by-pixel correlation.

The accuracies of the remote sensing burn severity classifications are dependent on the burn variability within the site. For example, Sites #2 and #3 yield the highest kappa values when burn severities are grouped into unburned and burned classes (K= 0.28 and K = 0.32, respectively). This is because these sites display a high degree of burn variability, and remote sensing classifications do not predict areas of low and moderate burn severity well. The highest kappa value for Site #1 is obtained by reclassifying the data into two classes, unburned to low burn severity, and moderate to high burn severity (K = 0.39). This is because Site #1 displays a low degree of burn variability and consists mostly of areas with high burn severity (80%). The most accurate comparisons for vegetation cover in Sites #1-3 occurred when NDVI values were reclassified into two classes. These classes include NDVI values from -1 to 0.2 and NDVI values from 0.2 to 1, and resulted in kappas of 0.33, 0.17, and 0.14 for Sites #1-3, respectively). It is not clear if this is a true improvement or is the result of reducing the number of classes (four for the original and two for the reclassification). Comparisons of geology were very accurate in Sites #1-3 (K = 1.0, K = 1.0, and K = 0.63, respectively); however, the compiled geologic map was based upon 1:100,00-scale field mapping performed by other geologists and was compared

to 1:24,000-scale field mapping done for this study, so this high degree of accuracy was expected.

Ground-truthing to assess the accuracy of the hazard maps created for Site #4 is beyond the scope of this study. Because this site was only validated against Sites #1-3, it should be ground-truthed more rigorously prior to being used by land managers in the SCNF. In order to perform ground-truthing, a validation strategy must be developed for selecting ground-truthing locations. This may be performed with grid or random point sampling. The ground-truth data will provide information regarding commission and omission errors, which may be used to evaluate the degree to which parameters included in the hazard maps are predicted correctly and incorrectly. Ground-truth data should also be assessed for which parameters contribute most significantly to landslide and erosion hazards in order to evaluate the ranking systems developed in this study.

ACKNOWLEDGEMENTS
I am grateful to Nancy Glenn, Glenn Thackray, and Paul Link for their expertise and guidance over the past three years. I thank the following people for their support and advice: Keith Weber, Linda Davis, John Welhan, Melissa Merrick, Chris Moller, Betsy Rieffenberger, and Jim Wolper. I feel lucky to have been part of the Geosciences Department Family – every member is supportive and encouraging, and their enthusiasm is contagious. This study was made possible by a fellowship from the NASA Sponsored Idaho Space Grant Consortium and grants from the Graduate Student Research and Scholarship Committee and the NASA Goddard Space Flight Center (ISU would like to acknowledge the Idaho Delegation for their assistance in obtaining this grant).

I thank my family for their love, patience, and unfailing support: Butch Wheeler, Mikki and Larrie Fitch, Del Sprague, Brian Sprague, Maxine and Don Foote, and Melanie and Alan Monson. Every good thing in my life is made possible by you. I am grateful to my best friends, who keep me grounded and in good spirits: Marcia Williams, Karen Edwards, Barbara Kracher, Duane DeVecchio, Tauna Butler, and Kebbie Wheeler. And to Butch Wheeler - the best husband, friend, and field assistant ever - it is difficult to articulate my love and gratitude. You make my world beautiful.

"It is never too late to be what you might have been." – George Eliot

LITERATURE CITED

Bailey, R.G., 1971, Landslide Hazards Related to Land Use Planning in Teton National Forest, Northwest Wyoming: U.S. Department of Agriculture Report, 131 p.

Benavides-Solorio, J., and MacDonald, L.H., 2001, Post-fire runoff and erosion from simulated rainfall on small plots, Colorado Front Range: Hydrological Processes, v. 15, p. 2931-2952.

Cannon, S.H., 2001, Debris-flow generation from recently burned watersheds: Environmental and Engineering Geoscience, v. 7, no. 4, p. 321-341.

Cannon, S.H., Bigio, E.R., Mine, E., 2001a, A process for fire-related debris flow initiation, Cerro Grande fire, New Mexico: Hydrological Processes, v. 15, p. 3011-3023.

Cannon, S.H., Kirkham, R.M., and Parise, M., 2001b, Wildfire-related debris-flow initiation processes, Storm King Mountain, Colorado: Geomorphology, v. 39, p. 171-188.

Carey, A., and Carey, S., 1989, Yellowstone's Red Summer: Flagstaff, AZ, Northland Publishing, 114 p.

Churchill, R.R., 1982, Aspect-induced differences in hillslope processes: Earth Surface Processes and Landforms, 7: 171-182.

Clayton, J.L., and Megahan, W.F., 1986, Erosional and chemical denudation rates in the southwestern Idaho batholith: Earth Surface Processes and Landforms, v. 11, p. 389-400.

Congalton, R.G., and Green, K., 1999, Assessing the Accuracy of Remotely Sensed Data: Principles and Practices: Boca Raton, FL, CRC Press, 137 p.

Cooke, R.U., and Doornkamp, J.C., 1990, Geomorphology in Environmental Management (2nd ed.): New York, NY, Oxford University Press, 410 p.

Crozier, M.J., Eyles, R.J., Marx, S.L., McConchie, J.A., and Owen, R.C., 1980, Distribution of landslips in the Wairarapa hill country: New Zealand Journal of Geology and Geophysics, v. 23, p. 575-586.

Doerr, S.H., Shakesby, R.A., and Walsh, R.P.D., 2000, Soil water repellency: its causes, characteristics, and hydro-geomorphological significance: Earth-Science Reviews, v. 51, no. 1-4, p. 33-65.

Dragovich, J.D., Brunengo, M.J., and Gerstel, W.J., 1993a, Landslide Inventory and Analysis of the Tilton River – Mineral Creek Area, Lewis County, Washington, Part 1: Terrain and Geological Factors: Washington Geology, v. 21, no. 3, p. 9-18.

Dragovich, J.D., Brunengo, M.J., and Gerstel, W.J., 1993b, Landslide Inventory and Analysis of the Tilton River – Mineral Creek Area, Lewis County, Washington, Part 2: Soils, Harvest Age, and Conclusions: Washington Geology, v. 21, no. 4, p. 18-30.

Dunne, T., and Leopold, L.B., 1978, Water in Environmental Planning: New York, NY, W.H. Freeman and Company, 818 p.

Easterbrook, D.J., 1999, Surface Processes and Landforms (2nd ed.): Saddle River, NJ, Prentice Hall, 546 p.

Ekren, E.B., 1988, Stratigraphic and structural relations of the Hoodoo Quartzite and Yellowjacket formation of Middle Proterozoic age from Hoodoo Creek eastward to Mount Taylor, central Idaho: U.S. Geological Survey Bulletin 1570, p. 1-17.

Environmental Systems Research Institute Inc., 2002, ArcView 3.3 and 8.2 Geographic Information System Software, Redlands, CA.

Evans, K.V., 1999, The Yellowjacket Formation of east-central Idaho, *in* Berg, R.B., ed., Belt Symposium III: Montana Bureau of Mines and Geology Special Publication 112, p. 17-30.

Evans, K.V., and Connor, J.J., 1993, Geologic map of the Blackbird Mountain 15-minute quadrangle, Lemhi County, Idaho: U.S. Geological Survey Miscellaneous Field Studies Map MF-2234, scale 1:62,500.

Fisher, F.S., and Johnson, K.M., 1995, Challis Volcanic Terrane, *in* Fisher, F.S., and Johnson, K.M., eds., Geology and Mineral Resource Assessment of the Challis 1° X 2° Quadrangle, Idaho: U.S. Geological Survey Professional Paper 1525, p. 41-43.

Gough, R.E., and Lamb, J., 2000, Fire-Resistant Plants for Montana Landscapes, available URL: http://www.montana.edu/wwwpb/pubs/mt200101.html, accessed April 13, 2003.

Gray, D.H., and Megahan, W.F., 1981, Forest vegetation and removal and slope stability in the Idaho batholith: USDA Forest Service Research Paper INT-271, 23 p.

Gritzner, M., Marcus, W.A., Aspinall, R., and Custer, S.G., 2000, Assessing landslide potential using GIS, soil wetness modeling and topographic attributes, Payette River, Idaho: Geomorphology, v. 37, p. 149-165.

Huete, A.R., 1988, A soil-adjusted vegetation index (SAVI): Remote Sensing of the Environment, v. 25, p. 295-309.

Huffman, E.L., MacDonald, L.H., and Stednick, J.D., 2001, Strength and persistence of fire-induced soil hydrophobicity under ponderosa and lodgepole pine, Colorado Front Range: Hydrological Processes, v. 15, p. 2877-2892.

Idaho Forest Products Commission, 2003, available URL: http://www.idahoforests.org/trees1.htm, accessed April 13, 2003.

Idaho Transportation Department, 1996, 1:100,000-Scale Metric Topographic Map of Challis, Idaho: scale 1:100,000.

Jensen, John R., 1996, Introductory Digital Image Processing (2nd ed.): Saddle River, NJ, Prentice Hall, 318 p.

Johansen, M.P., Hakonson, T.E., and Breshears, D.D., 2001, Post-fire runoff and erosion from rainfall simulation: contrasting forests with shrublands and grasslands: Hydrological Processes, v. 15, p. 2953-2965.

Keep Idaho Green, 2003, available URL: http://www.keepidahogreen.org/resident.htm,

accessed April 13, 2003.

Key, C.H., and Benson, N., 1999a, The Composite Burn Index (CBI): Field rating of burn severity, available URL: http://nrmsc.usgs.gov/research/cbi.htm, accessed September 30, 2002.

Key, C.H., and Benson, N., 1999b, The Normalized Burn Ration (NBR): A Landsat TM radiometric measure of burn severity, available URL: http://nrmsc.usgs.gov/research/ndbr.htm, accessed September 30, 2002.

Key, C.H., and Benson, N., 2002, Landscape Assessment, *in* Fire effects monitoring and inventory protocol, available URL: http://www.fire.org/firemon/lc.htm, accessed September 30, 2002.

Kimura, H., and Yamaguchi, Y., 2000, Detection of landslide areas using satellite radar interferometry: Photogrammetric Engineering and Remote Sensing, v. 66, no. 3, p. 337-344.

Kraemer, H.C., 1983, Kappa Coefficient: *in* Kotz, S. and N.L. Johnson, eds, Encyclopedia of Statistical Sciences: New York, NY, John Wiley and Sons, p. 352-354.

Koch, G.G., 1983, Hierarchical Kappa Statistics: *in* Kotz, S. and N.L. Johnson, eds, Encyclopedia of Statistical Sciences: New York, NY, John Wiley and Sons, p. 630-631.

Martin, D.A., and Moody, J.A., 2001, Comparison of soil infiltration rates in burned and unburned mountainous watersheds: Hydrological Processes, v. 15, p. 2893-2903.

McCarthy, D.F., 2002, Essentials of Soil Mechanics and Foundations (6th ed.): Saddle River, NJ, Prentice Hall, 788 p.

McKean, J., Buechel, S., and Gaydos, L., 1991, Remote Sensing and Landslide Hazard Assessment: Photogrammetric Engineering and Remote Sensing, v. 57, no. 9, p. 1185-1193.

Meyer, G.A., Pierce, J.L., Wood, S.H., and Jull, A.J.T., 2001, Fire, storms, and erosional events in the Idaho batholith: Hydrological Processes, v. 15, p. 3025-3038.

Meyer, G.A., Wells, S.G., Balling, R.C., Jr., and A.J.T. Jull, 1992, Response of alluvial systems to fire and climate change in Yellowstone National Park: Letters To Nature, v. 357, p. 147-150.

Moeremans, B., and Dautrebande, S., 2000, Soil moisture evaluation by means of multitemporal ERS SAR PRI images and interferometric coherence: Journal of Hydrology, v. 234, no. 3-4, p 162-169.

Nachtergaele, J., and Poesen, J., 1999, Assessment of soil losses by ephemeral gully erosion using high-altitude (stereo) aerial photographs: Earth Surface Processes and Landforms, v. 24, p. 693-706.

National Climatic Data Center, 2003, available URL: http://www.ncdc.noaa.gov/oa/climate/research/2003/feb/drought-national-overview.html#histfiles, accessed April 13, 2003.

National Interagency Fire Center (NIFC), 2001, available URL: http://www.nifc.gov, accessed October 16, 2002.

Pickup, G., and Marks, A., 2000, Identifying large-scale erosion and deposition processes from airborne gamma radiometrics and digital elevation models in a weathered landscape: Earth Surface Processes and Landforms, v. 25, p. 535-557.

Research Systems Inc., 2002, Environment for Visualizing Images (ENVI) Software, Boulder, CO.

Rieffenberger, B., 2000, USDA Forest Service Clear Creek Fire BAER Team Hydrology Report, Salmon-Challis National Forest, 21 p.

Ritter, D.F., Kochel, R.C., and Miller, J.R., 1995, Process Geomorphology (3rd ed.): Dubuque, IA, Wm. C. Brown Publishers, 546.

Ross, C.P., 1934, Geology and ore deposits of the Casto quadrangle, Idaho: U.S. Geological Survey Bulletin 854, p. 1-135.

Selby, M.J., 1993, Hillslope Materials and Processes (2nd ed.): New York, NY, Oxford University Press, 451 p.

Singhroy, V.H., Loehr, J.E., and Correa, A.C., 2000, Landslide risk assessment with high spatial resolution remote sensing satellite data: International Geoscience and Remote Sensing Symposium, Honolulu, 2000, Proceedings (URL: http://www.ccrs.nrcan.gc.ca/ccrs/rd/sci_pub/bibpdf/13012.pdf, accessed February 18, 2002).

Singhroy, V., and Mattar, K., 2000, SAR image techniques for mapping areas of landslides: International Society for Photogrammetry and Remote Sensing Conference, Amsterdam, 2000, Proceedings, p. 1395-1402.

Sohn, Y., and Rebello, N.S., 2002, Supervised and unsupervised spectral angle classifiers: Photogrammetric Engineering and Remote Sensing, v. 68, no. 12, p. 1271-1280.

Space Imaging, 2002, available URL: http://www.spaceimaging.com, accessed February 21, 2003.

Tysdal, R.G., 2000, Revision of Middle Proterozoic Yellowjacket Formation, Central Idaho: U.S. Geological Survey Professional Paper 1601-A, p. A1-A13.

United States Forest Service (USFS), 2001a, available URL: http://www.fs.fed.us/r4/sc, accessed October 16, 2002.

United States Forest Service (USFS), 2001b, A Report to the President in Response to the Wildfires of 2000, *in* National Fire Plan, available URL: http://www.fireplan.gov/president.cfm, accessed October 16, 2002.

Welhan, J., 2003, Geostatistics and Spatial Modeling: Idaho State University Department of Geosciences, Lecture Notes, p. 27-36.

Wilson, C.J., Carey, J.W., Beeson, P.C., Gard, M.O., and Lane, L.J., 2001, A GIS-based hillslope erosion and sediment delivery model and its application in the Cerro Grande burn area: Hydrological Processes, v. 15, p. 2995-3010.

Winston, Don, Link, P.K., and Hathaway, Nate, 1999, The Yellowjacket is not the Prichard and other heresies: Belt Supergroup Correlations, Structure and Paleogeography, east-central Idaho: *in* Hughes, S.S. and G.D. Thackray, eds, Guidebook to the Geology of Eastern Idaho: Pocatello, Idaho Museum of Natural History, p. 3-20.

VEGETATION CHANGE IN THE UPPER SNAKE, YELLOWSTONE, AND GREEN RIVER DRAINAGES: THE LAST 14,000 YEARS

Sharon R. Plager and Richard N. Holmer
Anthropological Research GIS Laboratory
Idaho State University
Pocatello, Idaho

ABSTRACT

Compiled pollen data from 28 cores indicate that the proportions of some plant species in Eastern Idaho and Western Wyoming have varied dramatically over the last 14,000 years. This information was used to examine how vegetation communities change over time. Discriminant analysis was used to determine the most influential species in community composition. The proportion of each discriminating species was interpolated for areas between cores using cokriging which allowed us to employ elevation. The general pattern of distribution in the predicted vegetation map for the historical period was comparable to the modern GAP data and provided the model for creating predictive maps for the notable vegetation peaks of the late Pleistocene and early and late Holocene.

Keywords: pollen coring, GIS, Idaho, historic.

INTRODUCTION

Humans have been exploiting the resources of eastern Idaho and western Wyoming for over ten thousand years. Near the center of our project area at Wasden Cave (Miller 1982), Folsom projectile points were found along with mammoth remains in deposits dating to 10,640 ± 85 BP, (AA-6833 accelerator date, Miller personal communication, 1997). Near the southwestern edge of the area, a twenty year old woman was buried with a spear point and bone needle 10,675 ± 95 years ago (Green, et al. 1998). In Yellowstone National Park near the eastern edge of the area, archaeological surveys and excavations have discovered large obsidian points which have provided hydration dates of 9,850 ± 278 years ago and 9,650 ± 248 years ago (Cannon 1993:8). These points are part of a broad collection of artifacts that document the exploitation of mammoth, bison, antelope, deer, and elk. To gain a better understanding of the resources available to early hunters and their prey from the Late Pleistocene into historic times, archaeologists attempt to reconstruct the environment in which they lived (Grayson 1998, Rhode 1999). Over the past several years, pollen cores have been collected from cave deposits on the Idaho National Engineering and Environmental Laboratory (INEEL) and from mountain lakes in eastern Idaho, Yellowstone National Park, Grand Teton National Park, and the Wind River Range (Figure 1).

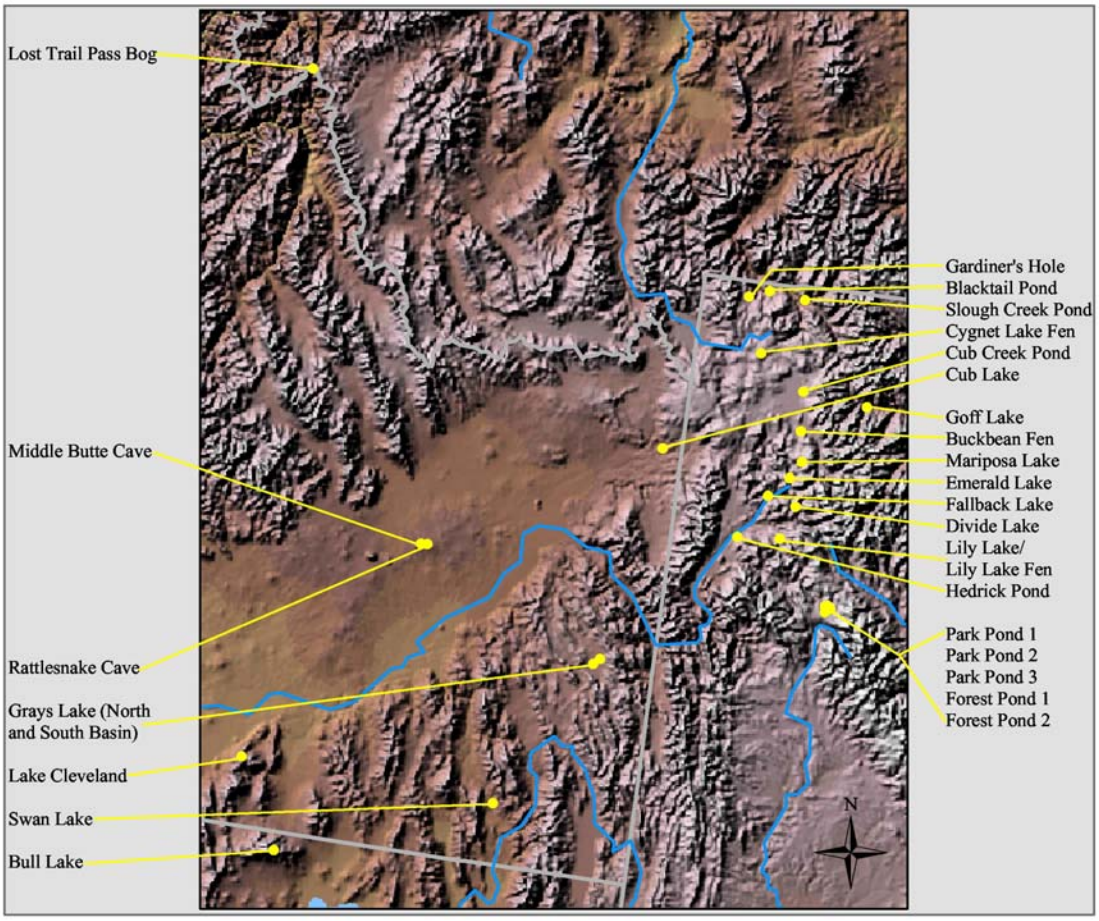

Figure 1. Shaded relief of the project area with core locations identified. The shaded relief was created by John Sterner at John Hopkins University Applied Physics Laboratory (Sterner 1995).

The local environment has fluctuated greatly as a result of global and regional weather fluctuations (regardless of human impacts) and there is no single "normal " or pristine environment that defines the Upper Snake River Basin. Therefore compiling what is known about "natural" fluctuations will provide a baseline to interpret the actual effects of past and modern societies and to appreciate what the immediate and long-term prospects are for environmental fluctuation. While pollen cores are typically used to recreate local vegetation change (Beiswenger 1991, Bright 1966, and Whitlock 1993), this research project explores the possibility of reconstructing how plant communities change over time on a regional scale.

Study Area

The study area (see Figure 1) extends 265 miles N-S by 230 miles E-W and encompasses an area of 60,950 square miles or nearly 40 million acres. The shaded relief shows the dramatic variation in topographic relief that characterizes the area which impacts its climate and consequent vegetation cover (Wigand 2003). The locations of the pollen cores are broadly dispersed across southeastern Idaho with one core from southwestern Montana and one from northern Utah. The pollen cores from western Wyoming are in closer proximity to one another with the five cores in the Wind River Range (Park Pond and Forest Pond locations) separated by only .9 to 2.3 miles. The furthest distance between pollen cores is 263 miles between Lost Trail Pass and Bull Lake with Bull Lake 259 miles from Slough Creek Pond and Lost Trail Pass 253 miles from the Wind River cores. This separation distance presents a number of difficulties when attempting to interpolate the vegetation between pollen cores, but it was anticipated that the Wind River Range cores would provide important information for modeling short-range spatial autocorrelation.

Pollen Database

We have compiled all published pollen data for the Upper Snake River and adjacent regions (see Table 1). Much of this data is available on the internet from the North American Pollen Database. When the raw pollen data was not available, data was extrapolated from published pollen diagrams. Two additional previously uninvestigated cores were included: a core from Bull Lake in northern Utah was analyzed by Van de Water and another core from the northern Grays Lake Basin was examined by Wigand (2003). Although the analysis varies among the locales, pollen was removed from the drilled cores at approximately every 10 cm. Plants were identified to family and genus and either raw counts or percentage of total pollen were recorded. All pollen counts have been converted to proportions to provide comparative data.

The pollen cores have been analyzed to varying degrees. For some cores, different species within a genus have been identified, such as *Pinus contorta* and *Pinus flexilis*, while in other cores, *Pinus* species were not differentiated. While the compiled database lists each core's raw data in the manner it was initially presented, additional variables have been added to combine species which were not consistently differentiated. Combined species include *Acer*, *Alnus*, *Ambrosia*, *Asteraceae*, *Ceanothus*, *Cercocarpus*, *Chenopodiaceae*/*Amaranthaceae*, *Ephedra*, *Eriogonum*, *Fraxinus*, *Galium*, *Juglans*, *Juniperus*, *Pinus*, *Populus*, *Potentilla*, *Prunus*, *Pseudotsuga*, *Ranunculus*, *Rosaceae*,

Sambucus, *Sarcobatus*, *Saxifragaceae*, *Scrophulariaceae*, *Shepherdia*, *Spiraea*, *Tsuga*, *Valeriana*, and *Xanthium*. In addition, all species of grass (*Gramineae*, *Poaceae*, and *Phragmites*) were combined. The following discussion refers to these combinations and the general patterns of their distribution. It should also be noted that this analysis deals only with terrestrial pollens which reflect changes in species distribution: aquatic pollens, spores and algae are included in some of the pollen analyses, but provide information regarding changes in aquatic systems.

Table 1. Locations of the pollen cores and the investigators that contributed data for this project. The number of sources that were used to interpolate each pollen cores chronology, as well as its age range in radiocarbon years BP are provided.

Core Location	**State**	**Investigator**	**Dates**	**Min. Age**	**Max. Age**
*Blacktail Pond	WY	Gennett 1977	4	0	11752
*Buckbean Fen	WY	Baker 1977	8	0	11500
Bull Lake	UT	Van de Water	5	2719	13398
*Cub Creek Pond	WY	Wright n.d.	3	128	11947
*Cub Lake	ID	Baker 1983	3	0	14096
*Cygnet Lake Fen	WY	Whitlock 1993	9	0	16484
*Divide Lake	WY	Whitlock 1993	5	0	12392
*Emerald Lake	WY	Whitlock 1993	6	459	12730
*Fallback Lake	WY	Whitlock 1993	3	8609	12173
*Forest Pond 1	WY	Lynch 1995	5	0	8703
*Forest Pond 2	WY	Lynch 1995	5	0	8687
*Gardiner's Hole	WY	Baker 1983	3	0	13850
*Goff Lake	WY	Wright n.d.	2	142	3710
Grays Lake - north	ID	Wigand 2003	4	72	4250
Grays Lake - south	ID	Beiswenger 1991	18	0	20717
*Hedrick Pond	WY	Whitlock 1993	6	0	17408
Lake Cleveland	ID	Davis, et al. 1986	5	0	12503
*Lily Lake	WY	Whitlock 1993	4	0	7507
*Lily Lake Fen	WY	Whitlock 1993	6	6286	12891
Lost Trail Pass Bog	MT	Mehringer, et al. 1977	16	0	15327
*Mariposa Lake	WY	Whitlock 1993	5	0	13369
Middle Butte Cave	ID	Davis, et al. 1986	6	2871	30407
*Park Pond 1	WY	Lynch 1995	3	180	4533
*Park Pond 2	WY	Lynch 1995	5	0	10328
*Park Pond 3	WY	Lynch 1995	5	394	10451
Rattlesnake Cave	ID	Davis, et al. 1986	6	0	13991
*Slough Creek Pond	WY	Whitlock and Bartlein 1993	6	0	13362
Swan Lake	ID	Bright 1966	4	0	12090

* Data is available from the North American Pollen Database.

METHODS

The project's objective was to produce vegetation maps for time periods identified as peak transitions by the data. If we could successfully predict modern vegetation based on our pollen core samples, we felt we could use the model to predict vegetation in earlier time periods. The pollen data indicate that some species, particularly sage, pine and grass, show dramatic fluctuations over time (Figure 2), while other species, particularly *Populus*, show almost no change even though *Populus* differentiates some plant communities from others. Therefore, we felt it was important to identify which species within our pollen samples were the most influential in distinguishing between the modern GAP vegetation classifications, rather than only using species that showed variation over time.

In selecting the most recent data for the last 200 years, only 22 pollen cores contributed data. Therefore, we included the most recent data from four more cores, Emerald Lake, Park Pond 3, Middle Butte, and Bull Lake to obtain data representative of the entire area. As some of the pollen cores have been analyzed at finer scales than others, they may contribute two or more data values for ages that fall within this range. Discriminant analysis indicated that 33 species had the most discriminating power. However, nine of these were not considered as they were present at four or less pollen locales. The remaining species determined to have the most predictive power were *Abies*, *Alnus*, *Ambrosia*, *Artemisia*, *Aster*, *Betula*, *Cercocarpus*, *Chenopodiaceae/Amaranthaceae*, *Ephedra*, *Eriogonum*, *grass*, *Juniperus*, *Picea*, *Pinus*, *Populus*, *Pseudotsuga*, *Quercus*, *Ranunculus*, *Rhamnaceae*, *Rosaceae*, *Rumex*, *Salix*, *Sarcobatus*, and *Thalictrum*.

Several interpolating methods were explored with the Wyoming data in an effort to find the best method for predicting vegetation between sampled locales. Unfortunately, the paucity of the data severely limits employing any interpolation method with any degree of accuracy. Relationships between species and other environmental variables were examined and elevation was found to have a weak correlation. As this project focused on determining general patterns of distribution, we felt that accuracy could be compromised to create a smooth surface and the capability of cokriging allowed us to capitalize on the correlation of species with elevation. In performing cokriging, we accepted the default coefficients calculated within ArcMap's Geostatistical Analyst. While adjustments were made to the search radius and the number of neighbors to include, these were attempted in an effort to produce predictions for the entire area and to smooth contours, not to improve accuracy or manipulate the distribution.

The shear size of the study area determined the resolution at which the analysis could be conducted. To comply with the limitations of our statistical software, we resampled concatenated digital elevation models (DEM) to produce a number of cells that would be manageable. This resulted in an image with a cell resolution of 316.683 m. Elevations associated with each cell's center point were used with the pollen data to create prediction maps for the 24 most influential species of the recent period.

The ISU GIS Training and Research Center had previously merged the GAP data for the center's specific area of concern (AOC) which includes Idaho, Montana, Wyoming, and Utah. As the AOC extends across four states, it was necessary to recode the GAP vegetation data from each state into a uniform system. We used the recoded vegetation coverage, which will be referred to as rcGAP, to distinguish it from each state's GAP analysis (Gap Analysis Program). For each cell, the rcGAP category was derived. Although, we refer to this as the historic map, we were really interested in how the vegetation landscape looked prior to Euro-American expansion into the area. Therefore we treated cells with rcGap codes such as agriculture or urban as missing data. Discriminant analysis was conducted based on the rcGAP vegetation categories using the predicted species distributions and elevation. Our first attempt produced a rather complex vegetation distribution simply because there were so many categories. In an attempt to simplify classifications into more general categories, we further combined the rcGAP classes into the following distinctive groups. All subsequent predicted classifications were based on these generalized vegetation groups which are organized by approximate elevation from highest to lowest.

Mixed Subalpine: Alpine fir, lodgepole pine, spruce, and whitebark pine are included in this classification in Idaho's GAP data. Within our predicted category, 37%

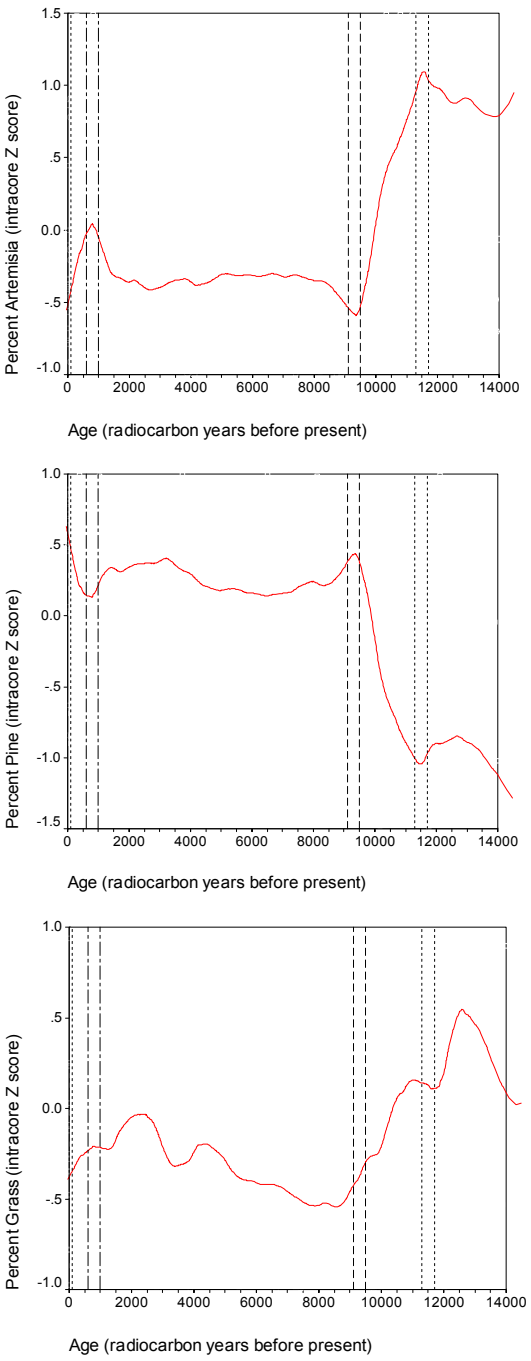

Figure 2. Fluctuations in the percent of sage, pine and grass over the last 14,000 years. Lines bracket the peak transition periods examined: single dotted line – present historic period; double dot and dash lines – late Holocene; double dash lines – early Holocene; and double dotted lines – late Pleistocene.

of the area was classed in the rcGAP as mixed subalpine, 21.7% was classed as whitebark pine, and 19.2% was classed as grassland. According to the discriminant analysis, this category has a comparatively small amount of grass and sagebrush cover.

Subalpine Meadow: Almost one third (29.3%) of the predicted subalpine meadow category was classified as subalpine meadow by the rcGAP with significant areas classed as mixed spruce and fir (23.4%), douglas-fir (7.3%), and lodgepole pine (23.3%). While the Idaho GAP Analysis defines this class as predominantly perennial montane or subalpine grass species, our predicted category includes more montane forbs and shrubs along with pine, spruce and fir which is consistent with the other rcGAP categories. Idaho's lodgepole pine class includes subalpine fir, Englemann spruce, whitebark pine, aspen and douglas-fir, as well as *Artemisia* spp. This is similar to what is found in the douglas-fir category with the addition of grand fir, ponderosa pine, and limber pine and shrubs such as serviceberry, snowberry, chokecherry, Oregon grape, and spirea. While *Asteraceae* and *Picea* occur in small amounts in each of the predicted categories, the subalpine meadow class contains the largest proportion.

Mixed Conifers: A number of different categories of the rcGAP comprise the predicted group mixed conifers. This is apparent when looking at how areas within the predicted group were formerly classed: 29.6% of predicted mixed conifer was classed as lodgepole pine in the rcGAP, 11.3% was classed as mixed subalpine, 10.1% was classed as douglas-fir, 7.7% was classed as grassland, and 9.2% was classed as big sagebrush. Our predicted group contains the third highest proportion of pine and fourth highest proportion of spruce within the pollen cores. Additional species include spruce, *Artemisia* spp., chenoams (*Chenopodeaceae*/*Amaranthaceae*), and various grasses.

Mixed Aspen/Conifer: *Populus* spp. occur in relatively small proportions within the pollen cores, yet we were able to differentiate this group with a relative degree of success. While areas within the predicted mixed aspen/conifer category were classed as mixed subalpine, douglas-fir, and lodgepole pine in the rcGAP, 23.4% of the area was classed as aspen and 26.7% was classed as big sagebrush. Perhaps the differentiating characteristic is that a 'median' amount of the discriminating species occurs in the mixed aspen/conifer group, except for juniper; it contains the highest proportion of J*uniperus* spp. of any of our predicted groups.

Mountain Sage: Within our predicted groups, the mountain sage category contains the highest proportions of *Artemisia* spp., *Betula*, *Ephedra* spp., *Eriogonum* and chenoams. This is the category referred to as montane shrub in the rcGAP, but we selectively named it mountain sage due to the dominance of sage and the fact that less than one percent of the predicted group was classed as montane shrub in the rcGAP. Within the mountain sage class, 33.6% of the area was formerly classed as big sagebrush, 17.8% as aspen, and 20.9% as douglas-fir. The Idaho GAP defines a warm mesic shrub category for southern Idaho as containing alder, serviceberry, Oregon grape, snowberry, willow, rose and various fruit-bearing shrubs: understory plants found in the douglas-fir category.

Riparian: The predicted riparian class has a high proportion of *Picea* and *Pinus* species and is most similar to the needleleaf dominated riparian class as defined in the Idaho GAP. This category includes douglas-fir, Englemann spruce, subalpine fir, maple, lodgepole pine, aspen and cottonwood. Comparatively, this predicted class has lower proportions mountain mahogany, chenoams, grass and juniper.

Grassland: In addition to various grasses, the predicted grassland class contains pine, spruce and some sagebrush, although it has the least amount of sage when other classes are compared. Discriminant analysis did reasonably well: 46.9% of the predicted grassland was classed by the rcGAP as grassland and 23.9% of the area was classed as sagebrush. Other grassland areas were classed as mixed xeric conifer, mixed subalpine and Douglas-fir. Interestingly, its proportion of pine is the highest compared to the other predicted categories, however, it is only slightly lower than in the mixed subalpine class. This is possibly due to the broad airborne distribution of pine pollen rather than stands of pine within the grassland.

Pinyon Pine/Juniper: The Idaho GAP defines the pinyon pine/juniper class as dominated by these two species, although mountain mahogany, serviceberry, *Artemisia* spp., bitterbrush, chokecherry, and snowberry may also occur. Only 8.4% of the area within predicted pinyon pine/juniper was classed as pinyon pine/juniper in the rcGAP; 16.8% of the area was classed as grassland and 53.2% of the area was classed as big sagebrush. The predicted class has a comparatively low proportion of pine, but its proportion of juniper is somewhat higher than average. The highest percent of mountain mahogany and *Abies* spp. occurs in this category.

Sagebrush Steppe: We combined the rcGAP sagebrush categories into one class, the sagebrush steppe. Following the descriptions given in the Idaho GAP, a variety of other plants could be found in association with *Artemisia* spp. depending on available moisture and elevation. These include grand fir, subalpine fir, mountain mahogany, lodgepole pine, ponderosa pine, douglas-fir, juniper, bearberry, Ceonothus, ninebark, chokeberry, snowberry, bitterbrush, greasewood, and bluebunch wheatgrass. Within the predicted sagebrush steppe group, 57.7% of the area was classed as big sagebrush in the rcGAP and 9.5% of the area was classed as grassland. The proportion of *Artemisia* spp. in the predicted sagebrush stepped is significant; however, it is not the highest compared to the other categories. Interestingly, there is almost as much pine as sagebrush, but again this is most likely a factor of the proliferation of *Pinus* pollen.

Sage/Grassland: Our predicted sage/grassland category contains the highest proportions of *Populus* spp., *Pseudotsuga* spp., *Quercus*, *Ranunculus*, and *Rosaceae* spp. when compared to the other categories. There is also a particularly high percent of grass and a comparatively high percent of *Artemisia* spp. and chenoams. This may account for the fact that 62.7 % of the area within predicted sage/grasslands was classed as big sagebrush within rcGAP.

Greasewood/Desert: Discriminant analysis repeatedly separated this category. Predicted greasewood/desert has the highest proportion of *Sarcobatus,* ragweed, and

grasses and the lowest proportion of pine. It also contains a significant amount of *Artemisia* spp. and chenoams. Comparing the predicted to rcGAP, 70.1% was classed as grassland in rcGAP, 10.1% was classed as big sagebrush, and 16.3% was classed as salt desert shrub. The Idaho GAP defines salt-desert shrub as budsage (*Artemisia spinescens*), shadscale (*Atriplex confertifolia*), 4-wing saltbush (*Atriplex spinosa*) and greasewood (*Sarcobatus vermiculatus*). As our pollen core data do not differentiate *Atriplex* spp., we elected to name the category greasewood/desert.

Using our combined classifications produced a generalized vegetation map (Figure 3) which we felt was comparative, at least visually, to the modern GAP data. Natural landscape features, such as sand dunes and lava, were recoded to match the reGAP data. In addition to the reconstructed historic vegetation distribution, we selected three earlier time periods in which to create vegetation maps because they appear to represent extremes in vegetation fluctuation (Figure 2). The three periods are:

Late Holocene Extreme: This period is generally known as the Medieval climate optimum or anomaly (Bettinger 1999:68) and dates to approximately 1100 – 600 years ago. It was a warm-dry period marked by a reduced distribution of pine when compared to earlier and later periods in the Holocene. Much of what today is coniferous forest was then subalpine meadowland, which also contained considerable amounts of sagebrush. The amount of grass was significantly greater than today but not as great as the Holocene peak around 2500 years ago.

Early Holocene Extreme: This period, dating to 9100 – 9500 years ago, was marked by a dramatic expansion of pine growth over earlier times spurred by the rapid warming at the onset of the Holocene but prior to the long-term drying effects of prolonged heat. The quantity and distribution of sagebrush, grass and pine is similar to historic vegetation cover. This period is probably equivalent to interstadial number seven recognized in millennial-scale climatic cycles throughout the northern hemisphere (Bond et. al 1997:1262).

Late Pleistocene Extreme: This period is probably the well-known Younger Dryas (10,000 – 11,200 years ago, Madsen 1999:79) although it seems to date a little earlier in our study area (11,300 – 11,700). This discrepancy may result from the interpolation of radiocarbon dates in pollen cores and the resultant averaging of many cores to produce the summary graphs shown in Figure 2. This period was marked by restricted and sparse pine distributions because most of the higher country was under ice and snow. Peripheral to the snow cover were coniferous forests although they did not extend into the lower elevations of the Snake River Plain, which supported much more grass than later climates making them ideal habitats for Pleistocene megafauna herbivores.

For each of the three earlier periods, pollen data was selected from age ranges that bracketed the noted extreme fluctuations. As for the recent historic period, it was sometimes necessary to either include a pollen core whose most recent date fell outside of the time range or extend the time range to include more core samples. Twenty-five cores contributed to the Late Holocene, 24 to the Early Holocene, and 22 to the Late

Pleistocene. Cokriging was used to create prediction maps for each of the 24 species within each of the time periods, with the exception of *Rhamnaceae*. This species did not occur in any of the cores during the Early Holocene or Late Pleistocene. However, we considered this to be an important factor and included its zero value in the discriminant function.

RESULTS

Vegetation maps for the four time periods are presented in Figure 3. The historic map shows what the eastern Snake River Plain and Yellowstone Plateau may have looked like prior to the urbanization, agriculture, forestry and mining impacts indicated in the modern GAP. Sagebrush steppe covered much of the lower elevations with mixed conifers extending across the Yellowstone Plateau and into the Island Park caldera region. A mixed subalpine forest was confined to the higher elevations of the Rocky Mountains while extensive grasslands dominated southwestern Montana. A mixed aspen/conifer forest surrounded what are now the Palisades and Blackfoot Reservoirs and pinyon/juniper forest extended northward from the Idaho/Utah border south of the Lake Walcott Reservoir. Jackson Lake was surrounded by an arc of mixed conifers but much of the landscape to the east and west was covered by subalpine meadow.

This was a significantly different landscape than that which characterized the late Holocene extreme. Subalpine meadow dominated areas which would later be dominated by sagebrush steppe, mixed aspen/conifer, and mixed conifers. Grasslands extended from Bear Lake northwest to the present American Falls Reservoir and across much of the region of the Henry's Fork. Mixed aspen/conifer forests were confined to the higher elevations of the Rockies and were bordered by mixed conifer and mountain sage vegetation. The mixed subalpine zone doesn't even occur. While the pinyon/juniper forest is still prevalent on the Idaho/Utah border a broad sage/grassland community surrounds the Lake Walcott Reservoir.

The predicted vegetation landscape for the early Holocene extreme is similar to the historic map. This is exactly what the data predict. Figure 2 shows the percent of pine, sage, and grass were at levels equivalent to recent data. The notable difference is that a sage/grassland zone doesn't occur in the early Holocene, indicating that this period may have been slightly drier or warmer than today.

The late Pleistocene was dramatically different. The predicted map indicates the entire Yellowstone Plateau, extending southwest into the area around Island Park, and including much of the Teton Range was in subalpine meadow. Much of this area was most likely under permanent snow, although the last vestiges of the Pinedale Glacier may have been visible in the Rocky Mountains. The mixed subalpine zone is extensive encompassing the mountain ranges of southeast Idaho except for the area around Bear Lake that is surrounded by subalpine meadow. The mixed aspen/conifer community is not as extensive as the subalpine zone, but drapes the mountain ranges to the northwest of the Snake River Plain. Sage/grasslands occupy the ranges south of the Snake River Plain while grasslands dominate the Plain. The distribution reflects a vegetation landscape adapted to considerably colder temperatures.

The paucity of data is apparent in the geometric boundaries of some of the vegetation zones, particularly visible in the Late Pleistocene which was based on data from only 22 pollen cores. These are also due to a violation of the assumption when using a kriging method that closely spaced data are more similar than data separated by greater distance. Within the compiled pollen data, this was often not the case. However, no effort has been made to make the maps more "realistic": the maps reflect the purely objective computation of probabilities for vegetation zone distribution.

In spite of these limitations, the general patterns appear to correlate with modern vegetation distribution and with what is known about the area from pollen and archaeological research. The percentage of land that falls within each of the vegetation zones is given in Table 2. While this helps to quantify vegetation change over time, again we are not implying any measure of accuracy. What is important is that, to our knowledge, this is the first attempt to produce a map, based on empirical data, of what the regional vegetation landscape may have looked like during the documented Late Pleistocene and Holocene extremes. The table shows that while the area within our vegetation zones may be similar in different time periods, the actual distribution as reflected in the predictive maps is significantly different.

Table 2. Area percentage of vegetation zones within each of the time periods mapped in Figure 3.

Classification	**Historic Period**	**Late Holocene Extreme**	**Early Holocene Extreme**	**Late Pleistocene Extreme**
Subalpine Meadow	5.4	44.9	3.3	41.8
Grassland	8.7	17.7	8.9	9.7
Mountain Sage	1.1	1.4	0	2.4
Greasewood/Desert	.4	1.7	.3	.2
Sagebrush Steppe	45.3	7.9	48.5	3.3
Pinyon/Juniper	3.4	5.7	3.6	0
Mixed Aspen/Conifer	7.2	6.0	4.8	.4
Mixed Coniferous	20.5	6.5	23.0	14.1
Mixed Subalpine	2.4	0	2.3	17.0
Riparian	0	.1	0	0
Sage/Grassland	.3	2.8	0	5.8
Barren or Open Water	5.3	5.3	5.3	5.3
Total Percent	100	100	100	100

CONCLUSIONS

The goal of this project was to gain an appreciation of how past climate changes are reflected in the landscape vegetation. We initiated this project without any preconception about the distribution of prehistoric vegetation other than it would correlate somewhat

with elevation. The maps solely reflect co-kriged predictions: the numbers speak for themselves.

Our pollen core samples are so few and the distances between most are so great, there is no way to know how well our maps represent the actual distribution of vegetation at these time periods. The only way to improve on this is to acquire more data, either with additional pollen cores, particularly along the Snake River Plain and in the ranges that border it, or with the analysis of unexamined existing cores from the project area. However, the predictive maps are much more revealing that we thought possible. We now have a model by which we can test additional time periods, perhaps exploring the millennial cycles noted by other researchers within the Great Basin (Madsen 1999). We have snapshots of the Holocene landscape and can begin to test these against the archeological data to address questions regarding how earlier inhabitants adapted to a changing environment and exploited and manipulated its resources. We may never have all the answers, but each gives us more insight into not only the past, but also the influence we have on our present environment.

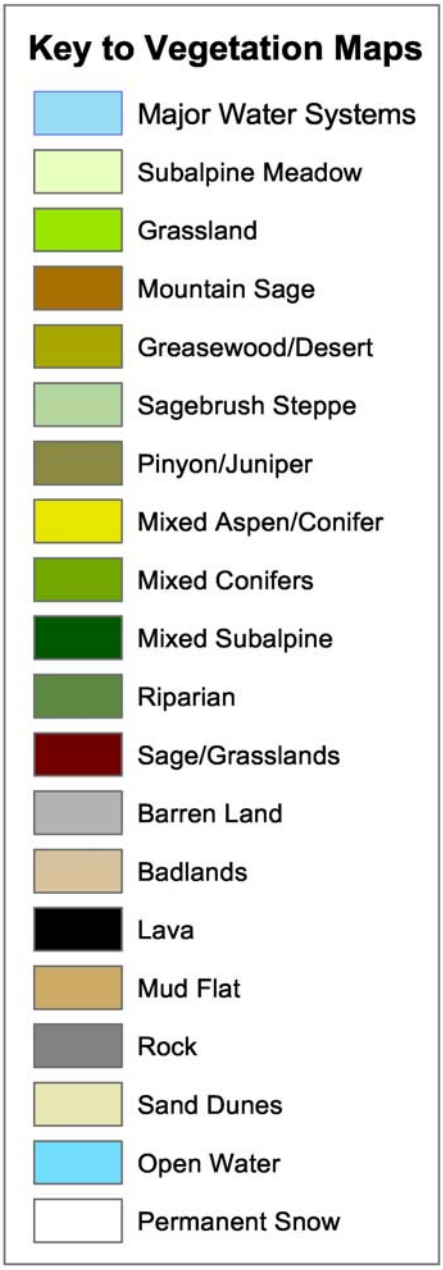

Figure 3. This legend is associated with the four maps on the following page. Each of the maps represents the general distribution of vegetation zones for a particular time period. The reader is cautioned that these are only generalized maps.

Historic Map 150 - 250 BP

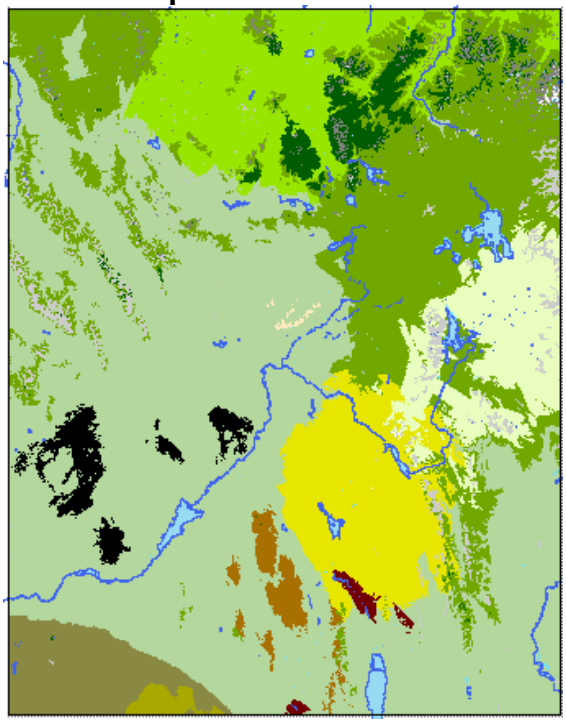

Late Holocene Extreme: 600 - 1000 BP

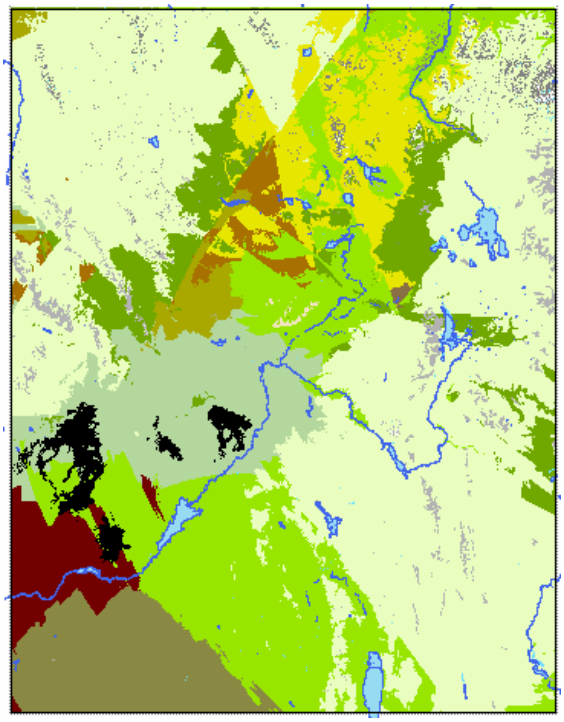

Early Holocene Extreme: 9100 - 9500 BP

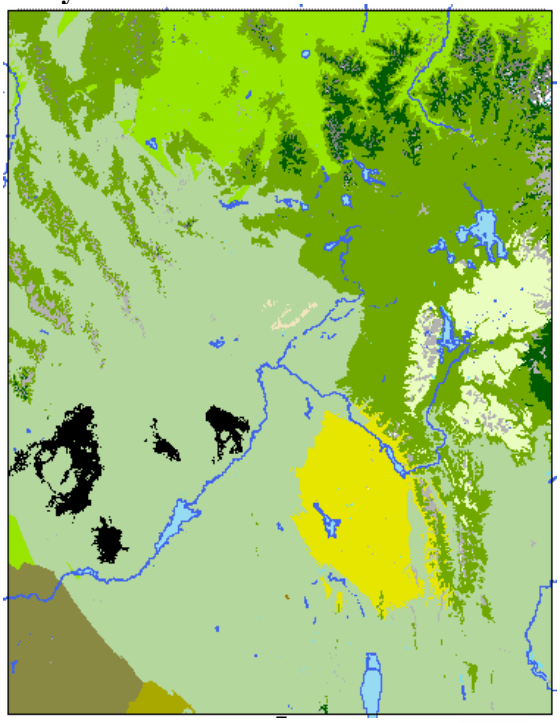

Late Pleistocene Extreme: 11300 - 11700

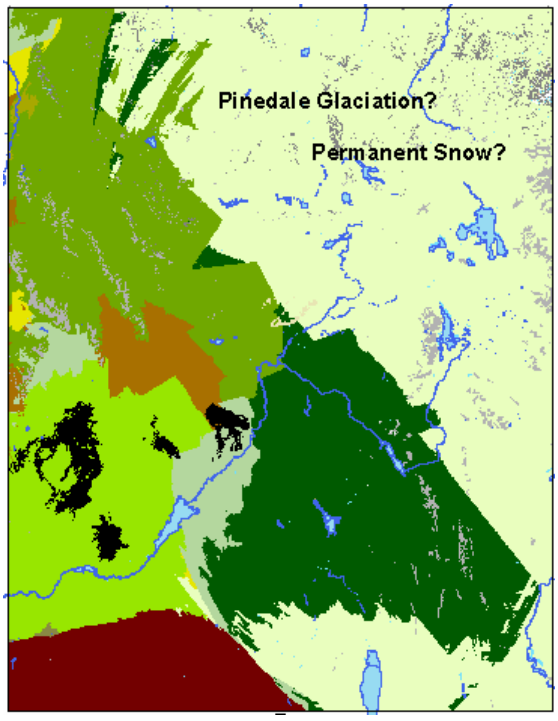

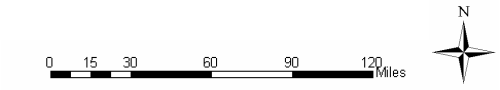

ACKNOWLEDGEMENTS
This study was made possible by a grant from the National Aeronautics and Space Administration Goddard Space Flight Center. ISU would also like to acknowledge the Idaho Delegation for their assistance in obtaining this grant.

LITERATURE CITED

Baker, R.G., 1976, Late Quaternary vegetation history of the Yellowstone Lake Basin, Wyoming. *United States Geological Survey Professional Paper* 729_E.

Baker, R.G., 1983, Holocene vegetational history of the western United States. *in* Wright, H.E., Jr., ed., Late-Quaternary environments of the United States, Volume 2 The Holocene. Minneapolis, University of Minnesota Press.

Beiswenger, J.M., 1991, Late Quaternary vegetational history of Grays Lake, Idaho: Ecological Monographs, v. 61, no.2, p.165-182.

Bettinger, R.L., 1999, What happened in the Medithermal. Beck, C., ed., Models for the Millennium: Great Basin Anthropology Today. Salt Lake City, UT, The University of Utah Press.

Bond, G., Showers, W., Cheseby, M., Lotti, R., Almasi, P., deMenocal, P., Priore, P., Cullen, H., Hajdas, I., Bonani, G., 1997, A pervasive millennial-scale cycle in North Atlantic Holocene and glacial climates: Science, v. 278, p. 1257-1266.

Bright, R.C., 1966, Pollen and seed stratigraphy of Swan Lake, Southeastern Idaho: Its relation to regional vegetational history and to Lake Bonneville history: Tebiwa, v. 9, no. 2, p.1-47.

Cannon, K.P., 1993, Paleoindian use of obsidian in the greater Yellowstone area: new evidence of the mobility of early Yellowstone people: Yellowstone Science, v. 1, no. 4, p.6-9.

Davis, O.K., Sheppard, P.S., and Robertson, S., 1986, Contrasting climatic histories for the Snake River Plain result from multiple thermal maxima: Quaternary Research, v. 23, p. 321-339.

Gap Analysis Program, http://www.gap.uidaho.edu/Projects/FTP.htm

Gennet, J.A., 1977, Palynology and paleoecology of sediments from Blacktail Pond, northern Yellowstone Park, Wyoming [M.S. thesis]: University of Iowa.

Grayson, D.K., 1998, The Desert's Past: A Natural Prehistory of the Great Basin: Washington, D.C., Smithsonian Institution.

Green, T.J., Cochran, B., Fenton, T.W., Woods, J.C., Titmus, G.L., Tieszen, L., Davis, M.A., Miller, S.J., 1998, The Buhl burial: a Paleoindian woman from Southern Idaho: American Antiquity, v. 63, no. 3, p. 437-456.

Idaho State University GIS Training and Research Center, http://giscenter.isu.edu/

Lynch, E.A., 1995, Origin of park-forest vegetation mosaic in the Wind River Range, Wyoming [dissertation]: University of Minnesota.

Madsen, D.B., 2000, Late Quaternary paleoecology in the Bonneville Basin: Utah Geological Survey Bulletin 130, 190 p.

Madsen, D.B., 1999, Environmental change during the Pleistocene-Holocene transition and its impacts on human populations. *in* Beck, C., ed., Models for the Millennium: Great Basin Anthropology Today. Salt Lake City, UT, The University of Utah Press.

Mehringer, P.J., Jr., Arno, S.F., and Peterson, K.L., 1977, Postglacial history of Lost Trail Pass Bog, Bitterroot Mountains, Montana: Artic and Alpine Research, v. 9, no. 4, p. 345-368.

Miller, S.J., 1982, The archaeology and geology of an extinct megafauna/fluted point association at Owl Cave, the Wasden site, Idaho: a preliminary report. *in* Ericson, J.E., Taylor,R.E., and Berger, R., eds., Peopling of the New World. Los Altos, CA, Ballena Press, Anthropological Papers No. 23, p.81-95.

Rhode, D., 1999, The role of paleoecology in the development of Great Basin archaeology, and vice-versa: *in* Beck, C., ed., Models for the Millennium: Great Basin Anthropology Today. Salt Lake City, UT, The University of Utah Press.

Sterner, R., 1995, Color landform atlas of the United States: John Hopkins University Applied Physics Laboratory.

Whitlock, C., 1993, Postglacial vegetation and climate of Grand Teton and southern Yellowstone National Parks: Ecological Monographs, v. 63, no. 2, p. 173-198.

Whitlock, C. and Bartlein, P.J., 1993, Spatial variations of Holocene climatic change in the Yellowstone region: Quaternary Research, v. 39, p. 231-238.

Wigand, P.E., 2003, Southeastern climatic transition region in the Northern Rockies, unpublished manuscript.

Wigand, P.E. and Rhode, D., 2002, Great Basin vegetation history and aquatic systems: the last 150,000 years: *in* Hershler, R., Madsen, D.B., and Currey, eds., Great Basin Aquatic Systems History. Smithsonian Contributions to Earth Sciences 33, Washington, D.C., Smithsonian Institution Press.

Wright, H.E., Jr., n.d., Pollen analyses at Mummy Cave and nearby areas, Northeastern Wyoming, [unpublished manuscript]: University of Minnesota.

EVALUATING DIFFERENT SCALES OF REMOTELY SENSED DATA TO PREDICT AMPHIBIAN HABITAT DISTRIBUTIONS

Jeremy P. Shive and Charles R. Peterson
Department of Biological Sciences
Idaho State University
Pocatello, ID 83209-8130
(e-mail: shivejere@isu.edu, petechar@isu.edu)

ABSTRACT
We evaluated three scales (spatial and spectral) of remotely sensed data to model wetland habitat distributions in two ecologically distinct wilderness landscapes. Two multispectral datasets, Landsat ETM+ (30 m, 6 bands) and ADAR 5500 (2 m, 4 bands), and one hyperspectral dataset, Hymap (3.5-4 m, 126 bands), were processed using numerous classification algorithms to map wetland features. The classifications were validated using traditional error matrices and also interpreted from the viewpoint of an ecologist conducting field surveys. The HyMap hyperspectral data produced the greatest classification accuracies of fine-scale wetland features; it was unmatched by the multispectral data. The hyperspectral data provide additional information used to distinguish habitat features and should be considered a valuable tool for future inventory and monitoring initiatives that require fine-scale comprehensive information across large spatial extents.

Keywords: hyperspectral, inventory and monitoring, scale, Frank Church-River of No Return Wilderness.

INTRODUCTION

Based on observations over the past two decades it has been recognized that amphibian populations are exhibiting global population declines, which has stimulated concern among herpetologists and conservation biologists around the world. In response to ongoing population declines, substantial effort has been invested in establishing broad scale inventory and monitoring initiatives to better understand current amphibian population distributions and relative abundance across large landscapes.

In most cases, inventory and monitoring programs have only recently begun and the collection of initial inventory data remains the primary objective. Following the inventory phase, repeated surveys can form the basis for a monitoring program. Monitoring specific key amphibian habitat features (e.g., shallow shorelines and emergent vegetation) can serve as a surrogate for organismal response to habitat alteration over time. Modeling habitat features may also provide insights concerning the effects of proposed management actions on population dynamics across broad spatial scales.

The ideal scenario for an inventory and monitoring program would be a comprehensive survey of all habitat available within the study area (Fellers 1997), but this is rarely possible because current amphibian habitat distribution is commonly unknown. Small wetland sites (i.e., several m^2) are not commonly detected using traditional methods of environmental mapping, such as USGS topographic maps and Digital Orthophoto Quarter Quadrangle (DOQQ) aerial photographs. Standard imagery or maps typically help identify potential habitat distribution and assist a researcher in designing the most appropriate sampling scheme or site selection process. Since these data sources do not always provide accurate information, ground based surveys are hindered due to the total number of hours needed to thoroughly inventory a region such as a forest or wilderness area.

Recent advances in remote sensing technologies and the numerous scale options (i.e., radiometric, spatial, and spectral) commercially available today significantly enhance researchers' abilities to design studies and investigate biological or ecological questions that previously could not be considered. In this study, we have taken a multi-scale approach to assess the applicability of current remote sensing technologies to model wetland habitat distribution in a wilderness area. The results are interpreted from an inventory and monitoring application perspective to propose the most appropriate remotely sensed data type for future broad scale amphibian conservation programs.

Study Area

The study area is located in the Frank Church-River of No Return Wilderness, Idaho (Figure 1). Two ecologically different landscapes within the study area were chosen as representative study sites. The first site is located along Big Creek, a fourth-order stream and major tributary to the Middle Fork of the Salmon River with elevations ranging from approximately 1100 m to 1900 m. Douglas Fir (*Pseudotsuga menziesii*) and Ponderosa Pine (*Pinus ponderosa*) are the dominant tree species within the drainage while Black

Cottonwood (*Populus balsamifera*), Water Birch (*Betula occidentalis*), and Green Alder (*Alnus viridis*) represent the tree species most commonly found in the riparian areas along Big Creek and local tributaries. Rocky Mountain Maple (*Acer glabrum*), Syringa (*Philadelphus lewisii*), and Prairie Rose (*Rosa woodsii*) comprise the majority of understory shrubs in the riparian area, while Giant Wildrye (*Elymus piperi*) and Idaho Fescue (*Festuca spp*.) characterize the drier upland hillsides. The second site is located in the Bighorn Crags, a sub-alpine region of the wilderness characterized by high elevation glaciated cirque basins with elevations ranging from approximately 2400 m to 2900 m. Sub Alpine Fir (*Abies lasiocarpa*), Engelmann Spruce (*Picea engelmanni*), and Whitebark Pine (*Pinus albicaulis*) characterize the forested uplands and valley floors. Beargrass (*Xerophyllum tenax*) and Grouse Whortleberry (*Vaccinium scoparium*) dominate the forest understory and sedge (*Carex spp*.) is commonly associated with mesic meadows and wetland habitat.

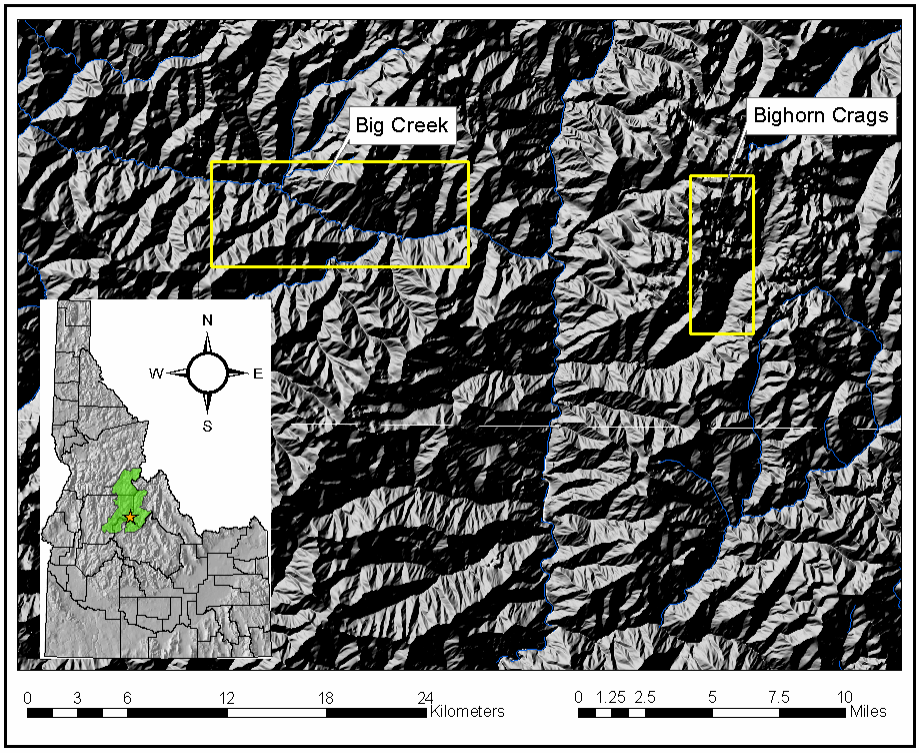

Figure 1. The location of the Frank Church-River of No Return Wilderness, Idaho shown in green, with the study area denoted by the orange star. The approximate area of the study sites are delineated by the yellow border.

METHODS

Image Acquisitions and Processing

We performed all image processing and image classifications using Research Systems Inc.'s ENVI® 3.5 (RSI, 2002) and all GIS analyses were conducted using Environmental Systems Research Institute, Inc.® ArcGIS 8.2.

Multispectral Data

The first multispectral dataset was collected on July 10, 2002 by NASA's Landsat 7 Enhanced Thematic Mapper Plus (ETM+) satellite. Landsat ETM+ uses an oscillating scanning mirror with +/- 5.78º angular displacement off-nadir, resulting in an image swath of approximately 185 km and an instantaneous field of view (IFOV) (i.e., spatial resolution) of 30 m for all spectral bands. The Landsat ETM+ sensor collects six spectral bands of 8-bit data in the visible and infrared region of the electromagnetic (EM) spectrum (Table 1).

The Landsat ETM+ data were received in the form of digital number (DN) values and we converted these data to at-sensor reflectance. The reflectance conversion process is calculated as:

$$L_\lambda = ((LMAX - LMIN)/255) \cdot DN + LMIN$$

Where, L_λ, is radiance ($W/m^2/sr/\mu m$) for each spectral band, LMIN and LMAX are the gains and bias information respectively that are obtained from the image header file, and DN represents the assigned digital number of a spectral band.

Reflectance, ρ_λ, for each band is calculated as:

$$\rho_\lambda = \frac{\pi \cdot L_\lambda}{ESUN_\lambda \cdot \cos\theta \cdot d_r}$$

Where L_λ is the radiance for each spectral band, $ESUN_\lambda$ is the mean exo-atmosphere irradiance for each band (Landsat 7 Science Users Handbook, Chapter 11, 2002) in units of $W/m^2/\mu m$, cosine θ ($\theta = 90^\circ - \beta$) where β is the sun elevation angle. The term d_r is defined as $1/d_{e\text{-}s}^2$ where $d_{e\text{-}s}$ is the relative distance between the earth and sun in astronomical units (Duffie and Beckman 1980). The term d_r is calculated as:

$$d_r = 1 + 0.033 \cos(DOY\ 2\pi/365)$$

Where DOY is the sequential day of year.

The second multispectral dataset was collected on July 31, 2002 by Positive System's Airborne Data Acquisition and Registration (ADAR) 5500 system. The ADAR 5500 system incorporates Kodak Professional DCS 420 digital frame cameras with a 39º across-track field of view and a 0.44 mrad instantaneous field of view (IFOV) for each pixel in the CCD array. The ADAR 5500 was configured to collect four spectral bands of 8-bit data in the visible and near-infrared regions of the EM spectrum (Table 1) with a spatial resolution of approximately 2 m.

Hyperspectral Data

Hyperspectral data were acquired on June 30, 2002 by the airborne hyperspectral sensor HyMap (Cocks et al. 1998). HyMap uses a whiskbroom sensor with a 61.3º field of view (512 across track pixels) with an IFOV of 2.5 mrad along track and 2.0 mrad across track. HyMap is typically flown on a twin engine fixed wing Cessna mounted with a gyro-stabilized platform and incorporates a Boeing C-MIGITS II Global Positioning System (GPS)/Inertial Monitoring Unit (IMU) that corrects for aircraft roll, pitch, and yaw caused by turbulence. HyMap collects 128 spectral bands of 12-bit data covering 0.44 μm – 2.5 μm spectral region with a 15 nm average bandwidth (Table 1). Spatial resolution of the hyperspectral data collected over the Big Creek and Bighorn Crags study sites were 4 m and 3.5 m respectively.

The raw radiance data ($\mu W/cm^2$ /sr/nm) collected by the HyMap sensor are influenced by incoming solar irradiance and atmospheric absorptions from gases such as water vapor, ozone, carbon monoxide, oxygen, carbon dioxide, nitrous oxide, and methane (Gao et al. 1993). In order to produce spectral signatures that can be compared with laboratory or ground-based spectra, and quantitatively evaluated, the radiance data must be converted into apparent reflectance. The data vendor provided the hyperspectral imagery already atmospherically corrected using a radiative transfer model ATREM (Gao et al. 1997). The reflectance data were also spectrally "polished" using the Empirical Flat Field Optimal Reflectance Transformation (EFFORT), which removes residual and cumulative calibration and model imposed errors (Boardman 1998a).

The Hymap data are collected on a pixel-by-pixel basis and therefore geometric corrections must be made to the data to insure that each pixel can be referenced to a real-world coordinate system and used with other spatial datasets. All of the pixel coordinates recorded during the flight are organized into an Input Geometry File (IGM) that preserves the spatial integrity of the ground pixel relationships (Boardman 1999). Then a Geometry Lookup Table (GLT) is created which provides the truly measured coordinate positions supplied from the onboard C-MIGITS II GPS/IMU that corrects for platform motion and topography (Boardman 1999). We applied the geometric correction files to the reflectance data which eliminated overlapping redundant pixels and resampled "gaps" in the data producing a geometrically corrected contiguous image.

We used the Minimum Noise Fraction (MNF) transform to segregate the noise dominated spectral bands from the "information rich" spectral bands, and to spectrally reduce the computationally expensive dataset. The MNF transform can be considered a two-step principal components analysis that accounts for correlated noise in the data caused by contiguous sequential spectral bands. The first step calculates a noise covariance matrix and decorrelates and rescales the noise in the data (Green et al. 1988). The second step is a standard Principal Component (PC) transformation where the transformed spectral bands are organized by decreasing variance (Green et al. 1988). We examined the MNF transformed images using ENVI's animation feature and considered the resulting eigenvalue plots to determine the dimensionality of each dataset. The assigned image

dimensionality (i.e., the significant MNF bands) served as the input for subsequent hyperspectral processing steps.

We used the Pixel Purity Index (PPI) and n-Dimensional Visualizer (nDV) to spatially reduce the dataset and identify the most spectrally "pure" pixels, or endmembers, in the imagery. The PPI repeatedly projects n-dimensional scatter plots onto a random unit vector cumulatively scoring the pixels with the highest and lowest values as well as any other pixels falling within a defined standard deviation. Pixels with extreme values are scored most often and theoretically represent the corners, or potential endmembers, of the multi-dimensional cloud of image pixels (Boardman 1993). The nDV rotates potential endmember pixels (i.e., the results from the PPI) in a user-defined number of spectral dimensions. We altered the number of spectral dimensions to expose endmember "corners" that are less evident in some collapsed dimensional axes. We selectively chose the most spatially distinct corners in the multidimensional cloud of data and exported each endmember pixel(s). This tool is interactively linked to the image and through repetitive investigations of the spatial distributions of endmember pixels, we were able to select image endmembers located within boundaries of features of interest (e.g., wetlands).

Image Classification

Multispectral Data

The intent of the classification process is to map the distribution of wetland habitat as an indicator of potential amphibian habitat. We are not abiding to a strict definition of a wetland and from this point forward we will refer to a wetland site generically as any location of standing water in the form of permanent lakes or ephemeral ponds and pools, but also wet meadows where water presence may be no more than a thin film or moist soil holding small puddles. These site descriptions characterize typical amphibian habitat in the study area and hence are the focus of our classification efforts.

The topography throughout the study area is characterized by steep slopes and ridges that produce an abundance of shadow influenced locations within both study sites. Shadows and water exhibit a similar spectral response pattern of very low reflectance, and consequently these two classes were continually misclassified and confused in the multispectral imagery. We decided the most accurate classifications of water features (i.e., wetlands) would be to distinguish them from the shadowed pixels in each image, and we paid close attention to selecting representative water and shadow training ROI's (Regions of Interest). We selected pixels in multiple training sites across the extent of each dataset to develop statistically representative ROI's needed for appropriate image classifications (Jensen 2000). We were not concerned with the ability to correctly classify surrounding vegetation features and collapsed all other image features into a single class labeled "everything else". This approach delineates a total of three spectral training ROI classes (i.e., water, shadow, and everything else) used to classify the Landsat ETM+ imagery. We attempted to classify an additional feature, sedge, in the ADAR 5500 imagery, but following preliminary visual assessment we determined the

Table 1. A comparison of the remotely sensed data specifications used in the study.

Sensor	Type of Imagery	Spatial Resolution	Spatial Extent*	Spectral Bands	Spectral Sampling	Spectral Range	Radiometric Resolution
HyMap	Hyperspectral	3.5 - 4m	2.5km x 20km	126	VIS 15nm	450nm - 890nm	12 bit
					NIR 15nm	890nm - 1350nm	
					SWIR1 13nm	1400nm - 1800nm	
					SWIR2 17nm	1950nm - 2480nm	
ADAR 5500	Multispectral	2m	2km x 3km (per frame)	4	Band 1(Blue)	460nm - 550nm	8 bit
					Band 2 (Green)	520nm - 610nm	
					Band 3 (Red)	610nm - 700nm	
					Band 4 (Near Infrared)	780nm - 920nm	
Landsat ETM+	Multispectral	30m	185km x 185km	6	Band 1 (Blue)	450nm - 515nm	8 bit
					Band 2 (Green)	525nm - 605nm	
					Band 3 (Red)	630nm - 690nm	
					Band 4 (Near Infrared)	750nm - 900nm	
					Band 5 (Infrared)	1550nm - 1750nm	
					Band 7 (Infrared)	2080nm - 2350nm	

* Estimates are approximate spatial extent; after georeferencing spatial extent may be reduced slightly due to topography

results were below an acceptable level of accuracy. This resulted in a total of three training ROI classes (i.e., water, shadow, and everything else) considered to classify the ADAR 5500 data.

We ran the Jeffries-Matusita ROI separability measure to quantitatively evaluate the statistical separability of the training ROI classes used for the multispectral image classifications (Richards 1999)(Table 2). The output separability values range from 0-2, with values falling below 1 suggesting poor or unacceptable separability and values above 1.9 indicating the classes have good separability (Richards 1999).

Table 2. Jeffries-Matusita ROI separability results for the multispectral training classes.

	Landsat ETM+		ADAR 5500	
	Big Creek	**Bighorn Crags**	**Big Creek**	**Bighorn Crags**
	Water	Water	Water	Water
Shadow	1.991	1.948	1.915	1.721
Everything Else	1.985	1.999	1.97	1.991

Big Creek Study Site
We used the Spectral Angle Mapper (SAM) classification algorithm for both the Landsat ETM+ and ADAR 5500 datasets at the Big Creek study site. The SAM classification algorithm determines the similarity between image spectra and training ROI spectra based on the angle between them calculated as a vector in n-dimensional space, where "n" equals the number of input bands or dimensionality (Kruse et al. 1993). Smaller angles represent better matches to ROI reference spectra. We adjusted the maximum allowable angle across a range starting at 0.1 radians up to 3.0 radians to determine the best acceptable angular tolerance. This algorithm is relatively insensitive to changes in scene illumination and albedo effects (Kruse et al. 1993), which may have contributed to the success of this approach applied to a landscape that is highly influenced by drastic changes in image brightness caused by topography and shadows.

Bighorn Crags Study Site
Following numerous attempts to apply traditional supervised classification algorithms to the Landsat ETM+ data in the Bighorn Crags study area, we concluded that the best approach was using a 2-D scatter plot incorporating two near-infrared spectral bands (i.e., Band 4 vs. Band 5). Water exhibits very low spectral response patterns in the near-infrared region of the EM spectrum and would expectedly be located near the lowest spectral values on both axis of the scatter plot. By exploiting this known spectral feature characteristic, we subjectively selected and iteratively refined a group of pixels located in the lower left corner of the 2-D scatter plot (Figure 2). We exported the selected pixels as ROI's and produced a "standing water" classification image.

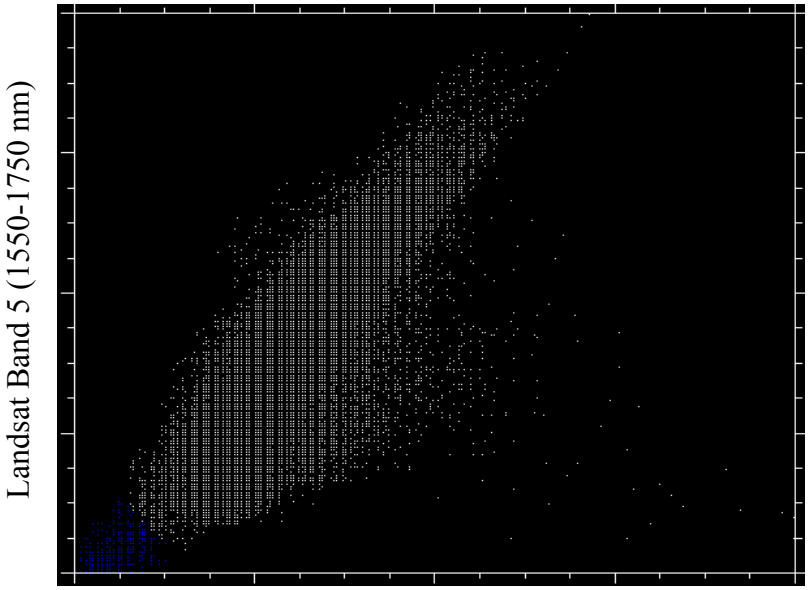

Figure 2. 2-D scatter plot used to create the Landsat ETM+ standing water classification map of the Bighorn Crags study site.

We used the Maximum Likelihood algorithm to classify the ADAR 5500 data. The Maximum Likelihood algorithm considers both spectral variance, plotted as a mean vector, and covariance of the training ROI's (Jensen 2000). The underlying assumption of this algorithm is a Gaussian distribution, which is a reasonable assumption for common spectral classes such as water (Jensen 2000). Based on the spectral response pattern and associated statistics of the ROI training classes, a probability density function is created that assesses the individual probability for each image pixel. We designated a probability threshold for each ROI training class determined through repetitive classification attempts, and any pixel falling within the designated threshold range is assigned to the corresponding ROI class.

Hyperspectral Data

Given the unique attributes of hyperspectral data, such as the ability to map endmember sub-pixel fractional abundances, we tested the Mixture Tuned Matched Filter (MTMF) classification algorithm (Boardman 1998b). Initially we ran MTMF on all image endmembers identified through the PPI and nDV image processing steps. We also experimented with traditional supervised classification algorithms in attempt to produce the most accurate wetland classifications.

Big Creek Study Site

Given the increased spectral resolution and range of the hyperspectral dataset, we were able to identify much finer-scale wetland habitat features than water alone. We identified Standing Water and Sediment (SWS) and Shallow Stream Water (SSW) image endmembers (Figure 3). We used these endmembers to classify wetland habitats associated with floodplain and stream features such as side-channels and backwater

pools. We also identified a wet meadow (WM) endmember representative of a mixture of sedges and grasses directly associated with water presence (Figure 4).

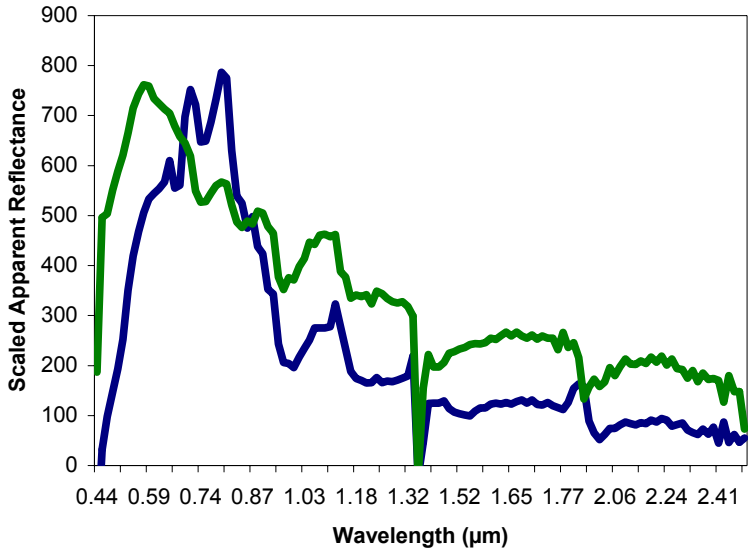

Figure 3. Shallow Water Sediment (SWS, shown in blue) and Shallow Stream Water (SSW, shown in green) endmember spectral profiles.

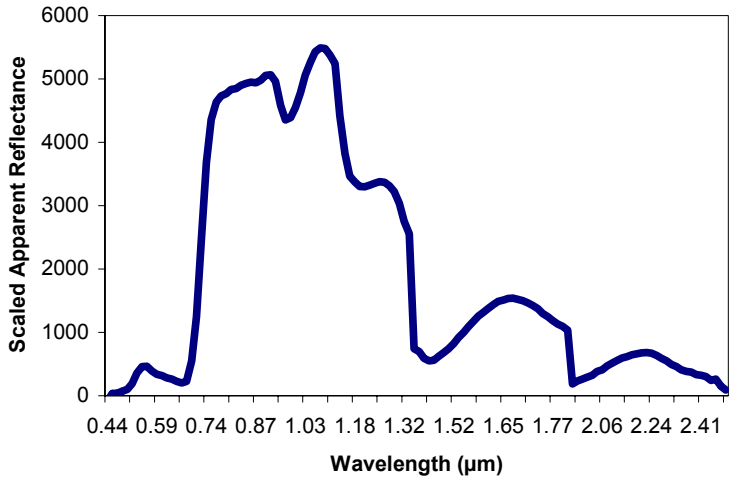

Figure 4. Wet Meadow (WM) endmember spectral profile.

We used the SAM algorithm to classify the SWS and SSW endmembers. We believe that the characteristics of the SAM algorithm (i.e., insensitivity to changes in illumination and albedo) contributed to the classification success for these features that commonly exhibit variable reflectance patterns due to surface turbulence of flowing water. We experimented with the same angular ranges described above for the multispectral

datasets, to assign the angle that produced the most accurate classifications while minimizing omission and commission errors.

We used the MTMF algorithm to produce a classification of sub-pixel fractional abundances for the wet meadow endmember. Although the goal was not to quantify the accuracy of fractional abundance value, this classification algorithm is potentially the best approach to identify small wetland features common to this study area. MTMF builds upon the strengths of both matched filtering and spectral unmixing algorithms while avoiding the disadvantages of both (Boardman 1998b). Matched filtering performs partial spectral unmixing and identifies the fractional abundance of a spectral endmember on a continuous scale without knowing all of the background endmember signatures (Harsanyi and Chang 1994, Boardman et al. 1995). Spectral unmixing takes advantage of the hyperspectral leverage (i.e., an overdetermined solution caused by a greater number of spectral bands than unknowns) to solve the linear mixed pixel problem (Boardman 1993). The combined strengths of these two algorithms provide a unique and robust method to map endmember fractional abundances.

MTMF results in two image outputs, the first being a Matched Filter (MF) image and the second an Infeasibility image. The best classification accuracies required the useful contribution of information from both resulting images combined into a single feature classification. We loaded the MF and Infeasibility images as the axes of a 2-D scatter plot diagram and subjectively selected, and iteratively refined, the pixels that exhibited high MF scores and low Infeasibility scores (Figure 5) to produce the final emergent sedge classification. Due to the spectral similarities in the vegetation present across the Cabin Creek floodplain, we were forced to select image pixels with a minimum MF threshold of 0.6.

Bighorn Crags Study Site

We were not able to identify any image endmembers that classified all water bodies (i.e., lakes, ponds, pools) well with the hyperspectral data, and consequently we classified standing water in the hyperspectral data using the same strategy described for delineating water in the Landsat ETM+ data. We loaded band 20 (0.727μm) vs. band 33 (0.9047μm), two near-infrared spectral bands, and selected all of the pixels that were located in the lower left corner paying close attention not to select non-water pixels (Figure 6). The 2-D scatter plot is interactively linked to the displayed image, and we focused on known areas of standing water (i.e., large ponds and lakes) to decide when the pixel selection began to overpredict non-target pixels.

We identified an Emergent Sedge (ES) endmember (Figure 7) located in the sedge dominated periphery of one of our training sites. This endmember was mapped and used as a proxy to help locate small emergent wetland sites and also wet meadow areas typically associated with amphibian foraging habitat in this study site. We used the MTMF algorithm to map sub-pixel abundances of the ES endmember. We loaded the MF and Infeasibility images as the axes of a 2-D scatter plot diagram and subjectively selected the pixels that exhibited high MF scores and low Infeasibility scores (Figure 8) to produce the final ES classification.

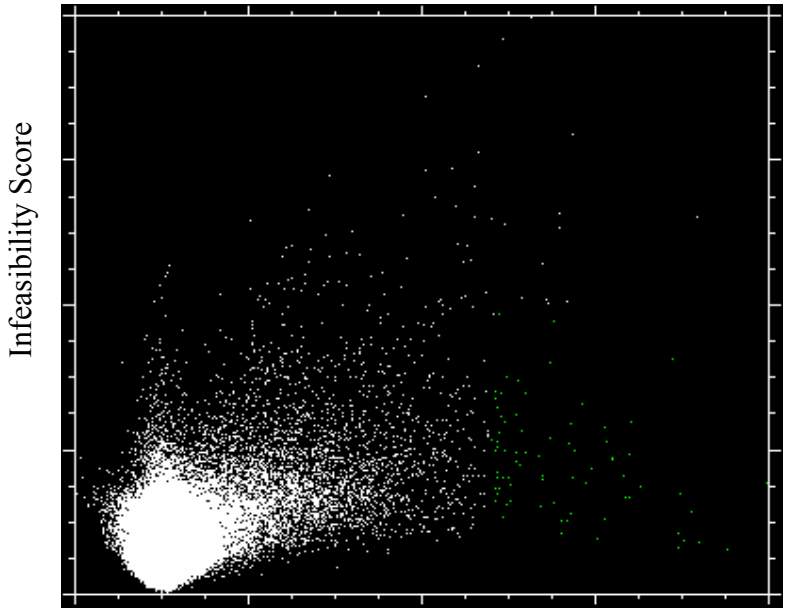

Figure 5. 2-D scatter plot of the Matched Filter and Infeasibility results from the MTMF classification algorithm applied to the wet meadow (WM) endmember. Final classified pixels are shown in green while the remaining background image pixels are shown in white.

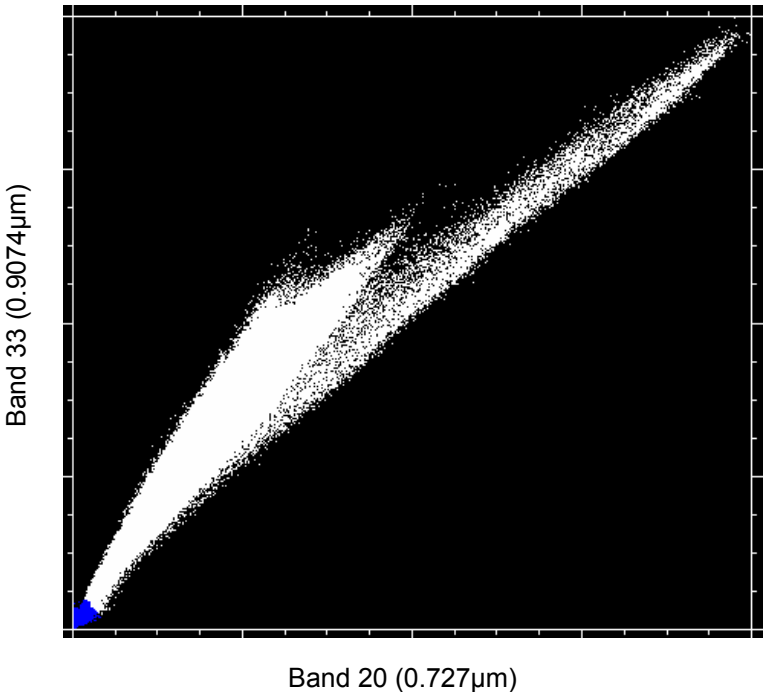

Figure 6. 2-D scatter plot showing the pixel selection used to create the standing water class. Final water pixels are shown in blue while all remaining image pixels are shown in white

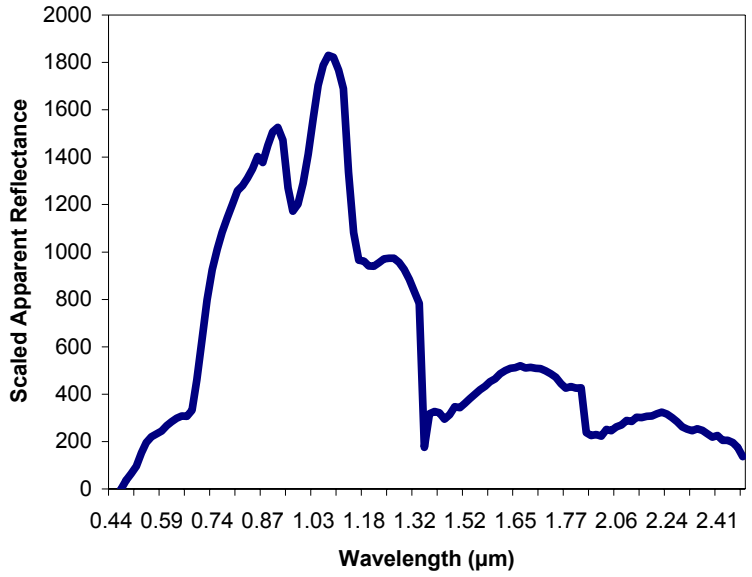

Figure 7. Emergent Sedge (ES) endmember spectral profile.

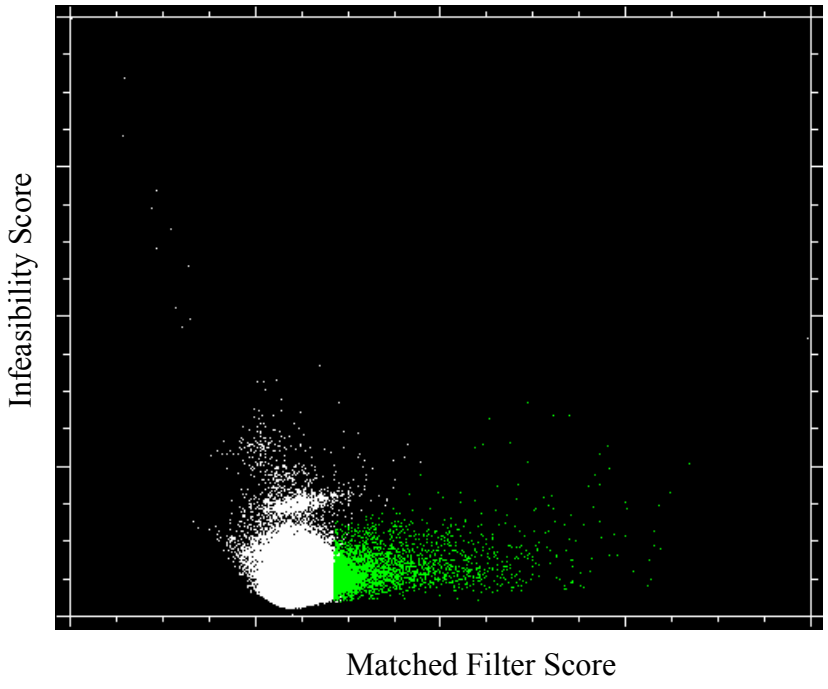

Figure 8. 2-D scatter plot of the Matched Filter and Infeasibility results from the MTMF classification algorithm applied to the emergent sedge endmember. Final classified pixels are shown in green while the remaining background image pixels are shown in white.

Accuracy Assessment

Error matrices serve as the basis for descriptive statistical techniques used to evaluate classification accuracy (Lillesand and Kiefer 1994, Congalton and Green 1999). Producer's accuracy is calculated by dividing the total number of correct pixels in a category by the total number of pixels actually identified from ground truth reference data (Congalton and Green 1999). Producer's accuracy represents the probability a true positive location on the ground is correctly classified. User's accuracy is calculated by dividing the total number of correctly classified pixels by the total number of pixels classified in that category (Congalton and Green 1999). User's accuracy represents the probability that a classified image pixel is actually that category on the ground (Story and Congalton 1986). Omission and commission errors are calculated by subtracting producer's and user's accuracy from 100% respectively.

Currently the ability to perform advanced image classifications has progressed in parallel to technological advances, but the corresponding ability to quantify accuracy has not followed this progression (Lillesand and Kiefer 1994). High spatial resolution data (i.e., 5m or less) commercially available from numerous sensors, challenges the capability of GPS receivers to accurately locate points on the ground when the topography is complex and canopy cover disrupts a clear view of the sky. Aside from the technical limitations of using GPS in many field study areas, image georeferencing procedures of airborne high spatial resolution data sometimes fail to provide highly accurate corrections. Even with a sophisticated GPS/IMU and ray tracing program recording X, Y, and Z coordinates for every image pixel (Boardman 1999), drastic fluctuations in ground elevation cause significant error in the georeferencing process. This means the coordinates of certain image pixels may be spatially skewed in a non-systematic direction, which makes locating individual pixels on the ground extremely difficult if not impossible. Similar to other validation studies involving high spatial resolution data (Aspinall 2002, Marcus 2002, Crabtree et al., *in press*), we used the classified imagery as a field map and navigated directly from it using obvious features (e.g., lake coves, stream bends, and rocky outcrops) as geographic references.

We chose to use groups or clusters of pixels as the sampling unit for the high spatial resolution (i.e., ADAR 5500 and HyMap) classification validation. The Landsat ETM+ spatial resolutions are within an expected positional range of accuracy common with current GPS receivers, which allowed us to consider individual pixels as a sampling unit. We did not want to exclude any sites large enough in spatial extent to fill a 30 m pixel, because many important wetland sites are much smaller than the spatial resolution of this imagery.

There are a number of suggestions published for developing a validation site selection scheme, each with their own advantages and disadvantages (Congalton 1991). Because the primary goal of this study was to identify wetland habitats that are low in abundance and widely dispersed throughout the scene, we felt the most appropriate validation was to visit all of the classified potential wetland sites. We walked the shorelines of lakes and visually searched meadows and backwater areas while in transit between predicted sites, and used previously collected field data from the study area (Charles R. Peterson, David

S. Pilliod, Crystal Strobl, and Jeremy P. Shive, unpublished data, Pilliod and Peterson 2001, Pilliod and Peterson 2002) as ground truth to evaluate omission errors.

CLASSIFICATION RESULTS AND DISCUSSION

Big Creek Study Site

The wetland locations within the Big Creek study site are a combination of primarily small ponds, wet meadows, and stream associated features such as pools and backwater channels. Many of the wet meadow sites have small ephemeral pools of water that were difficult to accurately detect. A total of 30 wetland sites exist within this study area based on past field surveys and newly located sites. Both multispectral datasets performed poorly at this study site while the hyperspectral data (combined) performed above average (Table 3).

Table 3. Accuracy assessment summary table for the Big Creek study site.

	Producer's Accuracy	User's Accuracy	Overall Accuracy	Omission Error	Commission Error
Landsat ETM+ (Water)	0%	0%	0%	100%	100%
ADAR 5500 (Water)	26.7%	72.7%	39.0%	73.3%	27.3%
HyMap (SWS)	43.3%	92.9%	59.1%	56.7%	7.1%
HyMap (SSW)	23.3%	100%	37.8%	76.7%	0%
HyMap (WM)	30.0%	56.3%	39.1%	70%	43.8%
HyMap (Combined)	83.3%	75.8%	79.4%	16.7%	24.2%

The Landsat ETM + water classification produced the poorest accuracy results possible for a remote sensing application with a producer's and user's accuracy of 0%. Even the largest pond within the study site (i.e., Bufo-Moose pond approximately 1400 m^2 in size) was not detected due to the large spatial resolution of the imagery. This site is a major source breeding pond for Western Toads (*Bufo boreas*) and Columbia Spotted Frogs (*Rana luteiventris*). The inability of this dataset to identify a single large wetland site questions the applicability of this imagery for inventory and monitoring efforts

Surprisingly the high spatial resolution of the ADAR 5500 data did not substantially contribute to a more successful classification of wetland habitat. The calculated producer's and user's accuracy were 26.7% and 72.7% respectively. Three wetland sites were falsely overpredicted and confused with the shadow class, while 73.3% (i.e., omission error) of the known wetland sites were missed. The ADAR 5500 imagery best identified stream associated features, such as side channels and pools, but did not identify wet meadows and small pool locations adequately. Our attempts to map an indicator variable, sedge, were not successful and consequently we were not able to accurately identify wet meadow features with the water class alone since the spectral response of these sites is dominated by vegetation presence. The single largest pond, Bufo-Moose

pond, was accurately identified while a smaller exposed pond located on the Cabin Creek floodplain was unexpectedly missed.

The HyMap hyperspectral data produced some of the highest classification accuracies for each individual endmember, and a combined accuracy that far exceeds the results from either multispectral dataset. The clear advantage of the hyperspectral data is the ability to identify multiple wetland features and indicator variables such as sedge presence to identify small sites. We calculated producer's and user's accuracy for the SWS endmember at 43.3% and 92.9% respectively. This endmember successfully identified most small ponds and pools while only slightly overpredicting one location in a forested riparian area.

The SSW endmember was used to complement the SWS classification by primarily identifying stream associated features, particularly side channels and backwater pools that we observed as late season Western Toad breeding sites in 2002. The producer's and user's accuracy for the SSW endmember were 23.3% and 100% respectively. These results illustrate the importance of considering multiple measures of classification accuracy. A user's accuracy of 100% (i.e., 0% commission error) simply means that every pixel that was classified as water in the scene is actually water on the ground. Reporting this result alone could mistakenly suggest an above average performance of this classification when in reality it performed poorly if the goal is to identify all wetland habitat in the study site.

The WM endmember was instrumental in identifying the wet meadow and ephemeral pool sites commonly missed by the other water related endmembers. The producer's and user's accuracy for the WM endmember were 30% and 56.3% respectively. The WM user's accuracy was the lowest reported at this study site illustrating the difficulty of accurately mapping this feature without overpredicting false positive sites. Even though 70% (i.e., omission error) of the total sites were missed, the true positive predicted sites located wet meadows that no other dataset was capable of predicting.

Individually, each HyMap endmember did not perform particularly well, but the utility of this imagery is that all of the features can be combined to produce one superior classification. We calculated a combined producer's accuracy of 83% (25/30) by summing all of the true positive locations among endmembers and divided by the total number of wetland sites. From an inventory and monitoring perspective the omission error is the most important measure of success while some overprediction (i.e., commission errors) is acceptable if the goal is identify all potential amphibian habitat in a study area.

From the standpoint of a herpetologist, the most significant result of the HyMap classification is identifying new sites that were not previously known from field surveys. We found a new backwater channel with breeding Western Toads and larval Columbia Spotted Frogs present. We discovered a second new backwater channel on the Cabin Creek floodplain that was not recognized through on the ground visual-assessment of the

area. We also identified a moderate sized forested pond representing a new potential breeding site with shallow water depths and an abundance of emergent vegetation.

Bighorn Crags Study Site

The Bighorn Crags study site is characterized by an abundance of high mountain lakes with forested pools and wet meadows dispersed throughout the landscape. A total of 48 wetland sites are present within this study site based on previous field surveys and one additional site identified through this research. The majority of wetland sites are lakes that on average are larger than the largest site in the Big Creek study site, and as a result the corresponding classification accuracies are much higher for all datasets (Table 4).

Table 4. Accuracy assessment summary table for the Bighorn Crags study site.

	Producer's Accuracy	User's Accuracy	Overall Accuracy	Omission Error	Commission Error
Landsat ETM+ (Water)	48.9%	100%	65.7%	51.1%	0%
ADAR 5500 (Water)	61.5%	100%	76.2%	38.5%	0%
HyMap (Water)	75%	94.7%	83.7%	25%	5.3%
HyMap (Sedge)	72.9%	89.7%	80.5%	27.1%	10.3%
HyMap (Combined)	91.7%	89.8%	90.7%	8.5%	10.2%

The Landsat ETM+ imagery produced the lowest classification accuracies with producer's and user's accuracy of 49% and 100% respectively. A producer's accuracy of 49% (i.e., 51% omission error) means that only half of the total true sites were actually identified. The predicted water sites were highly accurate with a commission error of 0%.

The wetland sites correctly identified consisted of large lakes and ponds while smaller ponds, emergent wetlands, and wet meadows were consistently missed likely due to their small spatial extent. Missed sites included the main source breeding location for Columbia Spotted Frogs, known as Frog Pond. A second crucial site completely missed was a smaller emergent wetland, named Axe Handle Meadow, that is the location of the only known Western Toad breeding site in the basin (David S. Pilliod, unpublished data).

The ADAR 5500 data produced slightly better results with producer's and user's accuracy of 61.5% and 100% respectively. The predicted wetland sites were again highly accurate (i.e., 0% commission error), but a number of small ponds and wet meadows were not identified and not reflected in this measure of accuracy. An omission error of 38.5% clearly depicts some limitations of this dataset, even when the wetland features are relatively large in size.

Frog Pond, the critically important Columbia Spotted Frog breeding site, was accurately identified while numerous wet meadows and forested ponds were missed. Axe Handle Meadow was missed again with this dataset and represents a significant error at a site

essential for understanding local Western Toad population status. The primary reason many of the wet meadow sites were missed is because we were not able to use an indicator variable, such as sedge presence, to assist in the identification of important wet and flooded meadow sites. Wet and/or flooded meadows are an important habitat type utilized by amphibian populations in the study area. These features are extremely difficult to predict using solely water features because the spectral response is highly influenced by vegetation presence. The limited number of spectral bands restricts the probability of correctly classifying these features, and imagery that provides an increased spectral range and spectral resolution will ultimately be needed to successfully model these types of wetland sites.

The Hymap hyperspectral data produced the highest classification accuracies of the datasets compared in this study. The water feature alone correctly classified more true positive sites than either multispectral datasets with producer's and user's accuracy of 75% and 94.7% respectively. Two sites were inaccurately overpredicted (i.e., 5.3% commission error) and confused with shadow. A total of 12 sites, which primarily consisted of wet meadows, were missed using this classification method.

The ES endmember yielded a slightly less accurate classification compared to the water feature with producer's and user's accuracy of 72.9% and 89.7% respectively. We evaluated the accuracy of this feature as a predictor of wetland presence and calculated accuracy based on ground truth data of all known wetland sites (i.e., a predicted sedge site was viewed as a predicted wetland site). This feature obviously did not correctly classify large deep lakes that lacked shallow shorelines with sedge present, but was extremely effective at identifying wet meadows and ephemeral pools missed by all other classified features and datasets. We assessed the accuracy of this feature explicitly (i.e., a predicted sedge site was evaluated as sedge and not a wetland) to assess how well the sedge classification actually performed at predicting sedge presence. We visited a total of 57 predicted sedge sites and calculated a producer's and user's accuracy of 98.3% and 91.8% respectively. Clearly the high accuracy of this feature supports future considerations to use sedge presence as a predictor variable for wetland presence, at least in the regions of the western U.S. where sedge presence is highly correlated to wetland and amphibian presence.

Although both the water feature and ES endmember produced higher accuracies than the multispectral datasets, the real advantage of the hyperspectral data is the capability to combine individual feature results for unparalleled accuracy results. We added all of the true positive predictions and divided by the total number of wetland sites present in the study site to calculate a combined producer's accuracy of 91.7% (44/48). All overpredicted sites that led to non-wetland locations were added to calculate a combined user's accuracy of 89.8%. This level of accuracy provides a near comprehensive prediction of all wetland sites present within the study site providing the detailed information necessary for effective inventory and monitoring programs.

One of the most significant results from the HyMap classification is the discovery of a new forested pond. We have a thorough and detailed understanding of the wetland

habitat available in this study site as a result of ongoing long term repeated survey (David Pilliod unpublished data). In fact, other than a single new pond discovered this summer every other wetland location was previously identified and surveyed. No amphibians were observed at this new site, but the characteristics of the pond (e.g., fishless) suggest that amphibians may utilize this location sometime during their active season.

Comparison against Traditional Methods

For a comparison to traditional site selection processes we used USGS 7.5 minute topographic (Topo) maps and DOQQ's to identify all wetland sites labeled on the map or clearly visible in the aerial photographs (Figures 9 and 10). The DOQQ's used in this study are black-and-white, but color DOQQ's are becoming available in many areas providing a more useful dataset for identifying wetland habitat. The Landsat ETM+ classification produced fewer true positive sites than the total recognized from Topo maps and DOQQ's (note: no DOQQ's exist over the Bighorn Crags study site). Across our study area, more wetlands would be accurately located if we used traditional sources instead of expending effort to classify the Landsat ETM+ imagery.

The ADAR 5500 data successfully identified more wetland sites than traditional Topo maps, but slightly less than the DOQQ's in the Big Creek study site (Figures 9 and 10). The combined processing time required to georeference the imagery and classify the ADAR 5500 data far exceeds the total amount of time needed to visually interpret DOQQ's. The greatest limitation of these data is the inability to accurately identify indicator variables, such as sedge presence, that can be used as a proxy for predicting wetland distributions.

The HyMap hyperspectral data clearly produced the greatest accuracies while providing a fine-scale level of information instrumental in understanding amphibian habitat distributions in the study area. Each individual endmember did not produce classification accuracies significantly better than the other datasets in this study excluding Landsat ETM+ (Figures 9 and 10). However, when all of the endmember accuracies are combined, this dataset yields the greatest accuracies accomplished in this study.

Assessment of Error and Bias

We performed all image classification efforts following a preliminary site survey and ground training data campaign. In addition, our background knowledge of the study area compiled through multiple years of previous field based surveys provides an informed perspective of the current amphibian habitat distributions. We made a number of subjective decisions concerning classification thresholds, training data pixel selection, and decisions on the final "best" classification map. These decisions are influenced by our familiarity with the study area and would expectedly differ from a classification effort performed with no background knowledge of the study area. Typically prior to inventory surveys little or no detailed background information is available for a study area potentially complicating the effort required to create a comparably accurate classification. It would be beneficial to repeat this study in an

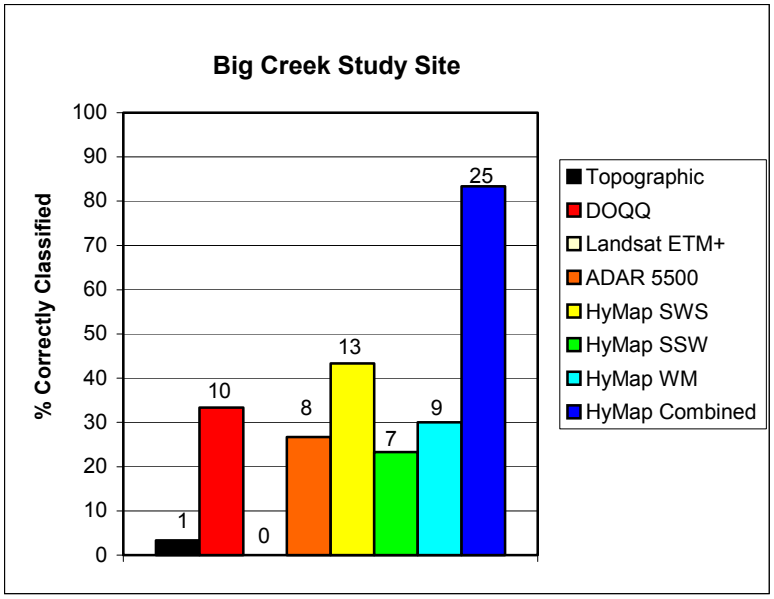

Figure 9. A comparison of correctly classified sites resulting from different data sources. The numbers above each dataset represents the total number of true positive sites predicted by each classified dataset of the 30 total wetland sites present in the Big Creek study site.

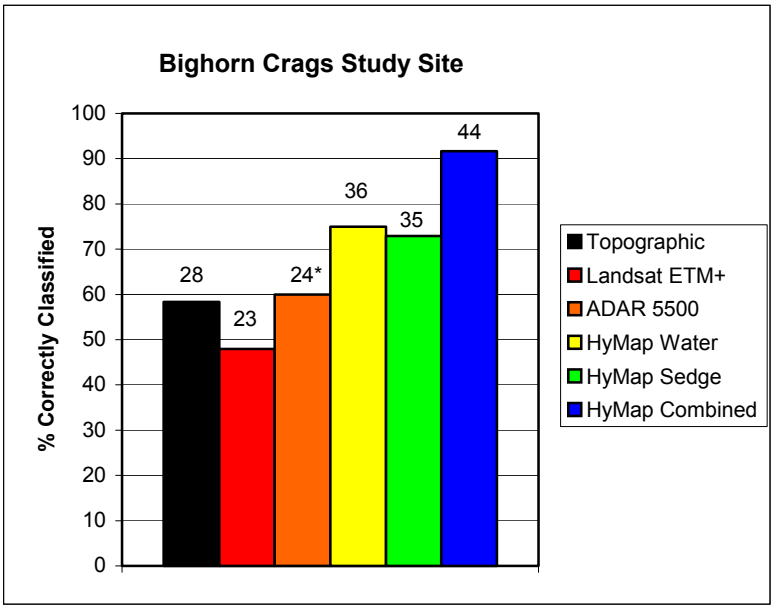

Figure 10. A comparison of correctly classified sites resulting from different data sources. The numbers above each dataset represents the total number of true positive sites predicted by each classified dataset of the 48 total wetland sites present in the Bighorn Crags study site. (* note: the ADAR 5500 coverage did not extend over the entire Bighorn Crags study site and consequently the total number of wetlands sites was reduced to 40)

unfamiliar region and compare the results to determine widespread application in inventory and monitoring programs.

We chose to navigate to all predicted sites using the final classification map as a reference opposed to using GPS and navigating using site coordinates. The high spatial resolution of the ADAR 5500 and HyMap imagery require coordinate accuracies consistently within 5 m of absolute true ground position. Without real-time differential correction capabilities, GPS coordinates collected in a region with rugged topography and forest canopy will rarely be accurate to within 5 m of absolute error. The georeferencing process contributes additional errors to image pixel coordinates and further lowers the probability of confidently locating individual pixels in the field. Until GPS accuracies increase and georeferencing algorithms advance, the assessment of high spatial resolution imagery will remain difficult and influenced by error.

Costs of Imagery

The total cost of each remotely sensed dataset needs to be evaluated if these technologies are going to be considered or actually become incorporated into inventory and monitoring programs typically constrained by funding. The financial reality of many long-term research initiatives limits the possibility of incorporating expensive technology that may only perform marginally better than a less expensive approach. A cost comparison of the imagery provides a perspective to consider accuracy and knowledge gained from a financial perspective.

Satellite based data will normally cost less than airborne imagery because many of the mobilization costs and acquisition logistics are no longer a substantial consideration. The Landsat ETM+ data was the most inexpensive data set acquired, regardless of the unfortunate geographic location of the study area that spans two adjacent Landsat scenes boundaries. A Landsat scene costs $600 for a Level 1G radiometrically and geometrically corrected dataset with each additional scene offered at a reduced rate of $250 (http://edcdaac.usgs.gov/pricing_policy.html). Considering the additional handling fee of $5, the total cost of the Landsat ETM+ data was $855 (Table 5).

The ADAR 5500 dataset is the second most expensive imagery collected and has a number of acquisition fees and financial considerations associated with a specific contracted collection. Many of the costs we are reporting reflect the logistical considerations for the contracted data collection of this project, and the costs may be variable depending on a different contract and extent of data collection. Mobilization fees that cover the estimated number of images contracted, and the corresponding estimated number of flight and standby days required, adds to a total of $4000. The image acquisition fees for the total area contracted in this data collection cost $11500, and includes expenses for flight operations engineer, insurance, and associated costs for the data capture. It is important to note that the contracted data collection covered a much larger spatial extent than this study area alone, and much of the data collected were not used for our research. This would lower this category total but it is hard to estimate how much cost would appropriately be deducted, so we approximated a cost of about 2/3

the total equaling $7660. There are also post capture processing fees of $2000 for vignetting corrections and band-to-band coregistration for all images.

The ADAR data are collected as overlapping frames imposing a large amount of processing time needed to georeference and mosaic the scenes into one image. Positive Systems, Inc. offers the DIME software package that is designed specifically for georeferencing and mosaicking ADAR 5500 data and costs $1700 for the site registration and on-site training. There are 25 free processing credits provided with the site license, but additional costs of "image credits" for $5 each are needed to process and save output images. We could not use this program for the Bighorn Crags study site (i.e., DOQQ's are required as a basemap layer), so we did not consider any additional image credit costs because they were not needed for our research. These additional costs are mentioned as considerations for larger studies incorporating this data type. Adding up all of acquisition expenses sums to a total of $15360 for the entire study area (Table 5).

The HyMap hyperspectral data was the most expensive dataset collected over the study area. HyMap data are priced on a per flightline basis of $6000, and included in these costs are image post processing services such as atmospheric and geometric corrections. We collected one flightline of hyperspectral data over the Bighorn Crags study area and two flightlines over the Big Creek study area creating a total cost of $18000 (Table 5). It is important to note that the Big Creek study area could have been covered in a single flightline if appropriately planned, and this would have reduced the total number of flightlines dropping HyMap behind the ADAR 5500 sensor in total costs. The reported costs reflect the value at the time of our data acquisition and have since lowered in price with cost reduction incentives for larger data collects.

Table 5. A comparison of imagery costs.

Sensor	Costs
Landsat ETM+	
Single Scene	600
(x2 w/ reduced cost)	250
Handling Charge	5
	$855
ADAR 5500	
Mobilization*	4000
Image Acquisition*	7660
Post Capture Processing*	2000
DIME Software	1700
	$15,360
HyMap	
Single Flightline*	6000
(x3)	18000
	$18,000

* Reported costs are variable

Processing Time

This category is an additionally important consideration that must be evaluated when suggesting the most appropriate imagery for amphibian inventory and monitoring initiatives. Total processing time is very difficult to evaluate because we expect considerable variability in the length of time needed for different people to perform the same processing steps. This will certainly influence the amount of time and effort needed to accomplish the necessary image processing steps. We provide a summary of the time we expended to process and classify each dataset.

We made some background assumptions while assessing the total processing time that can be compared between analysts. First, we assumed that an image analyst is already trained in traditional remote sensing principles, processing, and applications, and we did not account for learning time except when necessary (i.e., hyperspectral image processing). Secondly we also impose a requirement, as part of the preliminary processing step, 7 days or 56 hours of ground training data collection and/or ground reconnaissance at each study site to become familiar with the study area prior to any image processing effort.

The Landsat ETM+ data took the least amount of time to process and classify. The data were provided already mosaicked and the remaining image processing time consisted of converting the DN values to at-sensor reflectance. We estimated this step to take about 2 days, or 16 hours. The image classification process includes time for ROI training class selection and refining, and experimental testing of classification algorithm applications that we estimated to total 10 days, or 80 hours. Including the initial ground truth campaign, total time expenditure results in 19 days, or 152 hours, to fully process and classify the Landsat ETM+ data (Table 6).

The ADAR 5500 data took the second greatest amount of time to process and was almost identical to the amount of effort expended on the Landsat multispectral dataset. The DIME software training took 2 days, or 16 hours, to complete in which time the Big Creek scenes were georeferenced and mosaicked. We spent an additional day, or 8 hours, attempting to manually mosaic the Bighorn Crags images before deciding to leave them in the raw format due to undesirable results. Similar to the Landsat data, we estimated 10 days, or 80 hours, for image classification time including ROI selection and the testing numerous classification algorithms. Including the time needed for the ground truth campaign, the total estimated processing time for the ADAR 5500 data was 20 days or 160 hours (Table 6).

The HyMap hyperspectral data unquestionably took the greatest amount of time to process and classify attributed to the total time of learning the specifics of hyperspectral data analysis techniques and applications. Many of the common hyperspectral image processing steps are unique to this data type, and are not encountered working with multispectral data. We attended an hyperspectral training short-course that occurred over 5 days, or 40 hours, which formed the foundation of our knowledge of hyperspectral analyses. We suggest this training as a precursor for correctly and effectively processing

hyperspectral data, and consider this training part of the processing effort that should be included. We estimate the georeferencing procedures lasted 10 days, or 80 hours, with the majority of the time attributed to learning the correct processing steps specific to hyperspectral data and understanding various results. We performed data reduction techniques, such as the MNF transform, PPI, and the n-D Visualizer which lasted 15 days, or 120 hours, with much of the processing time a result of redundant testing of processing steps to better understand intermediate results. Finally, we estimate the image classification procedure took a total of 10 days, or 80 hours of time to complete with many repetitive steps interpreting the results and refining the input parameters. This results in a total of 47 days, or 376 hours, to complete the hyperspectral data analyses (Table 6).

Table 6. A comparison of categorized image processing times and associated time.

Sensor	Processing Step	Time (days)	Time (hours)
Landsat ETM+	Ground Training	7	56
	Reflectance Conversion	2	16
	Image Classification	10	80
		19	**152**
ADAR 5500	Ground Training	7	56
	Georeferencing/Mosaic	3	24
	Image Classification	10	80
		20	**160**
HyMap	Ground Training	7	56
	Hyperspectral Training	5	40
	Georeferencing	10	80
	Data Reduction	15	120
	Image Classification	10	80
		47	**376**

CONCLUSIONS

Illustrated through this comparative application and assessment, it is clearly recognized that different scales of remotely sensed data will produce varying accuracy results within the same study area. From an inventory and monitoring perspective, the dataset that provides the most cost-effective and comprehensive habitat information is the most desired. Our results provide insight into the relative performance of three vastly different dataset for predicting amphibian habitat and we offer some suggestions for further evaluation and future inventory and monitoring applications.

The Landsat ETM+ sensor has traditionally been viewed as a valid resource for numerous natural resource applications due to the consistency and availability of data. For some applications (e.g., forest fragmentation studies) the 30 m spatial resolution of this dataset may be appropriate because the scale of observation correctly corresponds to the scale of processes governing the feature of interest. Unfortunately many wetland sites most important for amphibians are typically not large lakes but smaller isolated ponds less than

30 m^2 in area. The results from both study sites reveal a significant limitation of this imagery for accurate identification of wetland habitat regardless of the inexpensive costs of these data.

The ADAR 5500 data performed below expected levels of accuracy even though this imagery exhibits the highest spatial resolution compared in this study. Given the fact that many of the wetland sites within the study are small in spatial extent, this dataset would expectedly classify these locations most accurately. We feel that the limited number of spectral bands contributed to the difficulties of distinguishing water features from other spectral classes such as shadow. The ADAR 5500 sensor collects only a single band in the near-infrared spectral wavelengths. We found that the near-infrared region was paramount in providing spectral information necessary for delineating water from other features, and because these data lack multiple near-infrared spectral bands, classifying water features was more difficult.

Aside from considering the accuracy statistics, potentially the most important result from the HyMap image classification is that new previously unknown wetland sites were discovered in areas that have been repeatedly surveyed on the ground. These results are similar to another study in Yellowstone National Park where new amphibian breeding sites were located in unexpected areas (Crabtree et al., *in press*). The ultimate goal of an inventory program is to comprehensively survey all available habitats within a study area, and the HyMap hyperspectral data exhibit the best potential for accomplishing this goal by providing near comprehensive identification of wetland habitat within the study area. The goal of monitoring programs is to understand how particular habitat features are changing over time. Given the ability to map fine scale wetland features, we can begin to subdivide predicted habitat into specific types of amphibian habitat such as breeding, foraging, and overwintering. These wetland features can be used as a surrogate to infer changing population status and habitat conditions across large landscapes. By identifying particular habitat features, such as the abundance of emergent sedge, we can begin to extrapolate distribution and occurrence predictions to other areas were there are no field data.

The hyperspectral data certainly have the capability to be successfully incorporated into inventory and monitoring programs, but warrants additional research to assess repeatability and application in diverse environmental landscapes. One immediate limitation would be the large cost and processing time associated with collecting hyperspectral imagery over large spatial extents. Costs have already begun to drop since we started this research and will expectedly continue to decrease as this technology becomes more common. Hyperspectral imagery should be considered a valuable tool for future inventory and monitoring programs with new potential applications yet to be explored.

ACKNOWLEDGEMENTS
This study was made possible by a grant from the National Aeronautics and Space Administration Goddard Space Flight Center. ISU would like to acknowledge the Idaho Delegation for their assistance in obtaining this grant. We would also like to thank Jim and Holly Akenson of the Taylor Ranch Research Station for their hospitality and logistical support during our visit to the Big Creek study site. We would also like to thank David Pilliod for all of his support, assistance, and suggestions with the Bighorn Crags study area.

LITERATURE CITED

Aspinall, R.J. 2002. Use of logistic regression for validation of maps of the spatial distribution of vegetation species derived from high spatial resolution hyperspectral remotely sensed data. Ecological Modelling 157: 301-312.

Boardman, J.W. 1993. Automated spectral unmixing of AVIRIS data using convex geometry concepts. *Summaries, 4th JPL Airborne Geoscience Workshop*, JPL Publication 93-26(1): 11-14

Boardman, J.W. 1998a. Post-ATREM polishing of AVIRIS apparent reflectance data since EFFORT: a lesson in accuracy versus precision. Proceedings of the 7th JPL Airborne Earth Science Workshop. JPL Publication 97-21(1): 53.

Boardman, J.W. 1998b. Leveraging the high dimensionality of AVIRIS data for improved sub-pixel target unmixing and rejection of false positives: Mixture Tuned Matched Filtering. AVIRIS 1998 Proceedings, Jet Propulsion Laboratory, Pasadena, Ca. 6.

Boardman, J.W. 1999. Precision geocoding of low altitude AVIRIS data: lessons learned in 1998. *AVIRIS 1999 Proceedings*, Jet Propulsions Laboratory, Pasadena, Ca. 6.

Boardman, J.W., F.A. Kruse, and R.O. Green. 1995. Mapping target signatures via partial unmixing of AVIRIS data. *Summaries, 5th JPL Airborne Earth Science Workshop*, JPL Publication 95-1: 23-26.

Cocks, T., R. Jenssen, A. Stewart, I. Wilson and T. Shields. 1998. The HyMap airborne hyperspectral sensor: the system, calibration and performance. Presented at the 1st EARSEL Workshop on Imaging Spectroscopy, Zurich, Switzerland.

Congalton, R.G. 1991. A review of assessing the accuracy of classifications of remotely sensed data. Remote Sensing of Environment 37: 35-46.

Congalton, R.G., and K. Green. 1999. *Assessing the Accuracy of Remotely Sensed Data: Principles and Practices*. CRC Press Inc., Boca Raton, Florida.

Crabtree, R.L., W.A. Marcus, K.Q. Halligan , J.W. Boardman, J.E. Norland, M. Mirik, C.R. Peterson, and R. Cooper. *In Press*. High Resolution Hyperspectral data for remote measurement of ecological variables: Evaluation and applications. Photogrammetric Engineering and Remote Sensing.

Duffie, J.A., and W.A. Beckman. 1980. Solar Engineering of Thermal Processes. John Wiley and Sons, New York. p.109.

Fellers, G.M. 1997. Design of amphibian surveys. In, D.H. Olson, W.P. Leonard, and R.B. Bury (eds). *Sampling Amphibians in Lentic Habitats*. Society for Northwestern Vertebrate Biology: 23-24.

Gao, B.C., K.B. Heidebrecht, and A.F.H. Goetz. 1993. Derivation of scaled surface reflectances from AVIRIS data. *Remote Sensing of Environment* 44: 165-173.

Gao, B.C., K.B. Heidebrecht, and A.F.H. Goetz. 1997. Atmosphere removal program (ATREM) Version 3.0 user's guide. Center for the Study of Earth from Space, University of Colorado, Boulder. 1-27.

Green, A.A., M. Berman, P. Switzer and M.D. Craig. 1988. A transform for ordering multispectral data in terms of image quality with implications for noise removal. IEEE Trans. Geosci. Remote Sens. Vol. 26(1): 65-74.

Harsanyi, J.C. and C.I. Chang. 1994. Hyperspectral image classification and dimensionality reduction: An orthogonal subspace projection approach. *IEEE Transactions on Geoscience and Remote Sensing* 32: 779-785.

Jensen, J.R. 2000. *Remote Sensing of the Environment, An Earth Resource Perspective*. Prentice Hall, Upper Saddle River, New Jersey.

Kruse, F.A., A.B. Lefkoff, J.B. Boardman, K.B. Heidebrecht, A.T. Shapiro, P.J. Barloon, and A.F.H. Goetz. 1993. The spectral image processing system (SIPS)-Interactive visualization and analysis of imaging spectrometer data. Remote Sensing of Environment 44: 145-163.

Lillesand, T.M., and R.W. Kiefer. 1994. *Remote Sensing and Image Interpretation*, 3rd Edition. Wiley, New York.

Marcus, W.A. 2002. Mapping of stream microhabitats with high spatial resolution hyperspectral imagery. Journal of Geographic Systems 4: 113-126.

Pilliod, D.S. and C.R. Peterson. 2001. Local and landscape effects of introduced trout on amphibians in historically fishless watersheds. Ecosystems 4: 322-333.

Pilliod, D.S., and C.R. Peterson. 2002. Evaluating effects of fish stocking on amphiban populations in wilderness lakes. In: Cole, D.N., S.F. McCool, W.T. Borrie, and J. O'Loughlin editors. Wilderness science in a time of change conference. Volume 5, Wilderness ecosystems, threats, and management. Proceedings RMRS-P-15-Vol-5. Ogden (UT): USDA Forest Service, Rocky Mountain Research Station. p 328-335.

Richards, J.A. 1999. Remote sensing digital image analysis. Springer-Verlag, Berlin. 240.

Research Systems, Inc. 2002. Environment for Visualizing Images User's Guide Version 3.5, Boulder, Colorado.

Story, M., and R. Congalton. 1986. Accuracy assessment: A user's perspective. Photogrammetric Engineering and Remote Sensing 52(3): 397-399.

POST-FIRE CONDITIONS OF RIPARIAN VEGETATION

Sara Richardson and G. Wayne Minshall
Idaho State University
Department of Biological Sciences
Pocatello, ID 83209-8130

INTRODUCTION

Our main objectives were: (1) to examine the summer 2000 post-fire conditions of riparian vegetation within several watersheds of the Frank Church Wilderness (Big Creek, Cabin Creek, Cliff Creek, Cougar Creek, Goat Creek, and Pioneer Creek) and other non-wilderness streams (Clear Creek and Waterfall Creek), (2) to determine historic fire "footprints," if possible, within Doe Creek and Waterfall Creek watersheds, and (3) to detect the presence of historic livestock grazing and its impacts on the vegetation, particularly through the presence of invasive species (Cabin Creek, Clear Creek, and Pioneer Creek).

Keywords: fire, grazing.

RESULTS

Clear Creek

The interest in Clear Creek was twofold: to examine riparian recovery following a large-scale fire and to locate possible areas of historic grazing by the occurrence of invasive species.

Reconnaissance fieldwork was conducted in July 2002, just after the imagery was flown. We recorded GPS points of large patches of homogenous vegetation and made observations of the general landscape and vegetation distribution after the fire in 2000 (Photos 1 and 2). A second field reconnaissance was conducted in October 2003 to verify vegetation maps. Additional GPS points were obtained at that time to record the distribution of vegetation and other interesting landmarks. We discovered a large blowout had occurred on the stream in late Summer 2003, expelling a large amount of sediment, ash, and large woody debris from the watershed (Photos 3 and 4). A local resident informed us the blowout occurred several kilometers upstream, at the confluence of Deadhorse Creek and Clear Creek. As a result of the blowout, Clear Creek changed its course and much of the vegetation along Clear Creek and its floodplain was buried under sediment (Photo 5).

Photo 1. Collecting GPS coordinates along Clear Creek, July 2002. Facing toward a debris dam on the far left of the photo.

Abundant riparian species of interest include birch (*Betula*), hawthorn (*Crataegus*), willow (*Salix*), wild rye (*Elymus*), poplar (*Populus*), and ponderosa pine (*Pinus ponderosa*). The invasive species most abundant in the Clear Creek watershed is cheat grass (*Bromus tectorum*).

Photo 2. Burned Douglas fir trunks with regrowth of fireweed and thimbleberry looking upstream along Clear Creek, July 2002. The trail is on the far right side of the photo.

Photo 3. Large woody debris that washed downstream during the Clear Creek blowout, Summer 2003. The stream changed direction 90° from its original course at this point. Photo was taken looking upstream in October 2003.

Photo 4. Large woody debris washed downstream during Summer 2003 blowout, as seen in October 2003. The orange vegetation on the far side of the floodplain is live hawthorn. Directly adjacent, on the right, are burned dead hawthorns.

Photo 5. Aerial view of mouth of Clear Creek watershed showing extent of mudflow (October 2003). Bright yellow areas on right side of photo above stream are large areas of cheatgrass.

Riparian Recovery

Due to the large blowout this past summer, much of the vegetation on the imagery is no longer there. This presented a problem during ground truthing in October. Therefore, we concentrated our efforts in a floodplain along Panther Creek, just downstream of the mouth of Clear Creek (Figure 1). The floodplain had almost all of the species of interest, and provided very useful data for verifying our vegetation maps. Figure 2 shows the distribution of classified vegetation along Clear Creek. The high accuracy of the species maps for the floodplain and surrounding areas unaffected by the mudflows leaves us confident that the vegetation maps along Clear Creek are quite accurate. Tree trunks of birch, poplar, and hawthorn that remain standing along lower Clear Creek provide further evidence of the accuracy of our vegetation maps. Table 1 lists the riparian species that were identified in the imagery and the area covered by each species within a 20m riparian buffer around Clear Creek. The most abundant species were burned poplar, ponderosa pine, and birch. We also were able to distinguish between burned and unburned vegetation for some species, including poplar and hawthorn (Figure 3).

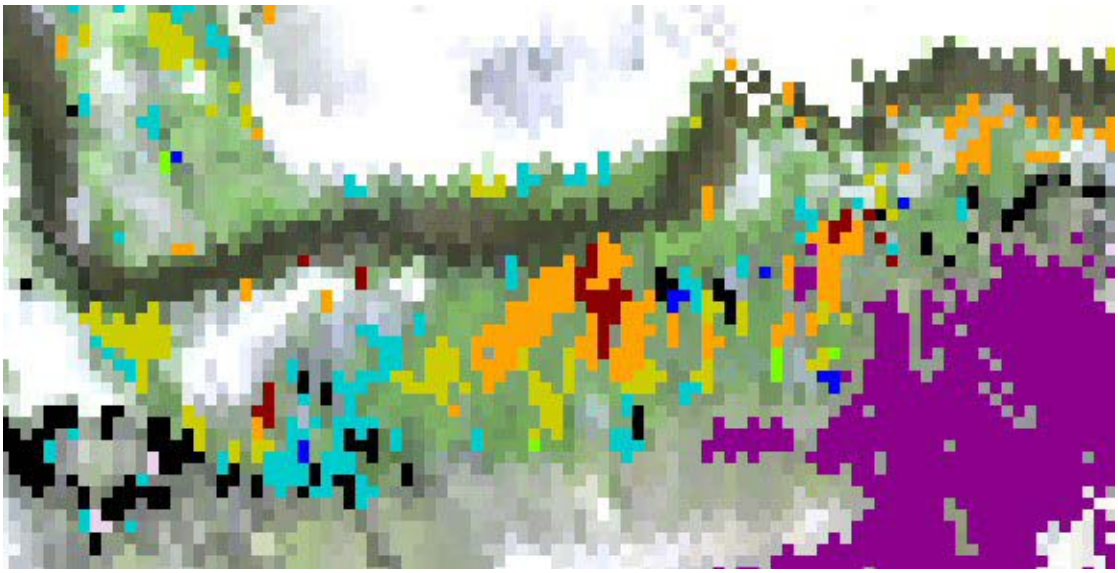

Figure 1. A true-color red-green-blue (RGB) composite of the floodplain surveyed in October 2003 along Panther Creek (shown as dark gray pixels), flowing from the upper right across the top of the image to the upper left, downstream of the mouth of Clear Crk.

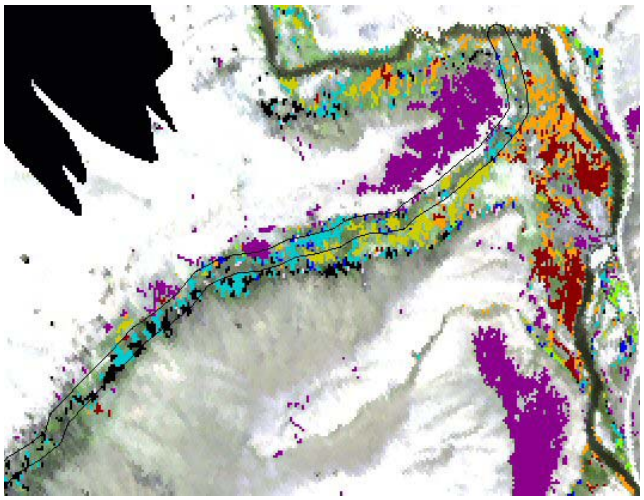

Figure 2. . True-color RGB composite of lower Clear Creek with the 20m buffer overlaid. As of Summer 203, the area along the buffer is under a layer of mud. Panther Creek flows from the lower right corner, along the right edge and exits in the upper center of the image. The floodplain surveyed in October 2003 is just to the left of where Clear Creek enters Panther Creek. After the mudflow, Clear Creek no longer turns to the left before emptying into Panther Creek; it now flows straight across the willow/rye grass flat. The black area in the upper left corner is the edge of the imagery. This imagery was flown July 2002.

Table 1. Composition of principal riparian vegetation within a 20m buffer zone along Clear Creek. The total area of the 20m buffer zone along Clear Creek is 106,436m^2. The total area of vegetation classified within the buffer is 27,094 m^2.

Species	% composition
Burned poplar	40.2
Ponderosa pine	24.3
Birch	14.9
Cheat grass	5.3
Willow	4.9
Burned hawthorn	4.0
Hawthorn	4.0
Ryegrass	2.1
Poplar	0.3

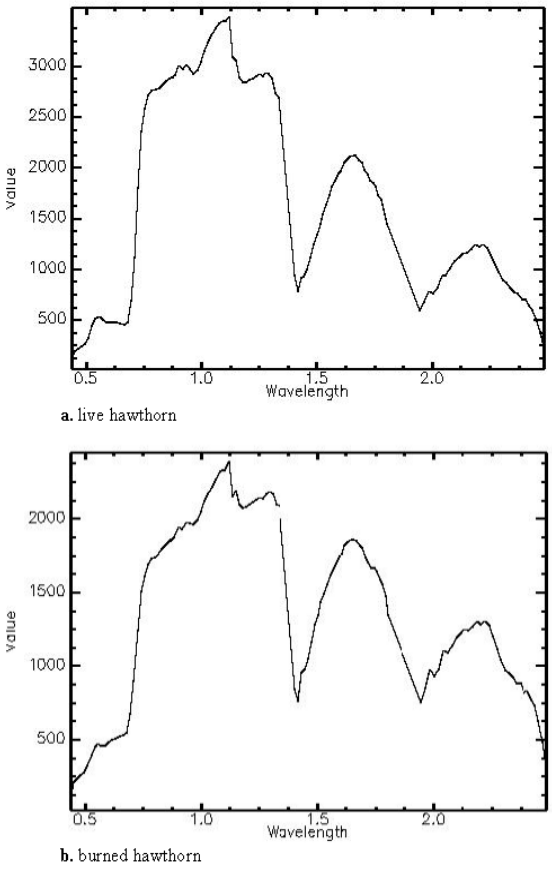

Figure 3. Unique spectral signatures of burned and live hawthorn along Clear Creek. The signatures look similar except at wavelength 0.7μm. The spectral signature for the live hawthorn shows an absorbance at 0.7 μm, whereas the spectral signature of the burned hawthorn shows not an absorbance, but a reflectance, at 0.7 μm.

Historic Grazing

We believe historic grazing occurred on a large elevated flat upstream of the mouth of Clear Creek because of the overwhelming abundance of cheat grass found there (Figure 4, Photo 6). There also are several hillsides upstream of Clear Creek, that mapped cheat grass in the imagery, and also suggest historic grazing. However, the large tract of cheat grass just upstream of Clear Creek (Figure 5) recently (2003) was sprayed by the Forest Service and is no longer as extensive as in 2002 when the imagery was flown.

Current Standing

This portion of the research is near completion. In the future we plan to examine the vegetation composition within two other riparian buffer zones 5m and 30 m, to gain a better understanding of the true size of riparian zones. We also will further examine the data using spectral unmixing to fine tune the percent composition of the vegetation within the buffer zones. Due to the heterogeneity of vegetation within the riparian zone, it is often difficult to identify large (5m) patches of homogenous vegetation as spectrally pure pixels. Spectral unmixing teases out the percentage of species within spectrally unpure pixels. Spectral unmixing will allow us to determine a larger percentage of the vegetation species composition along the riparian zone.

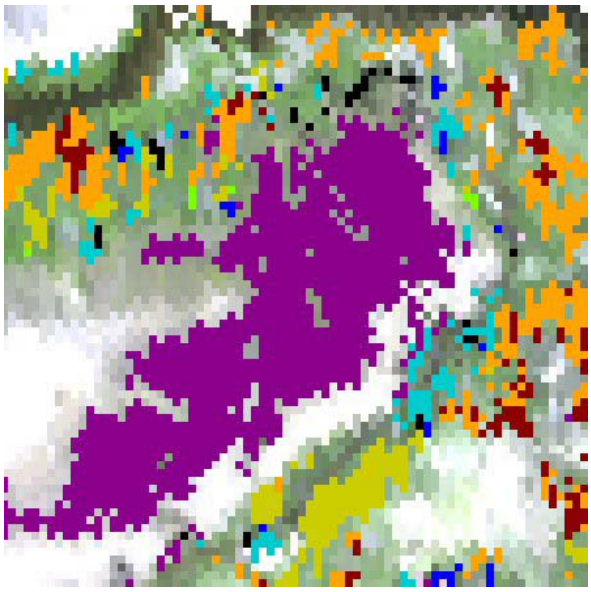

Figure 4. True-color RGB composite of a large tract of cheat grass (purple) located on elevated flat above Clear Creek, indicating historic grazing. Panther Creek runs across the top of the image. This imagery was flown July 2002.

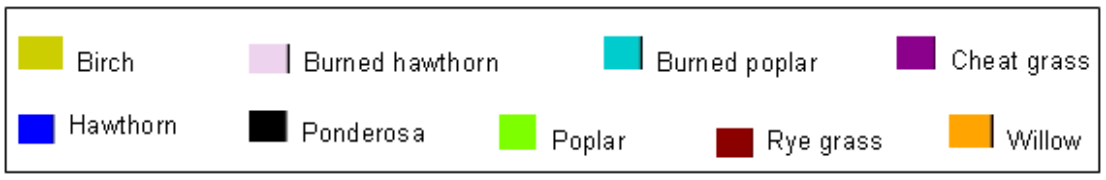

Photo 6. Large field of cheatgrass on hill above Clear Creek, October 2003. The dot on the right side of the field near the horizon is a 6ft. tall man.

Big Creek and its Tributaries

The interest in Big Creek was to examine riparian recovery following a large-scale fire; to quantitatively map its areal extent and relative (percent) species composition; to locate the boundary of a 60-year burn using marker trees that did not burn in the 2000 fire; and to verify accounts of historic grazing in Cave Creek, Cabin Creek, and Pioneer Creek by the occurrence of invasive species. The entire study area along Big Creek extends approximately 20km from just above Doe Creek to the Big Creek Gorge, approximately 6km above the confluence of Big Creek with the Middle Fork Salmon River. For each stream in which we examined riparian recovery, we applied a 20m riparian buffer (20m on each side of the stream) to measure relative species abundance.

Reconnaissance work was performed in summer 2003 to verify vegetation maps created in the spring. We recorded GPS points in large clumps of homogenous vegetation to help revise vegetation maps after field verification. Since the field season this summer, we have been revising the vegetation maps for several species. Results for Cabin Creek, Cliff Creek, Cougar Creek, Doe Creek, Goat Creek, and the middle section of Big Creek are given in this paper. Much of the imagery of Cave Creek, which was completely burned in 2000, was darkened by shadows, so we did not concentrate our efforts on this stream. We have identified some recovering vegetation along Cave Creek (mainly maple), but the results are not included in this paper.

Abundant riparian species of interest include Douglas fir (burned and live) (*Pseudotsuga menziesii*), birch (*Betula* sp.), cottonwood (*Populus* sp.), dogwood (*Cornus sericea*), maple (*Acer glabrum*), hawthorn (*Crataegus* sp.), prickly rose (*Rosa acicularis*), and Lewis mock orange (syringa) (*Philadelphus lewsii*). Invasive species of interest is cheat grass (*Bromus tectorum*).

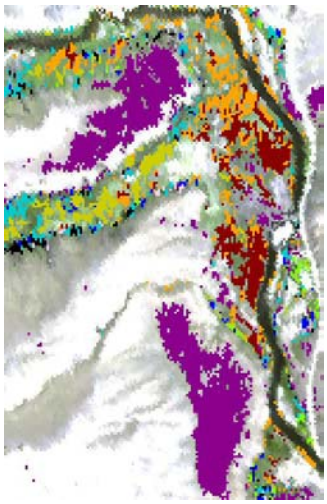

Figure 5. True-color RGB composite showing the location of cheat grass upstream of Clear Creek that was present when the imagery was flown (July 2002), but was recently (2003) sprayed with herbicides by the U.S. Forest Service. Also included, for reference, is the large field of cheat grass located on the elevated flat above Clear Creek (top left). Panther Creek flows from the lower right corner of the figure to the upper left corner.

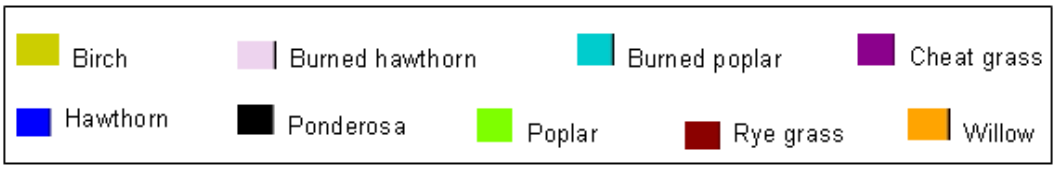

Riparian Recovery

We classified riparian vegetation on a 7km section of Big Creek, extending from approximately 3km upstream of Taylor Ranch to the Big Creek Gorge. The area of the 20m buffer is 324,285 m^2. We could identify vegetation only for 6% of the area (Table 2). This was due to (1) the buffer included Big Creek itself, which is quite large (6th order stream), and (2) the riparian is highly intermixed with many vegetation species, so it is often difficult to find large (5m) areas of homogenous vegetation.

Table 2. Composition of principal riparian vegetation within a 20m buffer zone along Big Creek. The total area of the 20m buffer zone along Big Creek is 324,285m^2. The total area of vegetation classified within the buffer is 18,190.5 m^2.

Species	% composition
Birch	30.4
Hawthorn	26.1
Cheat grass	14.3
Dogwood	10.6
Douglas fir	6.8
Mock orange	5.9
Burned Douglas fir	5.5
Maple	5.1
Prickly rose	0.6

Lower Cliff Creek burned completely during the 2000 fire (Photo 7); however, regrowth of vegetation was rapid (Photos 8 and 9). Much of the recovering riparian vegetation present in 2003 is maple, but it is not detected in the imagery. In fact, very little vegetation can be identified as spectrally pure in Cliff Creek after the fire (Figure 6), suggesting a variety of low vegetation interspersed with rock, ash, and charcoal. The difficulty in detecting the regrowth of maple along Cliff Creek is most likely due to the imagery being flown two years after the fire and the maple not being large enough to be detected by the 5m-pixel coverage. The most abundant species identified within a 20m riparian buffer zone were birch, hawthorn, and burned Douglas fir (Table 3). Most of the spectrally pure pixels identified were in the upper part of the imagery. Other recovering species along Cliff Creek that are not detected by the imagery are mountain hollyhock (*Iliamna rivularis*) and thimbleberry (*Rubus parviflorus*).

Photo 7. Cliff Creek in September 2000, one month after the fires. Looking upstream.

Photo 8. Cliff Creek in July 2001, showing re-growth of vegetation along the floodplain.

The upper basin of Cougar Creek was burned in 1998. The imagery covers the lower part of Cougar Creek, but does not extend to the fire boundary. We were able to classify almost 40% of the vegetation as spectrally pure. Birch and Douglas fir comprise 70% of the vegetation within the 20m riparian buffer zone (Table 4). Figure 7 shows the distribution of vegetation species along Cougar Creek.

Photo 9. Cliff Creek in July 2002, the same month the imagery was flown. There is more re-growth of low shrubs and fireweed (seen on the right bank, looking upstream).

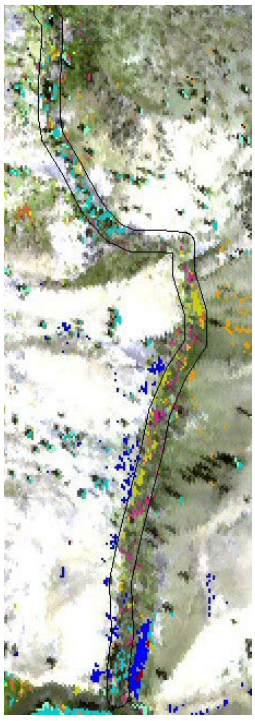

Figure 6. . True-color RGB composite of lower Cliff Creek, with the 20m buffer overlaid. Due to the severity of the burn in 2000, and the use of spectrally pure pixels, very little vegetation could be classified from the imagery, which was flown two years later, in July 2002. Big Creek flows from left to right at the bottom of the figure.

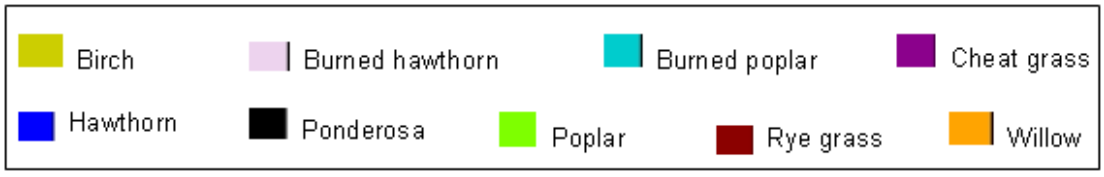

Table 3. Composition of principal riparian vegetation within a 20m buffer zone along Cliff Creek. The total area of the 20m buffer zone along Cliff Creek is 99,311 m^2. The total area of vegetation classified within the buffer is 12,124 m^2.

Species	% composition
Birch	31.4
Hawthorn	21.7
Burned Douglas fir	19.9
Maple	9.3
Douglas fir	6.5
Dogwood	5.5
Cheat grass	4.8
Cottonwood	0.4
Mock orange	0.4
Prickly rose	0.1

Table 4. Composition of principal riparian vegetation within a 20m buffer zone along Cougar Creek. The total area of the 20m buffer zone along Cougar Creek is 70,927 m^2. The total area of vegetation classified within the buffer is 26,944.5 m^2.

Species	% composition
Birch	40.7
Douglas fir	29.1
Maple	10.5
Dogwood	5.7
Hawthorn	3.9
Burned fir	3.7
Prickly rose	2.8
Cheat grass	2.3
Mock orange	1.3

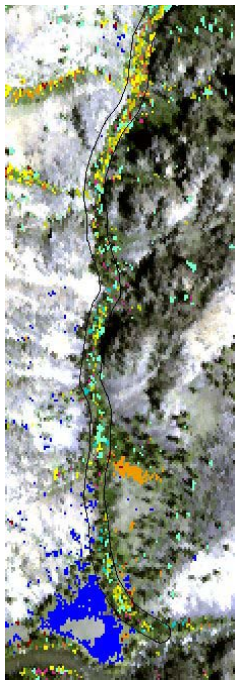

Figure 7. True-color RGB composite of lower Cougar Creek, with the 20m buffer overlaid. More vegetation was identified in the upper catchment than in the lower catchment. The large field to the left of Cougar Creek does have some cheat grass, but it is over-predicted in this composite. Big Creek flows from left to right across the bottom of the figure. The imagery was flown July 2002.

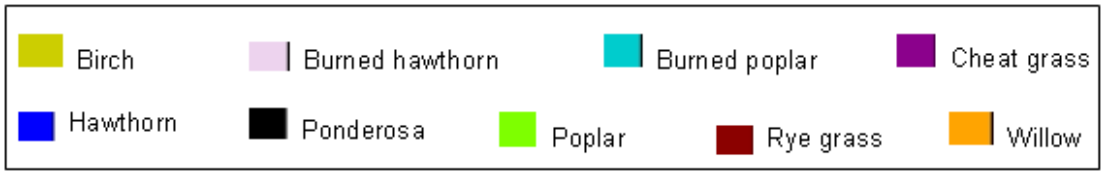

Goat Creek also was not burned in the 2000 fire. As in Cougar Creek, the imagery covers only the lower part of Goat Creek. Spectrally pure vegetation was classified for 56% of the vegetation within the 20m riparian buffer zone. Birch was the dominant vegetation, followed distantly by Douglas fir, prickly rose, and dogwood (Table 5). Figure 8 shows the distribution of vegetation species along Goat Creek.

Table 5. Composition of principal riparian vegetation within 20m buffer zone along Goat Creek. The total area of the 20m buffer zone along Goat Creek is 47,935 m^2. The total area of vegetation classified within the buffer is 27,053 m^2.

Species	% composition
Birch	38.0
Douglas fir	17.2
Prickly rose	14.2
Dogwood	13.7
Cheat grass	5.8
Maple	5.4
Hawthorn	3.1
Burned fir	0.7

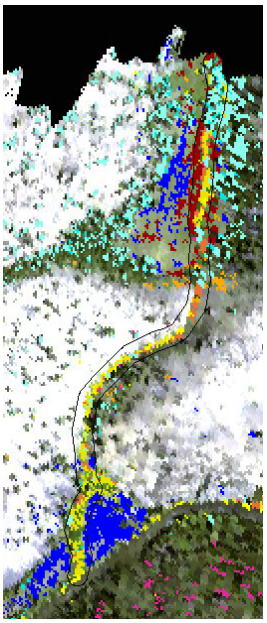

Figure 8. . True-color RGB composite of lower Goat Creek, with the 20m buffer overlaid. Birch is the dominant riparian species along Goat Creek. Imagery was flown July 2002. The black areas at the top of the figure are the edges of the imagery.

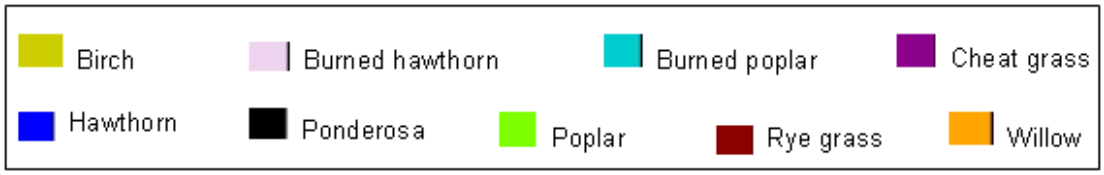

Historic Grazing

Large tracts of cheat grass were mapped along the hillsides around Cabin Creek, near the mouth of Pioneer Creek on a hill above Taylor Cabin, and in a field near the mouth of Goat Creek. There are accounts of grazing by homesteaders in the Cabin Creek drainage at the turn of the 20th Century. It is no surprise that most of the hillsides above Cabin Creek are covered with cheat grass (Figure 9). Most of the cheat grass is intermixed with other vegetation, namely tumble-mustard (*Sisymbrium altissimum*) and rabbitbrush (*Chrysothamnus*). A smaller tract of cheat grass was mapped along Pioneer Creek (Figure 10). The caretakers of Taylor Ranch previously grazed their horses along the hillside where the cheat grass was found. Although there are no historic accounts of grazing at the mouth of Goat Creek, a large field mapped out as predominantly cheat grass (Figure 11). The cheat grass at Goat Creek is intermixed with balsamroot (*Balsamorhiza*). The Goat Creek trail is used extensively by horseback riders and pack stock, so it is reasonable their animals would have grazed the field heavily over the years.

Historic Fire Footprints

Doe Creek catchment burned completely during the 2000 fire (Photo 10). However, there are isolated trees and small patches that did not burn during the fire. During field reconnaissance in Summer 2003 we found a large (5m) clump of live Douglas firs on a hillside above Doe Creek which did not burn in the 2000 fire (Photo 11). This stand is presumed to be around 60 years old, which is when a previous fire burned the entire

watershed. The spectral signature of this stand was used to locate other Douglas firs of the same age in the watershed, which are used to identify the historic fire "footprint."

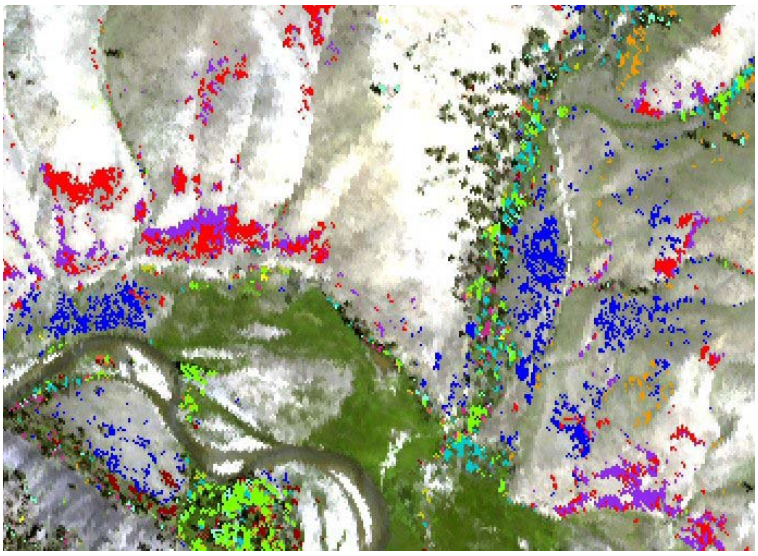

Figure 9. True-color RGB composite of lower Cabin Creek showing the distribution of cheat grass. These are located on well-drained sites and indicating historic grazing. There are three different cheat grass classifications, as indicated below in the color key. The imagery was flown July 2002

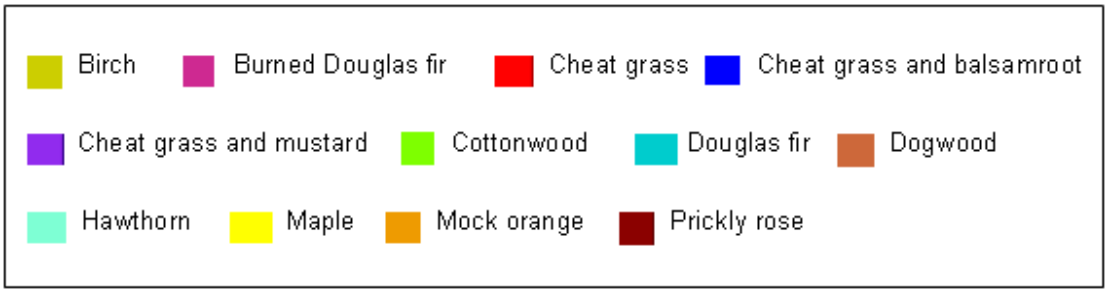

Preliminary results show the Douglas fir spectral signature is capable of finding some, but perhaps not all, 60-year old Douglas firs (Figure 12). It is not clear whether the spectral signature of the 60-year old Douglas firs is different from that of live Douglas firs of different ages, but this will be easy to determine for our existing coverages.

Current Standing

The historic grazing component of this research (Cabin Creek and Pioneer Creek) is near completion. We would like to further evaluate the percent composition of cheat grass versus other vegetation, such as tumble-mustard, rabbitbrush, and balsamroot. We will verify new vegetation maps in the field in Summer 2004, during our annual visit. Pertaining to the riparian recovery component, we plan to apply 5m and 30m buffer zones and quantify species abundance within these zones for all streams examined (Big Creek, Cliff Creek, Cougar Creek, and Goat Creek). We will determine the total vegetation cover, further refine the relative abundance numbers, and quantify the

abundance of rock, water, and other non-riparian vegetation. We will continue working on Doe Creek, revising the maps until all the 60-year old Douglas firs have been identified in the upper catchment.

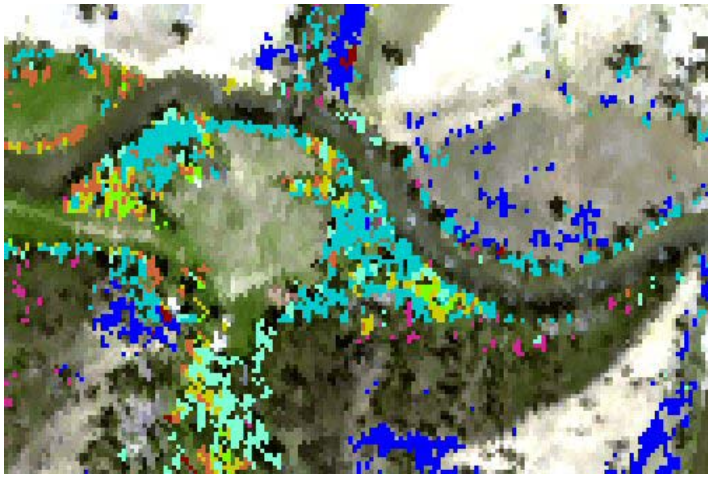

Figure 10. True-color RGB composite of Taylor Ranch, which lies between Pioneer Creek (left of center, bottom of figure) and Cliff Creek (top center). Big Creek flows from left to right along the middle of the figure. Cheat grass was identified on a hillside above Pioneer Creek (left side of figure). The large field downstream of Taylor Ranch (right side of figure) is largely cheat grass, but it is under-predicted in this field.

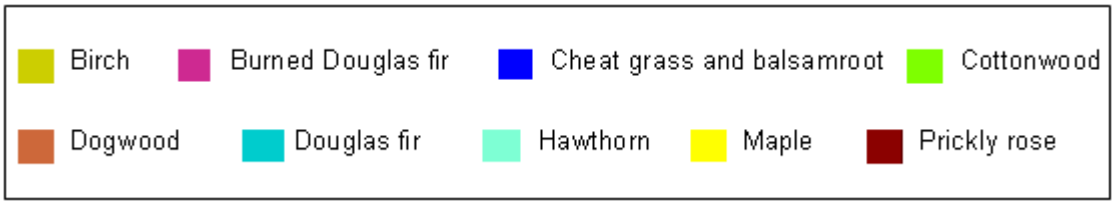

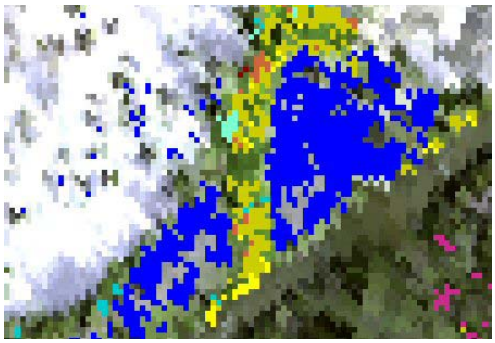

Figure 11. True-color RGB composite of the mouth of Goat Creek, showing the location of cheat grass. The imagery predicts well for cheat grass in these fields, which is intermixed with balsamroot. Imagery was flown July 2002.

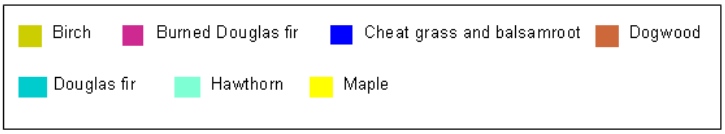

Photo 10. Doe Creek catchment as viewed from across Big Creek. This watershed was burned approximately 60 years ago and again in 2000. Most of the Douglas firs were burned in 2000; however, a few 60 year old trees can be seen on the far ridge line and near the mouth of the creek.

Photo 11. Looking upstream on Big Creek at Doe Creek coming in from the left. The large clump of Douglas firs on the hillside above the mouth of Doe Creek (right of center) is being used as a training point for 60-year old trees.

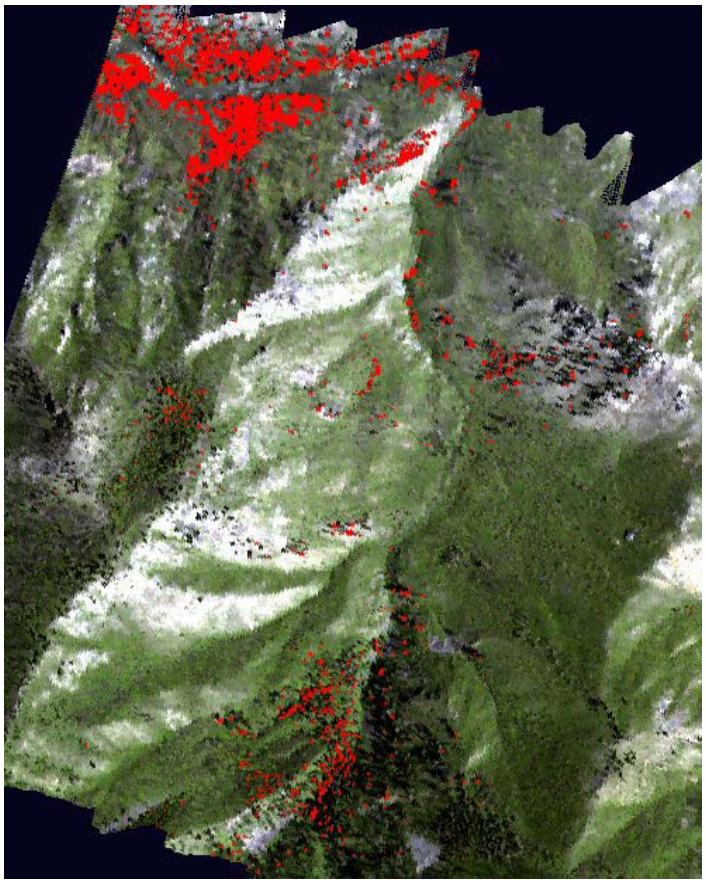

Figure 12. True-color RGB composite of Doe Creek catchment showing the location of living 60-year old Douglas firs (red). Doe Creek appears as a "ridge" extending from the bottom to the top in the center of the image. The mouth of Doe Creek lies just beyond the edge of the imagery in the upper right corner. Big Creek can be seen flowing between two large patches of Douglas firs in the upper left corner of the figure. The black areas in the upper left and upper right of the figure are the edges of the imagery. This imagery was flown July 2002.

ACKNOWLEDGEMENTS

This study was made possible by a grant from the National Aeronautics and Space Administration Goddard Space Flight Center. ISU would also like to acknowledge the Idaho Delegation for their assistance in obtaining this grant.